

**ANALYSIS OF MOVEMENT DISORDER-RELATED GENES FOLLOWING  
KNOCKDOWNS OF *ANO10*, *WDR81*, AND *VLDLR* IN ZEBRAFISH (*DANIO RERIO*)**

A THESIS SUBMITTED TO  
THE GRADUATE SCHOOL OF ENGINEERING AND SCIENCE  
OF BILKENT UNIVERSITY  
IN PARTIAL FULFILLMENT OF THE REQUIREMENTS FOR  
THE DEGREE OF  
MASTER OF SCIENCE  
IN  
NEUROSCIENCE

By  
Göksemin Fatma Şengül  
June 2018

ANALYSIS OF MOVEMENT DISORDER-RELATED GENES FOLLOWING  
KNOCKDOWNS OF *ANO10*, *WDR81*, AND *VLDLR* IN ZEBRAFISH (*DANIO  
RERIO*)

By Göksemin Fatma Şengül  
June 2018

We certify that we have read this thesis and that in our opinion it is fully adequate, in scope and in quality, as a thesis for the degree of Master of Science.

---

Michelle Marie Adams (Advisor)

---

Özlen Konu Karakayalı

---

Çağdaş Son

Approved for the Graduate School of Engineering and Science

---

Ezhan Karaşan  
Director of the Graduate School

## ABSTRACT

### ANALYSIS OF MOVEMENT DISORDER-RELATED GENES FOLLOWING KNOCKDOWNS OF *ANO10*, *WDR81*, AND *VLDLR* IN ZEBRAFISH (*DANIO RERIO*)

Göksemin Fatma Şengül

MSc in Neuroscience

Advisor: Michelle Marie Adams

June 2018

Movement Disorders are the neurological symptoms that cause alterations in normal motility, posture and muscle tone. Certain brain areas, such as the cerebellum, mediate correct motor control and functioning. When defects or congenital lesions occur in the cerebellum, neural disruption in motor coordination causes the development of a particular movement disorder known as cerebellar ataxia. The focus of this study was to examine how three genes of interest (*ano10*, *wdr81*, *vldlr*), contributing to multiple varieties of cerebellar ataxias, influence one another and other genes that are associated with this disorder. Mutations in *vldlr* and *wdr81* are associated with Cerebellar Ataxia Mental Retardation Disequilibrium Syndrome type 1 and type 2 (CAMRQ1 and CAMRQ2), respectively, whereas mutations in the *ano10* gene is responsible for the development of Autosomal Recessive Cerebellar Ataxia Type 3 (ARCA3). In this work, five key scientific findings were reported. Firstly, *in silico* analysis predicted a common Ca<sup>2+</sup> activated Casein Kinase 2 (CK2) domain in the protein sequences of the genes of interest and also predicted a common interacting UBC protein. These predicted interactions, a common CK2 domain and a UBC interacting protein may explain the observed

neurodegenerative phenotype in cerebellar ataxia. Secondly, the transcript level analysis (qPCR and RNASeq) of *ano10a*, *wdr81* and *vldlr* using zebrafish embryos collected from early embryonic and late larval stages showed that the three genes were expressed relatively higher at 1 hpf, 2 hpf and 5 hpf developmental stages than others and may suggest their importance in developmental processes. Additionally, the comparison of the expression patterns of *ano10a*, *wdr81* and *vldlr* during early embryogenesis indicated that three targeted genes were co-localized at diencephalon, midbrain (optic tectum) and cerebellum. These spatiotemporal results may restrict the involvement of these three genes selectively in early neurodevelopmental processes. Thirdly, this study also examined the expression level analysis of three targeted genes in 12 different adult tissues in a sexually dimorphic manner. Findings showed that genes of interest were expressed significantly higher at the eyes, brain and gonads (p-values < 0.05). Moreover, the gender specific examination in the 12 adult tissues revealed that *ano10a* and *wdr81* expression differed significantly at eyes, gills, liver and gonads (p-values < 0.05) whereas, *vldlr* gene expression was significantly different at swim bladder and gonads in male and female individuals (p-values < 0.05). Fourthly, the clustergram analysis indicated that three genes of interest were grouped within close families with each other and 9 additional cerebellar ataxia associated genes and may imply that targeted genes alter functions in the converging pathways. Finally, results from the clustergram analysis helped to design and carry out a study knocking down the expression of *ano10a*, *wdr81* and *vldlr* separately with MO antisense technology to examine the effect of the silenced mRNA on the expression levels of each other and 9 other highly correlated cerebellar ataxia-related genes. Single MO injections caused the significant upregulation of all

investigated genes especially at 72 hours after/post injection (hpi) (p-values < 0.05) when *ano10a* transcript was silenced suggesting either an activated compensatory mechanism or activated alternative disease specific cascade molecules in response to its absence. Taken together, the outcomes of functional knockdowns can pave the way for the development of novel therapeutic targets using inhibitors or antagonists of activated cellular pathway components or the enhancers of downregulated genes to prevent or at least slow down the progression of not only cerebellar ataxia but also several other neurodegenerative disorders.

**Key words:** Zebrafish, gene expression, movement disorders, cerebellar ataxia, *ano10*, *wdr81*, *vldlr*, morpholino injection, gene knockdown, sexual dimorphism, *in situ* hybridization, clustergram analysis, Bioinformatics analysis and qPCR.

## ÖZET

# **ZEBRABALIĞINDA HAREKET BOZUKLUĞUYLA İLİŞKİLENDİRİLEN ANO10, WDR81 VE VLDLR GENLERİNİN SUSTURULDUĞU MODELDE İNCELENMESİ**

Göksemin Fatma Şengül

Nörobilim Lisansüstü Programı, Yüksek Lisans

Tez Danışmanı: Michelle Marie Adams

Haziran 2018

Hareket bozuklukları hastalıkları, normal hareketlilik, duruş ve kas tonusunda değişikliğe neden olan nörolojik rahatsızlıklardır. Bilindiği üzere, beyincik dengeden ve kasların düzenli çalışmasından sorumlu olan önemli bir beyin bölgesidir. Beyincikte meydana gelen işlevsel kusurlar veya konjenital lezyonlar motor koordinasyonda bozulmalara sebepolarak, beyincik ataksisi diye adlandırılan hareket bozukluğunun gelişimine neden olur. Bu çalışmanın odak noktası, değişik serebellar ataksisi alt türlerinin ortaya çıkmasından sorumlu olan hedef genlerin (*ano10*, *wdr81*, *vldlr*) birbirleri ve serebellum ataksisi ile ilişkili diğer genler üzerindeki etkilerini incelemektir. Böylece hedef genler arasındaki ortak etkileşim paterni saptanmış olacaktır. *vldlr* ve *wdr81* genlerindeki mutasyonlar sırasıyla, Zihinsel Gerileme ve Denge Bozukluğu İçeren Beyincik Ataksisi Tip 1 ve Tip 2 (ZGDBA1 ve ZGDBA2) ile ilişkiliyken, *ano10* genindeki mutasyonlar, Otozomal Resesif Beyincik Ataksisi Tip 3' ün ortaya çıkmasından sorumludur. Bu çalışmada, yapılan deneylerin sonucunda beş önemli bilimsel bulgu elde edildi. Öncelikle, Biyoenformatik analizler sonucunda hedef üç genin de protein sekansında Kalsiyum iyonu tarafından aktive edilen Kazein Kinaz 2 (KK2) motifi ve üçünde etkileştiği Ubikitin C (UBC)

proteini olduğu gözlemlendi. Ortak olarak üçünde de var olduğu tahmin edilen bu KK2 motifi ve de üç genle de etkileşim halindeki UBC proteinin serebellum ataksisindeki sinirsel dejenerasyon fenotiplerinin ortaya çıkmasında etkili olabileceği düşünülmektedir. İkinci olarak, hareket bozukluğuyla ilişkilendirilen bu üç genin ifade düzeyleri qPCR ve RNASeq yöntemleri kullanılarak erken gelişimsel ve geç larval dönemlerde toplanmış olan zebra balığı embriyolarında gösterilmiştir. Yapılan deneyler sonucunda, hedef üç genin de 1 döllenme sonrası saat (dss), 2 dss ve 5 dss zaman dilimlerinde diğer zaman dilimlerine göre daha yüksek ölçüde ifade edildiği saptanmıştır. Bu da hedef genlerin özellikle gelişimsel işlevlerde önemli bir role sahip olduğunun göstergesi olabilir. Ek olarak, bu üç hedef genin embriyonik süreçte ortak ifadesi diyensefalon, orta beyin (optik tektum) ve serebellum bölgelerinde gösterildi. Bölgesel ve zamansal ifade analizlerinin sonuçları beraber değerlendirildiğinde, üç hedef genin de özellikle sinirsel gelişimle ilgili işlevlerde görev aldığı öngörülmektedir. Üçüncü olarak, erişkin zebra balığı organlarında, hedef genlerin ifade düzeylerine bakıldı. Üç gen de ortak olarak beyin, göz ve eşey organlarında diğer organlara kıyasla daha yüksek seviyede ifade edildiği gösterildi ( $p < 0.05$ ). Ayrıca cinsiyet dikkate alınarak yapılan incelemelerde, *ano10a* ve *wdr81* genlerinin gözler, solungaçlar, karaciğer ve eşey organlarındaki; *vldlr*'ın ise yüzme kesesi ve eşey organlarındaki ekspresyon seviyelerinin, dişi ve erkek bireyler arasında anlamlı farklılıklar gösterdiği saptandı ( $p < 0.05$ ). Daha sonra kümeleme analizi yapılarak, hedef genlerin birbirleriyle ve serebellum ataksisiyle ilişkilendiren diğer genlerle yakın ailelerde yer aldığı gösterildi. Bu durum ilgili genlerin kesişen yollardaki hücresel fonksiyonları değiştirebileceği fikrini akla getirdi. Son olarak, kümeleme analizi sonuçları ışığında planlanan etkileşim çalışmasında, üç hedef

genin, Morpholino oligonükleotit teknolojisi kullanılarak, ayrı ayrı susturulduğu durumda, hedef genlerin birbirlerinin ve serebellum ataksisiyle ilişkili diğer genlerin ifadesini nasıl değiştirdiği araştırıldı. Hedef genler arasından sadece *ano10a*'nın sustuğu koşulda, diğer iki hedef gen olan, *wdr81* ve *vldlr*'ın ve ayrıca çalışma kapsamında incelenen, serebellum ataksisi ile ilişkisi olan diğer genlerin çoğunun ifade düzeyini anlamlı olarak özellikle enjeksiyondan 72 saat sonrasında (sse) arttığı saptandı ( $p < 0.05$ ). Bu artışın hücrede *ano10a*'nın yokluğunu telafi edici bir mekanizma veya tam aksine hastalığın oluşumunu/ilerleyişini tetikleyen bir etki olduğu düşünülmektedir. Tüm bulunan sonuçlar dikkate alındığında, hedef genlerin susturulmasıyla aktive olan yolak antagonistlerinin/inhibitörlerinin ya da inhibe olan sinyal moleküllerinin aktivatörlerinin kullanılması yaklaşımı, ümit ediyoruz ki sadece serebellum ataksisini değil diğer başka sinirsel dejenerasyon içeren hastalıkları da tedavi edici nitelikte olacaktır.

**Anahtar kelimeler:** Zebra balığı, gen ifadesi, hareket bozukluğu hastalıkları, serebellum ataksisi, *ano10*, *wdr81*, *vldlr*, morpholino enjeksiyonu, gen susturma, cinsi çiftyapılılık, *in situ* hybridizasyon, kümeleme analizi, biyoenformatik analizi ve qPCR.



*To my dearest grandfather*

## **ACKNOWLEDGEMENTS**

When I chose the Department of Genetics in 2010 to take my undergraduate education, I wanted to be graduated with great success and continued to my way as a scientist. During my undergraduate education, my interest against neuroscience was arisen. Encountering with Dr. Michelle Adams was one of the great opportunities for me to start my scientific journey in the area of hard core neuroscience. Besides studying in my interested area, neuroscience, throughout my Master education, Dr. Michelle Adams also provided me with great motivation to pursue my aims, great laboratory environment to conduct my experiments enthusiastically, and great guidance and support to improve my academic knowledge. Therefore, I would like to present my endless gratitude to Dr. Michelle Adams.

I would like to thank to Dr. Özlen Konu Karakayalı for her contributions, feedbacks and kind collaborations for the progress of current study. I am also grateful to her for teaching Bioinformatics classes. The techniques, databases, programs and knowledge that I obtained through this lecture provided me to strengthen my hypothesis and to test my scientific questions with different perspectives. Therefore, I always felt and accepted that taking this course from Özlen Konu Karakayalı was the turning point of my project. Her acceptance to be a jury member for my defense was excellent proud for me.

I would like to express my special gratitude to Çağdaş Son for being my jury member, evaluating my thesis and giving feedbacks to enhance and improve my ideas in the text.

I would like to offer my gratitude to the dean of Science Faculty, Dear Professor Dr. Tayfun Özçelik. He was one of the most knowledgeable, kind and

respectful scientists that I met. It was great honor for me to be involved within the same project with him and to consult our ideas for the progression of this project. His collaboration, feedbacks and helps contributed a lot to bring our study into that much sophisticated and advanced stage.

I would like to thank to Professor Dr. Haluk Topaloğlu to accept being a great collaborator for us. He would be appreciated for his great knowledge, suggestions and clinical contributions to our studies whenever we asked for his help.

I also owe too much to Assoc. Prof. Güneş Özhan for her nice collaboration with us. She guided me about the troubleshooting of many experiments particularly on *in situ* hybridization and she also kindly shared her labs' optimized protocols with us.

I also owe to Assoc. Prof. Ayça Arslan-Ergül for being one of great role models for me. Her scientific enthusiasm, knowledge, ambitious and positive attitudes indicated how science can be that much enjoyable. Her great contributions and important suggestions about my project improved the quality of conducted work and impact of it. Therefore, I would be always grateful to her.

I would like to thank to my summer internship advisor Professor Cahir O'Kane (PhD) for giving me a chance to study in his lab at the Cambridge University. My supervisor, PhD student Alex Patto also will be always appreciated for his patient and guidance during my internship. It was a great opportunity for me to work with them in the area of neuroscience and to perform my experiments in such a precious scientific place where Watsons and Crick discovered DNA, genetic code of life.

I also would like to thank to Assoc. Prof. Ebru Erbay for accepting me into her lab as a Senior Student during my Bachelor studies. Studying under her guidance did not only help me to obtain myriad of experimental techniques but also, I developed my presentation skills and learned how to manage time efficiently in the hectic scientific environment. She taught me how to interpret coincidence like experimental outcomes that we can gain unintentionally by encouraging me to walk along the serendipitous path of discovery.

I want to thank to Dr. Naznoosh Somali and Dr. Hamid Syed for their patience and guidance during my senior studies in the laboratory of Dr. Erbay. Specifically, Dr. Syed even helped me for my current study whenever I had a question about the tricks of an experiment that I would perform for the first time. His wide knowledge and helpful attitude always prevent me losing time and making mistakes.

I want to thank to Dr. Begüm Kocatürk who is the Post-Doctoral Fellowship of the Dr. Ebru Erbay group and Instructor of the Neuroscience Graduate Program. She becomes one another great role model for me with her scientific ambition, enthusiasm and curiosity. She also taught me to pursue my research goals by believing them from heart and not to give them up even though there may be many obstacles throughout this scientific environment. I also did not forget to mention about her great friendship. Regardless of her academic status, she all the time approached to me as her friend or more likely as her little spoiled sister. She all the time supported me, rose my mode up whenever she felt I was unhappy, advised me and shared her experiences with me to see me as a successful and dedicated scientist as she is.

I would like to thank to Master of Science (MSc) Özge Burhan for her endless supports and friendship and as well as for being a good accompany of concert, cinema, shopping and makeup tutorials.

I would like to thank to PhD student Ayşe Gökçe Keşküş for her patience, and supports during our 7 years-old friendship. She was a wonderful listener and the representation of wisdom for me. Therefore, whenever I needed to take advice or I wanted to tell bad incidences that I have experienced, I found her and talked with her. After brief conversation, I left from her side feeling better than the beginning. She was a perfect collaborator as well. During our studies for this project, she helped a lot. She performed clustergram analysis (Figure 3.5) and obtained expression level graphs of the movement disorder-related genes of interest during early embryogenesis (Figure 3.2) by using qPCR and RNASeq data in Matlab®. Having such a great friend in your private life and scientific your lab environment has provided me to feel lucky. Therefore, Ayşe Gökçe has special place in my heart.

I would like to thank to PhD student Melek Umay Tüz-Şaşıık for her helps, guidance, patience and understandings throughout my Master studies. From the first day to the end of my experimental studies, she was all the time supported me, helped to design my experimental plans and solved my scientific problems whenever I stacked in those. She completely deserves her name meaning, Angel, by saving me from troubles and lightening my scientific burdens. I also want to present my gratitude to her for spending time to perform my morpholino injection experiments for the dose curve of *ano10a* and for the interaction studies with three genes of interest.

I would like to thank to MSc. Elif Tuğçe Karoğlu for her supports and friendship during my Master studies. She also provided me to have statistically significant data by performing sophisticated statistical tests in the context of this project. I also would like to emphasize her psychologist identity due to her Bachelor degree. She was the representative of wisdom for me. Therefore, I prefer to apply her advice whenever I have difficulty to make difficult decisions.

I would like to thank to Dilan Çelebi-Birand for her supports and helpful attitudes. She all the time put extra effort about my projects and helped whenever I need. I also want to thank her for the proofreading of my project applications, abstracts, posters and Turkish translations.

I would like to thank to Dr. Füsün Doldur-Ballı for her supports and helpful attitudes. She always shared her experiences even previously performed WDR81 and VLDLR morpholino injection dose curve gel image with us in the context of this project. Her well-written notebooks all the time enlighten my way whenever I hesitate about the steps of experiments.

I would like to thank to Assoc. Prof. Engin Durgun for his motivation and supports during my night-shift and officially holiday studies. I learned a lot from him how to become a good scientist, good suppose, good, father/mother, good advisor and good colleague. Therefore, he would be at the beginning of unforgettable persons of UNAM for me.

I would like to thank to my lab mates who provide me a suitable lab environment and help me whenever I need. Therefore, my special thanks go to Naz Şerifoğlu, MSc Begün Erbaba and Ilgım Narin Ardıç and to our former MSc student

Ayşegül Dede. If I did not conduct my projects in the environment did they provide, most probably I would not be that much productive. Therefore, I owe a lot to them.

I would like to acknowledge to Dr. Alper Devrim Özkan for her narrative and critical usage of English. Through his suggestions, I learned to write my thesis in a more proper and descent manner.

I have a chance to build strong friendships with people in the work place environment. There were so many perfect friends that I want to express my gratitude. I learned too much from them to grow as a more suitable researcher. Therefore, I would like to thank to PhD student Seylan Ayan for her short term supportive and scientific friendship. I also would like to thank to PhD student Nuray Gündüz for her supportive and stone like strong personality, to Dr. Aydan Yeltik for her understanding and protective personality, to PhD student Özlem Tufanlı for her nice and cute personality, to PhD student Kıvanç Güngör for his debater personality, to MSc Kıvanç Çoban for his colorful and cheerful personality, to MSc Özge Uysal for her realist and reliable personality, to MSc Oğuz Tuncay for his humorous sense of science, to MSc İdil Esen for her supportive personality, to MSc Uğur Teğın for his knowledgeable personality, to MSc Latif Önen for his helpful and computerized personality, to Onur Çakıroğlu for his caring personality, to Ulviye Quliyeva for her naive personality, to Gökçe Öz for her energetic personality, to Abdin Saateh for his old historical wisdom, to Koray for his critical approach, to Dr. Burak Güzelsoy for his cleaver thinking, to İrem for her short-term neighborhood, to Buket Gültekin for her pinky personality, to Zehra Veli for her sister-like protective and sensitive personality, to PhD student İnci Onat for her honest comments, to PhD student Zehra Tatlı-Yıldırım and PhD student Aslı Ekin for her sarcastic approach towards science,

to PhD student Aslı Dilber Yıldırım for her dedicative scientific approach, to MSc Hilal Bal for her enjoyable understandings of science, to Ünal Metin Tokat for his hardworking and honest personality, to Muzaffer Yıldırım for his doesn't care personality, to Kenan Sevinç for his outgoing personality, to MSc Çağla Eren-Çimenci for her enthuasiastic attitude to study my PhD in Canada, to Recep Erdem Ağhan for his offending personality, to MSc İdil Arıöz for her mother-like friendship, MSc Nurcan Haştar for her master chef abilities with microwave oven, to Nedim Hacıosmanoğlu for his lovely friendship, to Tuğberk Kaya for his creative and relax characteristics and to İrem Sözen for her excited personality. If I did not meet with them, I would not become that much confident and competent scientist. In addition, I would like to thank to my friends Fikret Piri, Semih Bozkurt and Abdullah Kafadengi from UNAM clean room for their happy good morning ceremonies. Through their morning conversations, I all the time started my day in an energetic and positive manner.

I would like to thank to UNAM administration office coordinators at the first place to Duygu Kazancı, Ayşegül Torun and Olcay Ündal for their collaborative and supportive attitudes.

I also would like to thank to Aunt Suna, Seycan, Şerife and Ümmühan for their endless power to collect our messy study areas and to clean our chemical containing laboratory environment. They were the invisible heroes of all scientific studies conducted in UNAM and MBG. Therefore, I would like to express my respect to their huge-effort requiring jobs.

I would like to thank to Tülay Arayıcı for her support in the Zebrafish Facility to separate breeder males and females. She was the best match maker for fish that I



saw in my life. I would like to thank to Gamze Aykut for her helps with regards to animal experiments. I would like to thank to MBG laboratory manager Pelin Makas and for her tidy and fair working understandings. I would like to thank to specifically Abdullah Ünlü as well. He was our liquid nitrogen supplier. Through his and his colleagues' efforts, we can reach to liquid nitrogen easily and abundantly to perform our animal experiments including I would like to acknowledge to my family. They deserve the biggest thanks at all. My mother Mihriban and my father Ünal dedicated their life only for my happiness and success. My brother Tanay also deserves most of the thanks for two reasons. First of them is that he guides me and encourage me to choose the department of Genetics. He all the time supported and helped me during my school education. Secondly, he and his beautiful wife Buket gave me the most beautiful meanings of life, Alp my nephew. Whenever I felt stressful, I all time spend time with Alp to become comfortable. After his birth, he became my little psychiatrist by supplying extra joy to my life.

I would like to dedicate my thesis to my grandfather. After her lost, I felt that I lost one of my best friends forever. His emptiness stayed and never be filled with any other emotion. His strong personality and mercy and as well as respective character always enlighten my way in this complicated life. I knew that he always watching me and wishing the best for me from the upper places. I always love him and try to become a successful and praiseworthy grandchild for him by discovering a cure against neurodegenerative disorders.

I would like to give my special gratitude to The Scientific and Technological Research Council of Turkey (TÜBİTAK) 1001 grant with 214S236 project number that provides scholarship support due to working on dietary regime of project's

animals, helping brain dissection of those animals, following the weight-height measurement of the sacrificed animals during the dissection, assisting the snap freezing of collected tissue samples in liquid nitrogen, learning and also using Tol2 transposon system to establish stable transgenic of mTOR fish lines which include the following four lines S2035T (Serine to Threonine), W2027F (Tryptophan to Phenylalanine) and W2027F (Tryptophan to Phenylalanine), S2035T (Serine to Threonine). After transgenic fish lines are generated, these animals would be used to study the effects of dietary regime on aging as a dimorphic manner. The process of generating transgenic zebrafish using Tol2 system would be explained in the conclusions and future aspects chapter.

## TABLE OF CONTENTS

<b>ABSTRACT .....</b>	<b>ii</b>
<b>ACKNOWLEDGEMENTS.....</b>	<b>ix</b>
<b>TABLE OF CONTENTS.....</b>	<b>xviii</b>
<b>LIST OF FIGURES .....</b>	<b>xxiii</b>
<b>LIST OF TABLES .....</b>	<b>xxvii</b>
<b>CHAPTER 1 .....</b>	<b>1</b>
<b>INTRODUCTION.....</b>	<b>1</b>
1.1. Movement Disorders.....	1
1.2. Cerebellar Ataxia .....	2
1.2.1. Cerebellar Ataxia Disorders.....	3
1.2.1.1. Behavioral Phenotypes of Patients with Cerebellar Ataxia .....	4
1.2.1.2. Alterations in Brain Structures in Patients with Cerebellar Ataxia.....	6
1.2.1.3. Relationships of Genes with Disease Phenotypes.....	11
1.2.1.3.1. Anoctamin 10 (ANO10).....	11
1.2.1.3.2. WD Repeat Containing 81 (WDR81) .....	15
1.2.1.3.3. Very-Low Density Lipoprotein (VLDLR).....	20
1.3. Zebrafish as a Model Organism.....	24
1.4. Morpholino Antisense Oligonucleotide Knockdown Technique.....	28
1.5. The Aims of the Study .....	32
<b>CHAPTER 2 .....</b>	<b>34</b>
<b>MATERIALS AND METHODS .....</b>	<b>34</b>
2.1. Subjects.....	34
2.2. Bioinformatics Tools .....	34
2.3. Acquisition of Adult Tissues.....	36
2.4. Collection of embryos during different developmental time periods for total RNA isolation and Whole Mount <i>In Situ</i> Hybridization (WMISH).....	37
2.5. Total RNA isolations from embryos and adult organ tissues .....	38
2.6. DNase treatment of isolated RNA samples.....	39

2.7. cDNA synthesis from DNase treated RNA samples .....	40
2.8. Quantitative Polymerase Chain Reactions (qPCR) of targeted genes.....	40
2.9. Whole Mount <i>In Situ</i> Hybridization (WMISH) using zebrafish embryos at various developmental and larval time points .....	41
2.9.1. RNA probe design and synthesis for <i>ano10a</i> .....	42
2.9.2. Performance of WMISH protocol and imaging .....	44
2.10. Analysis of the Expression of Cerebellar Ataxia-Related Genes Following the Knockdowns of <i>ano10a</i> , <i>wdr81</i> and <i>vldlr</i> .....	46
2.10.1. Dose Response Curve for Determining the Optimum Dose for the WDR81 Morpholino injections .....	48
2.10.2. Dose Response Curve for Determining the Optimum Dose for the VLDLR Morpholino injections .....	49
2.10.3. Dose Response Curve for Determining the Optimum Dose for the ANO10a Morpholino injections .....	50
2.10.4. Phenotypic measurements with morpholino injected, negative control injected and uninjected control embryos .....	51
2.10.5. Analysis of Cerebellar Ataxia-Related Genes of Interest following ANO10A, WDR81, VLDLR Morpholino Antisense Knockdown in Embryos .....	52
2.11. Statistical Analysis.....	54
<b>CHAPTER 3 .....</b>	<b>56</b>
<b>RESULTS .....</b>	<b>56</b>
3.1. <i>In Silico</i> Bioinformatics Analysis of <i>ano10</i> , <i>wdr81</i> and <i>vldlr</i> .....	56
3.2. Spatiotemporal Gene Expression Analysis Results of <i>ano10a</i> , <i>wdr81</i> and <i>vldlr</i> in Embryo and Adult Tissue Samples .....	60
3.2.1. The Gene Expression Analysis Results of <i>ano10a</i> , <i>wdr81</i> and <i>vldlr</i> in Embryo Samples .....	60
3.2.2. Pattern of Gene Expression Levels of <i>ano10a</i> , <i>wdr81</i> and <i>vldlr</i> in Adult Male and Female Zebrafish Organs .....	65
3.2.3. Spatial Localization of <i>ano10a</i> mRNA in Zebrafish Embryos at Different Developmental Time Periods.....	72
3.3. Clustergram Analysis of Cerebellar Ataxia Associated Genes.....	75
3.4. Morpholino Knock-Down Silencing Studies .....	77
3.4.1. Dose Curve Determination for ANO10a Morpholino.....	77
3.4.2. Quantification of ANO10a, WDR81 and VLDLR Morpholino (MO) Dose Curve Results.....	81

3.4.3. Consequences of Knocking Down with Morpholino Antisense Oligonucleotide One of the Targeted Genes of Interest into Zebrafish Embryos .....	85
3.4.3.2. Phenotypic Measurements of Single ANO10a, WDR81 and VLDLR Morpholino-Injected Embryo Samples .....	86
3.4.3.3. qPCR Gene Expression Analysis of Single Morpholino Injected Knockdown of ANO10a, WDR81 and VLDLR into Embryo Samples to Identify Potential Interacting Targets of the Genes of Interest .....	88
<b>CHAPTER 4 .....</b>	<b>97</b>
<b>DISCUSSION .....</b>	<b>97</b>
4.1. <i>In Silico</i> Analysis Revealed the Interactions of <i>ano10</i> , <i>wdr81</i> and <i>vldlr</i> with Neurodegeneration .....	97
4.2. The Expression Analysis of <i>ano10</i> Explained Its Importance in Developmental Processes and Its Association with Cerebellar Ataxia .....	97
4.3. The Expression Analysis of <i>wdr81</i> Explained Its Importance in Developmental Processes and Its Association with Cerebellar Ataxia .....	100
4.4. The Expression Analysis of <i>vldlr</i> Explained Its Importance in Developmental Processes and Its Association with Cerebellar Ataxia .....	102
4.5. The Clustergram Analysis Showed the Close Interaction among Three Genes of Interest and Highly Correlated 9 Other Cerebellar Ataxia Associated Genes with <i>ano10a</i> , <i>wdr81</i> and <i>vldlr</i> .....	104
4.6. The Regulatory Effects of <i>ano10a</i> Knockdown on the Expression of Cerebellar Ataxia Associated Genes .....	105
4.7. The Regulatory Effect of <i>wdr81</i> Knockdown on the Expression of Cerebellar Ataxia Associated Genes .....	113
4.8. The Regulatory Effects of <i>vldlr</i> Knockdown on the Expression of Cerebellar Ataxia Associated Genes .....	122
4.9. The overall upregulation of all investigated genes when <i>ano10a</i> gene silenced may activate a compensatory response in the biological systems .....	129
<b>CHAPTER 5 .....</b>	<b>132</b>
<b>CONCLUSIONS AND FUTURE PERSPECTIVES .....</b>	<b>132</b>
<b>Bibliography .....</b>	<b>142</b>

#### PERMISSIONS FROM THE REPRODUCED FIGURES OF PUBLISHED STUDIES 183

Figure 1.1. The anatomy of the cerebellum is illustrated. (A) The internal structures of the cerebellum including, cerebellar cortex in grey matter, and fastigial nucleus, globose

nucleus, emboliform nucleus in white matter were shown (Reused by courtesy of Professor Heshmat S.W. Haroun) [16].	183
Figure 1.1. The anatomy of the cerebellum is illustrated.(B)The functional structures of the cerebellum containing cerebrocerebellum, spinocerebellum and vestibulocerebellum were depicted (Reprinted with permission from Sinauer Association) [17].	184
Figure 1.2. Magnetic resonance imaging of patient with ARCA3 is represented. (A) Sagittal T1=weighted sequence is shown. (B) Transverse T1=weighted sequence is indicated (Reprinted with the permission of JAMA Neurology and by the courtesy of Professor Michel Koenig) [30].	185
Figure 1.3. (A) Computerized axial tomography (CAT) scan of CAMRQ1 affected individual with enhanced contrast is shown. (B) The coronal section of the brain is depicted. (C) The sagittal section of brain is illustrated. Reductions in the volumes of the cerebellum and vermis were clearly detected in all images (Reprinted with permission from John Wiley and Sons) [57].	187
Figure 1.4. MRI-based morphological analysis of control and CAMRQ2 affected individuals' brains are shown. (A) The midsagittal MRI images of control and CAMRQ2 affected individuals were illustrated. The highlighted numbers:(1) corpus callosum, (2) third ventricle, (3) fourth ventricle, (4) cerebellum on the right top image indicated brain areas where the volumetric changes became apparent. (B) The lateral and medial schematic representations of cortical regions are depicted. The highlighted numbers, (5) BA45, (6) BA44, (7) BA6, (8) precentral, (9) superior temporal, (10) superior parietal, (11) lateral occipital, (12) fusiform, (13) isthmus cingulated, (14) posterior cingulated, (15) frontal pole, (16) medial orbitofrontal, (17) temporal pole (Reprinted by the courtesy of Professor Tayfun Özçelik) [47].	188
Figure 1.5. The proposed topology and functional transmembrane domains of Anoctamin family member proteins are depicted (Reprinted with the permission from American Society for Pharmacology and Experimental Therapeutics) [77].	190
Figure 1.6. The schematic <i>in silico</i> representation of functional domains within the transmembrane WDR81 protein is depicted (Reprinted by the courtesy of Professor Michelle Adams and with the permission from Springer Nature BMC Neuroscience) [33].	191
Figure 1.7. A schematic representation of Reelin signaling pathway during early development (Reprinted with the permission from Aging and Disease) [123].	194
Figure 1.8. The depiction of orthologous genesamong zebrafish, human, mouse, and chicken genomes. This image was obtained from orthology relationships through Ensemble Campara 63. If a gene has been duplicated in one lineage, it is accepted as one single shared gene in the overlapping region (Reprinted with the permission from Springer Nature) [141].	196
Figure 1.9. Representation of the zebrafish organs. The upper image depicts a dorsal view of brain and nervous system whereas the picture below indicates internal organs. The abbreviations for the structures of the brain and nervous system; OB: Olfactory bulb, Tel: Telencephalon, Ha: Habenula, Ctec: Commissura tecti, TeO: Optic tectum,	

CCe: Corpus cerebelli, EG: Eminentia granularis, CC: Crista cerebellaris, LVB: Facial lobe, MO: Medulla oblongata, MS: Medulla spinalis (Reprinted with the permission from Birkhäuser Verlag) [144], (Reprinted with the permission from Special Issue Biomedical Ultrasound) [145].	197
Figure 1. 10. Lateral view of adult female (F) zebrafish is shown in above and male (M) zebrafish is shown in below. Abbreviations; wt: wild type, L: Left side of the bodies (Adapted from Elsevier) [149].	198
Figure 1.11. An illustration of splice-blocking morpholino (MO) effects. (A) The normal endogenous splicing mechanism is shown. (B) The first possible route of SD MO action is targeting the splice donor site and inhibiting the binding of U1 complex. (C) The second possible route of SA MO action is targeting to the splice acceptor side and inhibiting the binding of U2AF (AF) spliceosomal component thereby following the subsequent recruitment of the U2 complex. In both cases, the lariat formation process does not occur, the splicing event is halted and a new mRNA transcript is not generated. Abbreviations: splice donor site targeting morpholino (SD MO); Splice acceptor site targeting morpholino (SA MO) (Reprinted with the permission from Mary Ann Liebert, Inc) [154].	199
Figure 1.12. The mechanism of action of translation blocking morpholinos. A) The normal endogenous translation mechanism is depicted. B) The translation-inhibiting morpholino targets to the 5'UTR and prevents the scanning of 40S ribosomal subunit, thereby inhibiting the starting and elongation steps of the translation process (Reprinted with the permission from Mary Ann Liebert, Inc) [154].	200
Figure 3.4. Whole mount <i>in situ</i> hybridization (WMISH) was performed with Zebrafish embryos in order to show the localization of <i>wdr81</i> , <i>vldlr</i> , <i>ano10A</i> mRNA transcription certain common nervous system areas. (A) The expression pattern of <i>wdr81</i> in early developmental stages of Zebrafish (Doldur-Ballı <i>et al.</i> , 2015) (Adapted by the courtesy of Professor Michelle Adams and with the permission from the Springer Nature BMC Neuroscience) [33]. Abbreviations, Ce: cerebellum, Di: diencephalon, FB: forebrain region, HB: hindbrain region, Hy: hypothalamus, MB: midbrain region, MLF: medial longitudinal, OV: Optic vesicle, Le: Lens, hpf: hour post fertilization, dpf: day post fertilization [33].	201
Figure 3.4. Whole mount <i>in situ</i> hybridization (WMISH) was performed with Zebrafish embryos in order to show the localization of <i>wdr81</i> , <i>vldlr</i> , <i>ano10A</i> mRNA transcription certain common nervous system areas. (B) The expression pattern of <i>vldlr</i> in early developmental stages of Zebrafish (Imai, <i>et al.</i> , 2012) (Adapted from the Development, Growth&Differentiation) [215]. Abbreviations, Ce: cerebellum, Di: diencephalon, FB: forebrain region, HB: hindbrain region, Hy: hypothalamus, MB: midbrain region, MLF: medial longitudinal, OV: Optic vesicle, Le: Lens, hpf: hour post fertilization, dpf: day post fertilization [215].	204
Figure 5.1. The illustration of Tol2 transposon system. (A) The suitable recombination sites addition through PCR to the gene of interest vector in order to insert it into the pME is depicted. Although it is not shown in this figure, the inserts of p5E and p3E entry vectors are also exposed to similar restriction sites addition PCR amplification to	

make them also proper for the insertion into their specific pDONR plasmids by using BP reactions. (B) The schematic drawing of combination of three entry plasmids within the one expression pDest vector using LR reaction. Abbreviations in the figure stands for pDONR: donor plasmid, attB1-4, attP1-4, attL1-4, attR1-4: recombination specific sequences, p5E: 5' elements containing plasmid, pME: middle entry plasmid, p3E: 3' elements containing plasmid, EGFP: enhanced green fluorescent protein sequence (Adapted from John Wiley and Sons) [339]. ..... 205

## LIST OF FIGURES

FIGURE 1.1. THE ANATOMY OF THE CEREBELLUM IS ILLUSTRATED. (A) THE INTERNAL STRUCTURES OF THE CEREBELLUM INCLUDING, CEREBELLAR CORTEX IN GREY MATTER, AND FASTIGIAL NUCLEUS, GLOBOSE NUCLEUS, EMBOLIFORM NUCLEUS IN WHITE MATTER WERE SHOWN (REUSED BY COURTESY OF PROFESSOR HESHMAT S.W. HAROUN) [16]. (B) THE FUNCTIONAL STRUCTURES OF THE CEREBELLUM CONTAINING CEREBROCEREBELLUM, SPINOCEREBELLUM AND VESTIBULOCEREBELLUM WERE DEPICTED (REPRINTED WITH PERMISSION FROM SINAUER ASSOCIATION) [17]. ....	3
FIGURE 1.2. MAGNETIC RESONANCE IMAGING OF PATIENT WITH ARCA3 IS REPRESENTED. (A) SAGITTAL T1=WEIGHTED SEQUENCE IS SHOWN. (B) TRANSVERSE T1=WEIGHTED SEQUENCE IS INDICATED (REPRINTED WITH THE PERMISSION OF JAMA NEUROLOGY AND BY THE COURTESY OF PROFESSOR MICHEL KOENIG) [30]. ....	7
FIGURE 1.3. (A) COMPUTERIZED AXIAL TOMOGRAPHY (CAT) SCAN OF CAMRQ1 AFFECTED INDIVIDUAL WITH ENHANCED CONTRAST IS SHOWN. (B) THE CORONAL SECTION OF THE BRAIN IS DEPICTED. (C) THE SAGITTAL SECTION OF BRAIN IS ILLUSTRATED. REDUCTIONS IN THE VOLUMES OF THE CEREBELLUM AND VERMIS WERE CLEARLY DETECTED IN ALL IMAGES (REPRINTED WITH PERMISSION FROM JOHN WILEY AND SONS) [57]. ....	8
FIGURE 1.4. MRI-BASED MORPHOLOGICAL ANALYSIS OF CONTROL AND CAMRQ2 AFFECTED INDIVIDUALS' BRAINS ARE SHOWN. (A) THE MIDSAGITTAL MRI IMAGES OF CONTROL AND CAMRQ2 AFFECTED INDIVIDUALS WERE ILLUSTRATED. THE HIGHLIGHTED NUMBERS: (1) CORPUS CALLOSUM, (2) THIRD VENTRICLE, (3) FOURTH VENTRICLE, (4) CEREBELLUM ON THE RIGHT TOP IMAGE INDICATED BRAIN AREAS WHERE THE VOLUMETRIC CHANGES BECAME APPARENT. (B) THE LATERAL AND MEDIAL SCHEMATIC REPRESENTATIONS OF CORTICAL REGIONS ARE DEPICTED. THE HIGHLIGHTED NUMBERS, (5) BA45, (6) BA44, (7) BA6, (8) PRECENTRAL, (9) SUPERIOR TEMPORAL, (10) SUPERIOR PARIETAL, (11) LATERAL OCCIPITAL, (12) FUSIFORM, (13) ISTHMUS CINGULATED, (14) POSTERIOR CINGULATED, (15) FRONTAL POLE, (16) MEDIAL ORBITOFRONTAL, (17) TEMPORAL POLE (REPRINTED BY THE COURTESY OF PROFESSOR DR. TAYFUN ÖZÇELİK) [47]. ....	10
FIGURE 1.5. THE PROPOSED TOPOLOGY AND FUNCTIONAL TRANSMEMBRANE DOMAINS OF ANOCTAMIN FAMILY MEMBER PROTEINS ARE DEPICTED (REPRINTED WITH THE PERMISSION FROM AMERICAN SOCIETY FOR PHARMACOLOGY AND EXPERIMENTAL THERAPEUTICS) [77]. ....	13
FIGURE 1.6. THE SCHEMATIC <i>IN SILICO</i> REPRESENTATION OF FUNCTIONAL DOMAINS WITHIN THE TRANSMEMBRANE WDR81 PROTEIN IS DEPICTED (REPRINTED BY THE COURTESY OF PROFESSOR MICHELLE ADAMS AND WITH THE PERMISSION FROM SPRINGER NATURE BMC NEUROSCIENCE) [33]. ....	17
FIGURE 1.7. A SCHEMATIC REPRESENTATION OF REELIN SIGNALING PATHWAY DURING EARLY DEVELOPMENT (REPRINTED WITH THE PERMISSION FROM AGING AND DISEASE) [123]. ....	21



FIGURE 1.8. THE DEPICTION OF ORTHOLOGOUS GENES AMONG ZEBRAFISH, HUMAN, MOUSE, AND CHICKEN GENOMES. THIS IMAGE WAS OBTAINED FROM ORTHOLOGY RELATIONSHIPS THROUGH ENSEMBLE CAMPARA 63. IF A GENE HAS BEEN DUPLICATED IN ONE LINEAGE, IT IS ACCEPTED AS ONE SINGLE SHARED GENE IN THE OVERLAPPING REGION (REPRINTED WITH THE PERMISSION FROM SPRINGER NATURE) [141].	26
FIGURE 1.9. REPRESENTATION OF THE ZEBRAFISH ORGANS. THE UPPER IMAGE DEPICTS A DORSAL VIEW OF BRAIN AND NERVOUS SYSTEM WHEREAS THE PICTURE BELOW INDICATES INTERNAL ORGANS. THE ABBREVIATIONS FOR THE STRUCTURES OF THE BRAIN AND NERVOUS SYSTEM; OB: OLFACTORY BULB, TEL: TELENCEPHALON, HA: HABENULA, CTEC: COMMISSURA TECTI, TeO: OPTIC TECTUM, CCE: CORPUS CEREBELLI, EG: EMINENTIA GRANULARIS, CC: CRISTA CEREBELLAR IS, LVB: FACIAL LOBE, MO: MEDULLA OBLANGATIS, MS: MEDULLA SPINALIS (REPRINTED WITH THE PERMISSION FROM BIRKHÄ USER VERLAG) [144] , (REPRINTED WITH THE PERMISSION FROM SPECIAL ISSUE BIOMEDICAL ULTRASOUND) [145].	27
FIGURE 1.10. LATERAL VIEW OF ADULT FEMALE (F) IS SHOWN IN ABOVE AND MALE (M) ZEBRAFISHES SHOWN IN BELOW. ABBREVIATIONS; WT: WILD TYPE, L: LEFT SIDE OF THE BODIES (ADAPTED FROM ELSEVIER) [149].	27
FIGURE 1.11. AN ILLUSTRATION OF SPLICE-BLOCKING MORPHOLINO (MO) EFFECTS. (A) THE NORMAL ENDOGENOUS SPLICING MECHANISM IS SHOWN. (B) THE FIRST POSSIBLE ROUTE OF SD MO ACTION IS TARGETING THE SPLICE DONOR SITE AND INHIBITING THE BINDING OF U1 COMPLEX. (C) THE SECOND POSSIBLE ROUTE OF SA MO ACTION IS TARGETING TO THE SPLICE ACCEPTOR SIDE AND INHIBITING THE BINDING OF U2AF (AF) SPLICEOSOMAL COMPONENT THEREBY FOLLOWING THE SUBSEQUENT RECRUITMENT OF THE U2 COMPLEX. IN BOTH CASES, THE LARIANT FORMATION PROCESS DOES NOT OCCUR, THE SPLICING EVENT IS HALTED AND A NEW MRNA TRANSCRIPT IS NOT GENERATED. ABBREVIATIONS: SPLICE DONOR SITE TARGETING MORPHOLINO (SD MO); SPLICE ACCEPTOR SITE TARGETING MORPHOLINO (SA MO) (REPRINTED WITH THE PERMISSION FROM MARY ANN LIEBERT, INC) [154].	30
FIGURE 1.12. THE MECHANISM OF ACTION OF TRANSLATION BLOCKING MORPHOLINOS. A) THE NORMAL ENDOGENOUS TRANSLATION MECHANISM IS DEPICTED. B) THE TRANSLATION-INHIBITING MORPHOLINO TARGETS TO THE 5'UTR AND PREVENTS THE SCANNING OF 40S RIBOSOMAL SUBUNIT, THEREBY INHIBITING THE STARTING AND ELONGATION STEPS OF THE TRANSLATION PROCESS (REPRINTED WITH THE PERMISSION FROM MARY ANN LIEBERT, INC) [154].	31
FIGURE 2.1. THE DEPICTION OF PGEM-T EASY VECTOR AND GENE OF INTEREST LIGATION WAS ILLUSTRATED (ADAPTED FROM PROMEGA) [218].	44
FIGURE 2.2. THE REFERENCE POINTS FOR PHENOTYPE MEASUREMENTS ARE INDICATED BY THE YELLOW MARKINGS. (A) A YELLOW LINE DEPICTED IN THIS 4 DPF REPRESENTATIVE EMBRYO FROM A DORSAL VIEW SHOWS THE REFERENCE MEASUREMENTS FOR DISTANCE BETWEEN EYES (1), FOR THE EYE RADIUS (2), FOR THE HEAD SIZE (3) AND FOR BODY LENGTH (4). (B) THE YELLOW LINE MARKED ON THE LATERAL ILLUSTRATION OF 4 DPF REPRESENTATIVE EMBRYO INDICATES THE REFERENCE MEASUREMENT FOR YOLK SIZE (5). THE STANDARD CONTROL MORPHOLINO INJECTED EMBRYO IS USED IN THIS REPRESENTATIVE IMAGE AND THE PHOTO WAS CAPTURED WITH THE LEICA FLUORESCENCE MICROSCOPE.	53
FIGURE 3.1. STRING PROTEIN-PROTEIN INTERACTION DATABASE (VER.10) RESULTS. (A) THE COMMON INTERACTING PROTEIN UBC WITH THE PROTEIN PRODUCTS OF HUMAN <i>ANO10</i> , <i>WDR81</i> , <i>VLDLR</i> WAS INDICATED. (B) THE PREDICTED INTERACTION NETWORK AMONG THE PROTEIN PRODUCTS OF GENES OF INTEREST AND OTHER CEREBELLAR ATAXIA ASSOCIATED GENES WITH EACH OTHER AND WITH COMMON UBC PROTEIN WAS DEMONSTRATED. THE PURPLE LINES INDICATE	

- EXPERIMENTALLY-DETERMINED PROTEIN-PROTEIN INTERACTION NETWORK BETWEEN TWO PROTEIN PAIRS, THE YELLOW LINE MEANS THAT THE PREDICTED INTERACTION NETWORK WAS BASED ON TEXT MINING AND THE GREEN LINE DEFINES THE INTERACTION NETWORK WAS OBTAINED FROM THE CURATED DATABASES. .... 59
- FIGURE 3.2. (A) THE qPCR EXPRESSION ANALYSIS RESULTS FOR *ANO10A*, *WDR81*, *VLDLR* GENES. ZEBRAFISH EMBRYOS WERE COLLECTED AT 1 HPF, 2 HPF, 5 HPF, 10 HPF, 12 HPF, 18 HPF, 24 HPF, 48 HPF, 72 HPF, 5 DPF, 15 DPF AND 36 DPF TIME POINTS. THE EXPRESSION OF THE TARGETED GENES WAS NORMALIZED WITH HOUSEKEEPING GENE  $\beta$ -*ACTIN*. (B) THE BAR PLOT REPRESENTATION OF RNASeq EXPRESSION DATA FOR *ANO10*, *WDR81* AND *VLDLR* GENES. THE EXPRESSION DATA FROM ZEBRAFISH EMBRYOS THAT WERE COLLECTED AT DIFFERENT DEVELOPMENTAL TIME PERIODS RANGING FROM 2.25 HPF TO 5 DPF WAS OBTAINED THROUGH EXPRESSION ATLAS DATABASE. THE GRAPHS WERE CONSTRUCTED IN MATLAB® PROGRAM LANGUAGE. ABBREVIATIONS, HPF: HOUR POST FERTILIZATION, DPF: DAY POST FERTILIZATION. THE STANDARD ERROR FOR THE qPCR EXPRESSION ANALYSIS IN A PART WAS INDICATED AS + SE. .... 63
- FIGURE 3.3. qPCR EXPRESSION ANALYSIS RESULT OF *ANO10A*, *WDR81* AND *VLDLR* GENES IN ORGANS FROM THE MALE AND FEMALE ZEBRAFISH. ORGANS WERE COLLECTED FROM THREE FEMALES AND THREE ADULT MALES AND THE SAME ORGANS WERE POOLED FOR EACH GENDER. THE RELATIVE EXPRESSION NORMALIZED WITH  $\beta$ -*ACTIN* GENE AS AN INTERNAL CONTROL. THE PANEL GRAPHS AND STATISTICS WERE OBTAINED USING SPSS (IBM, ISTANBUL, TURKEY). IN GRAPHS, THE ORGANS COLLECTED FROM MALE ZEBRAFISH SPECIMENS WERE REPRESENTED VIA BLUE COLOR WHEREAS FEMALE ORGAN TISSUES WERE SHOWN WITH RED COLOR. THE STANDARD ERROR WAS INDICATED AS +SE AND P-VALUE < 0.05 WAS ACCEPTED AS SIGNIFICANCE CUTOFF. .... 68
- FIGURE 3.4. WHOLE MOUNT *IN SITU* HYBRIDIZATION (WMISH) WAS PERFORMED WITH ZEBRAFISH EMBRYOS IN ORDER TO SHOW THE LOCALIZATION OF *WDR81*, *VLDLR* AND *ANO10A* MRNA TRANSCRIPTION CERTAIN COMMON NERVOUS SYSTEM AREAS. (A) THE EXPRESSION PATTERN OF *WDR81* IN EARLY DEVELOPMENTAL STAGES OF ZEBRAFISH (DOLDUR-BALLI *ET AL.*, 2015) (ADAPTED BY THE COURTESY OF PROFESSOR MICHELLE ADAMS AND WITH THE PERMISSION FROM THE SPRINGER NATURE BMC NEUROSCIENCE) [33]. (B) THE EXPRESSION PATTERN OF *VLDLR* IN EARLY DEVELOPMENTAL STAGES OF ZEBRAFISH (IMAI, *ET AL.*, 2012) (ADAPTED FROM THE DEVELOPMENT, GROWTH&DIFFERENTIATION) [215]. (C) THE EXPRESSION PATTERN OF *ANO10A* DURING EARLY DEVELOPMENTAL STAGES OF ZEBRAFISH. ABBREVIATIONS, CE: CEREBELLUM, DI: DIENCEPHALON, FB: FOREBRAIN REGION, HB: HINDBRAIN REGION, HY: HYPOTHALAMUS, MB: MIDBRAIN REGION, MLF: MEDIAL LONGITUDINAL, OV: OPTIC VESICLE, LE: LENS, HPF: HOUR POST FERTILIZATION, DPF: DAY POST FERTILIZATION. .... 74
- FIGURE 3.5. (A) THE CLUSTERGRAM OF ALL CEREBELLAR ATAXIA RELATED GENES IN *DANIO RERIO* DEMONSTRATING THAT THE GENES OF INTEREST, *ANO10A*, *WDR81* AND *VLDLR* ARE CLUSTERED IN THE CLOSE FAMILIES INDICATING THEIR POTENTIAL COMMON ROLES IN THE CONVERGING PATHWAYS. (THE CLUSTER CONTAINING *ANO10A*, *WDR81* AND *VLDLR* ARE SHOWN WITH RED). CORRELATION BASED SIMILARITY MATRIX AND WARD (INNER SQUARED DISTANCE) LINKAGE WAS USED FOR THE CLUSTERGRAM CONSTRUCTION. (B) THE MAGNIFIED PORTION OF THE CLUSTERGRAM FOCUSED ON UPREGULATED CEREBELLAR ATAXIA DISORDER-ASSOCIATED GENES TOGETHER WITH *ANO10A*, *WDR81* AND *VLDLR*. THE RED COLOR CODE REPRESENTS POSITIVE CORRELATION WHEREAS BLUE COLOR CODE DEFINES NEGATIVE CORRELATION AMONG CEREBELLAR ATAXIA DISORDER-ASSOCIATED GENES. THE COEFFICIENTS WITH P-VALUES > 0.05) ARE ILLUSTRATED IN WHITE COLOR. .... 76
- FIGURE 3.6. A 2 % AGAROSE GEL ILLUSTRATING THE PCR PRODUCTS FROM THE MORPHOLINO (MO) INJECTED AND CONTROL GROUPS TO ASSESS THE EFFICACY OF THE THREE DIFFERENT DOSES OF SPLICE-BLOCKING ANO10A ANTISENSE MO. THE FOLLOWING NUMBERS, BETWEEN 1-16, DEFINED LOADED SAMPLES INTO THE WELLS. ABBREVIATIONS: M: DNA GENE RULER MARKER (SM301, THERMO SCIENTIFIC, US), THE NUMBERS DEFINED THE SAMPLES LOADED INTO THAT WELL. THE

LANES 1 AND 9 INCLUDED 24 HPF UNINJECTED EMBRYOS cDNA, LANES 2 AND 10 INCLUDED 24 HPF 2 NG STANDARD NEGATIVE CONTROL MO INJECTED EMBRYOS cDNA, LANES 3 AND 11 INCLUDED 24 HPF 2 NG ANO10A MO INJECTED EMBRYOS cDNA, LANES 4 AND 12 INCLUDED 24 HPF 4 NG STANDARD NEGATIVE CONTROL MO INJECTED EMBRYOS cDNA, LANES 5 AND 13 INCLUDED 24 HPF 4 NG ANO10A MO INJECTED EMBRYOS cDNA, LANES 6 AND 14 INCLUDED 24 HPF 8 NG STANDARD NEGATIVE CONTROL MO INJECTED EMBRYOS cDNA, LANES 7 AND 15 INCLUDED 24 HPF 8 NG ANO10A MO INJECTED EMBRYOS cDNA. THE LANES 8 AND 16 INCLUDED NEGATIVE CONTROLS WITHOUT cDNA TEMPLATES. PCR REACTIONS PRODUCTS IN LANES NUMBERED 1-8 WERE AMPLIFIED WITH *ANO10A* SPECIFIC MORPHOLINO CONTROL PRIMERS WHEREAS THE WELL NUMBERS 9-16 WERE AMPLIFIED WITH  $\beta$ -*ACTIN* SPECIFIC PRIMERS. .... 80

FIGURE 3.7. QUANTIFICATION OF MORPHANT AND WILD TYPE TRANSCRIPTS FROM BAND INTENSITIES OF THREE DIFFERENT DOSES OF ANO10A, WDR81 AND VLDLR MORPHOLINOS (MO) INJECTED AND UNINJECTED 24 HPF EMBRYO SAMPLES. THE BAND INTENSITIES OF UNINJECTED EMBRYOS OF EACH GENE WERE ACCEPTED AS A 100 % OF THE WILD-TYPE TRANSCRIPT. THE RATIO OF MUTANT TRANSCRIPTS WAS DETERMINED BY SUBTRACTING THE BAND INTENSITY OF THE WILD-TYPE TRANSCRIPT WITHIN THE MORPHOLINO-INJECTED EMBRYOS FROM THE BAND INTENSITY OF WILD-TYPE TRANSCRIPT WITHIN THE UNINJECTED EMBRYOS AND THIS VALUE WAS DIVIDED BY THE BAND INTENSITY OF THE WILD-TYPE TRANSCRIPT IN UNINJECTED EMBRYOS AND MULTIPLIED BY 100. THE BAND INTENSITIES IN ORDER TO CALCULATE *ANO10A* MORPHANT RATIO WAS OBTAINED FROM FIGURE 3.6 AGAROSE GEL IMAGE WHEREAS THE *WDR81* AND *VLDLR* MORPHANT RATIOS WERE CALCULATED FROM MEASURED BAND INTENSITIES AGAROSE GELS THAT WERE RUN BY FORMER PhD STUDENT FÜSUN DOLDUR-BALLI. THE BAND INTENSITIES WERE MEASURED THROUGH IMAGE J (NIH, SCIENTIFIC IMAGE ANALYSIS, BEDHESDA, MD, US) AND THESE QUANTIFIED BAND INTENSITIES WERE USED IN ORDER TO CALCULATE AND THEN GRAPH THE MORPHANT VERSUS WILD-TYPE TRANSCRIPTS IN THREE SPECIFIC DOSES OF MORPHOLINOS INJECTED AND UNINJECTED EMBRYOS FOR EACH INDIVIDUAL GENE USING GRAPH PAD PRISM SOFTWARE (GRAPH PAD SOFTWARE, INC., SAN DIEGO, CALIFORNIA, US). .... 84

FIGURE 3.8. THE MEASURED (A) DISTANCE BETWEEN EYES, (B) EYE RADIUS, (C) HEAD SIZE, (D) BODY LENGTH AND (E) YOLK SIZE DATA IN ALL 5 EXPERIMENTAL GROUPS, UNINJECTED CONTROL (BLACK), STANDARD CONTROL MO INJECTED (GREY), 4 NG ANO10A MO INJECTED (RED), 2 NG WDR81 MO INJECTED (BLUE) AND 2 NG VLDLR MO INJECTED (GREEN) ARE DEPICTED AND STATISTICALLY ANALYZED WITH GRAPH PAD PRISM SOFTWARE (GRAPH PAD SOFTWARE, INC., SAN DIEGO CALIFORNIA, US). THE STATISTICAL DATA IS EXPRESSED AS MEAN +SE, ONE-WAY ANOVA INDICATED NO STATISTICAL DIFFERENCES (P-VALUES > 0.05), THE NUMBER OF IN TOTAL 18; IN TOTAL  $n = 18$  EMBRYOS, INCLUDING 3 INDIVIDUALS FOR EACH EXPERIMENTAL GROUP. ABBREVIATIONS: UNINJECTED CONTROL (UNINJECTED), STANDARD CONTROL MORPHOLINO INJECTED (STD MO), ANO10A MO-INJECTED (ANO10A MO), WDR81 MO-INJECTED (WDR81 MO), VLDLR MO-INJECTED (VLDLR MO). .... 87

FIGURE 3.9. THE RELATIVE EXPRESSION FOLD CHANGE OF *WDR81*, *VLDLR*, *ANO10B*, *TTBK2B*, *GRID2*, *WWOX*, *STUB1*, *ATXN1A*, *FMRI*, *ITPR1B* AND *ATXN2* AFTER 24 HOURS POST INJECTION (HPI), 48 HPI, 72 HPI ANO10A MORPHOLINO (MO) KNOCKDOWN. THE  $2^{\Delta(\Delta CT)}$  VALUES WERE USED TO CONSTRUCT THE GRAPHS. THE  $\beta$ -*ACTIN* NORMALIZATION WAS PERFORMED TO CALCULATE  $\Delta CT$  BY SUBTRACTING THE CT OF GENE OF INTEREST FROM THE CT OF  $\beta$ -*ACTIN* AND  $\Delta\Delta CT$  VALUES WERE CALCULATED BY SUBTRACTING THE STANDARD CONTROL EXPRESSION OF EACH SAMPLE OF INTEREST FROM THE  $\Delta CT$  VALUES. MULTIPLE ANALYSIS OF VARIANCE (MANOVA) STATISTICAL TEST FOLLOWED BY PAIRWISE COMPARISON BONFERRONI CORRECTION. .... 94

FIGURE 3.10. THE RELATIVE EXPRESSION FOLD CHANGE OF *ANO10A*, *VLDLR*, *ANO10B*, *TTBK2B*, *GRID2*, *WWOX*, *STUB1*, *ATXN1A*, *FMRI*, *ITPR1B* AND *ATXN2* AFTER 24 HOURS POST INJECTION (HPI), 48 HPI, 72 HPI WDR81 MORPHOLINO (MO) KNOCKDOWN. THE  $2^{\Delta(\Delta CT)}$  VALUES WERE USED TO CONSTRUCT

THE GRAPHS. THE <i>BETA-ACTIN</i> NORMALIZATION WAS PERFORMED TO CALCULATE $\Delta$ CT BY SUBTRACTING THE CT OF GENE OF INTEREST FROM THE CT OF <i>BETA ACTIN</i> AND $\Delta\Delta$ CT VALUES WERE CALCULATED BY SUBTRACTING THE STANDARD CONTROL EXPRESSION OF EACH SAMPLE OF INTEREST FROM THE $\Delta$ CT VALUES. MULTIPLE ANALYSIS OF VARIANCE (MANOVA) STATISTICAL TEST FOLLOWED BY PAIRWISE COMPARISON BONFERRONI CORRECTION. ....	95
FIGURE 3.11. THE RELATIVE EXPRESSION FOLD CHANGE OF <i>WDR81</i> , <i>ANO10A</i> , <i>ANO10B</i> , <i>TTBK2B</i> , <i>GRID2</i> , <i>WWOX</i> , <i>STUB1</i> , <i>ATXN1A</i> , <i>FMRI</i> , <i>ITPR1B</i> AND <i>ATXN2</i> AFTER 24 HOURS POST INJECTION (HPI), 48 HPI, 72 HPI VLDLR MORPHOLINO (MO) KNOCKDOWN. THE $2^{\Delta(\Delta CT)}$ VALUES WERE USED TO CONSTRUCT THE GRAPHS. THE <i>BETA-ACTIN</i> NORMALIZATION WAS PERFORMED TO CALCULATE $\Delta$ CT BY SUBTRACTING THE CT OF GENE OF INTEREST FROM THE CT OF <i>BETA ACTIN</i> AND $\Delta\Delta$ CT VALUES WERE CALCULATED BY SUBTRACTING THE STANDARD CONTROL EXPRESSION OF EACH SAMPLE OF INTEREST FROM THE $\Delta$ CT VALUES. MULTIPLE ANALYSIS OF VARIANCE (MANOVA) STATISTICAL TEST FOLLOWED BY PAIRWISE COMPARISON BONFERRONI CORRECTION. ....	96
FIGURE 5.1. THE ILLUSTRATION OF Tol2 TRANSPOSON SYSTEM. (A) THE SUITABLE RECOMBINATION SITES ADDITION THROUGH PCR TO THE GENE OF INTEREST VECTOR IN ORDER TO INSERT IT INTO THE PME IS DEPICTED. ALTHOUGH IT IS NOT SHOWN IN THIS FIGURE, THE INSERTS OF p5E AND p3E ENTRY VECTORS ARE ALSO EXPOSED TO SIMILAR RESTRICTION SITES ADDITION PCR AMPLIFICATION TO MAKE THEM ALSO PROPER FOR THE INSERTION INTO THEIR SPECIFIC pDONR PLASMIDS BY USING BP REACTIONS. (B) THE SCHEMATIC DRAWING OF COMBINATION OF THREE ENTRY PLASMIDS WITHIN THE ONE EXPRESSION pDEST VECTOR USING LR REACTION. ABBREVIATIONS IN THE FIGURE STANDS FOR pDONR: DONOR PLASMID, ATTB1-4, ATTP1-4, ATTL1-4, ATTR1-4: RECOMBINATION SPECIFIC SEQUENCES, p5E: 5' ELEMENTS CONTAINING PLASMID, PME: MIDDLE ENTRY PLASMID, p3E: 3' ELEMENTS CONTAINING PLASMID, EGFP: ENHANCED GREEN FLUORESCENT PROTEIN SEQUENCE (ADAPTED FROM JOHN WILEY AND SONS) [339]. ....	138

## LIST OF TABLES

TABLE 2.1. QPCR PRIMER PAIRS FOR TARGET GENES, T <sub>m</sub> VALUES, PRIMER SEQUENCE, PRIMER LENGTH AND AMPLICON LENGTH ARE SHOWN. ....	41
TABLE 2.2. PRIMER LIST TO SYNTHESIZE <i>ANO10A</i> RNA PROBE IS PROVIDED. ....	44
TABLE 2.3. THE LIST OF PRIMERS IN ORDER TO TEST THE EFFECTS OF GENE SPECIFIC ANTISENSE MORPHOLINOS. ....	47
TABLE 2.4. THE SPLICE BLOCKING ANTISENSE MORPHOLINO (MO) OLIGONUCLEOTIDES SEQUENCES OF <i>Danio rerio</i> <i>ANO10A</i> , <i>WDR81</i> , <i>VLDLR</i> AND HUMAN BETA GLOBIN. ....	48
TABLE 3.1. MOTIF SCAN DATABASE RESULTS SHOW PREDICTED STATUS OF COMMON MOTIF, CASEIN KINASE 2 PHOSPHORYLATION SITES, IN THE PROTEIN SEQUENCES OF <i>WDR81</i> , <i>VLDLR</i> , AND <i>ANO10A</i> GENES, WHICH MAY INDICATE THEIR POTENTIAL FUNCTIONAL REGULATIONS THROUGH PHOSPHORYLATION. ....	58
TABLE 3.2. P-VALUES OF TIME POINT EXPRESSION DIFFERENCES FOR <i>ANO10A</i> GENE QPCR RESULT. ....	64
TABLE 3.3. P-VALUES OF TIME POINT EXPRESSION DIFFERENCES FOR <i>WDR81</i> GENE QPCR RESULT. ....	64
TABLE 3.4. P-VALUES OF TIME POINT EXPRESSION DIFFERENCES FOR <i>VLDLR</i> GENE QPCR RESULT. ....	65
TABLE 3.5. P-VALUES OF ORGAN TISSUES' EXPRESSION DIFFERENCES FOR <i>ANO10A</i> GENE QPCR RESULT. ....	69
TABLE 3.6. P-VALUES OF ORGAN TISSUES' EXPRESSION DIFFERENCES FOR <i>WDR81</i> GENE QPCR RESULT. ....	69

TABLE 3. 7. P-VALUES OF ORGAN TISSUES' EXPRESSION DIFFERENCES FOR <i>VLDLR</i> GENE QPCR RESULT.	70
TABLE 3. 8. P-VALUES OF MALE AND FEMALE'S ORGAN TISSUES EXPRESSION DIFFERENCES FOR <i>ANO10A</i> GENE QPCR RESULT.	70
TABLE 3. 9. P-VALUES OF MALE AND FEMALE ORGAN TISSUE EXPRESSION DIFFERENCES FOR <i>WDR81</i> GENE QPCR RESULT.	71
TABLE 3. 10. P-VALUES OF MALE AND FEMALE ORGAN TISSUES EXPRESSION DIFFERENCES FOR <i>VLDLR</i> GENE QPCR RESULT.	71
TABLE 3.11. SURVIVAL RATE OF 24 HPF EMBRYOS THAT WERE USED FOR THE DOSE CURVE EXPERIMENTS OF <i>ANO10A</i> ARE GIVEN.	79
TABLE 3.12. SURVIVAL AND MORTALITY RATES OF 24 HPF, 48 HPF, 72 UNINJECTED, ANTISENSE MO AND STANDARD CONTROL MO INJECTED EMBRYOS THAT WERE USED FOR THE ANALYSIS OF KNOCKDOWN STUDIES ARE ILLUSTRATED.	85

# CHAPTER 1

## INTRODUCTION

### 1.1. Movement Disorders

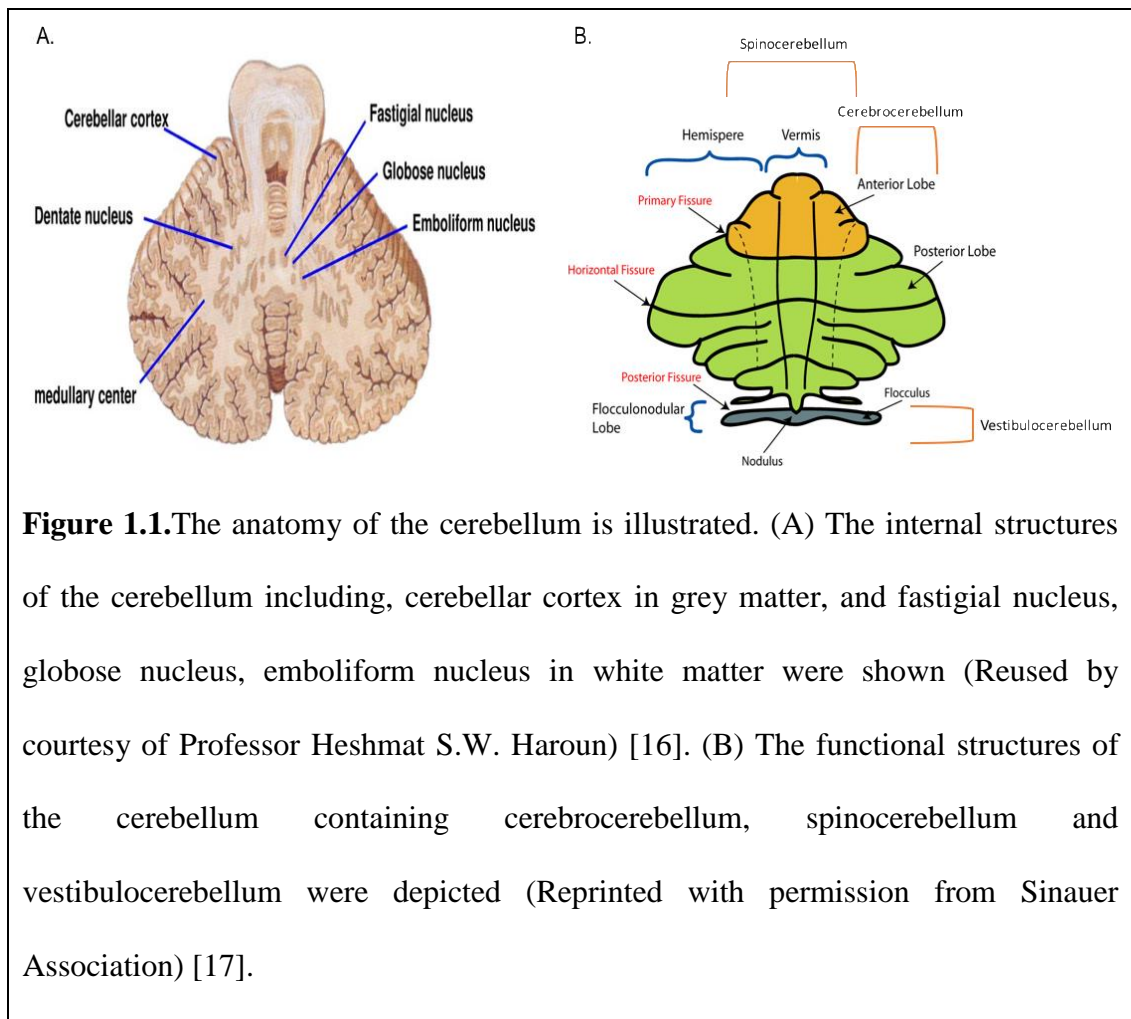
Movement Disorders (MDs) are neurological syndromes characterized by tremors, tics and dystonia that affect normal motility, posture, gaze and muscle tone. Movement-related disorders can result from defects or dysfunctions in the motor cortex, cerebellum, cerebral hemispheres, pyramidal and extrapyramidal systems and brain stem [1]. Approximately 5% of people under 40 years old and 20% of people older than 65 years old suffer from one of more than 40 different types of movement disorders all over the world [2], [3]. Movement disorders are classified under two headings as hypokinetic and hyperkinetic disorders. Hypokinetic movement disorders cause reduction in the rigidity of muscles and voluntary and involuntary muscle movements, as in the case of Parkinson's Disease (PD), Progressive Supranuclear Palsy (PSP), Multiple System Atrophy (MSA), and Cortical Ganglionic Degeneration (CGD) [4]–[7]. In contrast to hypokinetic movement disorders, hyperkinetic movement disorders such as Essential Tremor Syndrome (ETS), Huntington's Disease (HD) and Dystonia, are associated with increases in both the voluntary and involuntary muscle movements [8]–[14]. However, certain movement disorders are characterized as heterogenous which include the properties of both hypokinetic and hyperkinetic types. Ataxias are thought to be one of the most

common examples of this heterogeneous category. In this study, one specific type of ataxias known as Cerebellar Ataxia was examined.

## **1.2. Cerebellar Ataxia**

The cerebellum is a critical nervous system structure that plays a key role in performing motor movements [15] and its anatomy is depicted in Figure 1.1 [16], [17]. In terms of the anatomy of its structure, this indispensable brain region contains two hemispheres and a vermis area that connects these hemispheres together. As with the rest of the brain, the cerebellum possesses white and grey matter. The tightly folded grey matter of the cerebellum is located on its surface and involved in the cerebellar cortex formation, whereas the white matter is found in the core of the cerebellum and consists of dentate, emboliform, globose and fastigial nuclei [18]–[21]. In terms of functional structure, the cerebellum contains three compartments called cerebrocerebellum, spinocerebellum and vestibulocerebellum [18]–[21]. Specifically, the cerebrocerebellum plans movements and motor learning and also coordinates muscles and visual cues, including movement actions. Spinocerebellum is the second functional division of cerebellum and is important in the error correction of extremity movements. The third functional division of the cerebellum is the vestibulocerebellum, which is involved in the control of ocular reflexes and balance [18]–[22]. Due to its involvement in the control and regulation of motion and balance, impairments in the functioning of the cerebellum are often associated with the development of movement disorders. Cerebellar ataxia, the main disease of interest in the present study, occurs when the defects or congenital lesions in cerebellum are followed by neurological dysfunction in motor coordination [21],

[23], [24]. This disorder causes incoordination and unsteadiness in normal motility, balance, posture, gait, upper-lower limbs symmetry, and gaze [23], [25], [26]. This study focused on multiple varieties of the cerebellar ataxia movement disorder that will be explained in-depth in the upcoming section.



### 1.2.1. Cerebellar Ataxia Disorders

Autosomal Recessive Cerebellar Ataxias (ARCAs) are rare hereditary neurological disorders. ARCAs affect the normal functioning of central and peripheral nervous systems and sometimes cause malfunctions in other systems and organs. Therefore, they can be classified in the heterogeneous group of neuronal



diseases. There are numerous neurodevelopmental and neurodegenerative types of ARCAs, ranging from Friedreich Ataxia to Joubert Syndrome, as well as subtypes such as ARCA1, ARCA2 and ARCA3 [27]–[30]. This study specifically emphasized the ARCA3 subtype in order to understand the functional consequences of knocking down the causative *ano10* gene.

Cerebellar Ataxia Mental Retardation Disequilibrium Syndrome (CAMRQ) is an autosomal recessive neurodevelopmental disease that may or may not accompany the quadrupedal locomotion trait [31]–[33]. There are four distinct types of CAMRQ disorders (CAMRQ1-CAMRQ4). All these disease types are caused by missense mutations within the causative genes and the mutation results in the development of similar symptoms and phenotypes [33]–[37]. Specifically, the CAMRQ1 and CAMRQ2 subtypes were investigated throughout this study in the context of previously described ARCA3 subtype, and the functional knockdown experiments will be detailed to define the roles of the causative *wdr81* and *vldlr* genes.

#### **1.2.1.1. Behavioral Phenotypes of Patients with Cerebellar Ataxia**

Patients with the *ARCA3* phenotype start to manifest ataxia at an average age of 33 with an age range of 17 to 43 years old. This disease has a slow progression than other types of cerebellar ataxias. Corticospinal tract signs, including spasticity and problems in extensor plantar and diffuse tendon reflexes, are commonly encountered symptoms in this disorder. Patients under examination never exhibit peripheral neuropathy; so, the communication of brain and spinal cord with the rest of the body to coordinate movements seems quite normal. Hypermetric saccades and

gaze-evoked nystagmus were also recorded as oculomotor dysfunctions in some, but not all, patients with ARCA3. Truncating mutations in the causative *ano10* gene move the onset of disease to early juvenile or adolescence periods and also result in mental retardation (or cause cognitive decline if the disease is adult-onset) [30], [38]–[45].

**CAMRQ1** is a neurodevelopmental disorder affecting people at the very early periods of their life. The CAMRQ1 (MIM 224050) phenotype is characterized with quadrupedal locomotion and mental retardation. Consequently, these patients have little-to-no ability to develop their language. Motor development is also delayed in this disorder, which impairs the performance of motility-associated tasks. Therefore, patients with this disorder cannot walk before they are 3 years old, and this walking cannot be performed without the help of others before they are 6 years old [36]. Hypotonia and reduced muscle strength were also reported during the first few years of affected children. Exaggerated deep tendon reflexes, especially in lower limbs, are likewise present in some patients. The height of patients with this disorder is generally short. Although nystagmus never appears as a phenotype, strabismus was observed in some patients. In very rare cases, tremor, seizures and cataracts were detected [41]. Homozygous mutations of *vldlr*, another gene of interest for this study, give rise to the development of these disorder-related behavioral phenotypes [37], [46]–[48].

**CAMRQ2**, another subtype of cerebellar ataxia mental retardation disequilibrium syndrome, shares many of its symptoms with the CAMRQ1 syndrome

but there are some differences between these two subtypes that need to be emphasized. CAMRQ2 is also a congenital neurological disorder affecting people at early developmental time periods. Patients with CAMRQ2 (MIM 610185) also have mental retardation and a tendency to walk quadrupedally [49], [50]. Some patients with CAMRQ2 showed modest thoracic kyphosis, dysmetria and dysdiadochokinesia without any pyramidal tract findings. The heights of patients were generally short, as in the case of CAMRQ1. Although patients can grasp some basic words and convey their needs to other people, their cognitive functioning abilities are dramatically reduced [49], [51]. All these disease-related behavioral phenotypes were caused by a homozygous mutation within *wdr81*, which is the third gene of interest for this study.

#### **1.2.1.2. Alterations in Brain Structures in Patients with Cerebellar Ataxia**

Since all patients with described the mutations exhibit cerebellar signs such as gait ataxia, gaze-evoked nystagmus and mild-tremor in many movement-related disorders, it is important to highlight the differences in cerebellar anatomy, along with other nervous system structures [36], for each disorder of interest, allowing one to distinguish between similar phenotypes.

Magnetic resonance imaging has been used to show that patients with **ARCA3** developed cerebellar atrophy [33]. Cerebellar hypoplasia in ARCA3-affected brains was depicted in Figure 1.2, demonstrating the shrinkage in the size of cerebellums of ARCA3 patients [30]. In some patients, diffuse T2/FLAIR hyperintense and T1 hypointense patterns can be detected in the cerebellar hemispheres, whereas they are characterized with normal supratentorial structures, which corresponds to cerebrum

and diencephalon regions [40]. Other MRI findings indicated global brain atrophy that includes neuron loss in the central nervous system as indicated by neurodegeneration in cerebellum, brain stem and spinal cord was appeared as a result [40], [42], [52]–[56]. In the early onset, some rare congenital (developmental) defects such as dyskinesia in vermis, in cerebellar hemispheres or in some parts of the brain stem are observed [44].

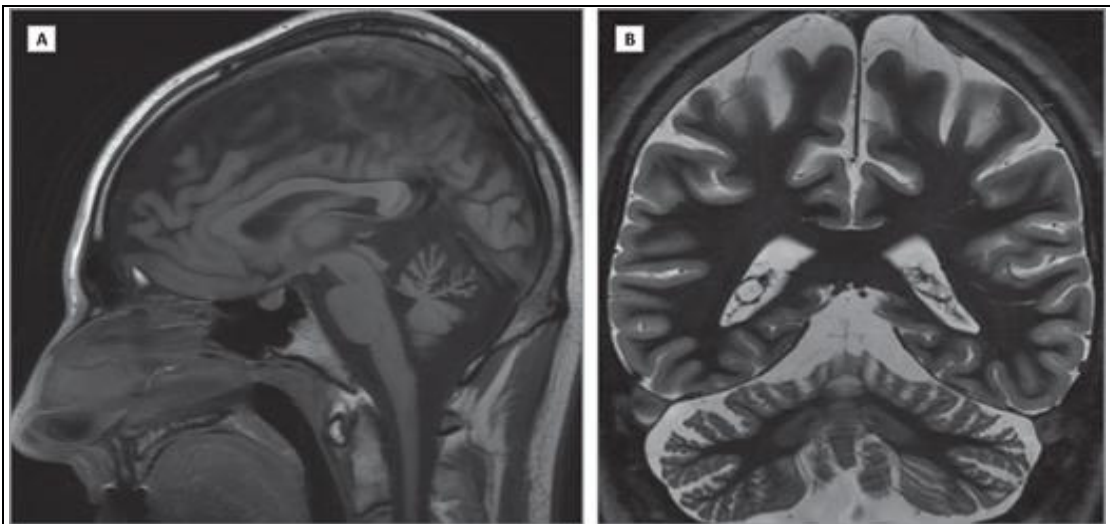
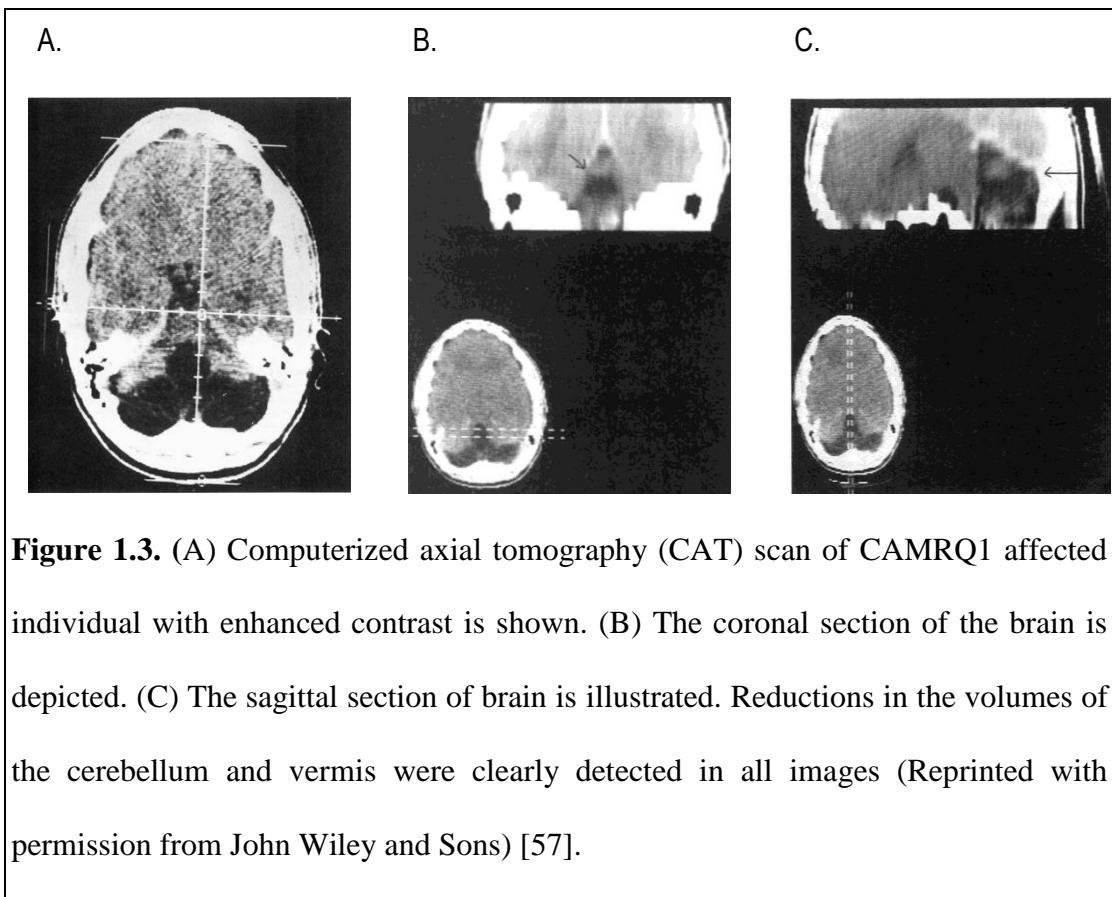


**Figure 1.2.** Magnetic resonance imaging of patient with ARCA3 is represented. (A) Sagittal T1=weighted sequence is shown. (B) Transverse T1=weighted sequence is indicated (Reprinted with the permission of JAMA Neurology and by the courtesy of Professor Michel Koenig) [30].

Cerebellar hypoplasia in the brains of the patients with *CAMRQ1* has been detected through computerized axial tomography technology [36], [57], [58]. Detailed neuroimaging studies also confirm cerebellar hypoplasia in all patients and have determined the affected regions to be the inferior portion of the cerebellum, as described in Figure 1.3 [57]–[60]. In addition, changes in the size of pons and

brainstem have been noted, with a dramatic reduction in the former and a less pronounced reduction in the later [34], [36], [46], [57], [61]–[63]. Although some patients have normal gyration of cerebral hemispheres, others have been recorded with mildly simplified gyration in the cerebral hemispheres with modest cortical thickening [57], [64], [65]. In 2008, Ozcelik *et al.* reported vermial hypoplasia with licencephaly and Turkmen *et al.* described moderate corpus callosum hypoplasia in CAMRQ1 patients, both in addition to the above-described cerebellar hypoplasia phenotype [37], [46].



As it is indicated in the MRI brain images of *CAMRQ2* patients in Figure 1.4, there is cerebellar hypoplasia phenotype that is similar to the CAMRQ1 and ARCA3 syndromes. The atrophy of inferior, middle and superior peduncles of the cerebellum

is also clearly present in this figure. Morphometric abnormalities in the corpus callosum, precentral gyrus, certain Brodman areas and some other cortical regions have likewise been noted in the C and D panels [47]. In addition, CAMRQ2 patients displayed hypogenesis and midline-clefting of the cerebellar vermis. The inferior portion of the cerebellar vermis is also incompletely formed, and the dentate nucleus appears degenerated in the cerebellar hemispheres of these patients. Besides these cerebellar alterations, changes in other nervous system structures have also been observed: The patients demonstrate with brain atrophy and moderate corpus callosum hypoplasia. However, patients showed no indication of dysplasia, grey matter heterotopia and abnormalities in the gyration of cerebral hemispheres [49], [66], [67].

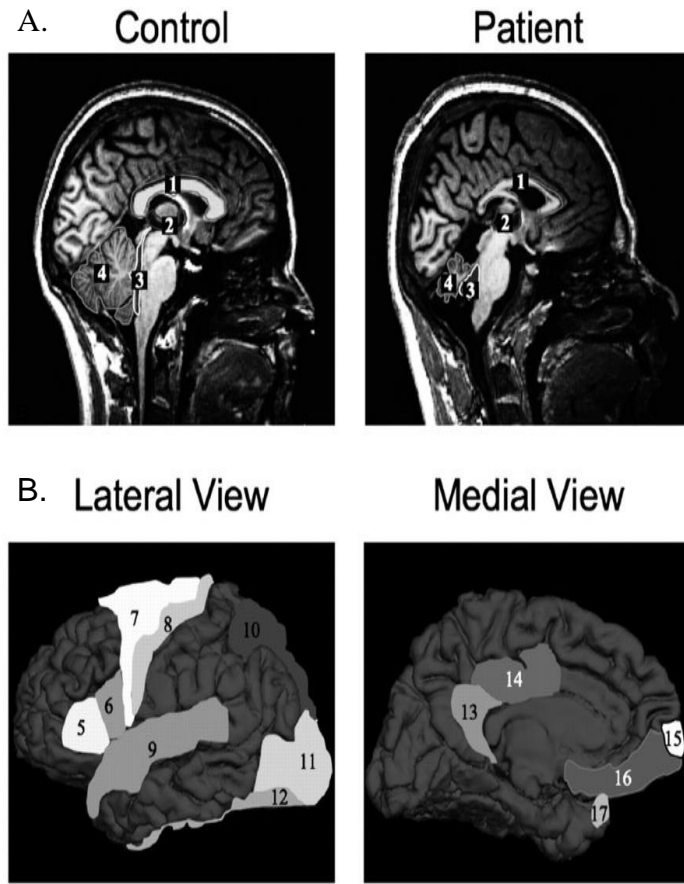


**Figure 1.4.** MRI-based morphological analysis of control and CAMRQ2 affected individuals' brains are shown. (A) The midsagittal MRI images of control and CAMRQ2 affected individuals were illustrated. The highlighted numbers: (1) corpus callosum, (2) third ventricle, (3) fourth ventricle, (4) cerebellum on the right top image indicated brain areas where the volumetric changes became apparent. (B) The lateral and medial schematic representations of cortical regions are depicted. The highlighted numbers, (5) BA45, (6) BA44, (7) BA6, (8) precentral, (9) superior temporal, (10) superior parietal, (11) lateral occipital, (12) fusiform, (13) isthmus cingulated, (14) posterior cingulated, (15) frontal pole, (16) medial orbitofrontal, (17) temporal pole (Reprinted by the courtesy of Professor Dr. Tayfun Özçelik) [47].

### 1.2.1.3. Relationships of Genes with Disease Phenotypes

#### 1.2.1.3.1. Anoctamin 10 (ANO10)

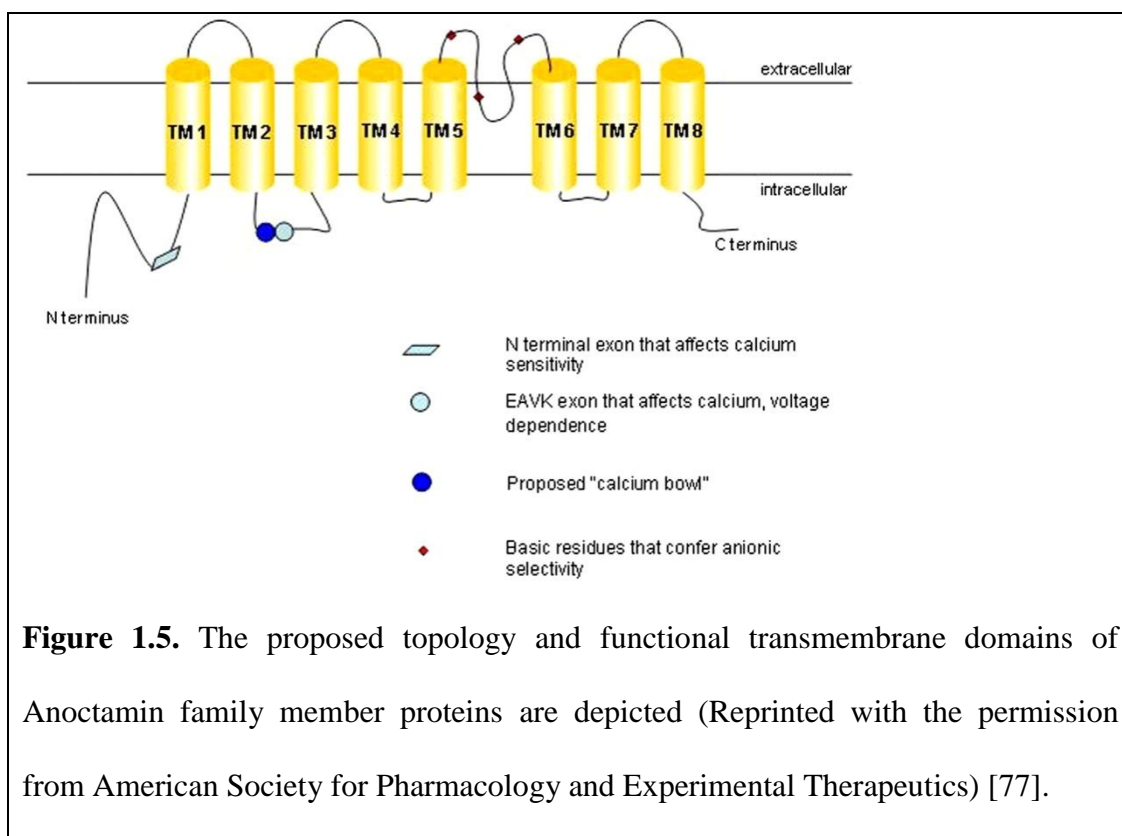
ANO10, Anoctamin 10, consists of 13 exons and belongs to the anoctamin protein family, also called the transmembrane 16 family. It encodes a transmembrane protein that serves as a calcium-activated chloride channel [68], [69]. *ano10* is composed of 8 transmembrane domains and contains cytosolic C- and N-termini. There are 17 different alternative splicing transcript variants for the human *ano10* gene and 14 of them are protein coding transcript variants while the rest do not encode a protein product [70]. Recent studies have suggested potential roles for this gene in certain cellular pathways: Wanitchakool *et al.* 2017 and Schreiber *et al.* 2016, for example, reported that *ano10* controls the intercellular calcium signaling [69], [71], [72] although its function remains unknown.

While the complete function of *ano10* is unknown, the presence of functionally-characterized family members allows for the deduction the roles of this gene in similar pathways. The function of uncharacterized member can also be confirmed by performing certain co-localization and/or co-expression experiments. Therefore, previous studies that detail the roles of the remaining *ano1-9* proteins, as well as the common features of the Anoctamin family in specific pathways, are useful for determining the function of *ano10*. In this context, *ano10* is likely to be involved in the transport of glucose and other sugars [73], bile salts [74]–[76], metal ions [76]–[78], organic acids [79] and amine compounds [78], [80], [81] and phospholipids [82], as well as in ion-channel transport [83], [84].



The structure of the Anoctamin family also provides considerable information about the function of its members. Therefore, the function of *ano10* can also be predicted through examining the general structure of Anoctamin family proteins. The general topology and functional structures of the Anoctamin family proteins are shown via Figure 1.5 [77]. In *ano10*, the first cytosolic loop is placed between transmembrane (TM) portions 2 (TM2) and TM3, and contains small rings of glutamate amino acids that serve to bind  $\text{Ca}^{2+}$ . The BK channel  $\text{Ca}^{2+}$  bowl is found juxtaposed to this  $\text{Ca}^{2+}$  binding domain [85], [86]. Xiao *et al.* 2011 demonstrated that if four glutamate amino acids are mutated to alanine residues in the  $\text{Ca}^{2+}$  bowl, then the overall  $\text{Ca}^{2+}$  sensitivity of the ion channel is mildly diminished [87]. This study also showed that the removal of the four, (EAVK) amino acid residues close to the  $\text{Ca}^{2+}$  binding domain results in a dramatic decrease in the  $\text{Ca}^{2+}$  sensing ability of the ion channel [87]–[91]. The re-entrant loop between TM5 and TM6 is also important for the function of *ano10*, and acidic substitutions of the basic amino acids in this region change the permeability of the membrane for ions. Specifically, this mutation increases the transport of more  $\text{Na}^+$  ions than  $\text{Cl}^-$  [86]. The TM1, TM4-5 and TM6-7 domains are highly conserved in all Anoctamin family proteins [90]. Among those transmembrane regions, TM1 is the most conserved segment. The consensus [IV]-x(3)-[FY]-G-x(5)-Y-F-x(2)-L motif was obtained through the multiple alignment of TM1 region sequences of all Anoctamin family members [87]. Therefore, TM1 in general and this motif in particular can be accepted as a functionally important domain for all Anoctamin family proteins [90]. TM5 and TM6 domains are rich in hydrophobic amino acids, and these two transmembrane regions are connected by a cytosolic re-entrant loop that contains conserved glutamic acid (E) residues. As

previously mentioned, glutamic acid residues assist in the binding of  $\text{Ca}^{2+}$  ions [75]. Yet another conserved sequence in the Anoctamin family consists of TM6 and TM7 transmembrane domains. The P-x(2)-P motif is found in all Anoctamin TM6s, while alanine (A) amino acid residues are conserved at the cytosolic side of TM7 domains, and proline (P) amino acid residues are likewise present on the extracellular region of TM7 [75].



Expression analyses and the Human Protein Atlas databases have described the expression data for the *ano10* gene under normal conditions [38], [92]. The highest expression of this gene is observed in the brain, especially in the cerebellum and occipital cortex, while relatively lower expressions have been recorded in muscle, retina and heart tissues, and minimal expression is present in the liver and

spleen [38], [92]. Therefore, alterations in this gene would likely have a big effect on nervous system development.

Anoctamin genes are also associated with tumorigenesis. Jun *et al.* reported in 2017 that Anoctamin family genes play important roles in the development of cancers [93]. *ano1* was upregulated in gastrointestinal stromal, breast and head-neck cancers [94]–[98]. *ano6* is involved in the development of breast cancer [99], while *ano7* is overexpressed in prostate cancer [100]. Through *in silico* experiments, *ano9* was shown to be overexpressed in colorectal, breast and lung cancers [101]. Recent biological and clinical research also shows *ano9*'s involvement in the pathogenesis of pancreatic cancer [102]. Another study has found a direct association between *ano10* and cancer [103]; however, the Human Protein Atlas database predicts this gene to be a favorable marker that is associated with endometrial, renal and colorectal cancers.

As discussed in the previous section, *ano10* was first associated with the ARCA3 disease phenotype in 2010, with the description of a homozygous frameshift c.1150-1151del (p.Leu384fs) mutation [43]. The same study also used high-throughput next-generation sequencing and Sanger sequencing to identify two other *ano10* mutations that were associated with ARCA. The first was a homozygous T>G nucleotide change at the position 1529 on the 10<sup>th</sup> exon of *ano10* [43]. This single nucleotide change results in a missense mutation through the substitution of a leucine residue with arginine at codon 510 (p.Leu510Arg) [43]. The second mutation observed in ARCA patients was a compound-heterozygous splice site

(c.1476+1G>T) and a frameshift mutation (c.1604del [p.Leu535X]) [104]. In 2016, a c132dupA duplication in the *ano10* gene was announced as the most common mutation for ARCA3 patients [42]. As shown by these examples, the analytical power provided by high-throughput sequencing technologies and homozygosity map analyses allows the precise identification of ARCA-associated genes and mutations [104], [105]. These developments, in turn, are crucial for the determination of additional cellular pathways to identify the mechanisms behind the development of cerebellar ataxia.

Based on the common properties of calcium-activated chloride channels and characterizations of other Anoctamin genes, it can be suggested that *ano10* plays a potential role in ion transport and calcium signaling and may affect the correct function of the nervous system [38], [69], [103], [106]. Recently, Wanitchakool *et al.* 2017 demonstrated that defects in certain cellular pathways, including calcium signaling and TNF-induced apoptosis, are present in *ano10* gene knockout mouse models [69]. However, further information is required to determine the complete set of functions associated with the absence of *ano10* gene during development, including its role in various cellular pathways and the onset of cerebellar ataxia.

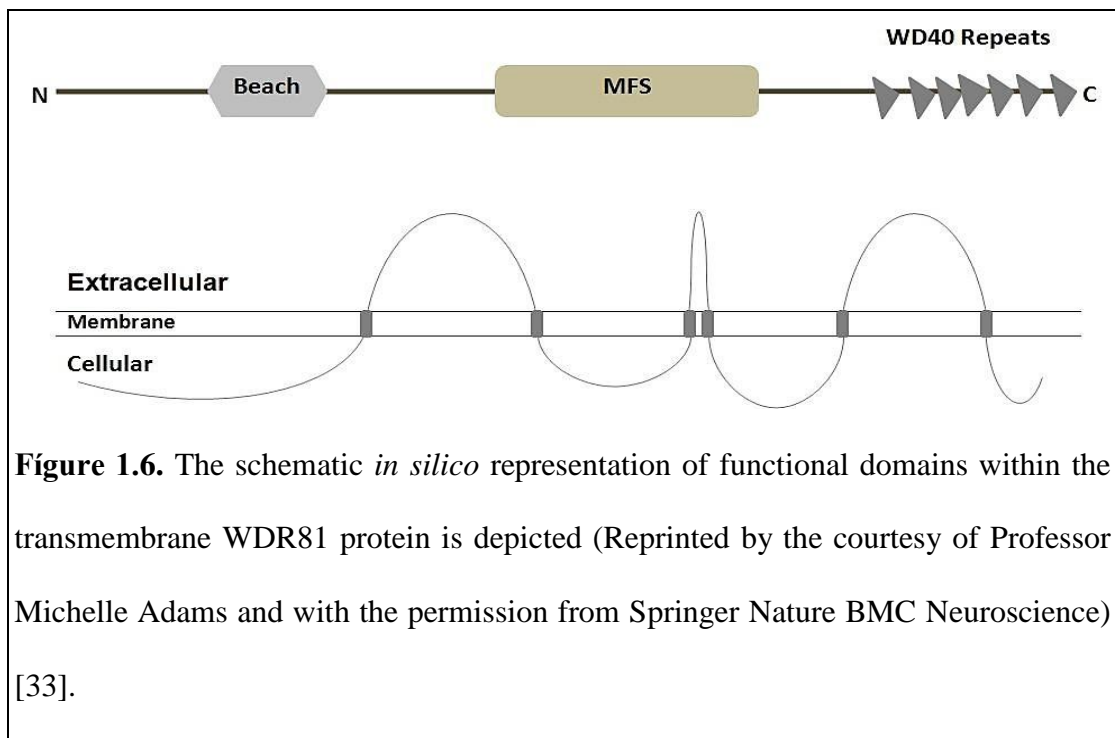
#### **1.2.1.3.2. WD Repeat Containing 81 (WDR81)**

The WDR81, WD repeat domain 81, gene contains 10 to 11 exons and encodes a multi-domain transmembrane protein, WD repeat containing 81 protein. This *wdr81* gene includes 4 alternative splicing transcript variants that encode a protein product as a result [33], [107]–[109]. Published research studies have

indicated the functions of this gene in the late endosomal pathways [110], ubiquitination pathway [111], autophagy pathway [111], Purkinje and photoreceptor cell survival [112].

Although some studies have previously predicted and suggested potential roles for the *wdr81* gene, functional characterization studies have yet to be completed for this gene. Therefore, functional domain analysis of WDR81 protein and its related family members is useful to determine the roles of this protein in cellular events and disease phenotype development. As it was indicated in Figure 1.6, there are 3 major domains within WDR81 protein that are known as the tryptophan-aspartic acid (WD) dipeptide repeat containing domain, Beige and Chediak-Higashi (BEACH) domain and major facilitator superfamily (MFS) domain. WDR81 contains six tandem copies of a transmembrane WD40 domain at the C terminus of the protein structure. The acronym of WD40 domain stands for a 40 amino acid length repeat that possesses tryptophan-aspartic acid (WD) amino acid residues at the end of each of the 6 copies. WD40 is one of the most common domains that can be countered in plenty of protein structures. It is also accepted as a top interacting motif found in many eukaryotic genomes [113]. WD40 repeat containing domains are mainly found in proteins involved in cell cycle regulation, transcription control, apoptosis, chromatin dynamics, vesicular transportation and assembly of cytoskeletal elements [110], [111], [114]. The second major domain in the *wdr81* protein structure is known as a BEACH domain. This BEACH domain includes protein mediating membrane-associated molecular recognition events such as vesicular trafficking, apoptosis, autophagy and synapse formation. As in the case of the WD40

domain, the BEACH domain serves as an interacting adaptor between signaling molecules. Therefore, both BEACH and WD40 domains give WDR81 the properties of scaffolding proteins that tether cellular signaling proteins to each other or to the DNA fragments [110], [113], [114]. The third important domain found in WDR81 is called as major facilitator superfamily (MFS) domain. This domain is described as one of the largest and variable families of transmembrane proteins placed in the genomes of living organisms including bacteria, archea and eukaryotes. MFS domain-containing proteins assist in transportation of small particles across the plasma membrane in response to chemical and osmotic ion concentration changes [115], [116]. They serve as a symporter, antiporter and uniporter on the cell membrane [110], [115], [116]. In conclusion, these three domains in the protein structure potentially indicate that WDR81 serves as a transmembrane protein that mediates a cascade of events in the certain signaling pathways based on its molecular recognition ability.



This *wdr81* gene is expressed mainly in the brain, especially in the cerebellum and corpus callosum. Its expression has also been detected in the neurons of Purkinje cells, brain stem, deep cerebellar nuclei and photoreceptor cells. Moreover, immunoelectron microscopy analyses revealed that the subcellular localization of *wdr81* protein was detected at the mitochondria of the Purkinje neurons [33], [108], [112]. In addition to published studies, Expression Atlas and Human Protein Atlas databases have demonstrated the expression data for the *wdr81* gene in several human tissues. The highest expression of *wdr81* is detected in the spleen, skin, female and male tissues especially in the ovary and seminal vesicle whereas relatively low expressions have been observed at the brain, muscle, lung and gastrointestinal track, and the relatively lowest expression was recorded in the adipose, kidney and endocrine tissues. There was no expression of *wdr81* at all in the pancreas according to these databases [107].

As described previously, the mutated *wdr81* gene is associated with the CAMRQ2 disease phenotype. The missense mutation p.P856.L was detected in the first exon of *wdr81* in some CAMRQ2 patients [28], [42]. The missense mutation, L1349P, in the *wdr81* gene was carried by *nur5* transgenic mice that were generated using N-ethyl-N-nitrosourea (ENU) mutagenesis. Due to the fact that mutant *nur5* mice line exhibits similar phenotypic and cellular consequences with CAMRQ2 disease containing patients, it is used as an animal model to understand the pathogenic mechanism of *wdr81* mutation in this disorder until a very recent conditional knock out *wdr81* mice line was introduced [112], [117], [118]. In addition to cerebellar ataxia, *wdr81* is also mutated in tumorigenesis. Donnard *et al.*

2014 reported that the expression of *wdr81* increases more than 10% in 23 colorectal cancer cell lines [119].

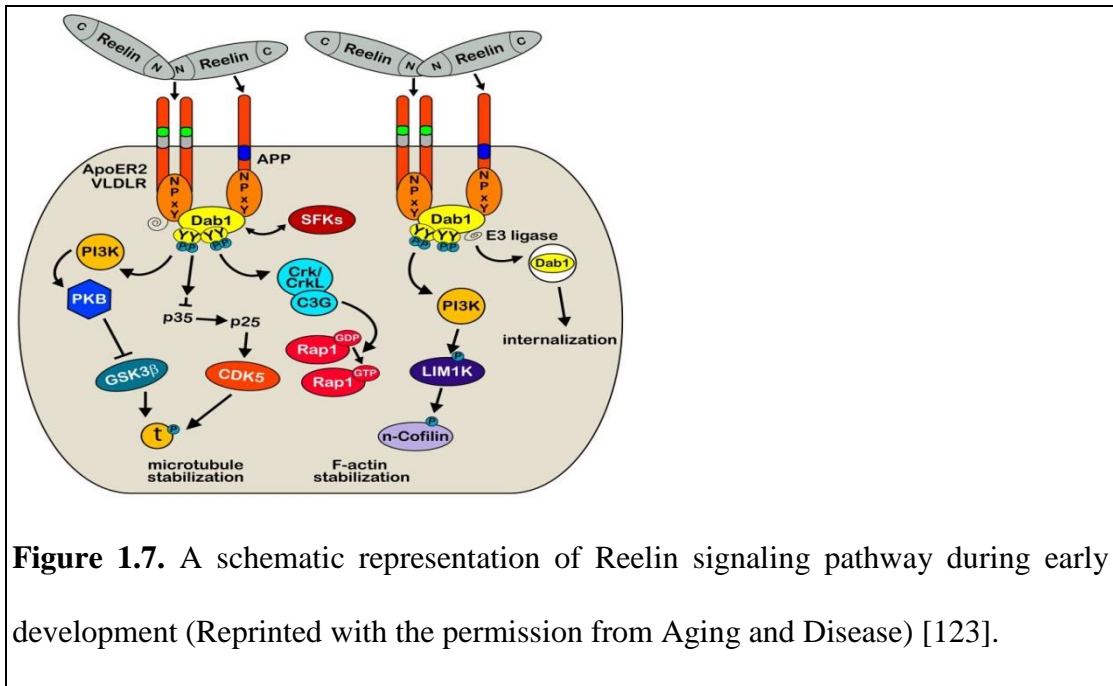
The causative relationship between *wdr81* and CAMRQ2 development still has not been elucidated specifically, although Liu *et al.*'s work has come closer to an explanation for the gene associated pathological mechanism in 2017 [111]. They demonstrated the interaction of *wdr81* with ubiquitin-positive protein foci by using conditional knock out *wdr81<sup>ff</sup>* mice model. When *wdr81* lost this interaction, ubiquitin proteins and the autophagy cargo receptor, p62, started to aggregate in the cortical and striatal neurons. Moreover, the BEACH domain of the *wdr81* recognizes another autophagy cargo receptor, LC3C, which facilitates the enclosure of ubiquitin proteins into autophagosomal vesicles, thereby degrading them and preventing their accumulation within the cytosol [111], [112]. All together these findings reveal that *wdr81* mediates and regulates the correct activity of p62 and LC3C to promote the autophagic degradation of ubiquitin proteins. When this gene is inactivated or mutated; therefore, the interactions among autophagy related proteins and *wdr81* are destroyed, the potential ubiquitin protein accumulation can cause the development of neuronal CAMRQ2 disorder. Although a recently-presented study by Liu *et al.* 2017 suggested logical causation between gene malfunctioning and potential CAMRQ2 development [111], the uncertainties in the function of *wdr81* and in the cascades of events behind the disease necessitate in-depth investigations regarding these issues.



#### 1.2.1.3.3. Very-Low Density Lipoprotein (VLDLR)

VLDLR is a gene that is composed of 19 exons [120] and encodes a membrane-bound receptor protein known as the very low-density lipoprotein receptor [121]. It contains 4 different alternatively-spliced transcript variants and three of them encode proteins, whereas one of them does not produce any protein product. This protein belongs to the low-density lipoprotein receptor family and is an important player of Reelin signaling and VLDL-triglyceride metabolism [120]–[122]. Reelin is the ligand for both the Apolipoprotein E Receptor (ApoER2) and VLDLR, and upon binding to its receptors, activates a downstream tyrosine kinase cascade to regulate cellular events such as microtubule or cytoskeletal element functions in neurons as depicted in Figure 1.7 [123]. The Reelin signaling pathway is involved in the coordination of Purkinje cell alignment in the developing cerebellum and controls neural migration in the developing brain, especially in the cerebral cortex and cerebellum [124]–[127]. This pathway also governs dendrite development and cortical layer formation within the developing hippocampus [128]. The Reelin signaling pathway is not only important for the development of the brain and other nervous system elements, but it also maintains adult synaptic plasticity, as determined by VLDLR knock-down experiments. In particular, the down-regulation of the *vldlr* gene causes reductions in synaptic puncta and glutamate receptor subunits [129]. In addition to its synaptic plasticity- and neural migration-related roles, VLDLR regulates the delivery of VLDL triglyceraldehydes to peripheral tissues [130]. The expression of *vldlr* gene was shown to be important in adipose tissue differentiation as well [131]. Therefore, *vldlr* accomplishes significant functions in the development of nervous system structures, migration of neurons at

the early embryonic stages, differentiation of adipocyte tissues and control of lipoprotein metabolism.



The *vldlr* gene expression is detected in blood vessels specifically localized at endothelial and smooth muscle cells through fluorescent *in situ* hybridization experiments [130], [132]. Moreover, the tissue specific expression analysis of this gene was done by Tacke *et. al.* using reverse transcriptase PCR technique in 2000 [130]. They detected the relatively high expression in heart, skeletal muscle and adipose tissue where active fatty acid metabolism takes place. However, this gene expression was absent in the liver tissue, which is also equally important for fatty acid metabolism [130]. Expression analyses and Human Protein Atlas databases have provided the expression data for the *vldlr* gene as being tissue-specific. The highest expression of this gene is encountered in the endocrine and female tissues especially at the parathyroid gland and ovary, while relatively lower expression has been

observed in the muscle tissue, and more or less, the same relative minimal expression was detected in the brain, liver, kidney, intestine and male tissues [133].

As described in the previous sections, mutations in the VLDLR gene were associated with CAMRQ1 neuronal disorder phenotypes [35]. Boycott *et al.* previously identified a homozygous deletion mutation in this gene in 2005 [62], and then Moheb *et al.* showed a homozygous single nucleotide change c.1342 C>T (p.R448X) in 2008 [48]. Turkmen *et al.* 2008 likewise discovered a homozygous c.2339delT mutation in the *vldlr* gene [37], while Ozcelik *et al.* 2008 found two homozygous mutations, denoted as a c.769C.T (p.R257.X) and a c.2339delT (p.I780TfX3) [46]. The heterozygous mutation c.1561G>C and duplication c.1711\_1712dupT were reported by Boycott *et al.* in 2009 [34]. In 2010, one study showed that a large deletion within the 5' untranslated region (UTR), encompassing exons 1-5, was related with certain phenotypes of CAMRQ1 [134]. In 2012, Ali *et al.* reported the homozygous c.2117G>T mutation in CAMRQ1 patients [35]. Recently, Dixon-Salazar *et al.* 2012 announced a new CAMRQ1 disease-associated homozygous mutation, c.1247\_53delGTTACAA, as a cause of the disease phenotype [63]. All those heterozygous or homozygous mutations in the targeted the *vldlr* gene proved a causative relationship between disease phenotype and gene. The involvement of ApolipoproteinE in the development of sporadic and familial AD suggested lipoprotein-containing receptor, *vldlr* as a potential disease-associated risk factor. In 2011, Okuizumi *et al.* performed multiple logistic regression analysis to confer a relative risk factor of this gene for AD [135]. This result indicated that *vldlr* was a susceptibility gene for potential AD development [135]. Therefore, this gene is

also associated with AD in addition to the focused cerebellar ataxia movement disorder.

Fortunately, the availability of abundant transgenic *vldlr*, *apoer2* and *reelin* mice lines were enabled the elucidation of the cellular functions of the *vldlr* gene in the signaling pathway(s) and/or in molecular events. Although no paper has claimed the exact pathological mechanism behind CAMRQ1 development when the *vldlr* gene is mutated or lost, its cellular function, the disruption of Reelin signaling pathway may be one of the important causes leading to the disease-associated phenotype. There might be two different scenarios in the disrupted Reelin signaling pathway to trigger the cerebellar ataxic-specific phenotypes. The first scenario is that since the Reelin signaling pathway undertakes the coordination of Purkinje cell alignment in the developing cerebellum, the malfunctioning *vldlr* gene interrupts the activation of downstream events and the cerebellum might not develop well enough and result in cerebellar hypoplasia, which is one of the most apparent phenotypes for CAMRQ1. The second way is that this signaling pathway is also responsible for the neuronal migration during the development of nervous system. The defected Reelin signaling again due to a mutation in *vldlr* gene may result in the inactivation of this pathway and then neural migration process cannot take place accurately and there may be hypoplasia not only in the cerebellar area itself but also in the whole brain including the corpus callosum, pons and brain stem, which is observed in patients with CAMRQ1 disease [34], [57]–[63], [136]. These two approaches explain how potential disease associated phenotypes occurs due to a mutant or non-functional *vldlr* gene.

### 1.3.Zebrafish as a Model Organism

While a wide variety of model organisms are used in biological experiments, data derived from the study of invertebrate animals such as worms and flies, as well as single-celled eukaryotes such as yeasts, are not always generalizable to human biology. The zebrafish, *Danio rerio*, is a very important vertebrate model organism and plays a crucial role in covering the deficiencies of non-vertebrate models in fields such as developmental biology, human disorders, aging, metabolism, neurophysiology, ethology and toxicology [137]–[140]. There are many reasons for using the zebrafish for the investigation of various research questions. Firstly, 70% of the protein-encoding human genes are orthologous to zebrafish genes (Figure 1.8) [141]. It is also known that 84% of the disease-causative genes have counterparts in *Danio rerio* [141]. Secondly, the zebrafish is a highly fecund animal that regularly produces hundreds of externally fertilized transparent embryos [141]. These transparent embryos are convenient for the visual monitoring of the onset and course of pathological conditions. Zebrafish models of human disorders provide an understanding of the mechanisms behind pathogenic processes and ultimately assist in the development of novel therapeutic interventions against a broad variety of human diseases [142], [143]. Moreover, reverse genetics approaches are easier to perform on zebrafish compared to mice. The manipulation of the zebrafish genome with either transient or stable genetic systems is not only useful to determine the severity or penetrance of a disease-associated phenotype, but also to reveal the functions of these disease-associated genes [142]. In the context of this thesis, stable transgenic line generation will be introduced in the Conclusions&Future Aspects chapter, while transient morpholino oligonucleotide microinjection technique will be

explained in detail in the following section. Thirdly, zebrafish have an integrated nervous system, including a brain and a spinal cord, and share many other vital organs with humans, such as the heart, kidneys and liver, as depicted in Figure 1.9 [141]–[145]. Zebrafish and mammalian organs can differ in terms of complexity and compartmental divisions. However, the presence of similar organs and the equivalent structures makes them quite useful as model organisms [146]. This issue can be exemplified by examining the structural similarities in the nervous system of *Danio rerio* and mammals. It is notable that the retinal cells, olfactory bulb, cerebellum and spinal cord structures found in the zebrafish nervous system are identical to their mammalian equivalents in terms of morphology and organization. However, the memory-associated hippocampus and emotional response-associated amygdala regions were not detected in the zebrafish brain. Ablation studies of the zebrafish telencephalon suggest that the dorsal part of this brain structure functions as a piscine equivalent of the hippocampus and amygdala [139], [146]. The mammalian visual cortex and corresponding visual areas are also not present in the zebrafish. Instead, the optic tectum region in the diencephalonic area of the zebrafish brain is mainly responsible for the visual processing of color detection, motion and direction. In addition to these basic vision-associated tasks, it is also demonstrated through earlier studies that the tectal nerves within the optic tectum region have the ability to perceive the texture, contrast, size and depth differences of an object [147]. Therefore, it can be concluded that the zebrafish optic tectum contains the V1 and V2 mammalian visual cortex structures. Fourthly, zebrafish lifespan is around 3-5 years, which is approximately 50% more than the other common animal model, which is the mouse [141], [148]. Therefore, zebrafish are more suitable as model organisms

for aging-related studies. Finally, zebrafish show pronounced sexual dimorphism, as shown in Figure 1.10 [149]. Phenotypic differences between genders suggest alternating selective pressure for male and female individuals. This phenotypic sexual dimorphism is generally associated with changes in gene expression patterns between male and female zebrafish. Indeed, microarray and qPCR analysis studies have reported wide-ranging sexually dimorphic gene expression in zebrafish. Therefore, it is important to test scientific hypotheses on both sexes to determine the whole picture for gene expression studies in zebrafish [150], [151]. For all those reasons, the zebrafish is commonly preferred as a promising model organism in a wide-range of scientific research, including the current study.

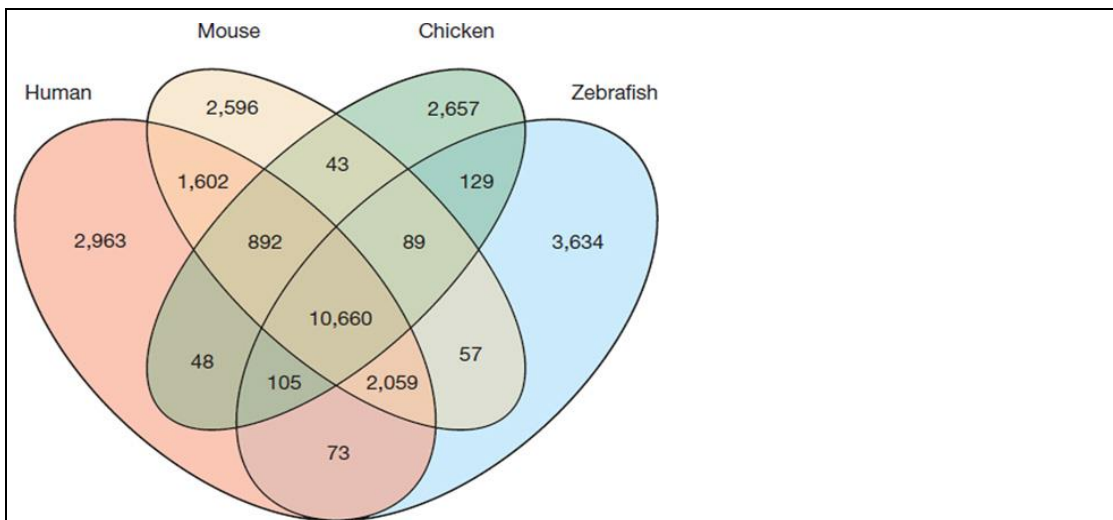
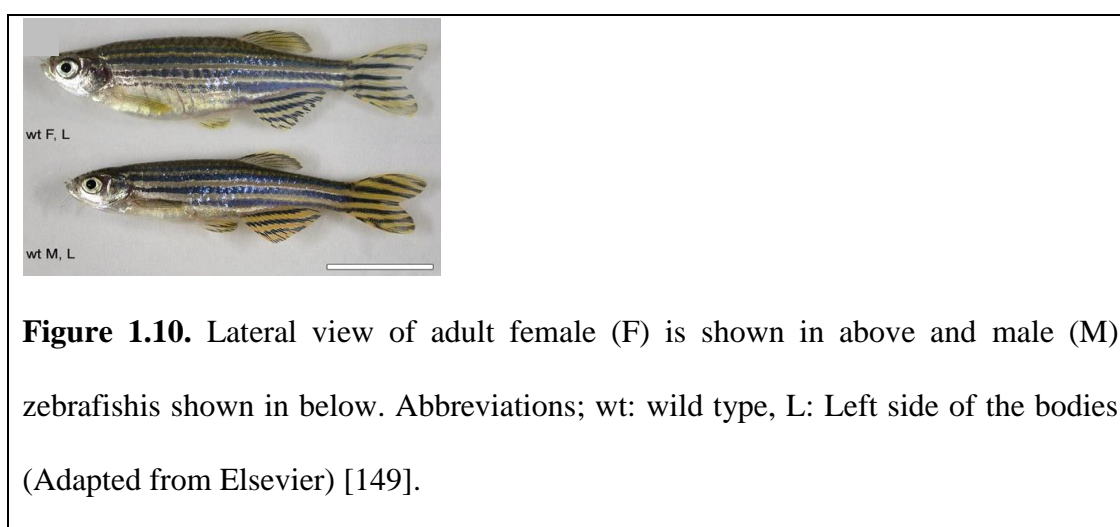
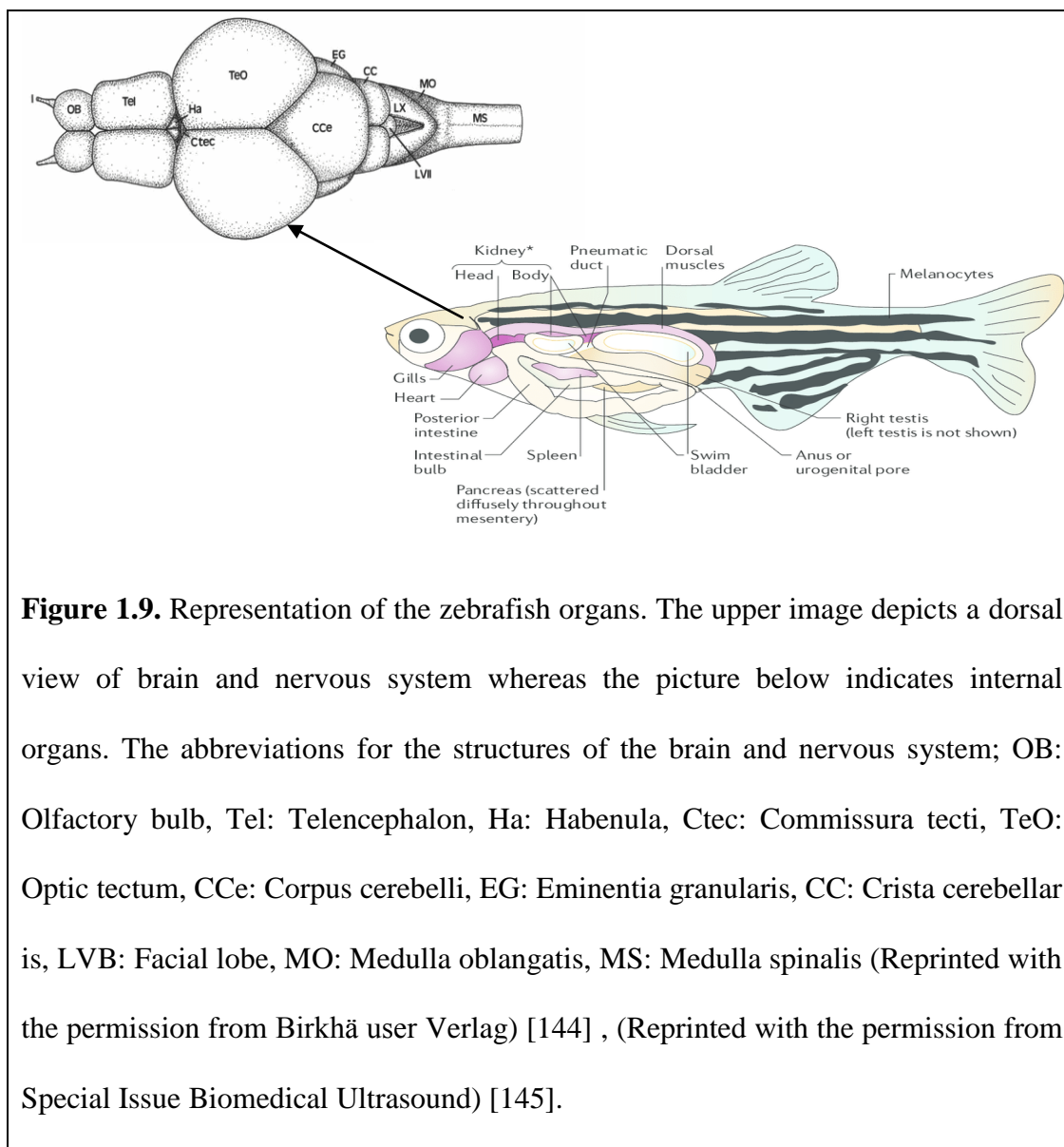


**Figure 1.8.** The depiction of orthologous genes among zebrafish, human, mouse, and chicken genomes. This image was obtained from orthology relationships through Ensemble Campara 63. If a gene has been duplicated in one lineage, it is accepted as one single shared gene in the overlapping region (Reprinted with the permission from Springer Nature) [141].





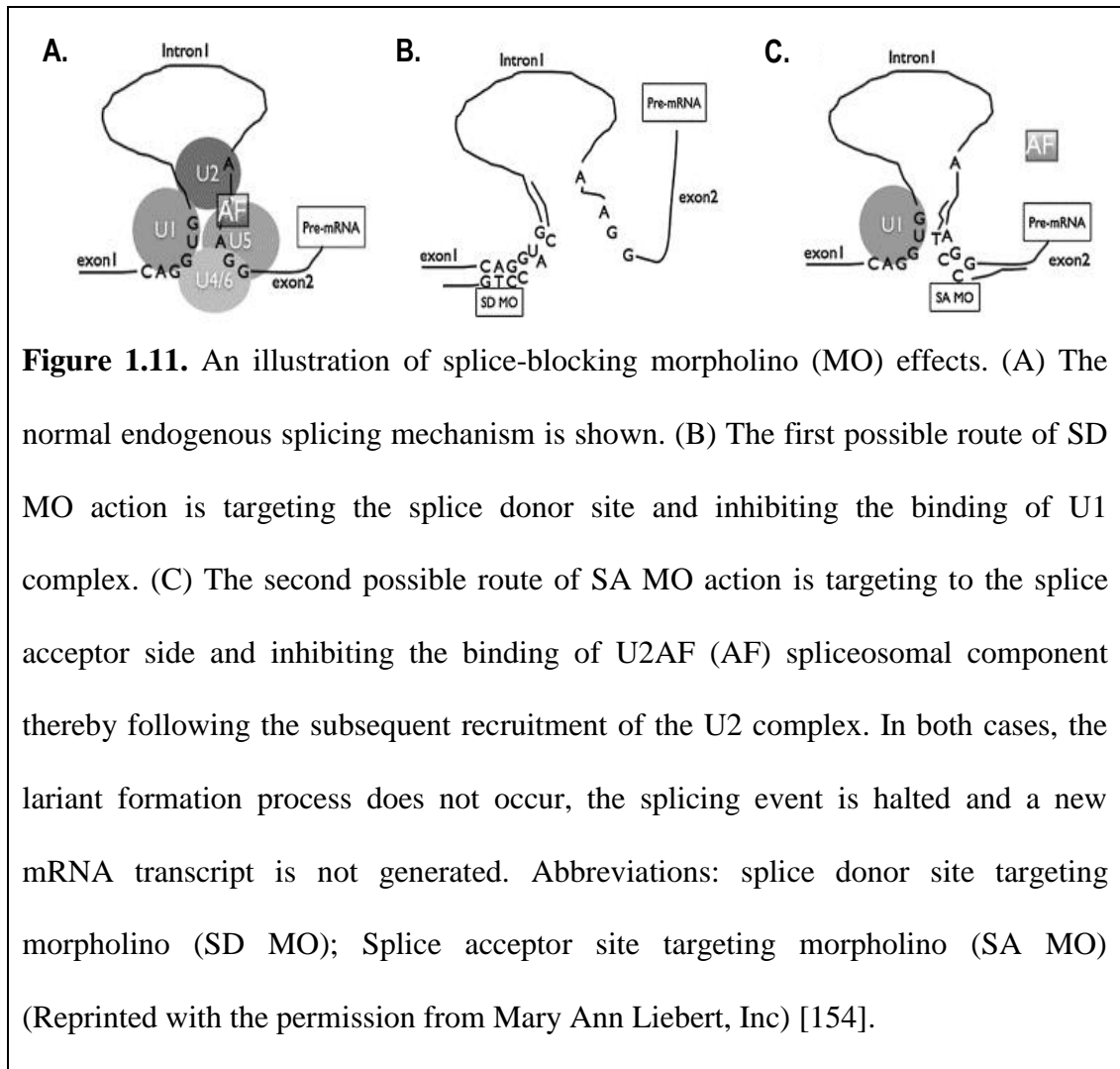
#### **1.4.Morpholino Antisense Oligonucleotide Knockdown Technique**

Though a considerable amount of research articles have drawn attention to the phenotype-driven forward genetics approach, there has been less emphasis on the equally important candidate gene-driven reverse genetics approach [152]. With its easily manipulable genome, the zebrafish is accepted one of the best-adapted models for this potent reverse genetics system that allows for the over-expression, knockdown and misexpression of the gene of interest to search for its cellular function [152]. In the context of current work, morpholino antisense oligonucleotide knockdown technique was applied in order to understand the interaction among the targeted genes. So, morpholino knockdown approach is detailed in the following parts of this section.

Morpholinos are approximately 25 base-pair length synthetic oligos that are commonly used to hamper the expression of targeted genes. Morpholinos consist of a phosphodiamidate backbone connected with a morpholino ring and nucleotide bases. Each nucleotide subunit of the morpholino oligonucleotide is attached to a methylenemorpholine ring, and non-ionic phosphodiamidate bonds link the morpholino rings of two sequential nucleotide bases. The morpholino oligonucleotide structure is strongly resistant to nucleases. Therefore, morpholinos remain stable against enzymatic degradation. The backbone of morpholino oligonucleotides does not contain a negative charge, which prevents their non-specific interaction with other cellular components. Therefore, they mostly bind to targeted sequences and are less likely toxic to the cells as a result. The morpholino

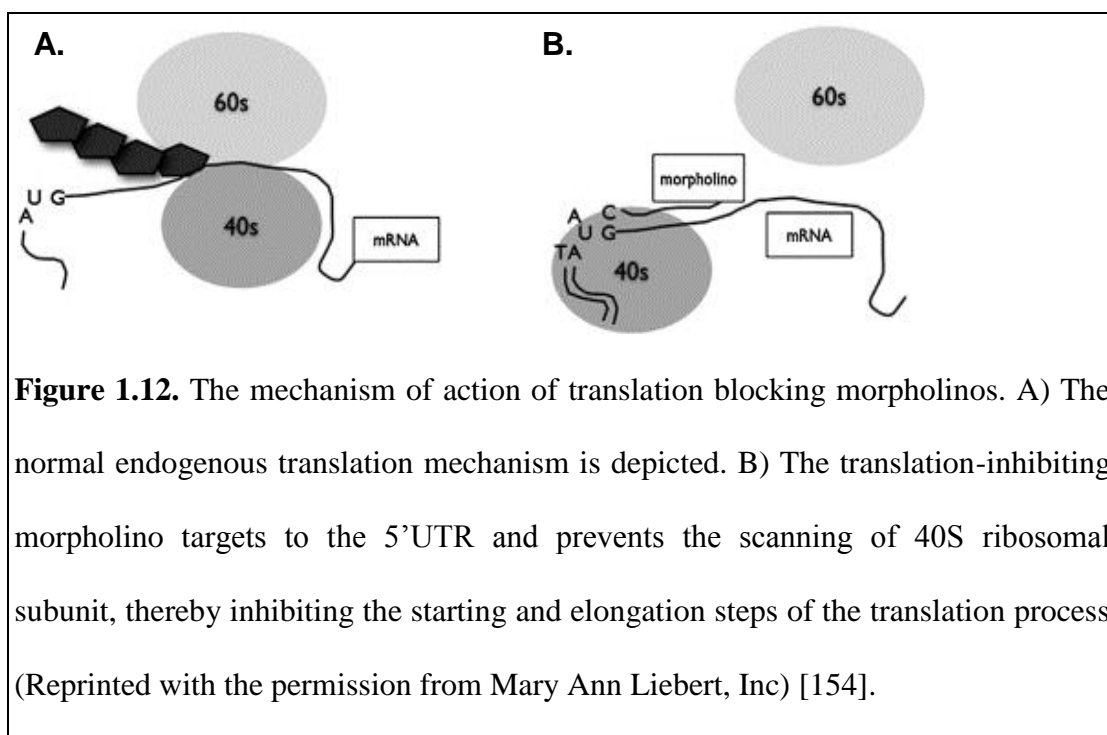
sequence can be designed to block translation, splicing or miRNA and ribozyme activities. However, splice- and translation-blocking morpholino oligonucleotides are the two types that are most commonly used for functional genomics applications in *Danio rerio* [153]–[156].

***Splice-blocking morpholinos*** are utilized to modify and control normal splicing events. These morpholinos affect and suppress pre-mRNA processing by inhibiting the activity of spliceosome components. As depicted in Figure 1.11, there are two distinct morpholino targeting splice sites [154]. Firstly, the morpholino specifically targets the splice donor site and hinders the binding of the U1 complex. Consequently, lariat formation cannot take place and the intron is inserted between two exons instead of splicing out to form the mature mRNA as depicted. This triggers premature stops and the nonsense-mediated decay of the transcript. In the second possibility, the morpholino targets the splice acceptor site and inhibits the binding of U2AF (AF), a core component of spliceosome. Therefore, the U2 spliceosomal RNA complex cannot be recruited and again the lariat formation is disrupted. In both cases, the binding of morpholinos to the targeted sites on the spliceosome components prevents the formation of lariat, thereby resulting in the production of a misspliced transcript. In order to assess the effects of splice-inhibiting morpholino injections on the targeted gene, the modified transcript can be checked using reverse transcriptase polymerase chain reaction (RT-PCR) and the shift can be visualized following gel electrophoresis. Moreover, alterations can be analyzed at the mRNA level through quantitative PCR (qPCR), *in situ* hybridization, microarray or Northern blot experiments [153], [154], [156]–[158].



**Translational-blocking** morpholino antisense oligonucleotides are used to modulate and control normal translation events. These translational blocking morpholinos block the translation initiation complex, which inhibit the protein synthesis. As depicted well in the Figure 1.12, the translational-inhibiting morpholinos specifically interact with the 5'-UTR of the complementary sense strands that is located in proximity to the AUG start site and strangle the scanning of the 40S ribosome [154]. This impedes the initiation and elongation of the translation process by the full ribosomal complex as occurs in the normal endogenous

translation mechanism. In order to detect the knock down of the protein expression using translational-inhibiting morpholinos, Western Blot experiments can be performed if the antibody exists against the targeted protein. If there is no available antibody against the protein of interest, the effect of morpholino on knockdown of translated protein product can be checked through the insertion of a hemagglutinin (HA) or green fluorescent protein (GFP) tag to downstream sequences of the gene of interest in the 5'-UTR. Therefore, the level of knockdown can be controlled by just using antibody against GFP or HA in the performed Immunoblotting experiments. The translation-blocking morpholino does not have the ability to degrade the targeted RNA instead it hampers the biological activity of this RNA until it is degraded with normal cellular events. Therefore, the RT-PCR technique is not a proper technique to control the effect of translation-blocking morpholinos as in the case of splice blocking morpholinos [153], [154], [156]–[158].



When introduced to zebrafish embryos at the 1-4 cell stage of development, the effects of these two types of morpholinos can last up to the 5th day of zygotic development, while the morpholino-specific phenotype starts to manifest within the first three days post fertilization (dpf) [156], [157]. Consequently, the experimental subjects were collected up to the third day of embryonic development, while microscopy imaging for phenotypic monitoring was continued up to 5 dpf in this work.

### **1.5. The Aims of the Study**

While it is possible to study the functional consequences of knocking down of each of these movement-disorder related genes individually, it is not known whether the absence of one gene affect the level of other related genes, and this might have clinical relevance for patients diagnosed with cerebellar ataxia disorders. In this study, the consequences of knocking-down three movement disorder-related genes (*ano10*, *wdr81* and *vldlr*) were determined using the zebrafish (*Danio rerio*) as a model organism. The current study encompassed five main research goals. The first aim of the study was to demonstrate the interactions between these three movement disorder-related genes and their protein products using Bioinformatics analysis. The second aim was to reveal the spatiotemporal mRNA expression level analysis of these movement disorder-related genes in zebrafish embryos and in adult zebrafish organs using qPCR. Thirdly, expression patterns of these three disease-causative genes were compared during early embryogenesis by whole mount *in situ* hybridization (WMISH) experiments to determine whether they were localized at similar nervous system regions of the zebrafish. Fourthly, clustergram analysis was

performed for all cerebellar ataxia-associated genes in order to understand how close the targeted causative genes were to each other, as well as to the other cerebellar ataxia related genes. Lastly, single splice-blocking morpholino microinjections were performed so order to determine the regulatory effects of gene of interests on each other and as well as on the other cerebellar ataxia-associated genes in converging pathways. Ultimately, this study is promising for the development of therapeutic interventions to improve the outcomes of cerebellar ataxia and similar movement disorders.

# CHAPTER 2

## MATERIALS AND METHODS

### 2.1. Subjects

Zebrafish (*Danio rerio*) AB strain were used and embryos were obtained from breeding pairs and grown in E3 medium. Both adult zebrafish and embryos were housed in the zebrafish facility in the Bilkent University Department of Molecular Biology and Genetics, and were maintained at 28° C under a 14 h light:10 h dark cycle. The animal ethics protocols for this study were approved by the Bilkent University Local Animal Ethics Committee (HADYEK). The ethics protocol with the number 2016/05 was approved on January 29, 2016 and with protocol the number 2016/22 was approved on July 15, 2016. Both protocols were used to perform adult animal and embryo experiments within the scope of this study.

### 2.2. Bioinformatics Tools

In order to show the analysis among targeted genes *ano10*, *wdr81* and *vldlr*, the String database (Ver. 10) was used [159]. To perform accurate protein interaction analysis with the String database, the previously published studies were utilized [160]–[164]. Secondly, the specific common domain within the protein products of the interested genes was determined using the Motif Scan database [165]. The Motif Scan bioinformatics tool searches for all known motifs in a given protein sequence. The existence of a particular domain sometimes can be helpful in order to infer the cellular function of a protein. In addition, the detection of common domains within

the different types of proteins that are regulating distinct cellular events can be beneficial to predict the novel functions of these proteins within the converging molecular pathways. Therefore, the common domain(s) were found in the protein products of the studied genes of interests. In order to obtain and interpret Motif Scan results the following articles were read [166]–[168]. Thirdly, the National Center of Biotechnology Information (NCBI) [169], Ensembl (release89) Genome Browser [170] and University of California Santa Cruz (UCSC) [171] databases were utilized to gather genomic information about the genes of interest, their mRNA and protein sequences and the knowledge about NCBI, USCS and Ensembl's resources, applications and updates were acquired through the papers [172]–[181]. Thirdly, in order to design primers for PCR, qPCR and probe synthesis the NCBI primer/Basic Local Alignment Search Tool (BLAST) [180], Primer3 [182] and Universal Probe Library (UPL) [183] online sources were utilized. Therefore, the following articles were taken as a reference for using BLAST [184]–[186], Primers3 [182], [187], [188] and UPL [189] tools in a conventional way and to design primers for different purposes. Fourthly, the EMBL-EBI [190], NCBI-BLAST [180] and Clustal Omega [191] bioinformatics sources gave the alignment results of query and subject sequences. These tools also were used to ensure the direction of inserted genes within the ligated plasmid vectors for determining the suitable restriction enzymes and RNA polymerases to synthesize antisense and sense gene specific probes. Papers with following reference numbers [192]–[199] were carefully read to understand the usage of databases and to interpret the obtained results from these tools. Lastly, the clustergram analysis was performed in order to understand how targeted genes were clustered with other cerebellar ataxia-associated genes. For this reason, the



“Cerebellar Ataxia” term was searched in the NCBI/Gene tool [200]. As a result of this query, the genes having causative association with multiple varieties of cerebellar ataxia disorders were selected. The Ensembl IDs were obtained for the zebrafish orthologous of selected genes through Ensembl database [170], [201] obtained manually. Ensembl IDs were used to gain baseline expression levels during different Zebrafish developmental stages. Therefore, the Expression Atlas [202] tool provided the baseline expression data from RNASeq at distinct zebrafish embryonic periods between early zygote to 5 days post fertilization (dpf) larvae. In order to generate expression data, they have performed experiments with 5 biological replicas including 360 embryos in total for each developmental stage and they calculated the average normalized expression value for each selected gene at the different time points. The downloaded RNASeq expression data was used to draw a graph for visualizing the hierarchical and unsupervised cluster analysis through inbuilt Matlab® (2016b) functions. The graph depiction using Matlab® codes was done by Neuroscience PhD student Ayşe Gökçe Keşküş. To use and grasp the NCBI/Gene [203]–[205] and Expression Atlas tools several articles [162], [206]–[214] were taken as a reference.

### **2.3. Acquisition of Adult Tissues**

In order to perform spatial expression analysis experiments of adult organ tissue samples from 8-10 months old male and female wild-type (AB) were taken. Firstly, the animals were euthanized in the ice including water and then the animals were decapitalized with a sterile surgical scalpel blade and the dissections of the organs were performed. In order to prevent RNA degradation of the collected tissue

samples, the dorsal part of the animals including the brain, eyes and gills, and the remaining body parts of the animals containing the heart, liver, gall bladder, swim bladder, kidney, spleen, fin, tail, gonads, intestine and muscles were dissected by two different individuals separately at the same time. For each animal, the gender was determined by examination of the gonads during the dissections. The collected tissue samples were put into properly labeled 1.5 or 2 ml eppendorf tubes and immediately immersed into liquid nitrogen to quickly and safely snap-freeze the tissues. The collected animal tissue samples were stored at  $-80^{\circ}\text{C}$  until the actual RNA isolation experiments were done. The acquisitions of tissues were done by me and PhD student Ayşe Gökçe Keşküş in a quick manner to prevent RNA degradation.

#### **2.4. Collection of embryos during different developmental time periods for total RNA isolation and Whole Mount *In Situ* Hybridization (WMISH)**

In order to perform temporal expression level analysis, samples were collected at the different developmental time periods including zygotic, larval and juvenile stages. The breeding setups usually were prepared generally prepared using 2 adult AB males and 2 adult AB females in the one individual breeding tank. Male and female animals were put into breeding tanks and isolated into two different parts of the tanks through separators. The separators were opened in the early morning and embryos were collected and they were incubated up until the specific developmental time periods in E3 Zebrafish embryo growing medium at  $28^{\circ}\text{C}$ . Samples from twelve different time periods 1 hour post fertilization (hpf), 2 hpf, 5 hpf, 10 hpf, 12 hpf, 18 hpf, 24 hpf, 48 hpf, 72 hpf, 5 days post fertilization (dpf), 15 dpf and 36 dpf were collected to perform qPCR expression analysis experiments. Approximately 40-

50 embryos were collected from 1 hpf, 2 hpf, 5 hpf, 10 hpf, 12 hpf, 18 hpf, 24 hpf, 48 hpf, 72 hpf, and 5 dpf developmental stages, and 8 larvae and 8 juvenile fish were collected from 15 dpf and 36 dpf time points. All samples were placed into the properly labeled 1.5 ml eppendorf tubes and then snap-frozen by immersing them into liquid nitrogen. After removal of the embryo samples from liquid nitrogen, they were stored at -80 °C until subsequent RNA isolation experiments were performed.

In order to examine the spatiotemporal expression analysis, WMISH experiments were performed for *ano10a* and embryo samples during different developmental stages at 6 hpf, 10 hpf, 24 hpf, 48 hpf, and 72 hpf were collected from a breeding setup of AB wild-type fish. The embryos were grown in an incubator in E3 embryo medium at 28°C and approximately 40-50 embryos for each time interval were put into properly labeled tubes. After fixation in 4% PFA (FB001, Invitrogen IC Fixation Buffer, Invitrogen, US) at 4°C overnight, they were dehydrated by a washing step in a methanol and PBS solution followed by storage in 100 % methanol at -20°C until the actual WMISH experiments were performed. These results were compared to the previously published reports of *wdr81* and *vldlr* [33], [215].

## **2.5. Total RNA isolations from embryos and adult organ tissues**

In order to perform expression analysis of the various zebrafish tissue organs and embryos that were collected at different developmental periods, total RNA isolation was performed. There were 40-50 embryo samples in each tube from 1 hpf, 2 hpf, 5 hpf, 10 hpf, 12 hpf, 18 hpf, 24 hpf, 48 hpf, 72 hpf and 5 dpf time periods, and 8 larvae samples in each tube from 15 dpf and 8 juvenile fish in each sample

tube from 36 dpf. For the adult tissues, 3 individual organs were pooled for each gender. The stored embryos and organ tissues were removed from  $-80^{\circ}\text{C}$  and permitted to come into room temperature in 5 minutes. Then, the RNA extraction protocol using Trizol reagent (15596018, Ambion, US) and ultrasound homogenizer (35019808, dr.hielscher, GmbH, Germany) was performed. The sonicator was adjusted to constant 80% Amplitude for 1 cycle and applied for 10-20 seconds in each run until the lysates becomes completely homogenized. To prevent contamination among samples, the tip of the sonicator was cleaned by washing firstly one time in 70% ethanol and then two times in DEPC (D5758-5ML, Sigma Aldrich, Germany)-treated ddH<sub>2</sub>O before immersed into different sample including tubes. After total RNA isolation protocol was performed, the concentrations of the samples were measured through NanoDrop 2000 Spectrophotometers (ND2000, Thermofisher Scientific, US). RNA concentration of each sample was diluted to 200 ng/μl and stored at  $-80^{\circ}\text{C}$  until subsequent DNase treatment reactions were prepared.

## **2.6. DNase treatment of isolated RNA samples**

Due to the concern of genomic DNA contamination in the isolated total RNA samples, which would result in amplification of the targeted gene specific region not only from the cDNA template but also from the contaminated genomic DNA during the qPCR experiments, DNase treatment was done to eliminate potential DNA contamination. After the total RNA samples were isolated, DNase treatment (AM1907, Turbo DNA free, Ambion, US) was performed. After this step, the DNase-treated RNA samples were removed and put into the  $-80^{\circ}\text{C}$  freezer until the cDNA conversion was performed from these RNA templates.

## 2.7. cDNA synthesis from DNase treated RNA samples

To synthesize cDNA (1708891, iScript cDNA Synthesis Kit, 100 reactions, BIORAD, US), 500 ng of DNase-treated RNA samples were used as a template. The total reaction was completed in a 20 µl volume by adding water, buffer and reverse transcriptase enzyme into RNA template in 200 µl reaction tubes. The reaction was incubated for 5 min at 25<sup>0</sup>C, for 30 minutes at 42<sup>0</sup>C and for 5 min at 85<sup>0</sup>C in a PCR machine with a heated lid (C1000™ Thermal Cycler, Biorad, Herkules, California, US). cDNA samples were kept at -20<sup>0</sup>C until they were used for the subsequent qPCR experiments.

## 2.8. Quantitative Polymerase Chain Reactions (qPCR) of targeted genes

The spatiotemporal expression level analyses of *ano10a*, *wdr81*, *vldlr* were performed using qPCR. The reaction was prepared in white plates (04 729 692 001, LightCycler 480 Multiwell plate, 96, Roche, Germany) by putting 2 µl cDNA, 2 µl of a Forward+Reverse primer mixture, which included 1µM concentration for each primer and all primers used for qPCR are given in Table 2.1, 10 µl SYBR Green 2x concentration Master Mix (04887352001, SYBR Green Master Mix, Roche, Germany), and 6 µl water (04887352001, PCR grade water (Roche, Germany) into each well. The performed qPCR experiments were repeated at least 3 times and the internal control *β-actin* was prepared for each repeat in order to normalize the data. The PCR conditions used for the amplification of gene specific fragments were, 95<sup>0</sup> C for 10 minutes, followed by 45 cycles of 95<sup>0</sup> C for 10 seconds, 60<sup>0</sup> C for 15 seconds, 72<sup>0</sup> C for 10 seconds and 40<sup>0</sup> C for 10 seconds. The Roche LightCycler 480

Systems (LCS 480, Roche, Germany) was benefited in order to perform qPCR experiments. After the PCR run was completed for each prepared reaction, Ct values were calculated through LCS480 software (Roche, Germany) applying AbsQuant/2<sup>nd</sup> derivative Max for Standards and Unknowns analyses [150], [216].

<b>Table 2.1.</b> qPCR primer pairs for target genes, T <sub>m</sub> values, primer sequence, primer length and amplicon length are shown.					
Gene	Primers	Sequence (5'>3')	T <sub>m</sub> (°C)	Primer length (bps)	Amplicon length (bps)
<i>ano10a</i>	Forward	CAGTGATGCGTCTCCGTTCA	60	20	121
	Reverse	CTCTGCTCCTCCATTACGCT	60	20	
<i>wdr81</i>	Forward	GCAGCACATGGCAGAACTC	60	20	89
	Reverse	TACGTGGGGCACTTCCAATC	60	20	
<i>vldlr</i>	Forward	GTGATGGGGACATGGACTGT	60	20	71
	Reverse	CACCTCGGCACAAGTTTTC	60	20	
<i>β-actin</i>	Forward	GCCTGACGGACAGGTCAT	60	18	94
	Reverse	ACCGCAAGATTCCATACCC	60	19	

## 2.9. Whole Mount *In Situ* Hybridization (WMISH) using zebrafish embryos at various developmental and larval time points

In order to examine the expression pattern of *ano10a* using zebrafish embryos at various developmental time periods, WMISH experiments were performed. These experiments not only revealed the spatiotemporal expression of the uncharacterized gene, *ano10a*, but also enabled comparison of the expression pattern of this gene with other cerebellar ataxia-related target genes, *wdr81* and *vldlr*. This permitted the examination of whether or not these genes were localized in similar nervous system regions at the same time or not.

### 2.9.1. RNA probe design and synthesis for *ano10a*

The cDNA coding sequence for ENSDART00000126041.1 mRNA transcript for the zebrafish *ano10a* gene was obtained from the ENSEMBLE genome browser [217]. The primers to amplify the desired region within the gene sequence were designed as previously described in the Bioinformatics Tools section and are given below in Table 2.2. As a template, wild-type (AB) zebrafish brain cDNA samples were used. Therefore, as described previously, two zebrafish brains were dissected. Total RNA isolation from these brains was performed using the RNeasy RNA isolation kit (74104, RNeasy mini kit for 50 preps, QIAGEN, Germany). After their concentration was measured with NanoDrop 2000 (ND2000, Thermofisher Scientific, US), the following DNase treatment (AM1907, Turbo DNA free, Ambion, USA) of these brains was done in order to eliminate potential genomic DNA contamination. Then, the 500 ng DNase-treated RNA samples were used to synthesize cDNA (05081955001, Transcriptor High Fidelity cDNA Synthesis Kit, Roche, Germany). The PCR products for one tube from these brain cDNA templates were prepared by putting 6.75 µl of 2X Phusion Master Mix (M036S, Phusion Master Mix Hot Start Flex, NEB, UK), 1.25 µl primix of 1 µM forward+1µM reverse primers as indicated in Table 2.2, 1 µl cDNA and 3.5 µl PCR grade water (AM9937, Ambion, USA). The desired DNA sequences within *ano10a* were amplified by following the PCR machine conditions that included 30 seconds at 94<sup>0</sup>C, 10 seconds at 94<sup>0</sup>C, 30 seconds at 63.4<sup>0</sup>C, 60 seconds at 72<sup>0</sup>C for 35 cycles, and 10 minutes at 72<sup>0</sup>C. The PCR products were run on a 0.8 % agarose gel for 30 minutes at 120 Voltage (V). In order to perform Thymine and Adenine (TA) cloning, the insert DNA sequence should have polyA tail. Therefore, the extra polyA tail addition step was

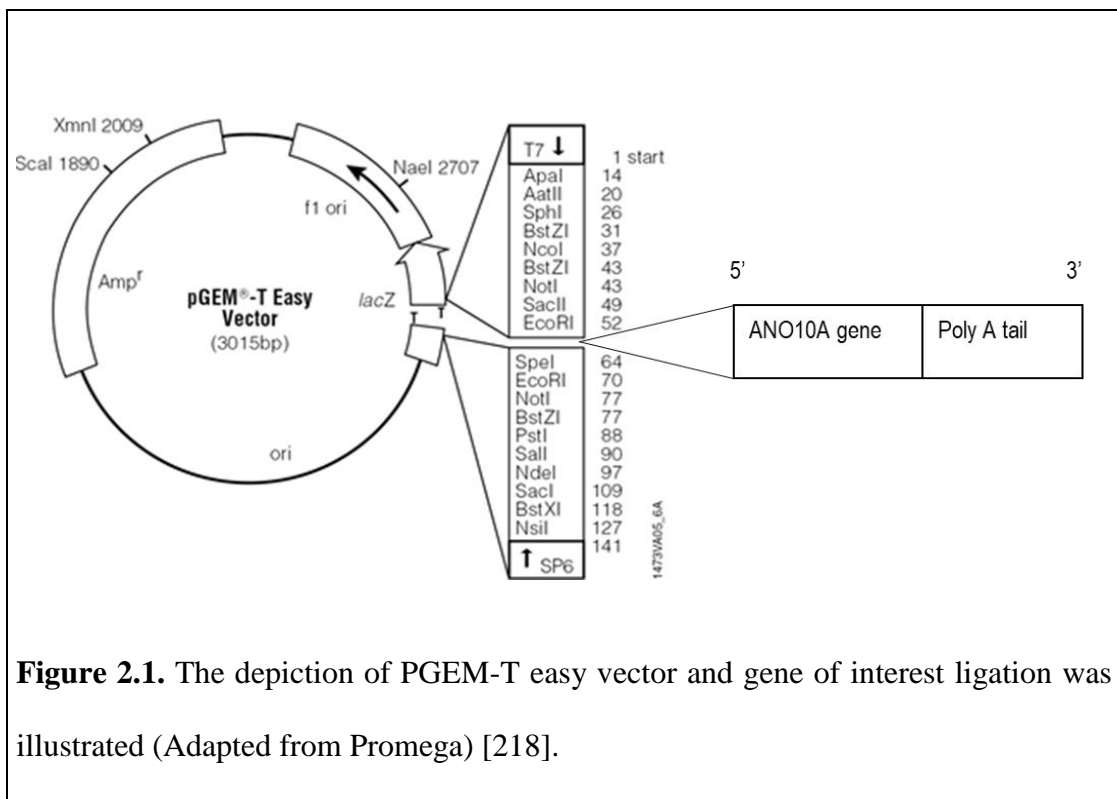
done by incubating PCR products with dATP in the presence of Taq polymerase (M0267S, Taq polymerase, NEB, UK) for 25 minutes at 72<sup>0</sup>C. The polyA tail added PCR products were stored at -20<sup>0</sup>C until proceeding to the next step. After the polyA tail addition, pGEM-T Easy Vector System (A1360, pGEM-T Easy Vector System I, Promega, US) was ligated with an *ano10a* insert sequence as depicted in Figure 2.1. [218]. The ligation product was transformed in bacteria and seeded onto ampicillin antibiotic containing agar plates. After overnight incubation of these plates at 37<sup>0</sup>C, the ampicillin resistant single colonies were grown in the LB medium and plasmid DNA was amplified via midiprep. This plasmid DNA was sequenced in order to understand the direction of the ligated insert. Since the insert was integrated into the vector in the 5'-3' direction manner, i.e. in the plus direction, SalI restriction enzyme (FD0644, Thermo Scientific, US) was used to linearize 1 microgram (µg) circular plasmid DNA for production of the sense probe template and ApaI (ER1411, Thermo Fisher Scientific, US) restriction enzyme was used to linearize 1 microgram (µg) circular plasmid DNA for the production of the antisense probe template. These restriction enzyme-digested linear plasmid DNA samples were run on a 0.8 % agarose gel for 30 minutes at 120V. After checking the correct size of expected band under UV light, gel extraction was performed. The DNA within this extracted gel was purified with a Zymoclean Gel DNA recovery Kit (D4007, Zymoclean Gel DNA Recovery Kit, US). Ultimately, the antisense probe synthesis reaction was catalyzed with SP6 enzyme mix (AM1320, MaxiScript SP6/T7 *In Vitro* Transcription Kit, Ambion, US) and labeled with dioxygenin (DIG) (11277073910, DIG RNA labeling mix, Roche, Germany) to detect during the last step of the WMISH experiments. In order to synthesize a sense probe, T7 enzyme mix (AM1320, MaxiScript SP6/T7 *In*



*Vitro* Transcription Kit, Ambion, US) was used and also labeled with DIG (11277073910, DIG RNA labeling mix, Roche, Germany).

**Table 2.2.** Primer list to synthesize *ano10a* RNA probe is provided.

Gene	Primers	Sequence (5'>3')	Tm (°C)	Primer length (bps)	Amplicon length (bps)
<i>ano10a</i>	Forward	GAGCTGAAGATGTGGGCTTG	63.4	20	736
<i>ano10a</i>	Reverse	TACAGGCACAGCAGAACGAA	63.4	20	736



## 2.9.2. Performance of WMISH protocol and imaging

The collected 6 hours post fertilization (hpf), 10 hpf, 18 hpf, 24 hpf, 48 hpf and 72 hpf wild-type zebrafish embryos were stored in 100% methanol at -20°C as described in the previous section 2.9.1. Collection of embryos during different developmental time periods was done for the WMISH experiments. They were taken

from the refrigerator and the rehydration of these developmentally different embryo samples was performed by washing them in methanol- and PBS-containing medium in a decreasing gradient of methanol. Since the zebrafish embryos' pigmentation starts during the early developmental time periods, a dechoriation step must be performed prior to the WMISH staining experiments in order to prevent background staining [219]. Therefore, bleaching of embryos was performed using a H<sub>2</sub>O<sub>2</sub>- and KOH-containing solution. After the bleaching step, proteinase K (P2308, Proteinase K, Sigma Aldrich, US) digestion was performed in order to eliminate the hybridization of probes with proteins [220]. The post-fixation of experimental samples again in 4% PFA was done. After post-fixation, embryos were incubated in the hybridization buffer in order to prepare samples for hybridization with probes. After this step, embryos were hybridized with *ano10a* gene-specific RNA probes. The samples were washed several times in order to get rid of unspecific probe binding. They were incubated with anti-dioxygenin antibody (11093274910, anti-dioxygenin-AP, Fab fragments, Roche, Germany). In order to visualize the mRNA expression, the color development step was performed. So, BM-purple which is a substrate for alkaline phosphatase was applied to the tissues for this purpose. The probes were labeled with DIG and the antibody to detect DIG-labeled probe reacts with alkaline phosphatase. When BM-purple reacts with alkaline phosphatase, the development of a purple color occurs wherever the mRNA of interest is localized. So, the expression pattern of a specific gene can be revealed as a result of WMISH experiments. In order to capture images of WMISH experiment results, Zeiss Sterio Microscope (Axio Zoom.V16, Zeiss, Oberkochen, Germany) was used.

## **2.10. Analysis of the Expression of Cerebellar Ataxia-Related Genes Following the Knockdowns of *ano10a*, *wdr81* and *vldlr***

Morpholino antisense oligonucleotides are used in studies designed to knockdown the expression of targeted genes and then examine the cellular response to this treatment. Therefore, the unknown roles of the targeted genes within the certain cellular events can be identified by silencing their expression. Morpholino oligonucleotides are usually composed of 25 base pair (bp) nucleotide sequences that include morpholino rings and thymine, adenine, guanine, cytosine nitrogen bases. The morpholino antisense oligonucleotide microinjection is generally applied to zebrafish embryos during early 1-4 cell zygotic stages. There are basically two types of morpholinos that can be constructed. They can be either designed to block translation of the mRNA into protein products or the pre-mRNA splicing process. Due to the absence of counter-reactive antibodies against *wdr81*, *vldlr*, *ano10a* for zebrafish, the translational blocking morpholinos were ideal for performing the current studies. Therefore, the splice-blocking morpholino antisense oligonucleotides were used in this study to knock down the expression of three movement disorder-related genes. There are 5 different consequences of splice-blocking injections into embryos. The morpholino injection may cause cryptic exons, cryptic introns, splicing out of the complete targeted exon, inclusion of complete targeted intron and splicing out of the targeted intron from the transcripts of the genes of interest [153], [154], [157], [221]. The primers designed to confirm the effects of the morpholino injections resulting in the knockdown of the three genes in embryos are provided below in Table 2.3. The antisense splice-blocking morpholino sequences for three genes of interest and negative standard control human *β-globin* morpholino

sequences are provided in Table 2.4. The standard control morpholino injections were done to ensure that the microinjection protocol did not provide any problems to the embryos and also to ensure that all phenotypic and genotypic changes were introduced by the silencing of the specific gene of interest not due to the injection process.

**Table 2.3.** The list of primers in order to test the effects of gene specific antisense morpholinos.

Gene	Primers	Sequence (5'>3')	Tm (°C)	Primer length (bps)	Amplicon length (bps)
<i>ano10a</i>	Forward Exon1	TGGGTGTCTAATGTGCAGGA	61	20	187 or 338
	Reverse Exon3	CCCACATCTTCAGCTCCAAT	61	20	
<i>wdr81</i>	Forward Exon3	CAGAACCAAAGCACAGCAAA	61	21	449 or 572
	Reverse Exon4	CCAAGTTTTCAGACAACCA	61	20	
<i>vldlr</i>	Forward Exon2	CGGTGTATTCCGTCTGTGTG	61	20	455
	Reverse Intron2	CCCGACAAAACATTCCTCC	61	20	
<i>β-actin</i>	Forward Exon45	GCCATCCTTCTTGGGTATGGAA	61	22	367
	Reverse Exon6	AGTCGGCGTGAAGTGGTAAC	61	20	

**Table 2.4.** The splice blocking antisense morpholino (MO) oligonucleotides sequences of *Danio rerio ano10a*, *wdr81*, *vldlr* and *human beta globin*.

Gene	Splice blocking morpholino sequence (5' > 3')
<b>ANO10A MO</b>	AAATGCCACGAGTCCCACCTCCATT
<b>WDR81 MO</b>	CACTTGTTCAAACCTTACCTAATAGT
<b>VLDLR MO</b>	ATGAGAAATTAAGCGACTCACCGCA
<b>β-GLOBIN MO</b>	CCTCTTACCTCAGTTACAATTTATA

#### 2.10.1. Dose Response Curve for Determining the Optimum Dose for the WDR81 Morpholino injections

Experiments to determine the optimum dose for injecting the *wdr81* splice-blocking morpholino were performed by a former PhD student, Dr. Füsün Doldur-Ballı. The details about all procedures can be found in her thesis in section 2.1.5.1. entitled as “*wdr81* Morpholino Dose Curve”. In her thesis, microinjections of three different doses (2 ng, 4 ng, 8 ng) of splice-blocking antisense *wdr81* morpholinos were injected and the survival rates for these injections were calculated. In short, the isolated RNA samples from 24 hpf embryos were converted into cDNA. These cDNA samples were amplified with primers for *wdr81* as shown in Table 2.3 in order to confirm the effects of the morpholino injections on the *wdr81* transcript sequence. Then, the amplified PCR products were run on the agarose gel. In this thesis, quantification of the band intensities of the PCR samples from these dose curve experiments were performed using ImageJ program (NIH, Scientific Image Analysis, Bethesda, MD, US) and this data was used in order to draw a graph comparing morphant vs. wild type transcripts with GraphPad Prism Software

(Graphpad, San Diego California, US). The quantified gel image was obtained from her thesis.

#### **2.10.2. Dose Response Curve for Determining the Optimum Dose for the VLDLR Morpholino injections**

In order to choose the minimum but the most efficient dose for morpholino oligonucleotide injections, 2 ng, 4 ng and 8 ng VLDLR splice-blocking morpholinos were prepared and injected in early zygotic zebrafish embryos, i.e., 1-4 cell stages. Similar doses of the standard control human BETA-GLOBIN ( $\beta$ -GLOBIN) morpholino were also injected as a negative control. There are two reasons to perform the negative control injection. Firstly, these types of injections will confirm that the process did not harm the embryos. Secondly, it confirms that any change in the *vldlr* transcript and embryo phenotype is occurring due to the specific antisense morpholino injections. In addition to splice-blocking and negative control morpholino injections, uninjected embryos were also included in the similar conditions as the splice-blocking and standard control morpholino injected embryos in E3 embryo medium at 28<sup>0</sup>C. These different doses of morpholino and standard control morpholino injected and uninjected embryos were collected at 24 hpf developmental time periods in a properly labeled 1.5 ml eppendorf tubes after the survival rates were recorded. They were snap frozen in the liquid nitrogen and stored at -80<sup>0</sup>C until RNA isolation experiments using Trizol reagent (AM9738, Ambien, US) as described with in the 2.5. Total RNA isolation from embryos and adult tissues section. Then, isolated RNA samples were treated with DNase (AM1907, Turbo DNA free, Ambien, US) and 500 ng DNase treated RNA samples were used as a

template in order to produce cDNA (1708891, iScript cDNA Synthesis Kit, 100 reactions, BIORAD, US). These cDNA samples were used to amplify specific region on *vldlr* transcript reactions through primers as supplied in Table 2.3. The PCR reactions were incubated at 95<sup>0</sup>C for 2 minutes, then 95<sup>0</sup>C for 30 seconds, 61<sup>0</sup>C for 30 seconds, 72<sup>0</sup>C for 40 seconds for 35 cycles and 72<sup>0</sup>C for 5 minutes. Since the control morpholino control reverse primer for *vldlr* caused annealing of intronic sequences, genomic DNA of 3 dpf embryos sample was used as a positive control and amplified in the same PCR conditions. All those samples were run on 1% agarose gel. The intensities of bands were calculated by ImageJ (NIH, Scientific Image Analysis, Bethesda, MD, USA) and they were used to draw a graph that compares morphant vs. wild type *vldlr* transcripts by using GraphPad Software (Graphpad, San Diego California, US). The quantified gel images were obtained from PhD student Füsün Doldur-Ballı.

### **2.10.3. Dose Response Curve for Determining the Optimum Dose for the ANO10a Morpholino injections**

At the 1-4 cell stages, the wild type embryos were injected with 2 ng, 4 ng and 8 ng *ano10a* splice blocking morpholinos and with 2 ng, 4 ng and 8 ng standard human BETA-GLOBIN morpholinos. As a negative non-injected control group, uninjected embryos were grown in the same conditions with the *ano10a* and standard control morpholinos injected embryos in E3 medium at 28<sup>0</sup>C. Embryos were collected at 24 hpf stage and snap frozen in liquid nitrogen and stored at -80<sup>0</sup>C. The total RNA was isolated using Trizol reagent (AM9738, Ambion, US) and treated with DNase (AM1907, Ambion, US). The cDNAs of these RNA samples were

synthesized (1708891, iScript cDNA Synthesis Kit, 100 reactions, BIORAD, US). These cDNA samples were amplified with specific primers as described in Table 2.3 following PCR conditions containing incubation at 98<sup>0</sup>C for 30 seconds, then at 98<sup>0</sup>C for 10 seconds, 64<sup>0</sup>C, at 72<sup>0</sup>C for 60 seconds for 35 cycles and 72<sup>0</sup>C for 10 minutes. The amplified PCR products were run on 2% agarose gel for 1 hour at 100 V. The band intensities of the PCR products were quantified with ImageJ (NIH, Scientific Image Analysis, Bethesda, MD, US) and these data were used to draw a bar plot that compares the wild type vs. morphant transcripts using GraphPad Software.

#### **2.10.4. Phenotypic measurements with morpholino injected, negative control injected and uninjected control embryos**

The morpholino injections for *ano10a*, *wdr81*, *vldlr* were performed during early embryogenesis. The knockdown of their expression may or may not induce changes in the phenotype of morpholino-injected embryo samples. Therefore, phenotypic measurements including the distance between eyes, the eye radius, the head size, body length and the yolk size were recorded for ANO10a, WDR81, VLDLR morpholino-injected and control groups embryo samples. The reference measurement places were marked and labeled with yellow color as indicated in the Figure 2.2. A 2 ng dose was used for the *wdr81* and *vldlr* morpholino injections and 4 ng dose for *ano10a* morpholino injections was applied to embryos. The proper 2 ng and 4 ng standard negative control and uninjected embryos were also included to compare the potential phenotypic changes in the measured parameters. The antisense targeted and standard control morpholinos injected embryos and uninjected control animals were grown in the E3 medium for 4 days. In order to capture images of the

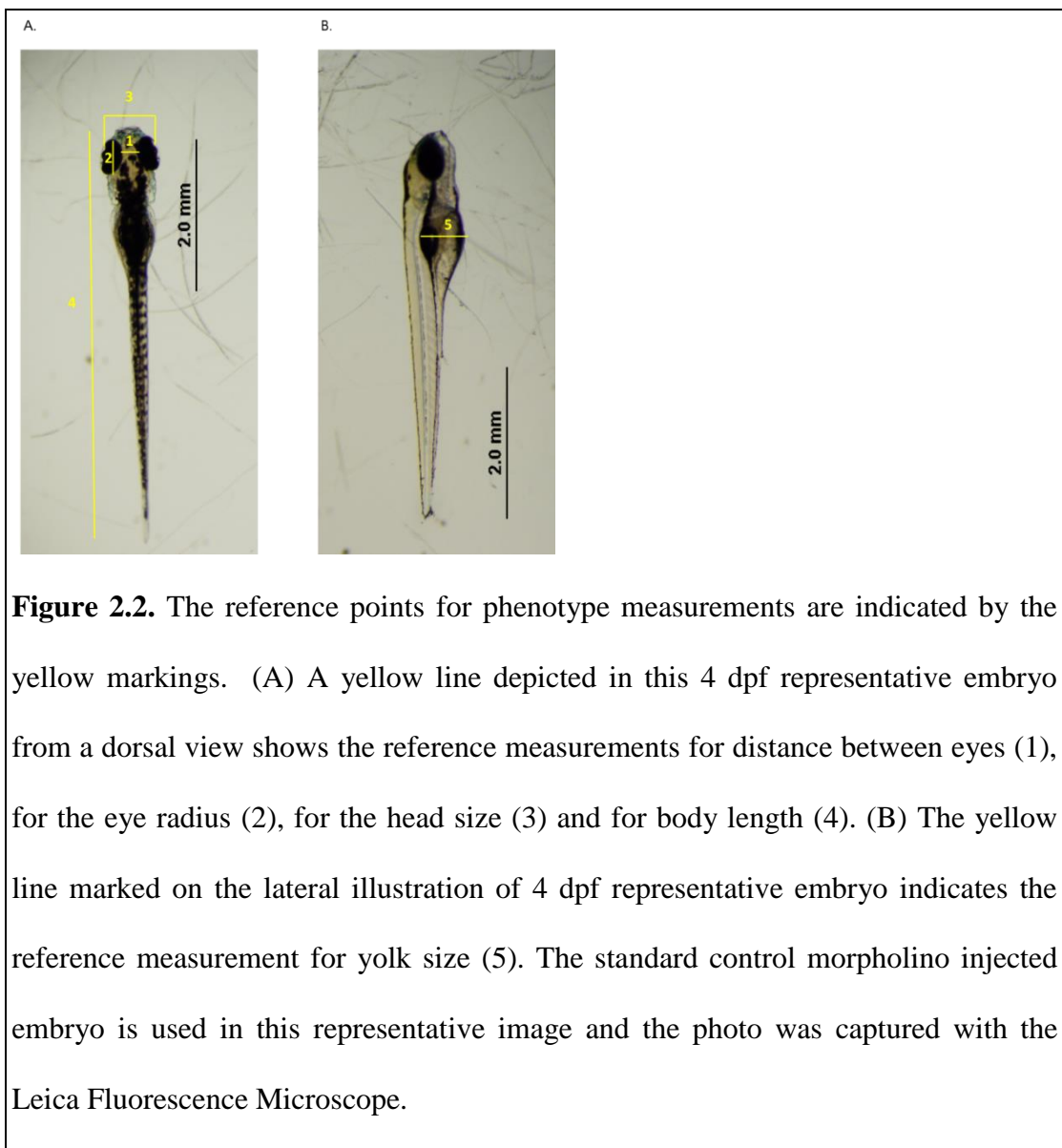


treated and control group embryos, they were put into small well plates that included E3 medium. Then, photos were collected using a fluorescence microscope (MZ10F, Leica Fluorescence Microscope, Leica, Germany) to detect changes in the movement of embryos. The embryos were anesthetized using 4 mg/ml Tricaine (MS222, Sigma-Aldrich, St. Louis, MO, US). The measurements of the phenotypic measurements including the distance between eyes, the eye radius, the head size, body length and the yolk size were performed with the ImageJ (NIH, Scientific Image Analysis, Bethesda, MD, US) quantification program. These measurements were done by a person who was both blind to experimental groups and sample IDs. Therefore, any bias of the phenotypic measurements would be eliminated for the gene of interest antisense morpholino-injected, standard control-injected and uninjected control embryos. These quantifications from the morphometric data were entered in the Graphpad Prism Software (Graphpad, San Diego California, US) in order to determine whether there were significant differences among the groups.

#### **2.10.5. Analysis of Cerebellar Ataxia-Related Genes of Interest following ANO10A, WDR81, VLDLR Morpholino Antisense Knockdown in Embryos**

The specific doses of 2 ng for *wdr81* and *vldlr* and 4 ng for *ano10a* antisense morpholinos were applied to embryos at the 1-4 cell stages. The proper standard control doses of 2 ng and 4 ng were also injected into a cohort of embryos. The antisense morpholino-injected, standard control-injected and uninjected embryos were incubated at the 28<sup>0</sup>C and collected at 24 hours post injection (hpi), 48 hpi and 72 hpi developmental stages. The embryos were snap-frozen in liquid nitrogen and stored at -80<sup>0</sup> C degrees until the experiments were performed. The RNA isolation,

cDNA synthesis and subsequent qPCR experiments and expression analysis were performed as stated in section 2.5-2.8 and the gene specific primers for qPCR that were used are supplied in Table 2.1. The normalization of the gene expression levels in this section was done in two steps. Firstly, the expression of the gene of interest was normalized according to the *beta-actin* expression levels in the same sample. Secondly, the obtained data was normalized to the standard control expression levels of each sample of interest.



## 2.11. Statistical Analysis

The statistical analysis of qPCR expression data from different developmental embryo samples and adult organ tissues and also qPCR expression data from interaction study for *ano10a*, *wdr81*, *vldlr* genes was performed using the SPSS (IBM, Istanbul, Turkey) program. One-way analysis of variance (ANOVA) statistical test with 12 levels for embryonic (1 hpf, 2 hpf, 5 hpf, 10 hpf, 12 hpf, 18 hpf, 24 hpf, 48 hpf, 72 hpf, 5 dpf, 15 dpf, 36 dpf) and for adult tissue (brain, eyes, gill, SB, heart, muscle, fin, liver, skin, gonads, intestine, tail) samples was applied on the provided expression data of *ano10a*, *wdr81* and *vldlr* genes. However, two-way multiple-analysis of variance (MANOVA) statistical test, between subjects, with the factors of time point with three levels (24 hpi, 48 hpi and 72 hpi) and injection condition (MO and standard control MO injected) on the organized qPCR expression data of 12 genes including targeted *ano10a*, *wdr81*, *vldlr* and 9 other cerebellar ataxia-associated genes. In addition, multivariate tests were done to illustrate whether interactions among experimental groups were significant or not. For univariate statistical analysis, a Bonferroni post-hoc comparison test was employed. A cut off of  $p < 0.05$  was used to indicate statistical significance. The statistical analysis of the qPCR experiment data was done by PhD student Elif Tuğçe Karoğlu and Ayşe Gökçe Keşküş. In order to perform the statistical evaluation of the clustergram analysis, a pairwise Spearman's correlation score was applied as a similarity score. A correlation coefficient (r) score with a p value  $> 0.05$  were considered as 0. The inner square distance (ward) linkage was used to construct the clustergram. The statistical part was done by PhD candidate/student Ayşe Gökçe Keşküş. In order to perform statistical analysis of the quantitative measurements of the eye radius, head size,

body size, distance between eyes and yolk size in the *ano10a*, *wdr81*, *vldlr* morpholino-injected, standard control morpholino-injected and uninjected control groups GraphPad Prism Software (GraphPad Software, Inc., San Diego California, US) was used. A one-way ANOVA statistical test was performed to compare the differences of these measurements among the 6 different experimental groups.

## CHAPTER 3

### RESULTS

#### 3.1. *In Silico* Bioinformatics Analysis of *ano10*, *wdr81* and *vldlr*

At the conception of this study, the common interaction of the three targeted genes of interest was that they were responsible for the development of multiple varieties of cerebellar ataxia movement disorders. There was no other published data that might indicate a similar role for these genes within a converging pathway. Therefore, bioinformatics analyses were done. The first employed tool was the Motif Scan and it resulted in the common  $\text{Ca}^{2+}$  activated Casein Kinase 2 motif within the protein sequences of three genes of interest. It is difficult to exactly state how many proteins include this CK2 domain; however, this domain is found in the proteins that take role in the cell-cycle regulation, apoptotic processes, transcription regulation, biological rhythms and cell proliferation [222], [223]. Although the protein products of ataxia-related genes do not participate any of the above listed cellular events, the detection of CK2 in the protein sequences of three cerebellar ataxia associated genes of interest may suggest their potential regulation through phosphorylation. The positions of predicted CK2 phosphorylation sites are provided in Table 3.1. Another bioinformatics tool, namely the String Database gave the predicted interaction among the protein products of three genes of interests and other cerebellar ataxia associated genes through a common Ubiquitin C (UBC) protein. The results of the protein-protein interaction network String database are provided in Figure 3.1. According to the String Database results, the different colors of lines carry distinct meanings. The

purple lines between UBC and ANO10, UBC and WDR81, UBC and VLDLR, UBC and TTBK2, UBC and WWOX, UBC and STUB1, UBC and ATXN1, UBC and ATXN2 depict an experimentally-determined protein-protein interaction network between two protein pairs, whereas the yellow line between WDR81 and VLDLR means that the predicted interaction network was based on text mining as suggested in the Gulsuner *et al.* 2008 paper [37], [46], [47], [61], [224]. The green line between STUB1 and UBC refers to the interaction network that was obtained from the curated databases.

**Table 3.1.** Motif Scan Database results show predicted status of common motif, Casein Kinase 2 phosphorylation sites, in the protein sequences of *wdr81*, *vldlr*, and *ano10a* genes, which may indicate their potential functional regulations through phosphorylation.

COMMON MOTIF CASEIN KINASE (CK2) PHOSPHORYLATION SITE	Status of motif in <i>wdr81</i>	Status of motif in <i>vldlr</i>	Status of motif in <i>ano10a</i>
	53-56	42-45	6-9
	224-227	121-124	27-30
	268-271	244-247	107-110
	312-315	290-293	120-123
	476-479	443-446	298-301
	494-497	546-549	385-388
	527-530	701-704	494-497
	561-564	710-713	625-628
	627-630	724-727	
	640-643	832-835	
	688-691	887-890	
	738-741	915-918	
	746-749		
	773-776		
	797-800		
	927-930		
	1053-1056		
	1064-1067		
	1129-1132		
	1187-1190		
	1192-1195		
	1204-1207		
	1212-1215		
	1226-1229		
	1280-1283		
	1343-1346		
	1355-1358		
	1409-1412		
	1433-1436		
	1527-1530		
	1579-1582		
	1590-1593		
	1673-1676		
	1717-1720		
	1813-1816		
	1967-1970		
	1989-1992		
	2017-2020		

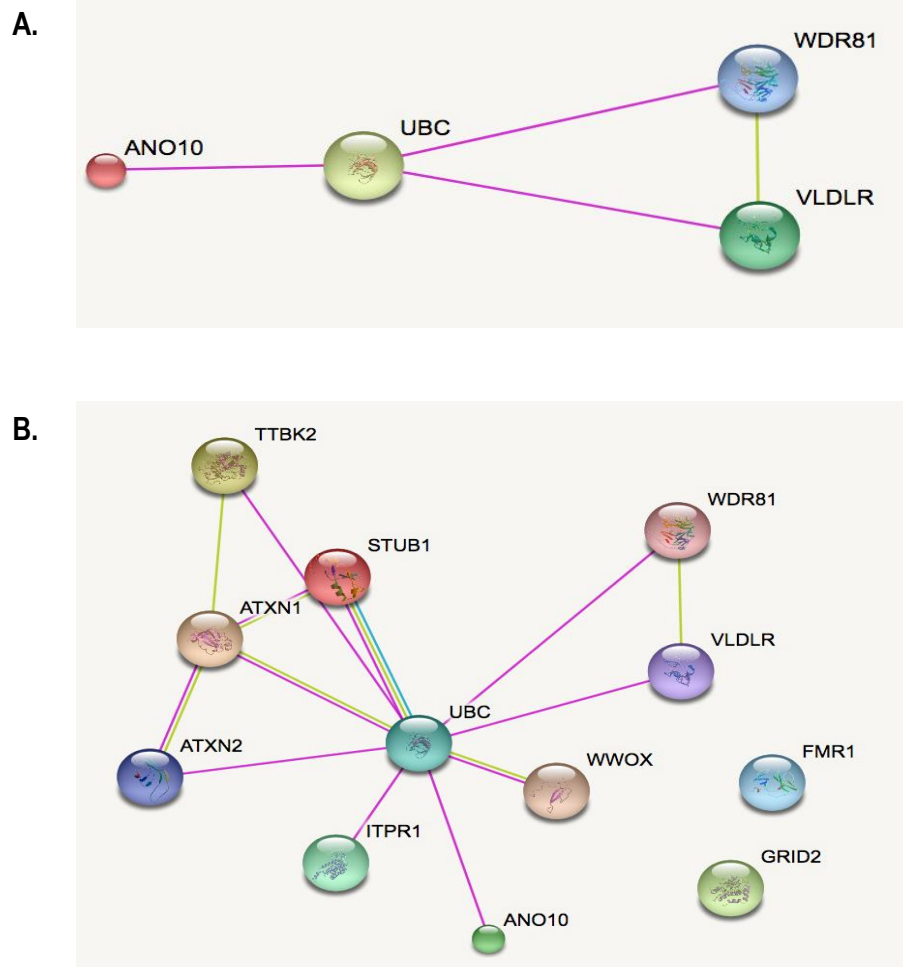


**Figure 3.1.** String protein-protein interaction database (Ver.10) results. **(A)** The common interacting protein UBC with the protein products of human *ano10*, *wdr81*, *vldlr* was indicated. **(B)** The predicted interaction network among the protein products of genes of interest and other cerebellar ataxia associated genes with each other and with common UBC protein was demonstrated. The purple lines indicate experimentally-determined protein-protein interaction network between two protein pairs, the yellow line means that the predicted interaction network was based on text mining and the green line defines the interaction network was obtained from the curated databases.



### **3.2. Spatiotemporal Gene Expression Analysis Results of *ano10a*, *wdr81* and *vldlr* in Embryo and Adult Tissue Samples**

#### **3.2.1. The Gene Expression Analysis Results of *ano10a*, *wdr81* and *vldlr* in Embryo Samples**

The gene expression level analysis result of *ano10a*, *wdr81* and *vldlr* during different developmental stages as measured by qPCR is depicted in Figure 3.2.A. According to Figure 3.2.A, the *ano10a* transcript has a variable expression during embryonic and larval time points. The levels of *ano10a* start at a high level and then the expression decreases dramatically after 5 hpf and starts to increase again at 18 hpf. A dramatic decrease was observed at 48 hpf and remained stable at 3 dpf, then at 5 dpf the expression started to increase again and the expression remained higher during larval stages with no significant decrease after 15 dpf. Statistical analysis demonstrated that the expression decreased significantly after 5 hpf (p-value < 0.05) and it was maintained in a similar range at 10 hpf and 12 hpf developmental stages. Then significant increases at 18 hpf (p-value < 0.05) followed by significant decreases at 48 hpf (p-value < 0.05) were observed and maintained in a stable manner at 3 dpf. The expression started to significantly increase at 5 dpf (p-value < 0.05) and this significant elevation continued until 15 dpf (p-value < 0.05). Although the expression at 36 hpf was still significantly higher than what was observed at 48 hpf, 72 hpf, 5 dpf (p-value < 0.05), an insignificant decrease was detected at 36 hpf in compared to the expression at 15 dpf. The statistical analysis for the *ano10a* gene qPCR results during different developmental time points are provided in Table 3.2.

The overall *wdr81* gene expression level was not as high as *ano10a* transcript during the stated developmental stages. As is depicted in Figure 3.2.A, the expression of *wdr81* was higher at the 1 hpf, 2 hpf and 5 hpf in compared to the rest of the developmental points, 10 hpf, 12 hpf, 18 hpf, 24 hpf, 48 hpf, 72 hpf, 5 dpf, 15 dpf and 36 dpf. Statistical analysis for *wdr81* gene qPCR analysis is given in Table 3.3 indicating the expression of *wdr81* dropped significantly (p-value < 0.05) after 5 hpf developmental stage. The expression of *wdr81* stayed more or less the same after that time period (p-values > 0.05). In other words, the expression of *wdr81* did not differ significantly for all time periods between 10 hpf and 36 dpf developmental stages.

The expression of *vldlr* transcript was the lowest as compared to *ano10a* and *wdr81* genes at the studied developmental time intervals (Figure 3.2.A). Statistical analysis indicated that the expressions of *vldlr* were significantly higher (p-values < 0.05) at the 1 hpf, 2 hpf and 5 hpf, than the rest of the other time points. The expression decreased significantly after 5 hpf (p < 0.05) and was marginally expressed at the remaining time periods with subtle and insignificant increases at the 18 hpf, 24 hpf, 48 hpf and 36 dpf (p-value > 0.05). The expression level of *vldlr* increased significantly at 15 dpf (p-value=0.049 < 0.05) as compared to the expressed transcript at 5 dpf. The statistical analysis of this gene's qPCR results for the distinct developmental time points is detailed in Table 3.4.

The bar graphs in Figure 3.2.B were generated in Matlab® using RNASeq expression data for the *ano10a*, *wdr81* and *vldlr* genes during embryonic and larval

stages. The expression of *ano10a* mRNA was high at the 2.25 hpf, 3 hpf, 4.33 hpf, 5.25 hpf, 19 hpf, 24 hpf, 30 hpf, 36 hpf, 48 hpf, 72 hpf, 4 dpf and 5 dpf as compared to the 6 hpf, 8 hpf, 10.33 hpf and 16 hpf developmental stages as shown in the Figure 3.2.B. The expression of *ano10a* transcript was lowest at the 8 hpf and the low expression continued until 19 hpf stage. The expression of this gene started to ascend after 10.33 hpf and showed quite similar expression values between 24 hpf and 5 dpf developmental stages. As it can be seen from the Figure 3.2, the qPCR expression pattern of *ano10a* was similar with those data obtained from RNASeq analyses. The higher expression of *ano10a* during early embryogenesis and later larval stages are similar in both the qPCR and RNASeq experiments.

According to Figure 3.2.B, the expression of *wdr81* was highest at the 2.25 hpf, 3 hpf and 4.33 hpf as compared to the rest of the stages. The expression of *wdr81* mRNA decreased at the 5.25 hpf developmental stage and kept the more or less similar expression levels between the 5.25 hpf and 5 dpf embryonic and larval time points. This higher expression profile was also indicated with qPCR results for *wdr81* at the early developmental points in Figure 3.2.A and p-values that were less than 0.05 were shown bold.

The obtained RNASeq expression pattern of *vldlr* gene is shown in Figure 3.2. According to Figure 3.2.B, this gene also showed the highest expression levels at the 2.25 hpf, 3 hpf and 4.33 hpf developmental time points. The expression of *vldlr* transcript decreased dramatically at 5.25 hpf stage and started to increase after the 24 hpf developmental period. The expression of *vldlr* continued to increase until 48 hpf

and was nearly stabilized after hatching (48 hpf-72 hpf). Extremely close expression profiles for the *vldlr* transcript at similar time points were seen from the qPCR and RNASeq analyses in Figure 3.2. This pattern was also similar for the *ano10a* and *wdr81* genes with the RNASeq and qPCR results being in parallel to each other.

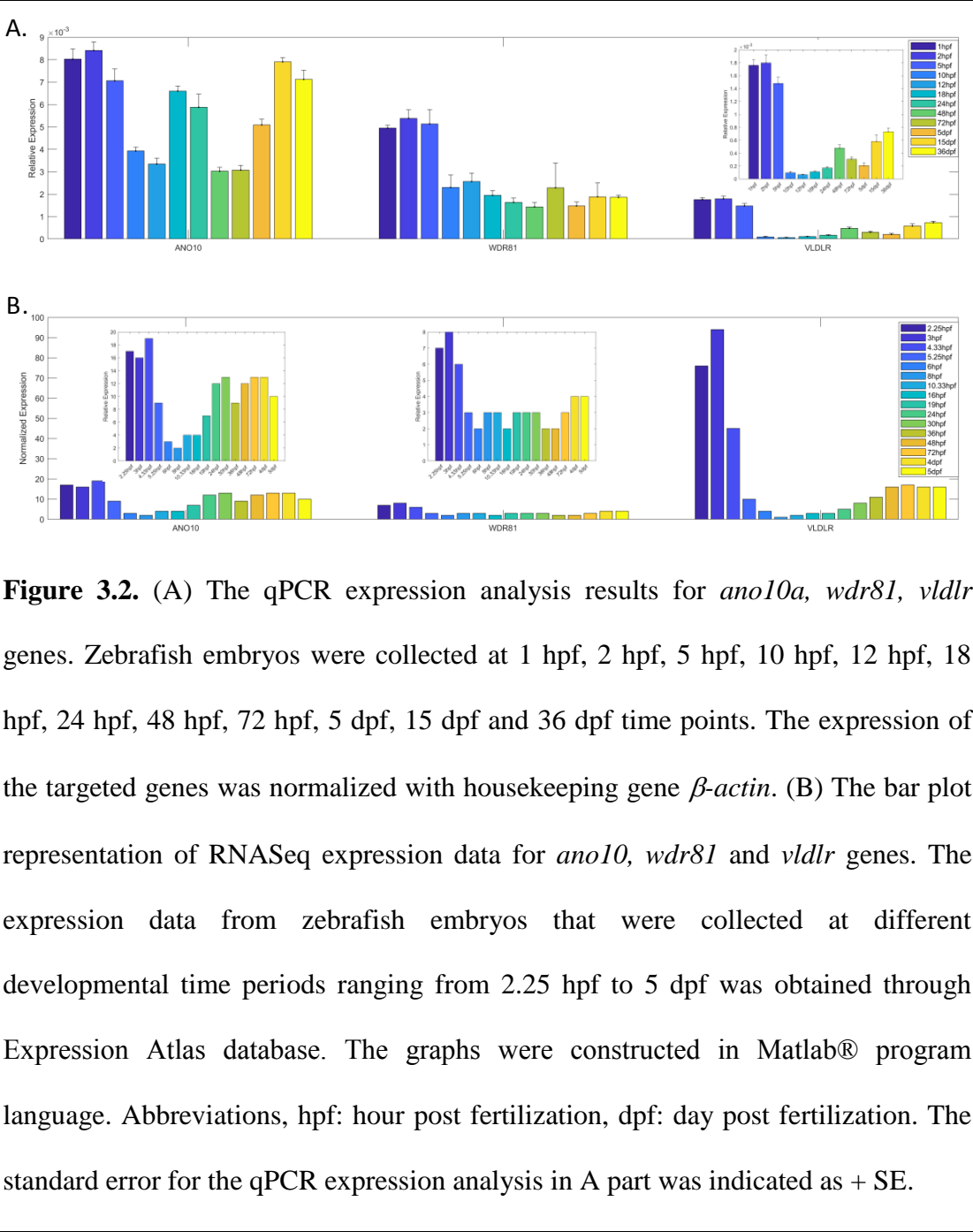


**Table 3.2.** p-values of time point expression differences for *ano10a* gene qPCR result.

	1 hpf	2 hpf	5 hpf	10 hpf	12 hpf	18 hpf	24 hpf	48 hpf	72 hpf	5 dpf	15 dpf	36 dpf
1 hpf		ns	ns	7,06E-08	2,78E-09	ns	0,008	4,97E-10	6,42E-10	7,00E-05	ns	ns
2 hpf	ns		ns	8,13E-09	3,59E-10	ns;p=0,058	0,001	6,85E-11	8,77E-11	6,78E-06	ns	ns
5 hpf	ns	ns		2,14E-05	6,59E-07	ns	ns	1,01E-07	1,34E-07	0,024	ns	ns
10 hpf	7,06E-08	8,13E-09	2,14E-05		ns	0,00035	0,026	ns	ns	ns	7,89E-07	1,47E-05
12 hpf	2,78E-09	3,59E-10	6,59E-07	ns		1,02E-05	0,001	ns	ns	ns;p=0,085	3,52E-08	4,59E-07
18 hpf	ns	ns;p=0,058	ns	0,00035	1,02E-05		ns	1,47E-06	1,97E-06	ns	ns	ns
24 hpf	0,008	0,001	ns	0,026	0,001	ns		0,000114	0,00015	ns	0,04	ns
48 hpf	4,97E-10	6,85E-11	1,01E-07	ns	ns	1,47E-06	0,000114		ns	0,01	6,64E-09	7,08E-08
72 hpf	6,42E-10	8,77E-11	1,34E-07	ns	ns	1,97E-06	0,00015	ns		0,018	8,52E-09	9,37E-08
5 dpf	7,00E-05	6,78E-06	0,024	ns	ns;p=0,085	ns	ns	0,01	0,018		0,0005	0,016
15 dpf	ns	ns	ns	7,89E-07	3,52E-08	ns	0,04	6,64E-09	8,52E-09	0,0005		ns
36 dpf	ns	ns	ns	1,47E-05	4,59E-07	ns	ns	7,08E-08	9,37E-08	0,016	ns	

**Table 3.3.** p-values of time point expression differences for *wdr81* gene qPCR result.

	1 hpf	2 hpf	5 hpf	10 hpf	12 hpf	18 hpf	24 hpf	48 hpf	72 hpf	5 dpf	15 dpf	36 dpf
1 hpf		ns	ns	0,022	ns;p=0,07	0,005	0,001	0,0005	0,021	0,001	0,01	0,003
2 hpf	ns		ns	0,003	0,011	0,001	0,00016	6,42E-05	0,003	7,68E-05	0,002	0,00044
5 hpf	ns	ns		0,01	0,031	0,002	0,0005	0,0002	0,009	0,0002	0,005	0,001
10 hpf	0,022	0,003	0,01		ns	ns	ns	ns	ns	ns	ns	ns
12 hpf	ns;p=0,07	0,011	0,031	ns		ns	ns	ns	ns	ns	ns	ns
18 hpf	0,005	0,001	0,002	ns	ns		ns	ns	ns	ns	ns	ns
24 hpf	0,001	0,00016	0,0005	ns	ns	ns		ns	ns	ns	ns	ns
48 hpf	0,0005	6,42E-05	0,0002	ns	ns	ns	ns		ns	ns	ns	ns
72 hpf	0,021	0,003	0,009	ns	ns	ns	ns	ns		ns	ns	ns
5 dpf	0,001	7,68E-05	0,0002	ns	ns	ns	ns	ns	ns		ns	ns
15 dpf	0,01	0,002	0,005	ns	ns	ns	ns	ns	ns	ns		ns
36 dpf	0,003	0,00044	0,001	ns	ns	ns	ns	ns	ns	ns	ns	

Abbreviations: ns means not significant,  $p < 0.05$  was accepted as a significance cutoff and p-values that were less than 0.05 were shown bold.

**Table 3.4.** p-values of time point expression differences for *vldlr* gene qPCR result.

	1 hpf	2 hpf	5 hpf	10 hpf	12 hpf	18 hpf	24 hpf	48 hpf	72 hpf	5 dpf	15 dpf	36 dpf
1 hpf		ns	ns	4,81E-16	2,60E-17	5,92E-17	1,71E-16	1,17E-13	2,66E-15	3,84E-16	1,04E-11	5,34E-11
2 hpf	ns		ns	2,45E-16	1,32E-17	2,97E-17	8,39E-17	5,06E-14	1,24E-15	1,86E-16	4,41E-12	2,03E-11
5 hpf	ns	ns		1,16E-13	6,36E-15	1,65E-14	5,61E-14	1,14E-10	1,37E-12	1,43E-13	1,18E-08	1,45E-07
10 hpf	4,81E-16	2,45E-16	1,16E-13		ns	ns	ns	0,035	ns	ns	0,005	2,11E-05
12 hpf	2,60E-17	1,32E-17	6,36E-15	ns		ns	ns	0,006	ns	ns	0,001	1,80E-06
18 hpf	5,92E-17	2,97E-17	1,65E-14	ns	ns		ns	0,023	ns	ns	0,003	7,37E-06
24 hpf	1,71E-16	8,39E-17	5,61E-14	ns	ns	ns		ns	ns	ns	0,015	4,41E-05
48 hpf	1,17E-13	5,06E-14	1,14E-10	0,035	0,006	0,023	ns		ns	ns	ns	ns
72 hpf	2,66E-15	1,24E-15	1,37E-12	ns	ns	ns	ns	ns		ns	ns	0,004
5 dpf	3,84E-16	1,86E-16	1,43E-13	ns	ns	ns	ns	ns	ns		0,049	0,00017
15 dpf	1,04E-11	4,41E-12	1,18E-08	0,005	0,001	0,003	0,015	ns	ns	0,049		ns
36 dpf	5,34E-11	2,03E-11	1,45E-07	2,10564E-05	1,80E-06	7,37E-06	4,41E-05	ns	0,004	0,00017	ns	

Abbreviations: ns means not significant,  $p < 0.05$  was accepted as a significance cutoff and p-values that were less than 0.05 were shown bold.

### 3.2.2. Pattern of Gene Expression Levels of *ano10a*, *wdr81* and *vldlr* in Adult Male and Female Zebrafish Organs

This study is the first to compare the tissue expression levels of the three genes of interest, *ano10a*, *wdr81* and *vldlr*, in adult male and female zebrafish organs. The mRNA transcript expression levels of these genes are depicted in Figure 3.3. As it was shown in Figure 3.3, the expression of *ano10a* was highest in the eye, brain, gill and gonad tissues, especially in the testis. The expression of this gene was moderate in the muscle, intestine, liver, skin, fin and tail tissues. The lowest expression of this gene transcript was observed in the swim bladder and heart tissues. The statistical analysis also indicated that there is a significant main effect among gender, gene and tissue dependent variables ( $p\text{-value} < 0.05$ ). The interaction

between gene and gender and tissue and gender were also significant for this gene (p-values < 0.05). Therefore, the statistical analysis showed that the expression levels of *ano10a* gene in males and females were significantly different in the eyes, gills, liver and gonad tissues (all p-values < 0.05). Additionally, the statistics also revealed that the overall expression levels of *ano10a* were higher in female tissues than in male tissues. The expression of *ano10a* were higher in females than in males at brain, eyes, gills, swim bladder, heart, fin, liver and tail whereas lower in females than in males at muscle, skin, gonads and intestine.

In Figure 3.3, the expression level analysis of *wdr81* in adult zebrafish tissues was also illustrated. The expression of *wdr81* was highest in the eyes, brain, gills and gonads, specifically in testis. The expression was modest in the liver, intestine, muscle, skin heart and swim bladder tissues. The lowest expression of the *wdr81* was seen at the fin and tail tissues. The statistical analysis also indicated the significant main effect among gene, gender and tissue dependent variables. The interactions between gender and gene and gender and tissue were also significant for this gene (p-values < 0.05). Therefore, the statistical analysis showed that the expression of *wdr81* was significantly different in eyes, gills, liver and gonads between two gender groups (all p-values < 0.05). Additionally, the sexually dimorphic expression pattern of *ano10a* and *wdr81* transcripts were detected in exactly the same organs in the eyes, gills, liver and gonads. As in the case of *ano10a*, the *wdr81* gene was highly expressed in the female tissues rather than male tissues. The *wdr81* gene was expressed higher in females than in males at brain, eyes, gills, swim bladder, heart,

fin, liver, skin, intestine and tail whereas the *wdr81* was expressed lower in females than in males at remaining muscle and gonads tissues.

In Figure 3.3, the expression level analysis of *vldlr* gene was also demonstrated. The expression of *vldlr* was highest in the brain, eyes, swim bladder and gonads, specifically in the egg tissues as opposed to previous two other targeted genes' higher expression levels in testis tissues. The expression of *vldlr* was moderate in the muscle and skin. The lowest expression of this gene was observed in the remaining organs including the gill, heart, fin, liver, intestine and tail. The statistical analysis also indicated the significant main effect among gene, gender and tissue dependent variables for *vldlr*. The interactions between gender and gene and gender and tissue were also significant (p-values < 0.05). Unlike *ano10a* and *wdr81*, the only significant difference between male and female individuals in *vldlr* gene expression was observed in the swim bladder and gonads (p-values < 0.05). Additionally, in similar to the expression levels of *ano10a* and *wdr81*, the *vldlr* gene was also expressed higher in female tissues rather than the male tissues. So, the expression of *vldlr* was detected higher in females than in males at eyes, gills, swim bladder, heart, fin, liver, skin, gonads and intestine whereas the expression of *vldlr* was observed lower in females than in males at brain, muscles and tail tissues. The detailed statistical analysis of the qPCR results of the targeted genes in 12 different organs from male and female specimens were performed using the SPSS program (IBM, Istanbul, Turkey). The comparison of the expression data for each gene and gender can be tracked examining the obtained p-values in Table 3.5-10. The p-values that were less than 0.05 were marked bold.



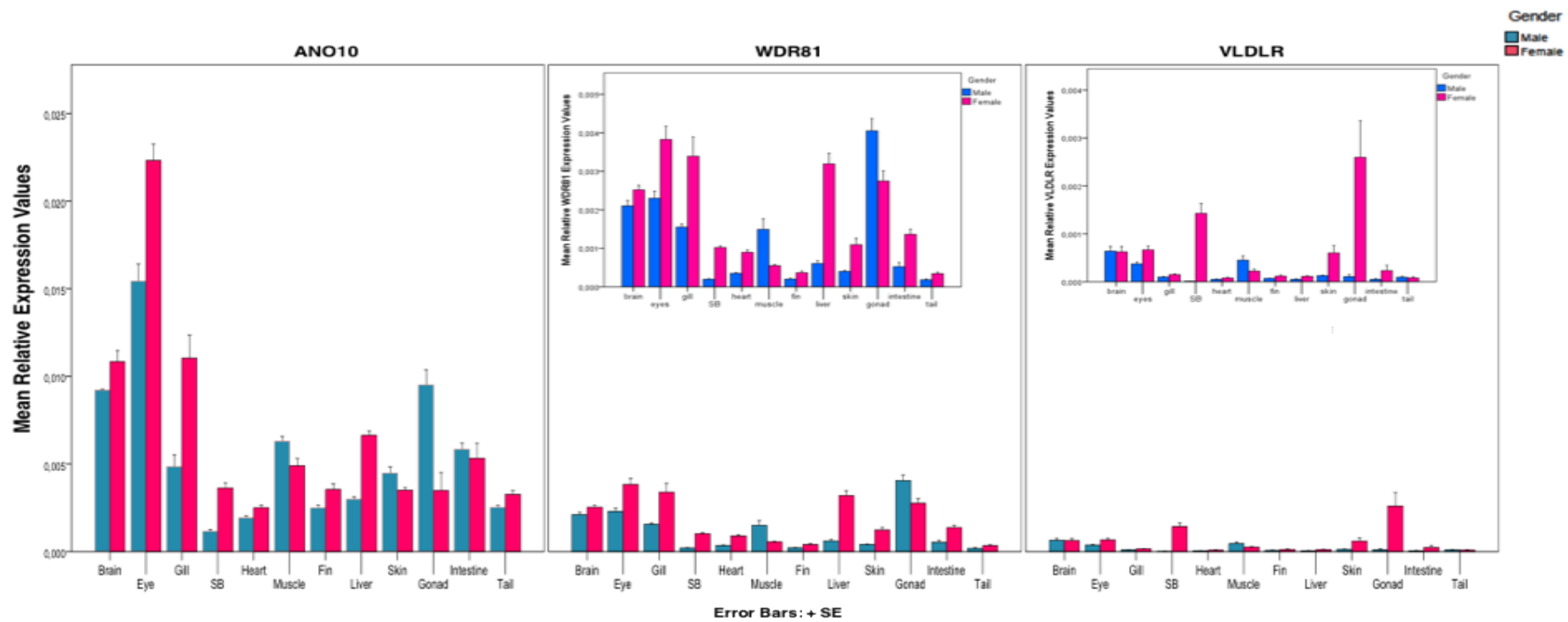


**Figure 3.3.** qPCR expression analysis result of *ano10a*, *wdr81* and *vldlr* genes in organs from the male and female zebrafish. Organs were collected from three females and three adult males and the same organs were pooled for each gender. The relative expression normalized with  $\beta$ -actin gene as an internal control. The panel graphs and statistics were obtained using SPSS (IBM, Istanbul, Turkey). In graphs, the organs collected from male zebrafish specimens were represented via blue color whereas female organ tissues were shown with red color. The standard error was indicated as +SE and p-value < 0.05 was accepted as significance cutoff.

**Table 3.5.** p-values of organ tissues' expression differences for *ano10a* gene qPCR result.

	Brain	Eye	Gill	SB	Heart	Muscle	Fin	Liver	Skin	Gonad	Intestine	Tail
Brain		1,71E-10	ns	3,09E-08	1,43E-08	0,007	3,98E-07	0,0042	1,95E-05	ns	0,006	2,38E-07
Eye	1,71E-10		2,42E-14	4,50E-24	2,25E-24	1,32E-18	4,71E-23	5,32E-20	2,07E-21	5,22E-17	1,21E-18	2,92E-23
Gill	ns	2,42E-14		0,00012	5,97E-05	ns	0,001	ns	0,029	ns	ns	0,001
SB	3,09E-08	4,50E-24	0,00012		ns	ns	ns	ns	ns	0,019	ns	ns
Heart	1,43E-08	2,25E-24	5,97E-05	ns		ns	ns	ns	ns	0,01	ns	ns
Muscle	0,007	1,32E-18	ns	ns	ns		ns	ns	ns	ns	ns	ns
Fin	3,98E-07	4,71E-23	0,001	ns	ns	ns		ns	ns	ns	ns	ns
Liver	0,00042	5,32E-20	ns	ns	ns	ns	ns		ns	ns	ns	ns
Skin	1,95E-05	2,07E-21	0,029	ns	ns	ns	ns	ns		ns	ns	ns
Gonad	ns	5,22E-17	ns	0,019	0,01	ns	ns	ns	ns		ns	ns, p=0,085
Intestine	0,006	1,21E-18	ns	ns	ns	ns	ns	ns	ns	ns		ns
Tail	2,38E-07	2,92E-23	0,001	ns	ns	ns	ns	ns	ns	ns, p=0,085	ns	

**Table 3.6.** p-values of organ tissues' expression differences for *wdr81* gene qPCR result.

	Brain	Eye	Gill	SB	Heart	Muscle	Fin	Liver	Skin	Gonad	Intestine	Tail
Brain		ns	ns	0,01	0,001	0,052	6,70E-05	ns	0,007	ns	0,026	2,38E-05
Eye	ns		ns	2,15E-07	2,59E-07	2,57E-05	1,40E-08	ns	3,05E-06	ns	1,06E-05	3,30E-09
Gill	ns	ns		0,00019	0,00022	0,012	1,21E-05	ns	0,002	ns	0,006	3,93E-06
SB	0,001	2,15E-07	0,00019		ns	ns	ns	0,052	ns	3,68E-09	ns	ns
Heart	0,001	2,59E-07	0,00022	ns		ns	ns	ns, p=0,059	ns	4,45E-09	ns	ns
Muscle	0,052	2,57E-05	0,012	ns	ns		ns	ns	ns	5,32E-07	ns	ns
Fin	6,70E-05	1,40E-08	1,21E-05	ns	ns	ns		0,004	ns	2,61E-10	ns	ns
Liver	ns	ns	ns	0,052	ns, p=0,059	ns	0,004		ns	0,008	ns	0,002
Skin	0,007	3,05E-06	0,002	ns	ns	ns	ns	ns		6,54E-08	ns	ns
Gonad	ns	ns	ns	3,68E-09	4,45E-09	5,32E-07	2,61E-10	0,008	6,54E-08		2,09E-07	5,24E-11
Intestine	0,026	1,06E-05	0,006	ns	ns	ns	ns	ns	ns	2,09E-07		ns
Tail	2,38E-05	3,30E-09	3,93E-06	ns	ns	ns	ns	0,002	ns	5,24E-11	ns	

Abbreviations: ns means not significant, SB means swim bladder and p-values < 0.05 was accepted as significance cutoff and p-values that were less than 0.05 were shown bold.

**Table 3. 7.** p-values of organ tissues' expression differences for *vldlr* gene qPCR result.

	Brain	Eye	Gill	SB	Heart	Muscle	Fin	Liver	Skin	Gonad	Intestine	Tail
Brain		ns	ns	ns	ns	ns	ns	ns	ns	ns	ns	ns
Eye	ns		ns	ns	ns	ns	ns	ns	ns	ns	ns	ns
Gill	ns	ns		ns	ns	ns	ns	ns	ns	0,002	ns	ns
SB	ns	ns	ns		ns	ns	ns	ns	ns	ns	ns	ns
Heart	ns	ns	ns	ns		ns	ns	ns	ns	0,001	ns	ns
Muscle	ns	ns	ns	ns	ns		ns	ns	ns	ns;p=0,063	ns	ns
Fin	ns	ns	ns	ns	ns	ns		ns	ns	0,001	ns	ns
Liver	ns	ns	ns	ns	ns	ns	ns		ns	0,001	ns	ns
Skin	ns	ns	ns	ns	ns	ns	ns	ns		0,042	ns	ns
Gonad	ns	ns	0,002	ns	0,001	ns;p=0,063	0,001	0,001	0,042		0,003	0,0012
Intestine	ns	ns	ns	ns	ns	ns	ns	ns	ns	0,003		ns
Tail	ns	ns	ns	ns	ns	ns	ns	ns	ns	0,0012	ns	

**Table 3. 8.** p-values of male and female's organ tissues expression differences for *ano10a* gene qPCR result.

Gender types and tissue names	Significance levels
Male brain-Female brain	ns
Male eye-Female eye	<b>p &lt; 0, 001 (***)</b>
Male gill-Female gill	<b>p &lt; 0, 001 (***)</b>
Male SB-Female SB	ns
Male heart-Female heart	ns
Male muscle-Female muscle	ns
Male fin-Female fin	ns
Male liver-Female liver	<b>p=0,007 &lt; 0, 01 (**)</b>
Male skin-Female skin	ns
Male testis-Female eggs	<b>p &lt; 0,001 (***)</b>
Male intestine-Female	ns
Male tail-Female tail	ns

Abbreviations: ns means not significant, SB means swim bladder and  $p < 0.05$  was accepted as significance cutoff and p-values that were less than 0.05 were shown bold.

**Table 3. 9.** p-values of male and female organ tissue expression differences for *wdr81* gene qPCR result.

Gender types and tissue names	Significance levels
Male brain-Female brain	ns
Male eye-Female eye	<b>p &lt; 0, 001 (***)</b>
Male gill-Female gill	<b>p &lt; 0, 001 (***)</b>
Male SB-Female SB	ns
Male heart-Female heart	ns
Male muscle-Female muscle	ns
Male fin-Female fin	ns
Male liver-Female liver	<b>p &lt; 0, 001 (***)</b>
Male skin-Female skin	ns
Male testis-Female eggs	<b>p=0,002 &lt; 0,01 (**)</b>
Male intestine-Female	ns
Male tail-Female tail	ns

**Table 3. 10.** p-values of male and female organ tissues expression differences for *vldlr* gene qPCR result.

Gender types and tissue names	Significance levels
Male brain-Female brain	ns
Male eye-Female eye	ns
Male gill-Female gill	ns
Male SB-Female SB	<b>p &lt; 0,001 (***)</b>
Male heart-Female heart	ns
Male muscle-Female muscle	ns
Male fin-Female fin	ns
Male liver-Female liver	ns
Male skin-Female skin	ns
Male testis-Female eggs	<b>p &lt; 0,001 (***)</b>
Male intestine-Female	ns
Male tail-Female tail	ns

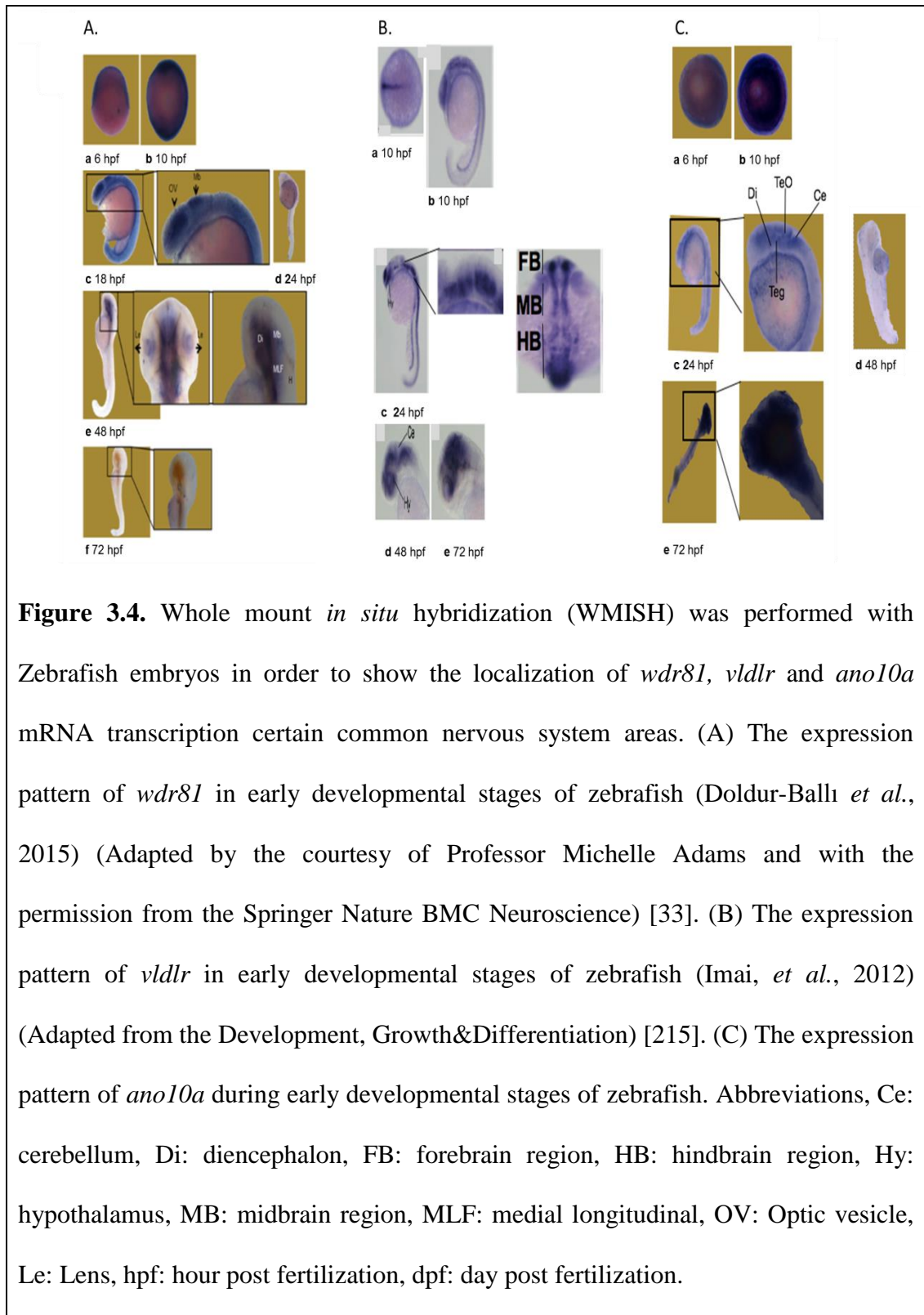
Abbreviations: ns means not significant, SB means swim bladder and  $p < 0.05$  was accepted as significance cutoff and p-values that were less than 0.05 were shown bold.

### 3.2.3. Spatial Localization of *ano10a* mRNA in Zebrafish Embryos at Different Developmental Time Periods

In order to determine the spatial localization of *ano10a* gene in zebrafish embryos at different developmental stages, whole mount *in situ* hybridization (WMISH) experiment was performed. This was done so that the spatial expression pattern of *ano10a* can be compared to the already published WMISH results for *wdr81* (Fig 3.4.A; Doldur-Balli *et al.*, 2015) and *vldlr* (Figure 3.4.B; Imai *et al.*, 2012) WMISH [33], [215]. The published *wdr81* and *vldlr* WMISH results were incorporated into this figure in order to compare the expression pattern of these three genes and as well as to detect whether these genes were expressed in the similar regions or not.

The comparison of *ano10a*, *wdr81* and *vldlr* expression patterns during early embryogenesis was depicted in Figure 3.4. As indicated from panel A and C of Figure 3.4, *ano10a* and *wdr81* expression was ubiquitous at the 6 hpf and 10 hpf developmental stages; however, the *vldlr* mRNA transcript started to show differential expression pattern earlier at 10 hpf stage in the midline of embryos, lying along the axial mesoderm, in addition to the ubiquitous expression as depicted in Panel B. The expression of *ano10a*, *wdr81* and *vldlr* mRNAs were co-expressed at the diencephalon, midbrain and cerebellar regions of 24-48 hpf embryos. Although the expression of *vldlr* and *wdr81* were localized in eye and optic vesicle at the 24 hpf and 48 hpf pharyngula stages respectively, there was no *ano10a* transcript neither in eye nor in optic vesicle yet during these developmental time periods. At the 72 hpf developmental time point, the expression of *wdr81* disappeared whereas the intense

expressions of both *ano10a* and *vldlr* were detected throughout the brain. The general expression profiles gained through the qPCR and RNASeq analyses of three targeted genes were in parallel with the results of WMISH. All these experimental results indicated that the expressions of *ano10a*, *wdr81* and *vldlr* mRNAs were high at the early developmental time points. The expression levels of *wdr81* and *vldlr* genes decreased and then stabilized later developmental stages 24 hpf, 48 hpf and 72 hpf, whereas the *ano10a* expression also decreased and stabilized during 24 hpf and 48 hpf and then the higher expression profile was retained after 72 hpf time points.



### 3.3. Clustergram Analysis of Cerebellar Ataxia Associated Genes

In order to understand the relationship among the *ano10a*, *wdr81*, *vldlr* genes, which are the primary interest of the current study, and other cerebellar ataxia disorder-associated genes, an unsupervised clustering analysis of all cerebellar ataxia causative genes based on their expression data was performed. In Figure 3.5.A, the clustergram of cerebellar ataxia disorder-related genes are illustrated. The Spearman's correlation coefficient-based similarity matrix was used to construct the clustergram. Based on this clustering analysis, it can be inferred that there were three distinct clusters, those of which that were a highly positive correlation cluster, no correlation cluster and a significantly negative correlation cluster with other groups. It should also be noted that the targeted genes of this study, *ano10a*, *wdr81* and *vldlr*, were grouped in the same cluster indicating their close relationship to each other. This relationship that there are 9 genes that were positively correlating with *ano10a*, *wdr81* and *vldlr* can be more clearly seen in Figure 3.5.B. These 9 genes were identified as *wwox*, *atxn1a*, *stxb1*, *fmr1*, *itpr1b*, *atxn2*, *ttbk2b*, *grid2* and *ano10b* and successfully showed the close clustering of *ano10a*, *wdr81*, and *vldlr* genes to each other and to the 9 additional cerebellar ataxia associated genes.





### 3.4. Morpholino Knock-Down Silencing Studies

#### 3.4.1. Dose Curve Determination for ANO10a Morpholino

In order to determine the correct dose for the ANO10a morpholino (MO) injections, the morpholino incorporation into zebrafish embryo genome was analyzed following the knockdown. In the course of this study, splice-blocking MOs were injected to the embryos at 1-4 cell stages. As discussed in the Chapter 2 Section 2.10, the splice-blocking MO injections may affect the genome of zebrafish embryo in 5 different ways. There may be cryptic exons, cryptic introns, splicing out of complete targeted exons, splicing out of complete targeted introns and incorporation of complete targeted introns in the mature mRNA transcript of the morphant animals [153], [154], [157], [221]. Since an exon 2-intron 2 targeting splice-blocking ANO10a MO was used in the current study, one of the expected mature mRNA transcript outcomes was the splicing out of complete exon2. Therefore, exon1-exon3-targeting primer pairs (Table 2.3) were used in order to control for the exon deletion from the targeted gene transcript. The expected morphant transcript should be composed of 187 bps in length whereas the wild-type PCR product should be 338 bps. When the morphant genotype was observed in more than 50% of the antisense morpholino-injected embryo groups, this dose was chosen as the correct amount to silence the expression of the targeted gene. The survival ratio of the morpholino-injected, negative standard control morpholino-injected and uninjected control are given in Table 3.11. Figure 3.6 illustrates the agarose gel electrophoresis image of the PCR products from the MO-injected and control groups to compare the efficacy of three different doses of the ANO10A MO on splicing. Two primer pairs were used in the PCR reactions. The first one was the MO specific *ano10a* primer pair that was

used in order to detect the effect of the MO injection on the normal splicing. The MO would cause the splicing out of exon 2 from the *ano10a* transcript. Therefore, instead of seeing a 338 bps band in the control groups, which is a band spanning exon1, exon2 and exon3, there would be a 187 bps length PCR product in the morphant transcript group. The second primer set was specific for  $\beta$ -actin and it was used as an internal control to ensure that the morpholino targeted only the *ano10a* transcript not any other genes. Therefore, regardless of treatment, all of the amplified PCR products should have a 367 bps band with more or less the similar intensity. The expected bands were observed as a result of this experiment. In the 2 ng, 4 ng and 8 ng morpholino-injected 24 hpf embryo samples (lanes numbered 3, 5, and 7 in Figure 3.6), the expected 187 bps band was detected and in the uninjected control (lane number 1 in Figure 3.6) and 2 ng, 4 ng and 8 ng standard control morpholino-injected 24 hpf embryo groups (lanes numbered 2, 4, and 6 in Figure 3.6), the expected 336 bps length wild-type band was obtained. In the  $\beta$ -actin primer amplified uninjected control 24 hpf embryo cDNA including sample (lane number 9), 2 ng, 4 ng and 8 ng MO-injected 24 hpf embryo cDNA including samples (lanes numbered 11, 13, and 15) and 2 ng, 4 ng and 8 ng standard negative control morpholino-injected 24 hpf embryo samples (lanes numbered 10, 12, and 14), the expected 367 bps band was detected. In the negative control samples (lanes numbered 8 and 16 in Figure 3.6) for *ano10a* and  $\beta$ -actin primers without any DNA templates, there were no band in these lanes, which indicated that none of the experimental sample was contaminated and those observed bands demonstrated specific and desired amplified regions within the targeted gene sequence.

**Table 3.11.** Survival rate of 24 hpf embryos that were used for the dose curve experiments of *ano10a* are given.

Sample ID	Survival Rate (%)	Mortality Rate (%)
24 hpf 2ng ANO10a MO injected	63,37	36,63
24 hpf 2ng standard control MO injected	65,31	34,69
24 hpf 4ng ANO10a MO injected	60,40	39,60
24 hpf 4ng standard control MO injected	68,18	31,82
24 hpf 8 ng ANO10a MO injected	53,70	46,30
24 hpf 8 ng standard control MO injected	56,25	43,75
24 hpf uninjected control	68,06	31,94

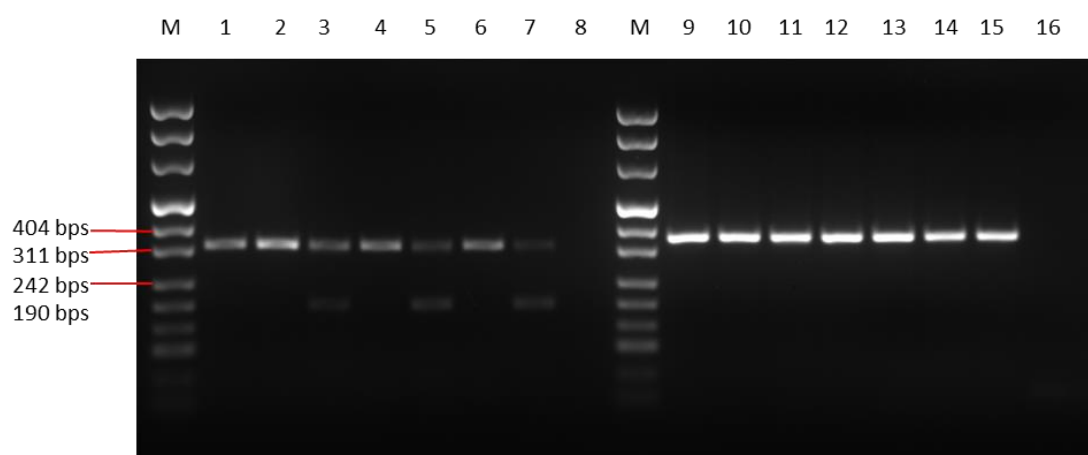


**Figure 3.6.** A 2 % agarose gel illustrating the PCR products from the morpholino (MO) injected and control groups to assess the efficacy of the three different doses of splice-blocking ANO10a antisense MO. The following numbers, between 1-16, defined loaded samples into the wells. Abbreviations: M: DNA gene ruler marker (SM301, Thermo Scientific, US), the numbers defined the samples loaded into that well. The lanes 1 and 9 included 24 hpf uninjected embryos cDNA, lanes 2 and 10 included 24 hpf 2 ng standard negative control MO injected embryos cDNA, lanes 3 and 11 included 24 hpf 2 ng ANO10a MO injected embryos cDNA, lanes 4 and 12 included 24 hpf 4 ng standard negative control MO injected embryos cDNA, lanes 5 and 13 included 24 hpf 4 ng ANO10a MO injected embryos cDNA, lanes 6 and 14 included 24 hpf 8 ng standard negative control MO injected embryos cDNA, lanes 7 and 15 included 24 hpf 8 ng ANO10a MO injected embryos cDNA. The lanes 8 and 16 included negative controls without cDNA templates. PCR reactions products in lanes numbered 1-8 were amplified with *ano10a* specific morpholino control primers whereas the well numbers 9-16 were amplified with *β-actin* specific primers.

### **3.4.2. Quantification of ANO10a, WDR81 and VLDLR Morpholino (MO) Dose Curve Results**

The indicated agarose gel image in Figure 3.7 was used to quantify the band intensities of the ANO10a MO-injected samples. However, the band intensities of WDR81 and VLDLR MO injected samples were quantified from the agarose gel results of former PhD student Füsün Doldur-Ballı. The band intensities of morphant versus wild-type transcripts in three distinct doses of targeted-gene specific MO-injected and uninjected 24 hpf embryo samples for each gene of interest were quantified with ImageJ. These quantified band intensities were used to obtain morphant versus wild-type transcript ratios using GraphPad Prism Software to determine the minimum correct dose for the MO injection.

The morphant percentage ratio was calculated by subtracting the band intensity of the wild-type transcript in the MO-injected embryo samples from the band intensity of wild-type transcript in the uninjected embryo samples and this value was divided by the band intensity of the wild-type transcript in uninjected embryo samples and multiplied by 100. Therefore, the ratio of the wild-type transcripts in the MO-injected and uninjected embryo samples were equal to the value of 100 minus the morphant percentage ratio and to calculate it as a percentage ratio, this result was multiplied by 100. These quantified band-intensity values were used in order to understand morphant versus wild-type phenotype in the three different doses of the MO-injected and uninjected control samples.

In Figure 3.7A, the percentage ratio of the morphant and wild-type *ano10a* transcripts are indicated. These ratios were calculated for three different doses of ANO10a splice-blocking MO injections and the correct dose for an efficient silencing was revealed. Based on the results of these calculations, there were 36.57% morphant transcripts and 63.43% wild-type transcripts within the 2 ng ANO10a splice-blocking MO-injected embryos whereas 64.64% morphant transcripts and 36.36% wild-type transcripts were contained within the 4 ng ANO10a splice-blocking MO-injected embryos. The 8 ng *ano10a* splice-blocking MO injected embryos included 85.26% morphant and 14.74% wild-type transcripts. So, the 4 ng injection dose was chosen as an optimal dose to apply in the knockdown studies.

The percentage ratios of morphant and wildtype *wdr81* transcripts are shown in Figure 3.7.B. These ratios were calculated for three distinct doses of WDR81 splice-blocking MO injections and the optimal dose to silence this gene was determined. Based on the results of these calculations, there were 85.22% morphant transcripts and 14.78% wild-type transcripts within the 2 ng WDR81 MO-injected embryos, whereas there were 88.34% morphant transcripts and 11.66% wild-type transcripts within the 4 ng WDR81 MO-injected embryos. The ratio of morphant transcripts was diminished to 85.78% and increased to 14.22% in the 8 ng WDR81-MO injected embryos. Due to potential off-target effects in the higher doses, a 2 ng WDR81 MO injection dose was chosen as an optimal dose in order to continue with further knockdown experiments.

The percentage ratios of morphant and wild-type *vldlr* transcripts are demonstrated in Figure 3.7.C. These ratios were also calculated for specific doses of VLDLR MO injections. Based on these calculations, there were 71.62% morphant transcripts and 28.38% wild-type transcripts of *vldlr* in the 2 ng VLDLR MO-injected embryos, whereas there were 75.10% morphant and 25.90% wild-type transcripts in the 4 ng VLDLR MO-injected embryos. The wild-type transcript ratio was 47.13% and the morphant transcript was 52.87% in the 8 ng VLDLR MO-injected embryos. Again due to the potential for off-target effects at higher doses, a 2 ng VLDLR MO-injection dose was chosen for the knockdown studies.



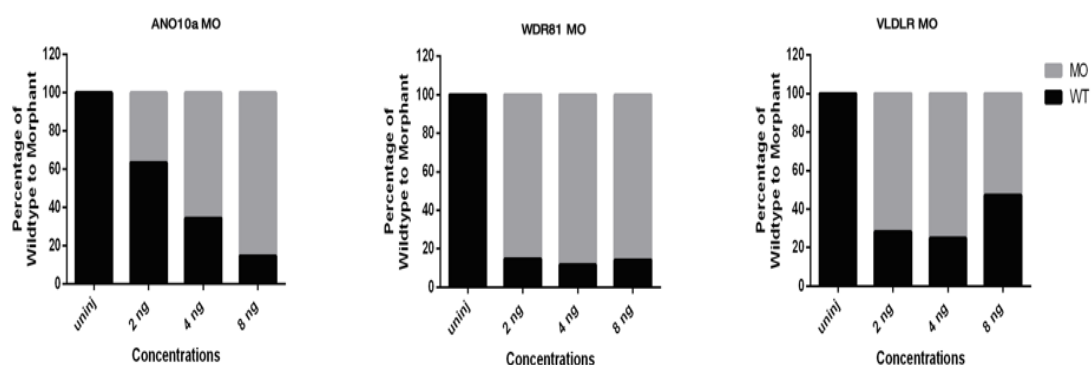


**Figure 3.7.**Quantification of morphant and wild type transcripts from band intensities of three different doses of ANO10a, WDR81 and VLDLR morpholinos (MO) injected and uninjected 24 hpf embryo samples. The band intensities of uninjected embryos of each gene were accepted as a 100 % of the wild-type transcript. The ratio of mutant transcripts was determined by subtracting the band intensity of the wild-type transcript within the morpholino-injected embryos from the band intensity of wild-type transcript within the uninjected embryos and this value was divided by the band intensity of the wild-type transcript in uninjected embryos and multiplied by 100. The band intensities in order to calculate *ano10a* morphant ratio was obtained from Figure 3.6 agarose gel image whereas the *wdr81* and *vldlr* morphant ratios were calculated from measured band intensities agarose gels that were run by former PhD student Füsün Doldur-Ballı. The band intensities were measured through Image J (NIH, Scientific Image Analysis, Bethesda, MD, US) and these quantified band intensities were used in order to calculate and then graph the morphant versus wild-type transcripts in three specific doses of morpholinos injected and uninjected embryos for each individual gene using GraphPad Prism Software (Graphpad Software, Inc., San Diego, California, US).

### 3.4.3. Consequences of Knocking Down with Morpholino Antisense Oligonucleotide One of the Targeted Genes of Interest into Zebrafish Embryos

#### 3.4.3.1. Survival Rates of Single ANO10a, WDR81 and VLDLR MO-Injected, Standard Control Injected and Uninjected Embryo Samples

As was done in the dose curve determination for ANO10a, WDR81 and VLDLR morpholino (MO) injections, the survival and mortality rate for those MO-injected, standard control MO-injected and uninjected embryos were recorded at the end of 24 hpf, 48 hpf and 72 hpf and they are provided in Table 3.12.

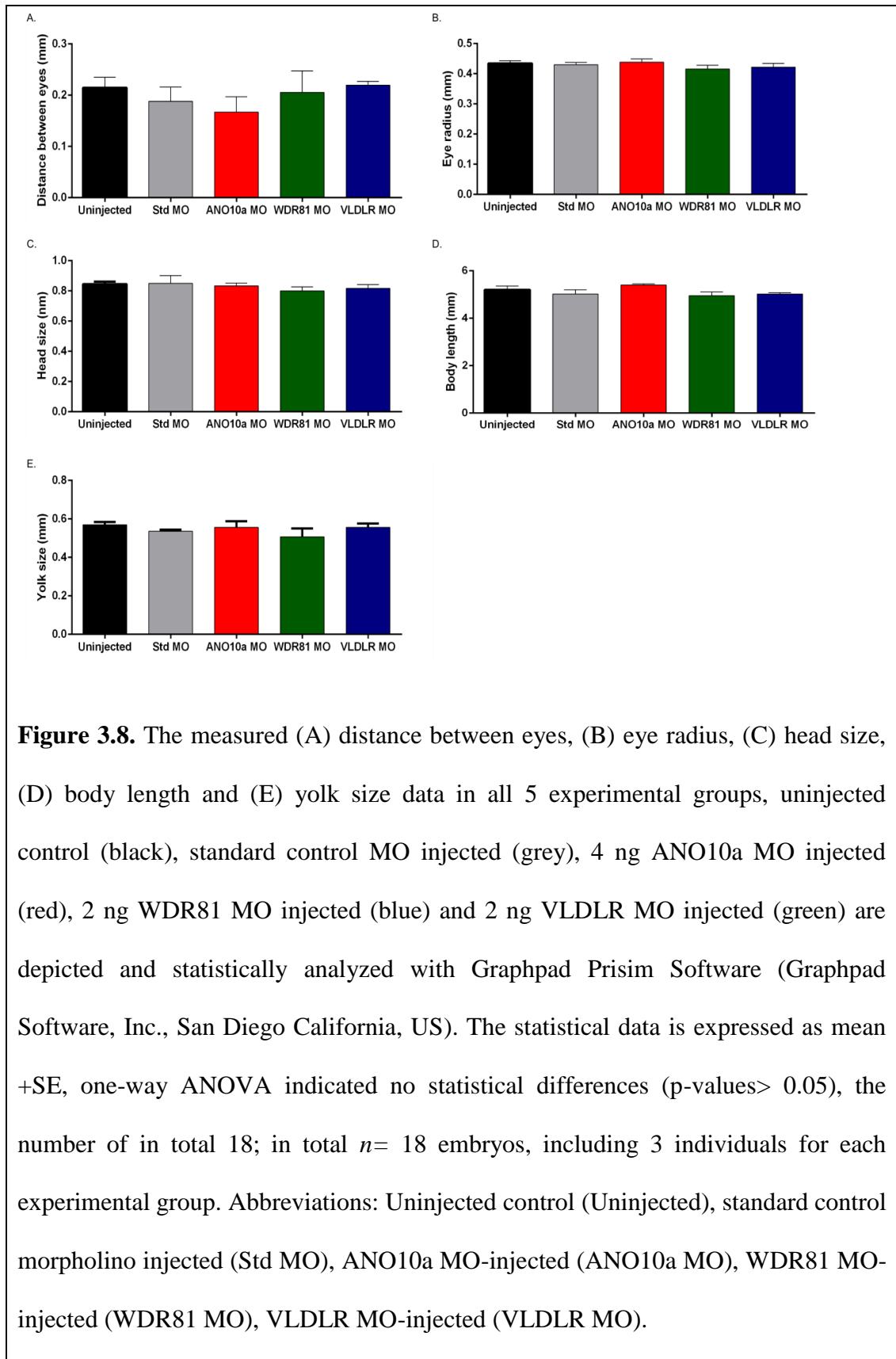
**Table 3.12.** Survival and mortality rates of 24 hpf, 48 hpf, 72 uninjected, antisense MO and standard control MO injected embryos that were used for the analysis of knockdown studies are illustrated.

Sample ID	Survival Rate (%)	Mortality Rate (%)
24 hpf 4 ng ANO10A MO injected	63,93	36,07
48 hpf 4 ng ANO10A MO injected	62,30	37,70
72 hpf 4 ng ANO10A MO injected	61,75	38,25
24 hpf 2 ng WDR81 MO injected	71,35	28,65
48 hpf 2 ng WDR81 MO injected	71,35	28,65
72 hpf 2 ng WDR81 MO injected	70,27	29,73
24 hpf 2 ng VLDLR MO injected	83,33	16,67
48 hpf 2 ng VLDLR MO injected	83,33	16,67
72 hpf 2 ng VLDLR MO injected	79,17	20,83
24 hpf standard control MO injected for ANO10A MO	77,66	22,34
48 hpf standard control MO injected for ANO10A MO	76,60	23,40
72 hpf standard control MO injected for ANO10A MO	70,74	29,26
24 hpf standard control MO injected for WDR81 and VLDLR MOs	70,00	30,00
48 hpf standard control MO injected for WDR81 and VLDLR MOs	69,21	30,79
72 hpf standard control MO injected for WDR81 and VLDLR MOs	68,68	31,32
24 hpf uninjected control	75,72	24,28
48 hpf uninjected control	73,23	26,77
72 hpf uninjected control	71,43	28,57

### **3.4.3.2. Phenotypic Measurements of Single ANO10a, WDR81 and VLDLR**

#### **Morpholino-Injected Embryo Samples**

After the quantitative measurements were obtained for the distance between eyes, the eye radius, the head size, body length and the yolk size of each sample from all the experimental group with ImageJ (NIH, Scientific Image Analysis, Bethesda, MD, US), this data was used to perform statistical analysis and the graphs are illustrated with the Graphpad Prism Software (Graphpad Software, Inc., San Diego, California, US) in Figure 3.8. The data show that the measured distance between the eyes, eye radius, head size, body length and the yolk size did not differ significantly in ANO10A, WDR81 and VLDLR MO-injected, standard control MO-injected and uninjected control groups. The corresponding statistical values were calculated for these measurements. The phenotypic categories that were compared within the 5 experimental groups in this study had the following p-values, F-values and degrees of freedom: the distance between eyes ( $F_{(4,10)} = 0.853$ ; p-value > 0.05), the eye radius ( $F_{(4,10)} = 0.7319$ ; p-value > 0.05), the head size ( $F_{(4,10)} = 0.4756$ ; p-value > 0.05), the body length ( $F_{(4,10)} = 1.1911$ ; p-value > 0.05) and lastly the yolk size ( $F_{(4,10)} = 0.8378$ ; p-value > 0.05).



### 3.4.3.3. qPCR Gene Expression Analysis of Single Morpholino Injected Knockdown of ANO10a, WDR81 and VLDLR into Embryo Samples to Identify Potential Interacting Targets of the Genes of Interest

qPCR experiments were performed with single ANO10a, WDR81 or VLDLR MO injected embryos. Firstly, statistical analysis was applied to determine whether there is any significant difference among 2 ng and 4 ng standard MO injected and uninjected groups. A two-way ANOVA statistical test was followed by pairwise comparison that did not show any significant difference (p-values > 0.05, data was not indicated) among 2 ng and 4 ng standard control morpholino and uninjected groups for *ano10a*, *wdr81*, *vldlr* in terms of the relative expression for 24 hours post injection (hpi), 48 hpi and 72 hpi developmental stages. The normalized data sets were used to compare the relative expression differences of targeted genes, *ano10a*, *wdr81*, *vldlr*, and additionally highly correlated genes, *ano10b*, *ttbk2b*, *grid2*, *wwox*, *stubl*, *atxn1a*, *fmr1*, *itpr1b* and *atxn2*, among single MO and standard MO injected groups at the 24 hpi, 48 hpi and 72 hpi time periods are significant or not. The normalization steps were described previously in the Chapter 2 Section 2.10.5.1.

The relative expression changes of 11 genes, those were *wdr81*, *vldlr*, *ano10b*, *ttbk2b*, *grid2*, *wwox*, *stubl*, *atxn1a*, *fmr1*, *itpr1b* and *atxn2* were shown at 24 hpi, 48 hpi and 72 hpi developmental time periods in the ANO10a MO used embryos. As observed in Figure 3.9, the absence of *ano10a* gene caused increase in the expression levels of all investigated genes at 24 hpi developmental stage as compared to the standard control MO injected embryos at the similar period. Even though the expression levels of some genes including *ano10b*, *ttbk2b* and *atxn1a*

have shown decreased expression in the ANO10a MO injected embryos relative to the standard control MO injected samples at 48 hpi, the remaining genes, *wdr81*, *vldlr*, *grid2*, *wwox*, *stxb1*, *fmr1*, *itpr1b* and *atxn2*, sustained the upregulated expression pattern as in the case of the 24 hpi developmental stage. All of the investigated genes again retained the increased gene expression profile as compared to the standard control MO injected samples at the 72 hpi developmental period. The obtained results from the ANO10a MO injected embryos at the investigated developmental stages, especially at 24 hpi and 72 hpi, suggested that other highly correlated genes increased their expression levels in order to compensate the absence of *ano10a*. When the graphs in Figure 3.9 were examined more closely, the investigated genes were grouped based on significant changes in their expression levels after *ano10a* expression was silenced using MO oligonucleotide technology. *vldlr*, *ttbk2b*, *grid2*, *wwox* and *fmr1* showed significant increases at the 72 hpi stage whereas *stxb1* and *itpr1b* upregulated their gene expression levels significantly at the 48 hpi developmental time point. The significant increase in the expression level of *wdr81* at the all of the investigated periods may indicate the close interaction of this gene with *ano10a* as confirmed by correlation coefficient score calculations ( $R^2_{ano10a-wdr81} = 0.79$ ). *ano10b* shows significant increases in its expression level at the 24 hpf developmental stage. Although the increased expression pattern was observed in all of the investigated genes at the 24 hpi developmental point, the significant increase was detected only in the *ano10b*, which is a paralog of the silenced *ano10a*, and this might suggest a similar function for both these genes in the cell. Therefore, as compared to the remaining genes, *ano10b* being the one significantly increased in its expression level at the beginning may indicate a

compensation for the absence of *ano10a* with their evolutionarily shared key functional properties. These common interaction pattern based on functionally grouped genes may give further insights in assigning novel functions to the *ano10a* gene as it will be discussed later.

The relative expression changes of *ano10a*, *vldlr*, *ano10b*, *ttbk2b*, *grid2*, *wwox*, *stub1*, *atxn1a*, *fmr1*, *itpr1b* and *atxn2* were indicated at the 24 hpi, 48 hpi and 72 hpi developmental time periods in the WDR81 MO injected embryos. As in the case of the ANO10a MO injected embryos, the investigated genes were grouped based on the common expression profile changes at the same time periods when the expression of *wdr81* was silenced during the same time point. Figure 3.10 illustrates the grouped genes in terms of similar expression pattern changes in response to the absence of the *wdr81* gene. *ano10a*, *vldlr*, *ttbk2b*, *grid2*, *wwox*, *atxn1a*, *fmr1*, *itpr1b* and *atxn2* were downregulated in all of the investigated time periods as compared to the standard control MO injected samples after *wdr81* gene was silenced. However, two genes behaved different than those mentioned above by keeping a downregulation pattern during the three subsequent time periods. *ano10b* exhibited a downregulation expression pattern in the WDR81 MO injected embryos at the both 24 hpi and 48 hpi stages as shared by above genes, and it showed insignificant upregulation at the 72 hpi time period, whereas *stub1* demonstrated decreased expression profiling at 24 hpi, then increased its level at 48 hpi, and this increase would not become a consistent trend as there was a little expression drop at the 72 hpi developmental time period. These genes were also grouped according to a similar significant expression pattern. The graphical details demonstrated that *vldlr*, *ano10b*,

*grid2*, *atxn1a*, *fmr1* and *atxn2* were significantly decreased in their expression levels after *wdr81* knockdown as compared to the standard control MO injected samples at 24 hpi and 48 hpi stages. Especially expression changes in *vldlr* gene were less than a quarter of the normal level within the first investigated time point. The 24 hpi may suggest the close interaction of *wdr81* with *vldlr* gene as confirmed with the calculated high correlation score ( $R^2_{wdr81-vldlr} = 0.79$ ). However, *wwox* and *itpr1b* showed significant decreases in their expression levels as compared to the expression levels of standard control MO injected embryos only at the 24 hpi developmental stage, whereas *ttbk2b* gene showed significant downregulation pattern at the 48 hpi time period. All these expression pattern trends and significant changes in the expressions grouped genes indicate potential novel functions of the *wdr81* gene as it will be discussed in the upcoming section.

The relative expression changes of the *wdr81*, *ano10a*, *ano10b*, *ttbk2b*, *grid2*, *wwox*, *stb1*, *atxn1a*, *fmr1*, *itpr1b* and *atxn2* were observed at the 24 hpi, 48 hpi and 72 hpi developmental stages in the VLDLR MO injected embryos in Figure 3.11. The genes were grouped based on similar expression profiles and then significant changes in specific genes were seen to not only to detect a pattern but also to obtain the most altered ones that would enable potentially giving a novel function to the silenced *vldlr* gene. The application of the VLDLR MO caused the most diverse groups as compared to the WDR81 and ANO10a MOs injected samples. *wdr81* and *stb1* genes increased their expression levels after the 24 hpi time period in the VLDLR MO injected groups as compared to the standard control injected embryos, then they slightly decreased their expression levels at the 48 hpi stage and again tend

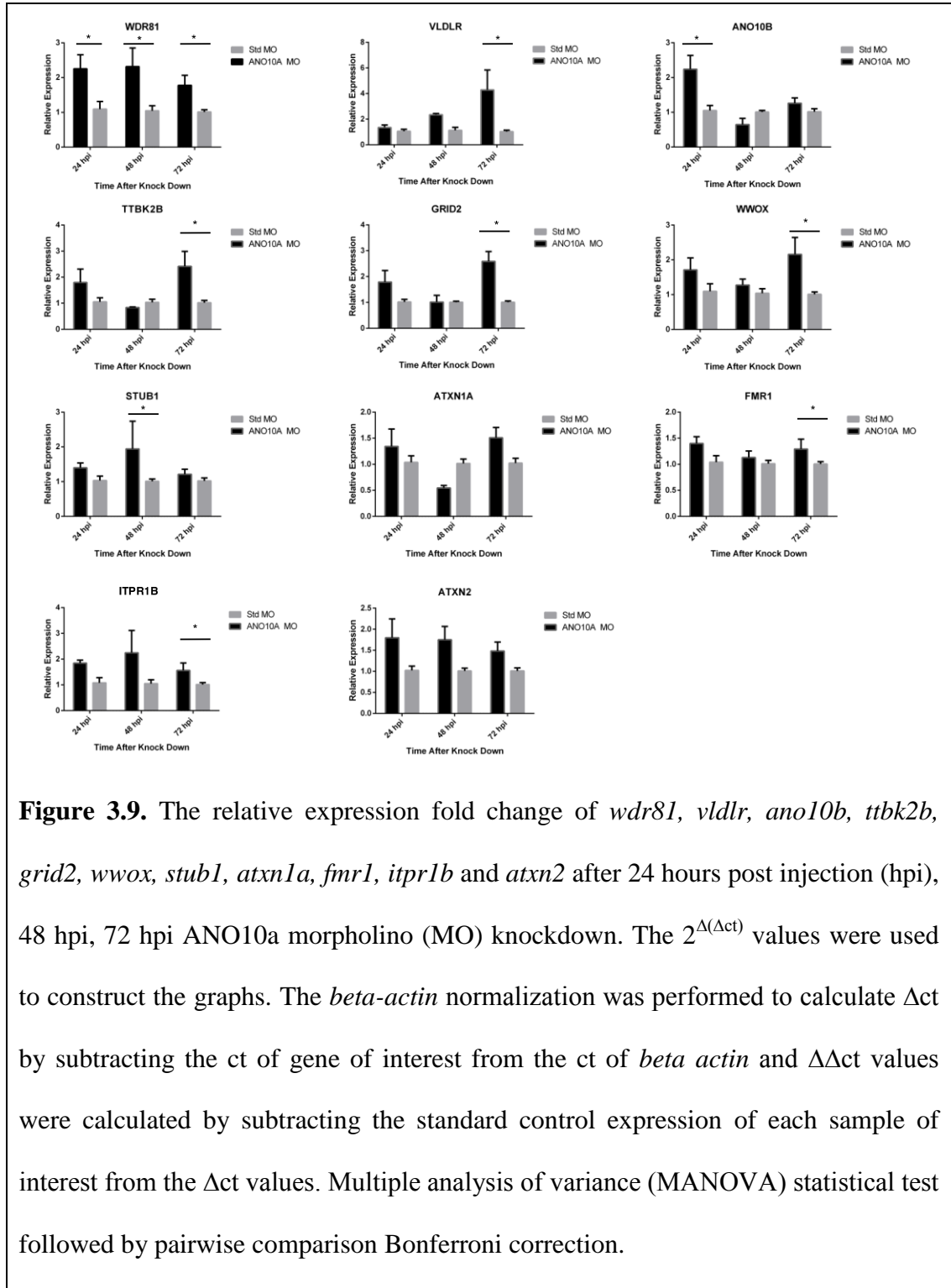


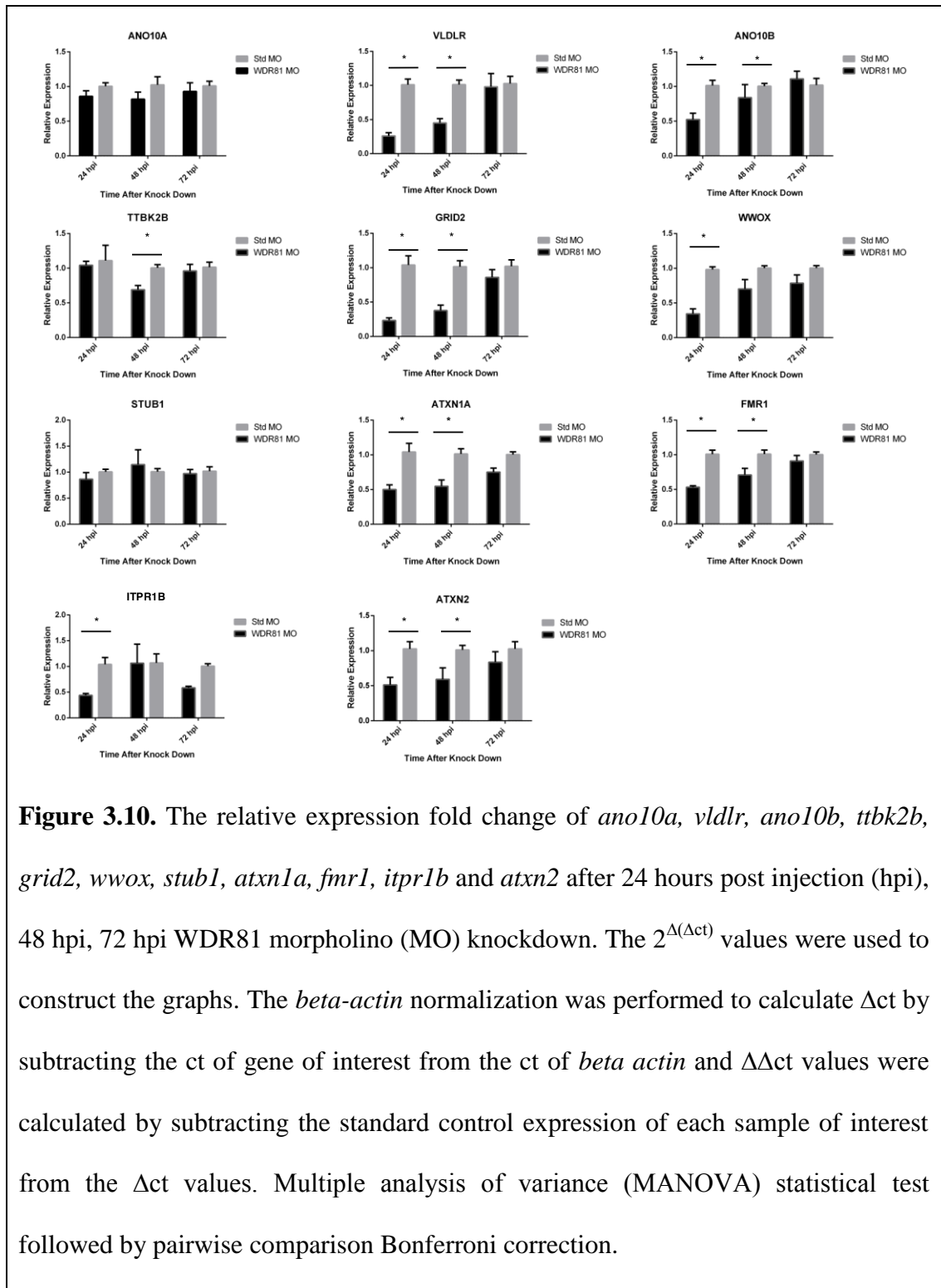
to compensate for the absence of *vldlr* by increasing their expression at the 72 hpi developmental point. *ttbk2b*, *grid2* and *fmr1* showed similar expression profiles at the same time points when the VLDLR gene was knocked down. These gene groups firstly decreased their expression levels in the VLDLR MO injected samples as compared to the standard control injected embryos at the 24 hpi stage. They sustained this downregulated expression pattern at the 48 hpi time period and this trend returned to the previous levels, by the activation of a potential compensatory mechanism at the 72 hpi developmental stage. There was another group of genes including *wwox*, *atxn1a*, *itpr1b* and *atxn2* that never overcame the absence of *vldlr* by showing downregulated expression levels throughout the three stages of investigation. Two genes showed an individual trend that was not shared by the other genes. *ano10b* was downregulated like most of the genes at the 24 hpi developmental stage as compared to the standard control MO injected samples. However, it upregulated its expression at the 48 hpi stage which different than these groups of genes. To our surprise, *ano10b* did not sustain this upregulation pattern until the 72 hpi period, and then the expression of this gene was decreased once more at 72 hpi in the *vldlr* gene silenced embryos as compared to the standard control injected samples. *ano10a* was the second to demonstrate a distinct pattern in which it showed upregulation at all investigated developmental stages in the VLDLR MO injected samples as compared to the standard control MO injected embryos. As shown in Figure 3.11 in the absence of the *vldlr* gene, *ano10b* and *atxn2* decreased their expression levels significantly in the VLDLR MO injected embryos as compared to the standard control MO injected groups at the 24 hpi developmental time period. The expression levels of *grid2*, *wwox*, *atxn1a* and *fmr1* genes were significantly

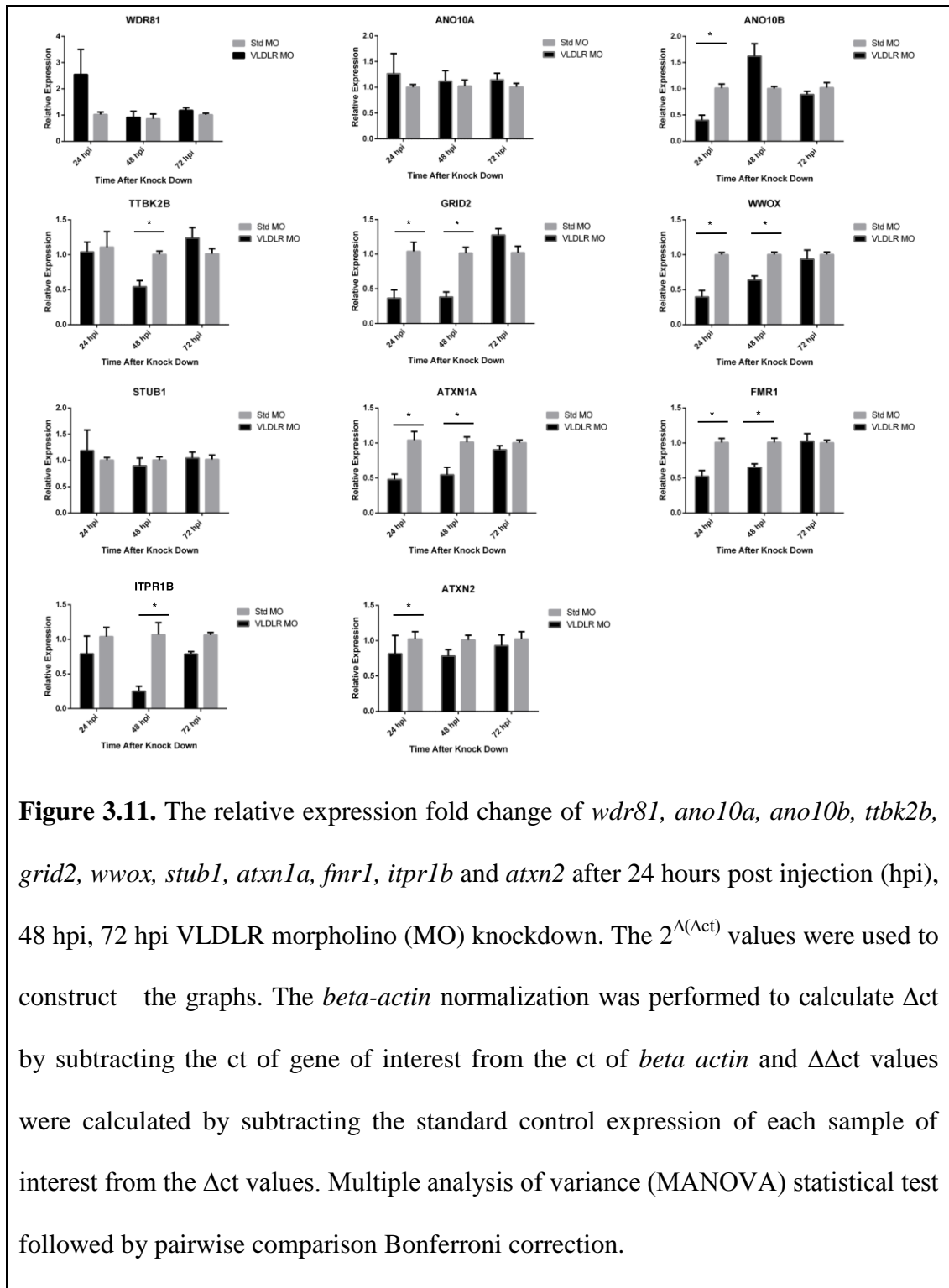
downregulated in the VLDLR MO injected embryos at both the 24 hpi and 48 hpi developmental periods. However, *ttbk2b* and *itpr1b* genes showed significant decreases in their expression levels only at the 48 hpi stage. All of these significant expression pattern changes might indicate different functions for the *vldlr* gene.

The reported effects of the single MO injections on the expression levels of the investigated genes could provide insight into potential new functions of *ano10a*, *wdr81* and *vldlr* genes. The obtained common interaction pattern from the results indicated that *wdr81* and *vldlr* were similar to each other as opposed to *ano10a* as was derived from the similar downregulation pattern in these genes at the investigated time points. Additionally, the activated compensatory mechanism in the all genes at the 24 hpi and 72 hpi time periods showed the critical importance of the *ano10a* gene especially during these developmental processes. One another important result of this study was the discovery or suggestion of novel therapeutic approaches against cerebellar ataxia. Since the knockdown of causative genes in this sense *ano10a*, *wdr81* and *vldlr* can be accepted as a potential mimicking of the disease environment, the upregulated genes could be delivered as a potential therapy to alter the disease phenotypes. For example, altering the levels of *wdr81*, *vldlr*, *ano10b*, *ttbk2b*, *grid2*, *wwox*, *stub1*, *fmr1* and *itpr1b* could be suggested for the treatment of ARCA3 when *ano10a* is mutated; similarly, changing the levels of *ano10a*, *ano10b*, *wdr81*, *ttbk2b*, *grid2*, *stub1* and *fmr1* might be delivered to the organism to eliminate the defected phenotypes in CAMRQ1 when *vldlr* is deficient; only *ano10b* can be accepted as an optional therapeutic for the CAMRQ2 if *wdr81* is depleted. If the combined phenotypes of the three different types of cerebellar ataxias

are detected in the patients, the *ano10b* gene could be a good therapeutic to diminish the negative effects of all three.







# CHAPTER 4

## DISCUSSION

### **4.1. *In Silico* Analysis Revealed the Interactions of *ano10*, *wdr81* and *vldlr* with Neurodegeneration**

The current study was designed to investigate the common interaction pattern among the cerebellar ataxia causative genes, *ano10a*, *wdr81* and *vldlr* by using the zebrafish model organism. The performed Motif Scan and String database *in silico* analysis generated the preliminarily supportive results in line with the pursued hypothesis. A common calcium-activated Casein Kinase 2 and predicted UBC interaction provided a link among *ano10*, *wdr81* and *vldlr* with neurodegeneration due to cerebellar ataxia phenotype when mutations took place in the targeted genes [225], [226]. Further integrative expression analysis was performed in order to resolve the interactive roles of these genes within the converging pathways.

### **4.2. The Expression Analysis of *ano10* Explained Its Importance in Developmental Processes and Its Association with Cerebellar Ataxia**

*ano10*, also called as TMEM16K, which belongs to the Anoctamin family with nine other members encoding a  $\text{Ca}^{2+}$  activated chloride channel transmembrane protein was the first gene to be focused on among the three target genes of interest. To gain the temporal differential expression profile of this *ano10a* gene at the early developmental time periods, embryo samples were used from 12 different developmental stages. The higher expression during early embryonic stages (between 1 hpf-5 hpf) and at the later larval time points (5 dpf, 15 dpf, 36 dpf) indicates the

importance of this gene not only on embryonic but also on the juvenile development as well in the intercellular calcium signaling events that occur [68]–[72]. The WMISH results for the *ano10a* gene also was confirmed using qPCR analyses with a higher expression profile of this mRNA transcript at the 6 hpf and 10 hpf early developmental stages. In Figure 3.4, the localization of *ano10a* gene is observed in the diencephalon, tegmentum, optic tectum and especially in the cerebellum, and this may explain why movement-related defects appear when *ano10* is mutated in the patients with ARCA3 [30], [38]–[45].

The expression variation among different tissues is a prerequisite to detect the importance of a gene within the physiologic and/or pathological conditions [227]. Thus, the differential expression analysis of the *ano10a* gene was performed in the 12 different adult tissue samples with respect to different genders and at a much broader organ range for the first time in zebrafish. As mentioned in Figure 3.3, the higher *ano10a* gene expression was obtained in the eye, brain and gill organs. The quantitatively higher *ano10a* expression localization in the eyes can indicate its association with the correct eye functioning and with the appearance of eye movement defects [228]. The previous published studies of Vermeer *et al.* 2010 and Balreira *et al.* 2014 support this idea with the observed abnormal eye movement phenotype, cataract and retinal degeneration when this gene was mutated [38], [229]. The brain tissue was one other organ that demonstrated a highly expressed level of the *ano10* gene. This brain specific differential expression of the *ano10* gene was also shown previously in 2014 using human tissues [38]. It has been pinpointed that the enhanced gene expression in brain may suggest increased neuronal activity and

huge alterations in the physiology and function of the brain cells [230], [231]. Additionally, the mutated or degraded mRNA transcript may result in neurological disorders [38], [41], [231]–[233]. Therefore, the upregulated *ano10* expression in brain may shed light on the brain controlled motor movement disturbances and neuronal death in cerebellum and brain stem in the patients with cerebellar ataxia when this gene contained a mutation [38], [40], [42], [44], [52]–[56]. Another organ showing upregulated *ano10* expression as illustrated in the Figure 3.3 of the current study was the gills. It is known that gills regulate ion exchange during cellular respiration [234], [235]. Since the *ano10* transmembrane protein acts as a calcium ion binding chloride channel, it may specifically assist the transportation of chloride ions in the gills. A defective *ano10* in gills may distort the chloride and calcium ion metabolism and this might imply mitochondrial dysfunction and thereby provide insight into the reduction in the rate of cellular respiration as observed in some patients with cerebellar ataxia [229], [236]. Although it may be underestimated in many studies, the spatial expression level analysis of *ano10* was done with respect to the gender of the fish. The progression of the differences among male and female individuals in the cerebellar ataxia associated phenotype exhibiting eye and gill organs due to differences in the level of the *ano10* expression may pose a new discussion point that the progression of disease may exhibit alterations based on gender as reported approximately 30 years ago in De Michelle's study [237].



#### **4.3. The Expression Analysis of *wdr81* Explained Its Importance in Developmental Processes and Its Association with Cerebellar Ataxia**

*wdr81*, also named as WD repeat domain 81 is a transmembrane protein encoding gene and is the second focused gene of interest in the current study. Although the complete functions of this gene were not elucidated yet, former papers exclaimed its role in the Purkinje and photoreceptor cell survival, and as well as in the ubiquitination, autophagy and late endosomal pathways [110]–[112]. As was previously stated with *ano10*, the same extensive expression analysis studies were performed. The embryo samples were collected from the 12 distinct developmental time points and the highest expression was observed at the first three stages, 1 hpf, 2 hpf and 5 hpf similarly to the *ano10* gene. This result may show the importance of *wdr81* in the early development. The expression of this gene drastically decreased after 5 hpf and did not show significant elevation once more among the investigated time stages in opposite with *ano10a*. Therefore, it can be still proposed that *wdr81* may be accepted as an important gene for the early embryogenesis but not for the later larval and juvenile stages in the refereed cellular signaling pathways as is required for *ano10*. This result also may explain one important issue as well. The observation of congenital defects in the CAMRQ2 disease appearing with a *wdr81* mutation may also indicate the key role of this gene notably during development [47], [111], [112], [238]. Although the current study repeated similar expression patterns in the evaluated embryonic and late larval stages as in the shown in Doldur-Ballı *et al.* 2015, the critical 18 hpf expression was not seen in the current results [33]. However, the confirmation of qPCR expression profile in the current study with RNASeq performed Ensembl Genome project (continuing, unpublished data) in the

Dr. Busch-Nentwich laboratory revealed that there is no apparent peak between 16 hpf-19 hpf stages [33], [202]. Therefore, this may suggest that the one presented in this thesis reflects a more consistent expression data during development by confirming the parallel expression profile with the obtained RNASeq expression analysis during quite similar time points [33], [202]. The higher temporal expression profile of *wdr81* during early embryogenesis and decreased transcript level of *wdr81* at the later larval stages were not contradicted with the WHISH results of previous paper [33] and may still emphasize how critical *wdr81* is especially for the developmental processes or pathways within the cell. This WHISH results also enabled the comparison of the spatial mRNA localization of *wdr81* with *ano10*. They both are co-expressed in the diencephalon, midbrain and cerebellum. This strong expression signal from the cerebellar region may explain the defected phenotype in the cerebellum when both of these genes are mutated. However, the absence or depletion of either of these two mRNA transcripts from the diencephalon and tectum regions could exclaim a reasonable connection why the motor control and sensory system defects in the patients with ARCA3 and CAMRQ2 are observed as behavioral phenotypes when these two genes do not display their functions properly [24], [30], [33], [38], [41], [45], [49]–[51], [63], [239]–[242]. Therefore, when the temporal and spatial expression results were combined for both *ano10a* and *wdr81*, the already suggested developmentally important role might be more specified as neuro-developmentally important [33].

The presented data from Figure 3.3 illustrated the differential expression in brain, eyes, gills and gonads similarly to the case of *ano10a*. Both developmental and

adult spatial expression pattern similarities of these two genes might suggest how alike they are to each other and might also support the idea that altering the function would affect converging pathways. These organ specific gradient expression patterns of *wdr81* and *ano10* especially in brain and eyes were in parallel with already published human data indicating how the current study is consistent with the previous results [33], [38], [41], [49]–[51]. The differential expression of *wdr81* in the gills might point to the involvement of the protein product of this gene in respiratory dependent energy metabolism [112]. Since gills are required for the respiration process of the fish as suggested in the *ano10a* discussion session, it is expected to observe problems with regards to respiration. If mutations occur in the *wdr81* gene, the cumulative depletion of this gene from the organism would also brake the respiration event in gills and thereby in some human patients the decreased respiration rate or respiratory chain deficiency can be obtained as a chronic phenotype of the cerebellar ataxia disorder [112], [229], [234]–[236], [243]. Although the gender effects have not been completely resolved yet in the progression or the development of cerebellar ataxia, the sexually dimorphic expression profile of *wdr81* in specifically disease associated organs e.g. eyes and gills might dictate the fact that gender would be a factor to encounter with phenotypes in earlier or later periods of the lifespan of people [237].

#### **4.4. The Expression Analysis of *vldlr* Explained Its Importance in Developmental Processes and Its Association with Cerebellar Ataxia**

Another gene of interest was *vldlr*, very-low density lipoprotein receptor (VLDLR), which is a membrane bound transmembrane receptor protein. *vldlr* is an

important component of the Reelin signaling cascade thereby ensuring the correct synaptic function, in the cortical development of the mammalian brain and in VLDL-dependent triglyceride metabolism [128], [130], [215]. As it can be seen from our results section, the *vldlr* gene is more likely to behave similarly to *wdr81* than to *ano10a*. The qPCR and RNASeq expression data analysis indicated that *vldlr* is an important gene especially for the zygotic developmental processes as suggested in the case of *wdr81* expression results during early embryogenesis [33], [243], [244]. The published study in Imai *et al.* 2012 examined the expression pattern of this gene during early embryogenesis [215]. The results showed that similar nervous system structures expressed *ano10a*, *wdr81* and *vldlr*. These regions were diencephalon, midbrain (especially tectum) and cerebellum (Figure 3.4). The expression of *vldlr* in these nervous system structures may provide insight into the pathogenesis of neurodevelopmental movement disorders. The mutation of *vldlr* may disrupt the neuronal migration in these brain areas and cause the appearance of functional deficiencies such as ataxic phenotypes as seen in CAMRQ1 [37], [239]–[243]. It is easy to connect the cerebellum associated disease phenotype in CAMRQ1, basically disturbed motor control, with the deficiency of this *vldlr* gene from the cerebellum. When this gene is mutated or defective in the diencephalon and midbrain during early development, they may be associated sensory and motor control defects in patients with CAMRQ1 [37], [239]–[243], [245].

The expression of *vldlr* in the adult zebrafish tissues also indicated parallel conclusions with the spatiotemporal mRNA transcript data at the early developmental stages. The relatively higher expression of *vldlr* gene was also

detected in eyes and brain as shown in the organ specific expression results of *ano10a* and *wdr81* genes. The differential expression of *vldlr* gene in brain and eyes can explain the alterations in the brain activity during the voluntary walking, abnormalities in the correct motor functions of the extremities and defected eye movement phenotypes e.g. in the patients with CAMRQ1 when this gene is mutated [37], [46], [47]. These results were not completely similar with the published study by Tiebel *et al.* 1999 that indicated the higher expression of this gene in heart and modest expression in kidney, muscle, adipose, and brain tissues of the mouse model. The experiments were done using Northern blotting technique. The qPCR is usually accepted as more sensitive and reliable than this technique for the quantitative expression analysis [246]. Therefore, the recent study results could be more trustable than the previous published data. The current work also evaluated the expression of *vldlr* gene in a sexually dimorphic manner. *vldlr* was differentially expressed in the swim bladder and in gonads between the two genders. The expression of this *vldlr* gene in one of the movement controlling organs, swim bladder, in a dimorphic manner may clarify the effect of gender on the development of disease phenotype at the earlier or later lifespan of the organism [237], [247].

#### **4.5. The Clustergram Analysis Showed the Close Interaction among Three Genes of Interest and Highly Correlated 9 Other Cerebellar Ataxia Associated Genes with *ano10a*, *wdr81* and *vldlr***

The clustergram analysis of RNASeq expression data enabled to determine how functionally close these targeted genes are to each other. The results of clustergram analysis indicated that the three target genes, *ano10a*, *wdr81* and *vldlr* were clustered within close families and this analysis additionally provided 9 highly

correlated genes with targeted disease causative genes. It would be a valuable contribution to science if the interactions among targeted genes and as well as these additionally determined 9 other cerebellar ataxia genes were studied. Therefore, as a next step, the single knockdowns of targeted genes were performed by injecting morpholino (MO) oligonucleotides to the 1-4 cell staged zebrafish embryos. In the absence of one targeted gene, the gene expression changes in the remaining two and additional 9 other cerebellar ataxia associated genes were revealed as a result of the interaction study.

#### **4.6. The Regulatory Effects of *ano10a* Knockdown on the Expression of Cerebellar Ataxia Associated Genes**

Firstly, ANO10a MO was used to silence transcript of *ano10a* gene and the changes of expression levels of two other targeted genes, *wdr81* and *vldlr*, and 9 other cerebellar ataxia associated genes were examined within three developmental time periods. Although the overall increased expression profile of all investigated genes was obtained especially at 24 hpi and 72 hpi developmental stages, the significant upregulation pattern in almost-all of the investigated genes were detected at 72 hpi time period in the *ano10a* gene silenced group as compared to the standard MO injected siblings. This significant upregulation especially at the 72 hpi developmental stage may suggest the activated compensatory mechanism or may trigger the disease associated phenotypes when *ano10a* gene was silenced.

It was expected to detect significant increases in the expression level of *ano10b* when its evolutionarily paralog (with more than 50 % gene coding sequence

complementation) *ano10a* was transcriptionally silenced [248]. This can be interpreted as the functionally similar paralog may take over the absence of the other. Therefore, *ano10b* increased its expression to two times of its normal level to compensate the downregulated *ano10a* activity mainly in the intracellular  $\text{Ca}^{2+}$  signaling pathway [69], [248], [249].

The increase of the *wdr81* gene expression (with at least two times of the normal levels during this stage) along the whole experimental process may be a good indicator of the interaction between two studied genes *wdr81* and *ano10a*. It is known that *wdr81* plays a role in the phosphatidylinositol phosphate-3 kinase (PI3K) pathway as a negative regulator [250]. The significant increase in the expression of *wdr81* when *ano10a* was silenced may suggest that *ano10a* may be a negative regulator of *wdr81* so that *ano10a* may alter the activity of the PI3K pathway by on *wdr81*. Therefore, the association between *wdr81* and *ano10a* genes may propose the involvement of *wdr81* and *ano10* in this pathway to regulate the endosomal fusion, recycling, sorting and early to late transport [250]. The indirect decrease in the activity of PI3K due to the knockdown of *ano10a* may further affect the functioning of converging pathways by regulating the occurrence of post-translational modifications in the components of these signaling pathways. For example, the inactivation of PI3K pathway may result in the downregulation of AKT and Mammalian Target of Rapamycin (mTOR) signaling pathways by regulating the activity of downstream kinases. As a result, these decreased AKT and mTOR activity may affect the cellular proliferation, survival, growth and metabolic processes. It was shown by Courtney *et al.* and Lui *et al.* 2010 that the inactivation of PI3K pathway

was promote the apoptosis of tumor cells [251], [252] so that the potential PI3K inhibitors or negative regulators may serve as an intervention against distinct cancer types [251]–[254].

Although the significant increase in the expression level of *vldlr* gene as compared to the standard control MO injected state (four times more *vldlr* transcript than the normal cellular levels of the *vldlr* transcript) was detected at the 72 hpi developmental stage when *ANO10a* gene was silenced, the general increased expression pattern was conserved along the three days of experimentation as in the case of *wdr81* and nine other cerebellar ataxia associated genes. This obtained result was consistent with the predicted interaction of *ano10* and *vldlr* in the String database, in Figure 3.1 and as well as with a high correlation coefficient between *ano10* and *vldlr* ( $R^2 = 0,68$ ) in the clustergram analysis in Figure 3.5. Therefore, it can be suggested that *ano10* and *vldlr* genes could play a key developmentally important role in cortical neuron development and these two genes may also be in close association to regulate the Reelin signaling pathway in the adult brain [124]–[128]. The increased activity in the *vldlr* regulated pathways such as Reelin signaling in response to the absence of *ano10a* may further activate the downstream components via post-translational modifications. The binding of VLDLR receptor with Reelin ligand causes the activation of Dab1 with phosphorylation by tyrosine kinases. The phosphorylation of Dab1 activates other kinases which ensure the stabilization of cytoskeletal elements. The regulation of cytoskeletal elements by phosphorylation induces the increased activity in the hippocampal dendritic spines [255], [256]. Therefore, it can be predicted that the *ano10a* knockdown dependent



*vldlr* activation may result in increased synaptic plasticity and learning capacity through the activation of signaling components by phosphorylation.

As opposed to the compensatory activation of *wdr81* and *vldlr* genes in response to the ANO10a MO injection, *ttbk2b*, Tau Tubulin Kinase 2B, significant upregulation at the 72 hpi developmental stage may explain the neurodegenerative mechanism behind the cerebellar ataxia when the *ano10* gene is mutated [257]. The overexpression of *ttbk2* drives the hyper phosphorylation of proteins which lead to the mislocalization and accumulation of these phosphorylated proteins and as an inevitable outcome neurodegenerative diseases are sometimes observed [258]. Therefore, it may be suggested that increased *ttbk2* as a result of *ano10* silencing may cause an increase in the total phosphorylation rate of proteins triggering protein aggregate formations thereby neurodegenerative phenotypes in the ARCA3 patients [257]–[260].

One another gene that increased its expression significantly at 72 hpi developmental stage after *ano10a* silencing was *grid2*, glutamate ionotropic receptor delta type subunit 2. *grid2* is an excitatory neurotransmitter receptor selectively expressed in the cerebellar Purkinje cells. The *grid2* gene may try to compensate the absence of *ano10a* especially in the developing cerebellum by ensuring the approximately three times the normal increased neuronal activity to prevent cerebellar dysfunction in the brains of patients with ARCA3 [261]–[264].

The significant gene expression increase (two-fold increase) at 72 hours after ANO10a MO injection was gained in *wwox*, ww domain containing oxidoreductase. This *wwox* acts as a tumor suppressor gene to induce controlled cell death through transforming growth factor beta 1 (TGFB1) [265] and tumor necrosis factor TNF [266] signaling pathways. When the activity of these pathways increases, further post-translational modifications help to convey signal towards downstream pathway elements. The phosphorylation, ubiquitination and N-acetylglucosaminylation (N-GlcNacetylation) of TNF signaling components whereas ubiquitination, phosphorylation, acetylation and ribosylation of TGFB1 pathway elements may activate either cell proliferation, differentiation, survival processes or apoptosis and necrosis mechanisms [267], [268]. These post translational modifications also may activate immune response [267]–[269]. So, it can be predicted that *ano10* may take role in the regulation of above referred pathways by further affecting the activity of signaling molecules through post translational modifications and specifically the potential activation of immune response may show that *ano10* could be involved in the cellular defense mechanism as its family member *ano6* [269].

The significant overexpression of *stb1*, STIP1 homology and u-box containing protein 1, which functions as an ubiquitin ligase and modulates the activity of chaperon complexes [270]–[273], 48 hours after ANO10a MO injection was also observed. This increased *stb1* expression in response to the silenced *ano10a* might be interpreted in two different ways to elucidate the unknown functions of *ano10a*. It may firstly show that *ano10a* may negatively regulate the cellular activity of *stb1*. Therefore, the *ano10a* knockdown may trigger the

ubiquitin dependent protein degradation. This situation may secondly suggest the involvement of *ano10a* in the ubiquitin proteasome system; therefore, *stubl* increased its expression level to compensate the absence of *ano10a* to in the process of protein degradation. Actually, this implication was also proposed as a result of String database *in silico* analysis. It predicted the interaction of *ano10* with a UBC protein (Figure 3.1) and thereby involving *ano10* in the process of ubiquitin-mediated protein degradation [159].

The significant overexpression of *itpr1b*, inositol 1, 4, 5 trisphosphate receptor type 1B, was shown in the ANO10a MO injected embryos at 48 hpi developmental stage. As it is well known that *itpr1* controls the release of  $\text{Ca}^{2+}$  from the endoplasmic reticulum [274]–[277]. The intracellular signal transmission along the Inositol trisphosphate pathway can be mainly provided through post translational modifications especially by phosphorylation. When the *itpr* receptor binds to its ligand, the Receptor Tyrosine Kinases (RTKs) phosphorylates Phospholipase C (PLC) isozyme which then cleaves Phosphatidylinositol 4,5-bisphosphate ( $\text{PIP}_2$ ) into two separate molecules, 1,2-diacylglycerol (DAG) and Inositol 1,4,5-trisphosphate ( $\text{IP}_3$ ).  $\text{IP}_3$  interacts with *itpr* and causes the release of  $\text{Ca}^{2+}$  ions by opening the  $\text{Ca}^{2+}$  ion channels [268], [278], [279]. The influx of intracellular  $\text{Ca}^{2+}$  ions has regulatory function on several biological events such as synaptic plasticity in cerebellar Purkinje cells, muscle contraction, glycolysis, gluconeogenesis, cell cycle regulation, growth and clathrin mediated vesicle coating [280], [281]. It can be proposed from above described pathway that *itpr1* works to regulate intracellular  $\text{Ca}^{2+}$  ions storage as *ano10* does to ensure the correct functioning of referred biological systems [274]–[277].

Therefore, it may not be surprising that *itpr1* increased its expression two times to cope with the decreased activity of *ano10* in the intracellular  $\text{Ca}^{2+}$  ion regulation.

The upregulation of *atxn2*, Ataxin 2, gene throughout the three days after ANO10a MO injection may also try to compensate the absence of *ano10*. It has been shown that the *atxn2* gene modulates the activity of endocytosis, ribosomal translational, mammalian target of rapamycin (mTOR) pathway and mitochondrial functions. It was also shown that the gain of function in the *atxn2* led to neuronal atrophy [282]–[285]. Therefore, the upregulation in the *atxn2* gene after *ano10* gene silencing can be interpreted in two different ways. Firstly, *ano10* gene may take roles in the *atxn2* involved referred cellular events including endocytosis, RNA metabolism, mTOR signaling and mitochondrial function. Secondly, the absence of *ano10* caused increase in *atxn2* gene that may trigger the neuronal atrophy phenotype in the cerebellum of patients with ARCA3. Additionally, it can be also suggested that potential *atxn2* inhibitors can be used in order to diminish the cumulative defects of *atxn2* upregulation and *ano10* knockdown in cerebellar ataxia disorder. Another gene *atxn1a*, Ataxin 1A, was also increased in its expression significantly at the 72 hpi developmental stage of the *ano10a* knockdown. This *atxn1* is critical in RNA processing, with a similar function to *atxn2*, and it also adjusts cerebellar bioenergetics proteome through glycogen synthase kinase 3 beta/mammalian target of rapamycin (Gsk3b/mTOR) pathways [286], [287]. The upregulation of *atxn1* can contribute to the development and progression of cerebellar ataxia associated phenotypes that appear as a result of ARCA3 when *ano10* is mutated. The increased *atxn1* caused increases in the number of inhibitory neurons resulting in inhibition of

the action potential in the cerebellar region and eventually the development of cerebellar ataxia [288], [289]. So, in the ARCA3 types specifically *atxn1* inhibitors or Gsk3b inhibitors can be suggested as therapeutics to at least decrease the negative effects of disease-associated phenotypes.

The significant expression increase at the 72 hpi developmental stage was demonstrated in another gene, *fmr1*, fragile X-mental retardation 1. This gene plays crucial functions in the neuronal development and synaptic plasticity cellular processes by taking roles in the translational control and RNA transport related pathways [290], [291]. The increased *fmr1* gene can be interpreted in two different ways. It may try to compensate for the absence of *ano10a* in the neurodevelopmental processes or as shown in the previous paper, the increased mRNA levels of *fmr1* caused RNA toxicity, which is responsible for the development of disease phenotypes [292]–[294]. Therefore, it may be predicted that the silenced *ano10a* and increased *fmr1* gene may drift the cerebellar ataxia pathogenesis into a more complicated situation. As a practical approach, if the increase of *fmr1* gene in response to *ano10a* knockdown supports the second proposed approach above, then potential *fmr1* inhibitor injections may be warranted to decrease the severity of cerebellar ataxia pathogenesis. The detected upregulation of all investigated genes in the knockdown of *ano10a* may be used either to assign novel functions to the *ano10a* by examining these genes or to suggest their potential inhibitors as therapeutics for the cerebellar ataxia if these increased gene levels trigger the development of disease phenotypes.

#### 4.7. The Regulatory Effect of *wdr81* Knockdown on the Expression of Cerebellar Ataxia Associated Genes

Alterations in the expression level of 11 genes (two of them were targeted genes; the remaining 9 were chosen according to Clustergram Analysis) including, *ano10a*, *vldlr*, *ano10b*, *ttbk2b*, *grid2*, *wwox*, *stubb1*, *atxn1a*, *fmr1*, *itpr1b* and *atxn2* genes were also detected in the WDR81 MO injected embryos at 24 hpi, 48 hpi and 72 hpi developmental stages (Figure 3.10). The overall downregulatory effect of *wdr81* knockdown on the expression of two targeted (*ano10a* and *vldlr*) and 9 highly correlated (*ano10b*, *ttbk2b*, *grid2*, *wwox*, *stubb1*, *atxn1a*, *fmr1*, *itpr1b* and *atxn2*) genes was detected. Although *ano10b* and *stubb1* showed increased transcript levels in response to *wdr81* silencing, these changes in the expression levels were not significant as compared to the standard control injected embryos and also the compensatory effect on the expression levels did not occur as fast as the ANO10a MO injected group, the increased expression in *ano10b* and *stubb1* was observed after the 48 hpi developmental period.

The first investigated gene *ano10a* was downregulated in its expression at the 24 hpi, 48 hpi and 72 hpi developmental points when the *wdr81* gene was silenced. As it was remarked previously, *ano10* is a transmembrane protein encoding gene and responsible for the regulation of intracellular  $\text{Ca}^{2+}$  signaling [69], [71], [72]. Additionally, it is thought that this gene also plays roles in the transportation of glucose [73] and other sugars [73], bile salts [74]–[76], metal ions [76]–[78], organic acids [79], amine compounds [78], [80], [81] and phospholipids [82]. The decrease in the *ano10a* expression after the *wdr81* gene was silenced using MO technology

may still confirm that *wdr81* and *ano10a* may interact with each other in converging pathways. The influence of *ano10a* knockdown on the expression level of *wdr81* gene also implied the similar interpretation as discussed in the previous paragraph. Therefore, *ano10a* and *wdr81* may be involved in the transportation of ions, glucose, organic acids and above mentioned chemical molecules [73]–[82] or in the intracellular  $\text{Ca}^{2+}$  signaling [69], [71], [72] or in the PI3K pathway [250].

The *ano10b* gene, which is the paralog of *ano10a*, was also included in the *wdr81* knocked down group and the expression level changes at 24 hpi, 48 hpi and 72 hpi developmental stages as compared to the standard control MO injected samples were examined. The changes in the expression levels of *ano10a* and its paralog *ano10b* were not exactly same. Although both genes decreased their expression levels as compared to the standard control MO injected embryos at the 24 hpi and 48 hpi developmental stages, the changes in the expression levels of *ano10b* at those time periods were significant but the changes in the expression levels of *ano10a* were not. The second difference was that the downregulation pattern in *ano10b* altered its direction and its expression was upregulated at 72 hpi as the downregulation expression pattern of *ano10a* continued at the 72 hpi time period. These differences between two paralogs may be caused by approximately 50% difference in their coding sequences. The significant decrease in the *ano10b* at both the 24 hpi and 48 hpi developmental stages also may support the correlation analysis done with Clustergram. The correlation coefficient of *ano10b* and *wdr81* ( $R^2 = 0,73$ ) was slightly higher than the correlation coefficient of *ano10a* and *wdr81* ( $R^2 = 0,72$ ). Additionally, the upregulation in the level of *ano10b* at the 72 hpi developmental

stage may indicate that *ano10b* and *wdr81* may have closer interactions than *ano10a* and *wdr81*. Therefore, the regulatory influence of *ano10b* would be more than *ano10a* on the *wdr81* related pathways such thing as PI3K [250] which indicates the neofunctionalization between two different paralogs.

The expression level of another targeted gene *vldlr* decreased to less than one third of its normal level at 24 hpi and to less than half at the 48 hpi developmental stages. The decreased expression of *vldlr* was protected at the 72 hpi developmental point; however, the downregulation of this gene at that stage was not significant as in the case of 24 hpi and 48 hpi periods. The significant downregulatory effect of WDR81 MO on the *vldlr* gene may not only confirm the high correlation coefficient between these two genes ( $R^2 = 0,79$ ) obtained from the previous clustering analysis but also may suggest that *wdr81* may act as an activator of the *vldlr* in the Reelin [124]–[129] and/or triglyceride [130] signaling pathways. Therefore, it is not surprising that *wdr81* knockdown would cause decreased activity in above referred pathways by influencing the transmission of signal along the intracellular elements. In terms of the Reelin signaling pathway, the decreased *vldlr* expression may affect the RTKs activity and this may cause decreased phosphorylation of downstream Dab1 molecule. As a result, the congenital defects in developing cerebellum can be encountered and the mechanisms of both neuronal migration and synaptic function can be disrupted as well [295]. The *wdr81* knockdown dependent downregulated *vldlr* activity may also pose a threat for the triglyceride metabolism as suggested in Tacke *et al* 2000 [130]. The deficiency in the level of *vldlr* may decrease the uptake of VLDL-triglyceride through the periphery and may alter the serum triglyceride



balance [130]. Thus, it is proposed that *wdr81* may be involved in the *vldlr* regulated Reelin signaling pathways and triglyceride metabolism [124]–[130], [295].

The tau and tubulin kinase *ttbk2b* also showed a decreased expression pattern among the all investigated time points as compared to the standard control MO injected siblings. Although the significant decline in the expression level of *ttbk2b* was detected at 48 hours after the WDR81 MO injection, the decreased expression profile observed at the 24 hpi, 48 hpi and 72 hpi developmental stages was similar to *ano10a* and *vldlr*. The downregulation of *ttbk2b* in response to the *wdr81* silencing may indicate that *wdr81* may be a positive regulator of the cellular events that are mediated by the *ttbk2*. In addition to the previously discussed kinase role of this gene on the activity of certain cellular proteins [258]–[261], *ttbk2* is also responsible for the ciliogenesis event requiring the coordination of motor driven transport, membrane trafficking and selective import of cilium specific proteins from a barrier at the ciliary transition zone [296]. If this *ttbk2* gene is mutated or its expression is decreased, the inevitable impairments in the ciliogenesis mechanism result in defects in CNS [297]. Therefore, the locomotion and body posture related problems can be triggered by the impaired ciliogenesis due to the decreased activity of *ttbk2* as a result of a deficient *wdr81* gene in patients with CAMRQ2 [49]–[51].

The excitatory glutamate neurotransmitter receptor encoding *grid2* gene also showed a downregulated expression pattern at the 24 hpi (declined to less than quarter), 48 hpi (declined to less than one third) and 72 hpi developmental stages when WDR81 MO was used. The downregulation of *grid2* was significant at the 24

hpi and 48 hpi stages in response to the standard control MO injected siblings. The downregulation trend was sustained 72 hours after WDR81 MO knockdown but there was no significant decrease in the expression of *grid2* between MO injected and standard control injected groups. This gene is involved in synapse organization and modulation of synaptic communication. Moreover, it is necessary for the development and correct functioning of the movement associated brain area, cerebellum. It was shown in Hills *et al.* 2013 that *grid2* gene deletion caused cerebellar ataxic and atrophic phenotypes in mice [263], [298]. Therefore, the *wdr81* knockdown dependent *grid2* downregulation may induce and speed up the progression of cerebellar defects in patients with the CAMRQ2 movement disorder.

The decreased expression pattern also was observed in the WW repeat containing oxidoreductase, *wwox* gene among all of the investigated time periods in response to the WDR81 MO injection. The expression of this gene significantly decreased to the less than half of the endogenous level at the 24 hpi. Although the downregulated *wwox* expression profiles were maintained at both the 48 hpi and 72 hpi developmental periods, the changes in the levels of *wwox* expression at 48 and 72 hpi were not significantly different than their standard control MO injected siblings. The decreased *wwox* gene was thought to decrease the activity of *wwox* involved in cellular pathways such as the TGFB1 and TNF signaling pathways [265], [266]. When the signal transmitted through TNF pathway was downregulated due to the *wdr81* knockdown dependent *wwox* downregulation, it causes the inactivation of intracellular kinases, extracellular signal-regulated kinase (ERK), janus kinase (JNK) and mutagen activated kinase (p38) [299]. Therefore, cells may become more prone to

cancer development and may not induce enough immune response against the pathogen invaders. However, if the TGFB1 pathway activity decreases due to the downregulated *wwox* expression level, the downstream signal transduction elements, serine-threonine kinases, cannot activate the SMAD proteins through phosphorylation [300]. So, TGFB1 may not work as an anti-proliferative agent anymore; whereas, it may serve as an oncogenic factor and cells ones more would be more susceptible to develop tumors as in the case of inactivated TNF signal transduction [301], [302]. Moreover, the deficiency in the *wwox* was also detected in the cerebellar ataxia [303]. Therefore, the downregulation of the *wwox* due to the defective or decreased *wdr81* may lead to more severe neurological symptoms in CAMRQ2 such as cognitive decline, optic atrophy and hearing loss in addition to the main clinical features appearing as uncoordinated gait, upper extremity control loss, and the impairment of speech, swallowing and eye movement [47], [304].

The other gene, *stub1*, changed its expression level in response to *wdr81* silencing at the 24 hpi, 48 hpi and 72 hpi developmental stages. Apparently, there were no consistent and significant differences in its expression levels after the knockdown of *wdr81* as compared to the standard control MO injected siblings. The changes in the expression level of *stub1* at the 24 hpi and 72 hpi developmental stages were less than the standard control MO injected groups whereas the expression level of it at the 48 hpi time periods was higher than the standard control MO injected siblings. Actually, this result is not completely contradicting the previous results but interestingly different than was expected. Since *stub1* plays a role in the ubiquitin proteasome pathway to degrade misfolded proteins [270]–[273],

it was strange not to see any significant changes in its expression when the predicted UBC interaction containing (Figure 3.1) and ubiquitinated protein degradation facilitator [111], *wdr81* was silenced. It can be thought that although *wdr81* may have interactions with many ubiquitin proteins, it may not have to participate in the ubiquitination process. It may most probably be included by the proteasome system after a protein is ubiquitinated. So, the level of upstream ubiquitin ligase protein encoding *stb1* gene expression was not altered due to *wdr81* deficiency.

The decreased expression profile seen in another gene was *atxn1a* after the WDR81 MO was applied to zebrafish embryos. The expression of this gene was decreased to half of its endogenous level at the 24 hpi and 48 hpi stages ( $p$ - values  $< 0.05$ ) and the expression was still less than the standard control MO injected siblings at the 72 hpi developmental stage ( $p > 0.05$ ) but this difference was not significant as in the case of first two time periods. The significant decline in the *atxn1a* would disrupt especially the Gsk3b pathway thereby the bioenergetics homeostasis in cerebellum and as well impairing the RNA processing [286], [287]. Thus, likewise as with the overexpression of *atxn1*, the downregulation of it may also explain the severe ataxia symptoms due to disrupted cerebellum bioenergetics in CAMRQ2 when the causative gene *wdr81* was knocked down. The *atxn2* was another gene showed to decrease its gene expression profile at the 24 hpi, 48 hpi and 72 hpi developmental stages in response to the *wdr81* silencing as compared to their standard control MO injected siblings. The expression of this gene was decreased to the half of its endogenous expression at the 24 hpi and 48 hpi developmental stages ( $p$ -values  $< 0.05$ ) and the mRNA transcript of *atxn2* was still less than the standard

control MO injected siblings at the 72 hpi stage but there were no significant differences between WDR81 MO injected and standard control MO injected groups at that time period. The decreased *atxn2* expression after WDR81 MO injection may dysfunction RNA metabolism, mTOR signaling, mitochondrial function and endocytosis cellular processes [282]–[285].

The effect of *wdr81* knockdown on *atxn2* may impair the activity of referred pathways showing the indirect regulatory roles of *wdr81* gene in those pathways through *atxn2*. The second interpretation of the decreased *atxn2* after *wdr81* gene silencing may suggest ameliorations against cerebellar degeneration as opposed to the triggered disease symptoms. It was published previously in Van den Heuven *et al.* 2014 and Pulst *et al.* 2016 that the *atxn2* gene silencing using antisense oligonucleotide has slowed down the progression of motor phenotype and recovered the impaired action potential in cerebellum [303], [305]. Thus, the decreased *atxn2* in *wdr81* deficient CAMRQ2 neurological syndrome may try to improve the potential degenerative phenotypes in cerebellum providing hope to produce interventions not only for CAMRQ2 but also for patients with other types of neurodegenerative disorders.

The *fmr1* gene also exhibited decreased gene expression at the 24 hpi, 48 hpi and 72 hpi developmental stages in response to WDR81 MO injection. The changes in the expression level of *fmr1* at 24 hpi and 48 hpi developmental time points were significant (p-values < 0.05) and the expression was still lower than the expression of standard control MO injected siblings at the 72 hpi time point but there was no

significant difference between these two groups at that stage (p-value > 0.05). The downregulated *fmr1* gene due to the silenced *wdr81* may cause impaired RNA transportation and translational control of neurodevelopmental processes and synaptic plasticity [292]–[294]. Moreover, the absence of *fmr1* gene is proposed to give rise to the development of mental retardation [306]. So, the *wdr81* knockdown dependent downregulation of *fmr1* gene may not only confirm the critical importance of *wdr81* gene in neurodevelopment and neuronal connections but also regulate the the observed mental retardation and cognitive impairment symptoms in CAMRQ2 patients when *wdr81* was mutated due to the decreased *fmr1* gene activation. As predicted through the metabotropic glutamate receptor (mGluR) theory, the decreased *fmr1* stimulates mGluR1 and mGluR5 which triggers the internalization of  $\alpha$ -amino-3-hydroxy-5-methylisoxazole-4-propionic acid receptors (AMPA) and eventually leads to long-term depression (LTD), underlying the reason behind cognitive decline [307]. This theory might offer new directions for therapies related to the mental retardation phenotype in CAMRQ2 by inhibiting the overactivity of mGluR with their proper antagonists.

The *itpr1b* also decreased its expression level at the 24 hpi, 48 hpi and 72 hpi developmental stages when the *wdr81* gene was silenced. Although the decreased expression profile was observed among all three time periods, the significant expression decrease, to less than quarter of its endogenous expression (p-value < 0.05) was only obtained 48 hours after *wdr81* knockdown. Interestingly, there were no significant decreases in the expression of *itpr1b* at the 24 hpi and 72 hpi developmental stages compared to the standard control MO injected siblings (p-

values > 0.05). The decreased expression of *itpr1b* after *wdr81* gene knockdown may cause defects in the phosphorylation of PLC isozyme by RTKs and therefore inactivate PLC cannot cleave PIP<sub>2</sub> into IP<sub>3</sub> and DIG molecules. The IP<sub>3</sub> cannot interact with *itpr1* and cannot trigger the opening of intracellular Ca<sup>2+</sup> channels. As a result, *wdr81* knockdown dependent *itpr1* gene downregulation may cause reduction in the Ca<sup>2+</sup> release from the endoplasmic reticulum [268], [278], [279], [308]. Therefore, the indirect effect of *wdr81* in the regulation of Ca<sup>2+</sup> metabolism would also affect the activity of several other Ca<sup>2+</sup> dependent cellular processes such things as cell division and muscle contraction [280], [281]. Furthermore, it was proposed that the deleterious mutations in *itpr1* cause cerebellar ataxia [308]. So, as in the case of *ttbk2b*, *grid2*, *wwox*, *atxn1a* and *fmr1*, in CAMRQ2 syndrome, *wdr81* deficiency dependent decreases in *itpr1* gene expression may worsen or increase the severity of cerebellar ataxia associated phenotypes.

#### **4.8.The Regulatory Effects of *vldlr* Knockdown on the Expression of Cerebellar Ataxia Associated Genes**

The third and last single knockdown was performed with the targeted *vldlr* gene. The expression level changes of two targeted genes, *wdr81* and *ano10a* and 9 highly correlated cerebellar ataxia associated genes were studied. The VLDLR MO caused the most diverse response in the expression levels of the genes. Some of the investigated genes increased their expression at certain developmental stages such as *wdr81*, *ano10a*, *ano10b*, *ttbk2b*, *grid2* and *stub1* whereas many of genes decreased their expression profile in response to the silencing of *vldlr*. The obtained upregulation pattern was not significant for none of them; however, the decreased

expression pattern for many investigated genes was significant at certain investigated developmental stages. Therefore, the effects of VLDLR MO can be accepted as more similar to WDR81 MO downregulatory response rather than the ANO10a MO upregulation pattern. The effects of *vldlr* silencing on the expression of the investigated genes and related pathways can be discussed in the following manner.

There were no significant changes in the expression levels of the two other targeted genes *wdr81* and *ano10a* at the 24 hpi, 48 hpi and 72 hpi developmental stages. However, the higher expression of these genes when the VLDLR MO was used as opposed to the standard control MO injected siblings demonstrated that these genes activate compensatory mechanisms to fulfill the decreased activity of *vldlr*. The increased expression of these genes may indicate that *wdr81* and *ano10a* may be involved in the cellular pathways that are regulated by the *vldlr*. So, the *wdr81* and *ano10a* may play roles in the cortical layer formation, Reelin signaling pathway and triglyceride metabolism. Additionally, it can be also derived that *vldlr* may serve as a negative regulator for the *wdr81* and *ano10a* containing pathways. For example, the decreased *vldlr* expression would increase the activity of PI3K and intracellular  $\text{Ca}^{2+}$  signaling pathways. The increased PI3K pathway activity is considered a hallmark of cancer [309] whereas the influx of  $\text{Ca}^{2+}$  into cells is thought to initiate apoptotic cascades [310]. Neurons are one of the most fragile cells whose activities are perturbed as a result of excess  $\text{Ca}^{2+}$  influx [310]. Fortunately, the changes in the expression levels of these two genes were not significant so that the above predicted speculations about their regulatory activities in the referred cascades would not appear as a result of *vldlr* knockdown. The expression of *ano10b* was affected



differently from the *vldlr* knockdown than its paralog *ano10a*. Its expression dropped significantly to the half of its normal level at the 24 hpi stage and the expression level changes of this gene show no significant differences as compared to standard control MO injected groups at the 48 hpi and 72 hpi time periods, its expression was increased at 48 hpi and was followed by a decrease in gene expression at the 72 hpi periods. Therefore, the silenced *vldlr* mainly caused downregulation in the *ano10b* expression and thereby *ano10b* associated pathways. Interestingly, *vldlr* deduces the activity of intracellular  $\text{Ca}^{2+}$  signaling not on *ano10a* but on *ano10b* gene. This may be again explained by the neofunctionalization of paralogs.

The expression level of *ttbk2b* decreased to half of its endogenous expression at 48 hpi stage. This *vldlr* dependent decrease in *ttbk2* disrupts the ciliogenesis mechanism which causes impairments in the CNS [297]. Therefore, the observed gait and body posture disturbances in patients with CAMRQ1 can be derived from the causative *vldlr* dependent decreased *ttbk2* activity. The expression of *grid2* significantly decreased to half of its endogenous level at 24 hpi and 48 hpi developmental stages (p-values < 0.05).

This downregulated expression pattern may negatively affect the activity of *grid2* regulated synaptic events [263]. Furthermore, the importance of *grid2* in the developing cerebellum also may explain the cerebellar ataxia and atrophy phenotypes when this gene is deficient especially during embryonic and the early childhood [298]. Therefore, it can be suggested that the *vldlr* knockdown dependent *grid2* downregulation may hasten and trigger the progression of cerebellar ataxia

symptoms in patients with CAMRQ1. The *wwox* gene also showed a significantly decreased expression pattern at 24 and 48 hours after VLDLR MO injection as compared to the expression levels of standard control MO injected groups.

The decreased expression pattern for *wwox* was maintained also at the 72 hpi developmental stage; however, there were no significant differences between the VLDLR MO injected and standard control MO injected siblings at that time period. In short, the injected VLDLR MO may have decreased the expression of *wwox* and this leads to the inactivation of intracellular pathway kinases of TGFB1 and TNF signaling cascades [265], [266], [299], [300]. These inactivated kinases of these two pathways such as JAK, p38, ERK and serine threonine kinases cannot phosphorylate and these pathways cannot activate downstream pathway elements so that the cells may not arise immune response against pathogens and they may induce tumor development [299]–[302]. Furthermore, the deficiency of this gene is associated with cerebellar ataxia [303]. Therefore, the *vldlr* dependent *wwox* expression level decrease in the patients with CAMRQ1 may trigger more complicated and serious symptoms such as cognitive decline, hearing loss and optic atrophy combined with general ataxia phenotypes including uncoordinated walking, disturbed body posture, impaired speech, swallowing and eye movement.

The following expression level analysis was performed on the gene, *stabl*. Interestingly, there were no significant differences in the expression levels of the *stabl* gene between the VLDLR MO injected groups and standard control MO injected siblings at the 24 hpi, 48 hpi and 72 hpi developmental stages. This was

interesting because of the fact that *stub1* and silenced gene *vldlr* was supposed to interact with each other in the ubiquitin proteasome pathway. Actually, this idea was not supported with already published papers; but, the predicted interaction between *vldlr* and UBC protein (Figure 3.1) was the reason to expect a change in the expression level of ubiquitin ligase gene, *stub1* in response to *vldlr* knockdown. As discussed previously, the unaffected expression profile of *stub1* after *vldlr* gene silencing may not completely refute the interaction and potential role of *vldlr* gene in the ubiquitin pathway. This gene may be involved by the proteasome system after a protein is ubiquitinated. Therefore, the upstream actual ubiquitination process responsible gene expression may not be affected from the decreased level of *vldlr*.

The *atxn1a* also decreased its expression level in all investigated time periods after *vldlr* gene was silenced in compared to the standard control MO injected groups. The expression level significantly declined to half of its endogenous level at the 24 hpi and 48 hpi developmental stages (p-values < 0.05). Although the level of decreased expression was sustained at the 72 hpi stage, there were no significant differences in the expression level of *atxn1a* between *vldlr* gene silenced and standard control MO injected siblings at that period. The decreased *atxn1a* expression may influence the action of Gsk3b pathway and this would most probably distort the bioenergetics balance in the cerebellum [286], [287]. Additionally, downregulated *atxn1a* may hamper the RNA processing steps [286], [287]. The disrupted RNA and bioenergetics homeostasis especially in the cerebellum may clarify the observed CAMRQ1 phenotypes in *vldlr* gene deficient patients that may be owing to a more complex background than the apparent one. Disease

development or progression may be affected from the *vldlr* interacting genes and clearly due to its cellular functions *atxn1* may be just one of these genes. The expression level of *atxn2* gene also decreased at the 24 hpi, 48 hpi and 72 hpi developmental stages when the VLDLR MO was injected to the embryos as compared to the standard control MO injected siblings. Although the decreased expression pattern was detected at all of the investigated stages, the expression of *atxn2* in the VLDLR MO injected embryos was significantly less than the standard control MO injected siblings only at 24 hpi stage (p-value < 0.05). This statistically meaningful decreased expression of *atxn2* may negatively affect the activity of RNA metabolism, mTOR signaling, mitochondrial processes and endocytosis [282]–[285]. This regulatory effect of *vldlr* on *atxn2* can assign unknown functions to the *vldlr* gene in above referred pathways. Actually, the same hypothesis for *wwox*, *ttbk2*, *grid2* and *atxn1a* genes may not be applicable for this gene. Contrarily, *atxn2* downregulation might carry therapeutic purposes. It was proposed that the silenced *atxn2* gene can decelerate the progression of motor defects and can restore the impaired neuron firing in cerebellum [302], [305]. Thus, as opposed to the expected results, *vldlr* gene deficient CAMRQ1 patients may try to recover the degenerations in cerebellum by decreasing the *atxn2* mRNA or protein level using inhibitors or interfering RNAs.

The *fmr1* gene also declined its expression significantly at the 24 hpi and 48 hpi developmental stages (p-values < 0.05) when the VLDLR MO was injected as compared to the standard control MO injected embryos. This statistically significant decrease in the expression of *fmr1* may induce defects in mRNA splicing, mRNA

stability and mRNA transportation steps, which may exert special importance especially for neuronal development and synaptic communication processes [292]–[294]. The indirect effect of *vldlr* on these cellular events may illustrate that *vldlr* may take role in the regulation of RNA homeostasis. Additionally, the characterized mental retardation phenotype of patients with CAMRQ1 may be connected with decreased *fmr1* due to mutated or insufficient *vldlr* function. One of the advantages of this connection may be that at least the cognitive impairment symptoms in CAMRQ1 disorder can be eliminated by restoring the activity of influenced *fmr1* downstream elements. Therefore, this possibility once more may enable the discovery of novel therapeutics against cerebellar ataxia.

The effect of *vldlr* knockdown on the expression level of *itpr1b* at 24 hpi, 48 hpi and 72 hpi developmental stages was downregulatory. Although the decreased *itpr1b* expression pattern of VLDLR MO injected embryos differs significantly (decreased to approximately a quarter of its endogenous expression) from the standard control MO injected groups only at the 48 hpi stage (p-value < 0.05), the reduction of *itpr1b* may distort the  $\text{Ca}^{2+}$  ion homeostasis thereby  $\text{Ca}^{2+}$  ion activated pathways activity in other experimental time periods as well [274], [308], [311]. Actually, the influence of  $\text{Ca}^{2+}$  influx especially in the *vldlr* controlled neuronal and synaptic functions may suggest a cross-interaction between *itpr1b* and *vldlr*. The downregulated *vldlr* may decrease the expression level of *itpr1* and this would impair the entrance of  $\text{Ca}^{2+}$  ions to cells, which then may downregulate the *vldlr* activated synaptic plasticity. Therefore, the encountered CAMRQ1 disorder as a result of

deficiency in *vldlr* gene may be actually triggered by the disturbance in the activity of interacting *itpr1* function.

The single MO injection study of *ano10a*, *wdr81* and *vldlr* showed a potential functionally close interaction of these genes with each other, which may indicate that these genes can share the same or similar functions within the converging pathways [312]. Moreover, the regulatory influence of targeted gene silencing also on the expression levels of the 9 other cerebellar ataxia associated genes may enable the discovery of novel roles for the *ano10a*, *wdr81* and *vldlr* as discussed above. However, all of the function of these genes and their interactions will need to be validated at the protein level and this future direction, as well as others; will be discussed in the next chapter. Nevertheless, the unmasking of the interaction pattern among genes may also suggest new therapeutic avenues against cerebellar ataxia by using antagonists or inhibitors for the overactivated cascades by supplying the inactivated downregulatory elements. Through this way, the war not only against multiple types of cerebellar ataxias but also against all other neurological disorders can be defeated.

#### **4.9. The overall upregulation of all investigated genes when *ano10a* gene silenced may activate a compensatory response in the biological systems**

The increased expression of all genes when *ano10a* silenced may propose the activated compensatory mechanism in the cellular events. This situation significantly observed only when ANO10a MO was used to silence the *ano10a* gene and was not encountered when both WDR81 and VLDLR MOs injected to knockdown those

genes. This may indicate that *ano10a* knockdown can activate a compensatory mechanism on the other investigated genes to ensure similar developmental outcomes and ensure the transduction of signals through several biological pathways despite the minor differences in genetic makeup or in the environmental conditions. The activated compensatory response after the *ano10a* silencing has been attributed to a myriad of different reasons. However, four most common ideas would be discussed in this section. Firstly, the genetic robustness is aroused due to the fact that *ano10a* may be a redundant gene whereby the absence of one gene can be compensated by another or others with the similar functions and similar expression patterns as detailed for each silenced gene in the above sections [313]–[322]. Secondly, the compensatory mechanism can also be activated through tightly regulated cellular signaling, metabolic and transcriptional networks. If the cellular function of a particular gene is disrupted in a signaling pathway due to mutations or knockout/knockdown agents, this would alter the function through the converging pathways. Thus, it can be implied that *ano10a* gene may take role in the same or interacting pathways thereby sustaining the cellular wellness and rescuing the defected outcome [322]–[326]. Another robustness that also brings a reasonable explanation is the dosage compensate mechanism that is activated in male flies to have two fold increase in transcribed genes from their single X chromosome and equalize the levels of gene expression with two active X chromosomes including female flies [322], [327], [328]. On the contrary, in the mammals, one of two X chromosomes is inactivated by undergoing the heterochromatin structure and this ensures the similar developmental stages between two different genders [322], [329]–[331]. This robustness cannot be proper system for the zebrafish model

organism that was used throughout the course of this study to test the proposed hypothesis; since, the sex chromosomes have not identified for this animal, yet [322], [332]. Lastly, the compensated mechanism was appeared as a result of the knockdown of *ano10a* may suggest that *ano10a* may be a housekeeping gene [322], [333]. As it is well-known, the housekeeping genes undertake essential functions in the cellular events. Therefore, when a mutation takes place in the specific housekeeping gene or if it is knockout or when its activity is decreased by using knockdown technology, it is expected that the loss of housekeeping gene may be deleterious for survival or may trigger the development of certain disorders [333]. However, most of the time, when a housekeeping gene is mutated, deleted or silenced, there were no such expected outcomes would be observed as a [333]. This situation can be explained through genetic compensation mechanism. The defected activity of a housekeeping gene can be retained through the relevant family members or through its evolutionarily paralogue(s) so that the cells survive and they do not show any disease associated behavioral phenotypes. The activated compensatory mechanism when *ano10a* gene was silenced may imply that *ano10a* may be a redundant gene [322]–[326] or it may be a housekeeping gene [322]. Additionally, the genetic robustness can be appeared due to altered function in the converging pathways or dosage compensation mechanism [322]. However, the absence of sex chromosomes in the zebrafish refutes the dosage compensation system in the context of the current study [332].



# CHAPTER 5

## CONCLUSIONS AND FUTURE PERSPECTIVES

The findings of current study provided important conclusions into the role of *ano10*, *wdr81* and *vldlr* in the context of cerebellar ataxia. Firstly, the results from the bioinformatics analysis of the targeted genes with the String Database predicted that the protein products of ANO10, WDR81 and VLDLR are interacting with common UBC protein. This can be further interpreted that the protein products of the genes of interest may play a role in neurodegenerative development in cerebellar ataxia due to protein accumulation depending on or independent from the disruptions in the ubiquitin degradation pathway. The Motif Scan database results gave a common  $\text{Ca}^{2+}$  activated Casein Kinase (CK) 2 domain in the protein sequences of targeted genes. The involvement of CK2 in the phosphorylation of neurodegenerative disorder-related proteins and/or co-localization with their protein aggregates [334] may explain the observed neurodegenerative phenotypes in cerebellar ataxia when CK2 hyperphosphorylates *ano10*, *wdr81* and *vldlr*. Thirdly, the expression level analysis of *ano10a*, *wdr81* and *vldlr* was shown in zebrafish embryos that were collected from 12 different developmental stages. Obtained results show that the expression level of three targeted genes were detected relatively higher at 1 hpf, 2 hpf and 5 hpf time points than the rest of the other embryonic and larval time points, which may emphasize that these genes play important roles in developmental processes. Moreover, the performed RNASeq transcript analysis during early

embryogenesis was in parallel with above findings. Furthermore, the expression pattern comparison of these three genes during early embryogenesis revealed that *ano10a*, *wdr81* and *vldlr* were co-localized at the diencephalon, midbrain (tectum) and cerebellum. This observation may restrict the importance of three targeted genes selectively in neurodevelopment. Fourthly, it was the first time that the mRNA transcript level analysis of *ano10a*, *wdr81* and *vldlr* genes in 12 different adult animal tissues was performed. There were no other studies in zebrafish that indicated the expression levels of these three genes using such a big range and sexually dimorphic perspective. The findings demonstrated that *ano10a*, *wdr81* and *vldlr* were expressed relatively higher in the brain, eye and gonads. Additionally, the analysis in males and females indicated that the expression of *ano10a* and *wdr81* were significantly different in eye, gills, liver and gonads (p-values < 0.05), whereas *vldlr* mRNA transcript was significantly different in the swim bladder and gonads (p-values < 0.05). Fifthly, the clustergram analysis illustrated that the targeted genes of interest were clustered in close families with each other and other cerebellar ataxia associated genes. This result can be interpreted that they may act in the converging pathways and undertake some regulatory roles to help with the correct functioning of each another. The clustergram analysis led to the design and performance of interaction studies by knocking down the expression of each target gene of interest separately using a MO oligonucleotide approach to search for the effect on the expression of other two target genes and 9 other cerebellar ataxia associated genes. Single MO injections resulted in significant upregulation in the expression levels of almost-all investigated genes 72 hours after/post injection (hpi), especially when particularly *ano10a* was silenced. This data might suggest activated compensatory

mechanisms or disease associated signals in the cell. Taken together, the consequences of the functional knockdowns of three targeted genes will aid in the discovery of potential therapeutic targets that could lead to potential interventions against the onset of cerebellar ataxia.

As future directions for this current line of investigation, certain experiments could be designed and performed in order to further do research and determine the novel functions of the targeted genes, *ano10a*, *wdr81* and *vldlr* genes and their potential protein products in the cellular pathways. Firstly, double (*ano10a-wdr81*, *ano10a-vldlr*, *wdr81-vldlr*) and triple (*ano10a-wdr81-vldlr*) knockdown combinations of *ano10a*, *wdr81* and *vldlr* genes could be done with embryos to detect different the responses of the investigated genes to a more severe phenotype than the single knockdowns (*ano10a*, *wdr81*, *vldlr*). This would provide the assignment of novel functions to the genes of interest and also discovery of potential therapeutic targets for intervening in the early onset of cerebellar ataxia. Although knockdown studies give clues about the regulatory roles of the silenced genes, sometimes the partial knockdown of a gene may indicate specific changes in the altered cellular functions or direct disease-related phenotypes due to the fact that there may be a sufficient level of expression in these embryos. Moreover, the risk of off-target effects in the mRNA silencing with MO needs to always be kept in mind as a potential handicap for the knockdown studies. The possibility of targeting irrelevant mRNA sequences in addition to or instead of the intended gene may produce false-positive phenotypes and functions for the gene of interest. So, knockout or mutagenesis systems could be used instead of knocking down of the

genes of interest. To generate knockout zebrafish, the Tol2 mediated gene trapping method or CRISPR/Cas9 technique could be applied [335]–[337]. These transgenesis systems can produce genetically ablated or mutated stable transgenic zebrafish lines for long term functional characterization of the target genes of interest and disease-model of cerebellar ataxia in the future. Basically, the Tol2 system applies asite specific recombination (through *att* sites) that is also known as multisite Gateway technology to create genomic modulation in a quick manner. The Tol2 system is injected with a plasmid DNA and transposase enzyme mRNA to the embryos. The preparation of plasmid DNA in order to give a complete expression construct requires certain cloning and PCR amplification steps. Firstly, the suitable recombination sites are added to the three entry system DNA fragments through PCR reactions and then inserted into the proper donor plasmid (pDONR) vectors via BP reactions. These three entry plasmid vectors are known as 5' elements plasmid (p5E) including promoter sequences, middle entry plasmid (pME) containing coding sequences (gene of interest fragment) and the last one is called as 3' elements plasmid (p3E) including polyA tail to synthesize a fully functional mRNA transcript and a reporter gene to follow the expression of the insert. Additionally, the usage of the tissue-specific promoter enables the labeling of specific structures through fluorescent signal containing reporter transgenes in live embryos and this would cause the knock in or knock out of targeted gene(s) only at the particular tissues not throughout the whole organism. Furthermore, the availability of the promoters that allow the expression of genes when certain conditions are fulfilled also makes it possible to control transcription temporally. For example, the *hsp70* gene promoter could be used in order to induce the overexpression of gene of interest(s) under heat

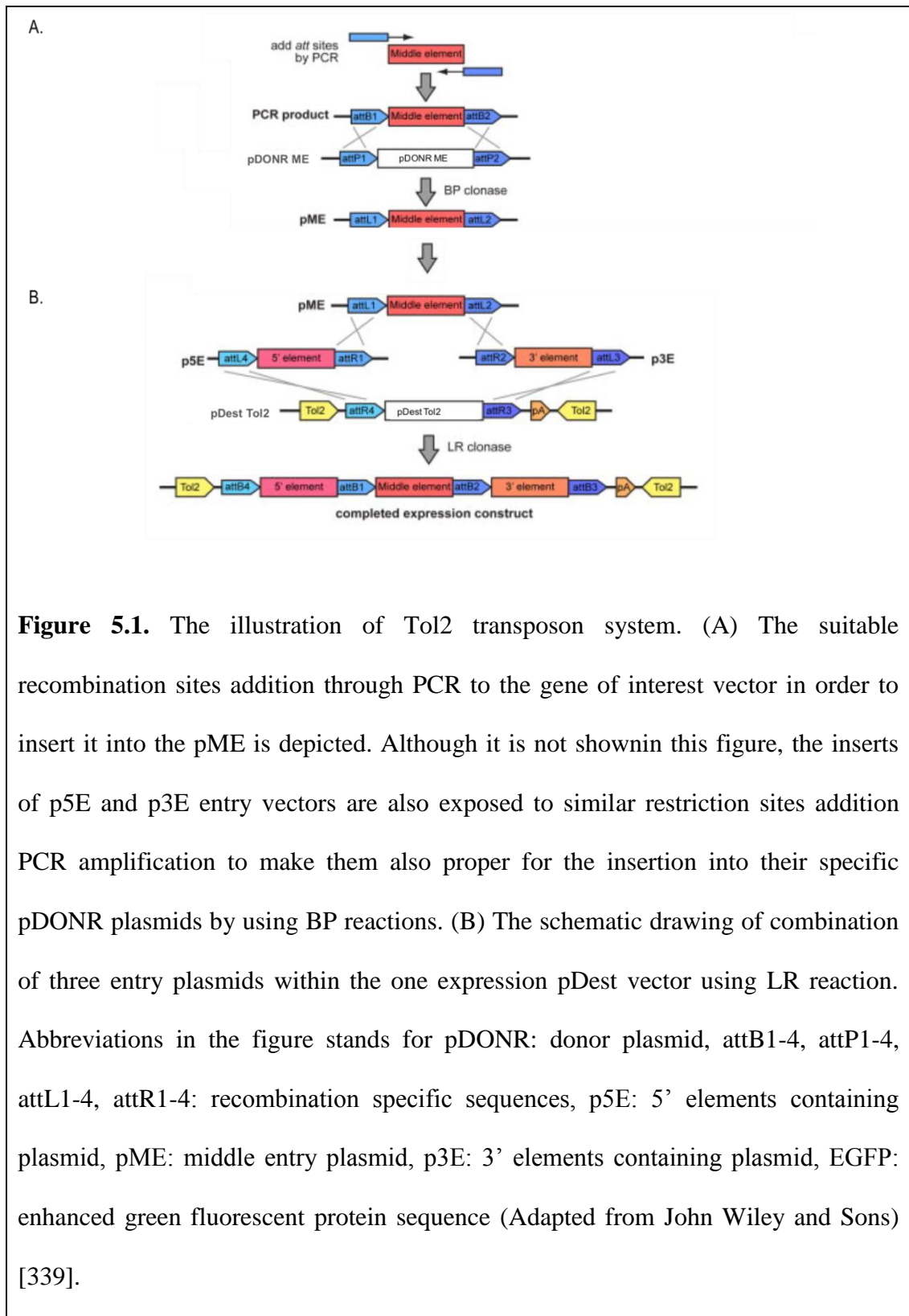
shock. Secondly, these three plasmids p5E, pME and p3E are combined within the destination (pDest) vector through LR reactions. After that point, the three entry plasmids containing pDest are known as the expression construct [338]–[344]. Then, this generated final expression vector in which gene of interest is inserted for this case, which is depicted in Figure 5.1, is given to the embryo with the transposase mRNA [339].

As previously mentioned the Tol2 system can be successfully used in order to knock in to overexpress the wild type or mutated genes of interest. This approach also can be utilized so as to inhibit the expression of targeted proteins or their transcript variants through gene trapping method. The gene trapping system provides the insertion of reporter fluorescent protein into the intronic sequence of the expressed gene to terminate the transcription at the polyadenylation site. Therefore, the truncated or nonfunctional protein is transcribed as a result. From that perspective, the Tol2 mediated transgenesis technique can help eliminate the action of specific genes or their protein products in living organisms to determine the functions of novel genes during early development and as well as at the level of adult animal. This Tol2 system is a more efficient method than the already applicable *Sleeping beauty*, *Tc3* and *I-SceI* meganuclease, *Gal4/UAS* systems [342], [345]. The conditional knockout of *wdr81* and multiple varieties of *vldlr* in mice were applied in a myriad of research experiments to answer diverse scientific questions. The absence of an *ano10* knock out mouse might encourage the generation of transgenic zebrafish with the easier and more efficient Tol2 system. Additionally, to resolve the mechanism behind the causes of cerebellar ataxia, generally ataxic phenotype

exhibiting model animals are used in scientific studies. By using the Tol2 transgenesis knock out or knock in approach, one can delete or mutate the causative genes, *ano10a/b*, *wdr81* and *vldlr* in this case and try to generate the disease model of cerebellar ataxia, which would aid in the development of therapeutics in the future.

In the single injection of ANO10a MO, WDR81 MO and VLDLR MO, the experimental samples were collected 24, 48 and 72 hours after the MO injection and those samples were processed to use in the interaction studies to reveal the regulatory effect with each other and with other cerebellar ataxia associated genes. These time periods were chosen to see the gradual effect of single MO injections on the expression of cerebellar ataxia associated genes during early developmental periods. However, these investigated time stages can be changed based on the results of qPCR, RNASeq and WMISH. Instead of 24 hpi developmental stages, earliest stages between 2 hpi-5 hpi can be chosen since the most significant overexpression of three genes of interest were detected at that range. Additionally, the investigated time periods may be determined from the developmental stages when the specific organ or structure develops so that the effect of the silenced gene on the development of particular organ can be also elucidated as well. Since in the current study, cerebellar ataxia causative and associated genes were investigated, it would be reasonable if specific developmental stages when brain and eye develop can be chosen. So, the developments of most of the organs start between at 24 hpf and 48 hpf stages. Accordingly, in addition to the 24 hpi and 48 hpi developmental stages, 27 hpi, 30 hp, 33 hp 36 hpi, 39 hpi, 42 hpi and 45 hpi developmental stages should be included

as well to detect the importance of silenced gene on the developing brain and eyes tissues [346]–[349].



Microarray experiments also could be performed to obtain the gene expression profile from single (*ano10a*, *wdr81*, *vldlr*), double (*ano10a-wdr81*, *ano10a-vldlr*, *wdr81-vldlr*) and triple (*ano10a-wdr81-vldlr*) morphant models. In this method, the differentially expressed genes between morphant and negative control MO injected groups could be detected and common or individually affected mechanisms among the different morphant models might be identified. Additionally, whole transcriptome analysis with microarray could be useful in order to validate the Clustergram analysis result, Figure 3.5, of the current study. Ultimately, the obtained differentiated genes the result from whole transcriptome analysis can enable the discovery of novel roles of *ano10*, *wdr81*, *vldlr* genes in a myriad of cellular cascades.

*In situ* hybridization studies using adult zebrafish brain tissue sections also could be performed in order to obtain the common spatial expression patterns of these three genes. The co-expression of these genes in similar nervous system structures also may indicate the converging functions of these genes in the cellular cascades. Furthermore, the gene expression pattern using the *in situ* hybridization method in adult brain tissues could be done using a sexually dimorphic design. In this case, the expression pattern differences between male and female brains for the target genes of interest could be determined as well.

One of the potential important results could be obtained by combining *in situ* hybridization with an immunostaining technique. Certain neuronal and glial markers could be used to co-localize the expression of targeted mRNA in the neuronal or glial



cells. This could be beneficial to detect whether these three movement disorder related genes are found mainly in neurons or glia cells. Alternatively, a GFP-GFAP zebrafish transgenic line versus a neural specific line could be used to directly determine if the expressed genes are primarily in the glial or neuronal cells. Furthermore, bromodeoxyuridine (BRDU) labeling could be performed in order to detect whether they are expressed on proliferating neurons or not.

Although the performed experiments were done using *anin vivo* animal system, an *in vitro* primary neuronal cell cultures experiment could be applied in order to study the roles of the targeted genes in neuronal migration. Previous studies indicated the importance of *vldlr* and *wdr81* in neuronal migration during early embryogenesis [30], [33], [112], [125]. As the potential regulatory role of *ano10a* on the expression of *vldlr* and *wdr81* and also on the expression of 9 other cerebellar ataxia associated genes during the early developmental stages was suggested in this study, it could be inferred that *ano10a* may be involved in the neuronal migration pathway as well. To check whether this hypothesis is true or not, an experimental setup would need to include overexpressed *ano10a*, silenced *ano10a* and suitable negative control groups. The scratch assay might be done in order to measure the migration rates of neurons in the experimental groups. The same experiments could be conducted for the other two genes of interest, *wdr81* and *vldlr* to indicate that those three targeted genes may be involved in neuronal migration processes, and this would give a chance to compare the rate of migration among three genes as well.

The absence of counter-reactive Zebrafish antibodies against *ano10a*, *wdr81* and *vldlr* prevents the investigation of changes at the protein level. If scientists could develop proper antibodies to detect these proteins, firstly Western blot experiments can be performed in order to determine the wild type protein expression of these genes in the certain adult tissues. Secondly, knockdown experiments with translational blocking morpholinos could be done in order to check the changes in the levels of protein products of the targeted genes during early embryogenesis. Thirdly, the previously performed study stating a potential regulatory role of *ano10a*, *wdr81* and *vldlr* knock downs on the expression of the investigated genes using qPCR could be validated. The direct interaction among the protein products of the genes of interest could be confirmed with co-immuno precipitation experiments, which would be possible only when antibodies against targeted proteins are available.

## Bibliography

- [1] S. Fahn, J. Jankovic, and M. Hallett, *Principles and Practice of Movement Disorders*. 2011.
- [2] H. S. Singer, J. W. Mink, D. L. Gilbert, and J. Jankovic, *Movement Disorders in Childhood*. 2016.
- [3] A. Mandal, "Types of movement disorders," 2017. [Online]. Available: <https://www.news-medical.net/health/Types-of-movement-disorders.aspx>. [Accessed: 31-Oct-2017].
- [4] "Movement Disorders Program - Introduction," 2017. [Online]. Available: [http://neurology.emory.edu/programs\\_centers/programs/movement/index.html](http://neurology.emory.edu/programs_centers/programs/movement/index.html). [Accessed: 29-Oct-2017].
- [5] K. D. Flemming and L. K. Jones, *Mayo Clinic Neurology Board Review: Basic Sciences and Psychiatry for Initial Certification*. 2015.
- [6] J. L. Vitek and M. Giroux, "Physiology of hypokinetic and hyperkinetic movement disorders: model for dyskinesia," *Ann. Neurol.*, vol. 47, no. 4 Suppl 1, pp. S131–S140, 2000.
- [7] "Movement Disorders: An Update.," *Can. J. Neurol. Sci.*, vol. 30.
- [8] D. J. Lanska, "Chapter 33 The history of movement disorders," *Handbook of Clinical Neurology*, vol. 95, no. C. pp. 501–546, 2009.
- [9] O. Suchowersky and C. Comella, *Hyperkinetic movement disorders*. 2012.
- [10] R. M. Kurlan, P. E. Greene, and K. M. Biglan, "Hyperkinetic Movement Disorders," *Oxford Univ. Press*, 2015.
- [11] W. F. Abdo *et al.*, "The clinical approach to movement disorders," *Nat. Rev. Neurol.*, vol. 6, no. 1, p. 2937, 2010.

- [12] “Neurology and Neurosurgery.” [Online]. Available:  
[http://www.hopkinsmedicine.org/neurology\\_neurosurgery/centers\\_clinics/movement\\_disorders/ataxia/conditions/index.html](http://www.hopkinsmedicine.org/neurology_neurosurgery/centers_clinics/movement_disorders/ataxia/conditions/index.html). [Accessed: 01-Nov-2017].
- [13] J. Benito-León and E. D. Louis, “Update on essential tremor,” *Minerva Medica*, vol. 102, no. 6. pp. 417–440, 2011.
- [14] D. Tarsy and D. K. Simon, “Dystonia,” *N. Engl. J. Med.*, vol. 355, no. 8, pp. 818–29, 2006.
- [15] U. Wolf, M. J. Rapoport, and T. A. Schweizer, “Evaluating the affective component of the cerebellar cognitive affective syndrome.,” *J. Neuropsychiatry Clin. Neurosci.*, vol. 21, no. 3, pp. 245–53, 2009.
- [16] H. S. Haroun, “Cerebellar Nuclei and Connections in Man,” *Anat. Physiol Biochem Int J*, vol. 1, no. 1, pp. 1–8, 2016.
- [17] P. Tibbetts, :“Principles of Cognitive Neuroscience,” *The Quarterly Review of Biology*, vol. 83, no. 3. pp. 309–310, 2008.
- [18] F. Müller and R. O’Rahilly, “The human brain at stages 21-23, with particular reference to the cerebral cortical plate and to the development of the cerebellum,” *Anat. Embryol. (Berl.)*, vol. 182, no. 4, pp. 375–400, 1990.
- [19] E. Keller, “The cerebellum,” 1989. [Online]. Available:  
<http://teachmeanatomy.info/neuro/structures/cerebellum/>. [Accessed: 02-Nov-2017].
- [20] F. Barahona, M., Leo, Ercinas, J., P., Mora, Pasqual, R., Querol, Linera, J., Alvarez, presmanes, Y., gañan, GIL, M., Á., “Structural and Functional anatomy of cerebellum. More than a motor conception,” in *European Society of Radiology*, 2011, pp. 1–36.

- [21] J. D. Schmahmann, “An Emerging Concept: The Cerebellar Contribution to Higher Function,” *Arch. Neurol.*, vol. 48, no. 11, pp. 1178–1187, 1991.
- [22] J. Voogd and M. Glickstein, “The anatomy of the cerebellum,” *Trends in Cognitive Sciences*, vol. 2, no. 9, pp. 307–313, 1998.
- [23] “Ataxia.” [Online]. Available: <https://www.mayoclinic.org/diseases-conditions/ataxia/symptoms-causes/syc-20355652>. [Accessed: 02-Nov-2017].
- [24] M. Anheim, “Autosomal recessive cerebellar ataxias,” *Rev. Neurol. (Paris)*, vol. 167, no. 5, pp. 372–384, 2011.
- [25] M. Anheim, C. Tranchant, and M. Koenig, “The Autosomal Recessive Cerebellar Ataxias,” *N. Engl. J. Med.*, vol. 366, no. 7, pp. 636–646, 2012.
- [26] M. Ferrarin, M. Gironi, L. Mendozzi, R. Nemni, P. Mazzoleni, and M. Rabuffetti, “Procedure for the quantitative evaluation of motor disturbances in cerebellar ataxic patients,” *Med. Biol. Eng. Comput.*, vol. 43, no. 3, pp. 349–356, 2005.
- [27] F. Palau and C. Espinós, “Autosomal Recessive Cerebellar Ataxias.” 1 (2006): 47. PMC,” *Orphanet J. Rare Dis.*, vol. 1, no. 47, 2006.
- [28] N. Whaley, S. Fujioka, and Z. K. Wszolek, “Autosomal dominant cerebellar ataxia type I: A review of the phenotypic and genotypic characteristics,” *Orphanet J. Rare Dis.*, vol. 6, no. 1, p. 33, 2011.
- [29] P. Khemani, “Chapter 71 – The Inherited Ataxias,” in *Rosenberg’s Molecular and Genetic Basis of Neurological and Psychiatric Disease*, 2015, pp. 811–832.
- [30] M. Renaud *et al.*, “Autosomal recessive cerebellar ataxia type 3 due to ANO10 mutations: delineation and genotype-phenotype correlation study.”

- JAMA Neurol.*, vol. 71, no. 10, pp. 1305–10, 2014.
- [31] U. Tan, “A new syndrome with quadrupedal gait, primitive speech, and severe mental retardation as a live model for human evolution,” *Int. J. Neurosci.*, vol. 116, no. 3, pp. 361–369, 2006.
  - [32] O. E. Onat *et al.*, “Missense mutation in the ATPase, aminophospholipid transporter protein ATP8A2 is associated with cerebellar atrophy and quadrupedal locomotion,” *Eur. J. Hum. Genet.*, vol. 21, no. 3, pp. 281–285, 2013.
  - [33] F. Doldur-Balli *et al.*, “Characterization of a novel zebrafish (*Danio rerio*) gene, *wdr81*, associated with cerebellar ataxia, mental retardation and dysequilibrium syndrome (CAMRQ),” *BMC Neurosci.*, vol. 16, no. 1, p. 96, 2015.
  - [34] K. M. Boycott *et al.*, “Mutations in *VLDLR* as a cause for autosomal recessive cerebellar ataxia with mental retardation (dysequilibrium syndrome).,” *J. Child Neurol.*, vol. 24, no. 10, pp. 1310–1315, 2009.
  - [35] B. R. Ali, J. L. Silhavy, M. J. Gleeson, J. G. Gleeson, and L. Al-Gazali, “A missense founder mutation in *VLDLR* is associated with Dysequilibrium Syndrome without quadrupedal locomotion,” *BMC Med. Genet.*, vol. 13, no. 1, p. 80, 2012.
  - [36] C. L. Kniffin, “Cerebellar ataxia, mental retardation, and dysequilibrium syndrome 1; CAMRQ1,” 2016. [Online]. Available: <https://www.omim.org/entry/224050>. [Accessed: 03-Nov-2017].
  - [37] S. Türkmen, K. Hoffmann, O. Demirhan, D. Aruoba, N. Humphrey, and S. Mundlos, “Cerebellar hypoplasia, with quadrupedal locomotion, caused by

- mutations in the very low-density lipoprotein receptor gene,” *Eur. J. Hum. Genet.*, vol. 16, no. 9, pp. 1070–1074, 2008.
- [38] S. Vermeer *et al.*, “Targeted next-generation sequencing of a 12.5 Mb homozygous region reveals ANO10 mutations in patients with autosomal-recessive cerebellar ataxia,” *Am. J. Hum. Genet.*, vol. 87, no. 6, pp. 813–819, 2010.
- [39] H. Maruyama, H. Morino, R. Miyamoto, N. Murakami, T. Hamano, and H. Kawakami, “Exome sequencing reveals a novel ANO10 mutation in a Japanese patient with autosomal recessive spinocerebellar ataxia,” *Clin. Genet.*, vol. 85, no. 3, pp. 296–297, 2014.
- [40] T. Chamova *et al.*, “ANO10 c.1150\_1151del is a founder mutation causing autosomal recessive cerebellar ataxia in Roma/Gypsies,” *J. Neurol.*, vol. 259, no. 5, pp. 906–911, 2012.
- [41] M. Renaud *et al.*, “Autosomal recessive ataxia due to ANO10 mutations; full and novel phenotypic data in an Irish pedigree,” *Movement Disorders*, vol. 31, p. S344, 2016.
- [42] L. Chamard, G. Sylvestre, M. Koenig, and E. Magnin, “Executive and attentional disorders, epilepsy and porencephalic cyst in autosomal recessive cerebellar ataxia type 3 due to ANO10 mutation,” *Eur. Neurol.*, vol. 75, no. 3–4, pp. 186–190, 2016.
- [43] M. Koenig, “Rare Forms of Autosomal Recessive Neurodegenerative Ataxia,” *Seminars in Pediatric Neurology*, vol. 10, no. 3, pp. 183–192, 2003.
- [44] S. Di Donato, C. Gellera, and C. Mariotti, “The complex clinical and genetic classification of inherited ataxias. II. Autosomal recessive ataxias,”

- Neurological Sciences*, vol. 22, no. 3. pp. 219–228, 2001.
- [45] M. Manto and D. Marmolino, “Cerebellar ataxias,” *Curr. Opin. Neurol.*, vol. 22, no. 4, pp. 419–429, 2009.
  - [46] T. Ozcelik *et al.*, “Mutations in the very low-density lipoprotein receptor VLDLR cause cerebellar hypoplasia and quadrupedal locomotion in humans,” *Proc. Natl. Acad. Sci. U. S. A.*, vol. 105, no. 11, pp. 4232–6, 2008.
  - [47] S. Gulsuner *et al.*, “Homozygosity mapping and targeted genomic sequencing reveal the gene responsible for cerebellar hypoplasia and quadrupedal locomotion in a consanguineous kindred,” *Genome Res.*, vol. 21, no. 12, pp. 1995–2003, 2011.
  - [48] L. A. Moheb *et al.*, “Identification of a nonsense mutation in the very low-density lipoprotein receptor gene (VLDLR) in an Iranian family with dysequilibrium syndrome,” *Eur. J. Hum. Genet.*, vol. 16, no. 2, pp. 270–273, 2008.
  - [49] S. Turkmen, K. Hoffmann, O. Demirhan, N. Aruoba, N. Humphrey, and S. Mundlos, “Cerebellar hypoplasia and quadrupedal locomotion in humans as a recessive trait mapping to chromosome 17p,” *J. Med. Genet.*, vol. 43, no. 5, pp. 461–464, 2006.
  - [50] C. L. Kniffin, “Cerebellar ataxia, mental retardation, and dysequilibrium syndrome 2; CAMRQ2,” 2016. [Online]. Available: <https://www.omim.org/entry/610185>. [Accessed: 03-Nov-2017].
  - [51] A. M. Alazami *et al.*, “Accelerating novel candidate gene discovery in neurogenetic disorders via whole-exome sequencing of prescreened multiplex consanguineous families,” *Cell Rep.*, vol. 10, no. 2, pp. 148–161, 2015.



- [52] N. Dupre, F. Gros-Louis, J. P. Bouchard, A. Noreau, and G. A. Rouleau, "SYNE1-Related Autosomal Recessive Cerebellar Ataxia," in *GeneReviews*, 1993.
- [53] Y. Shi *et al.*, "Identification of CHIP as a novel causative gene for autosomal recessive cerebellar ataxia," *PLoS One*, vol. 8, no. 12, 2013.
- [54] R. Attali *et al.*, "Mutation of SYNE-1, encoding an essential component of the nuclear lamina, is responsible for autosomal recessive arthrogryposis," *Hum. Mol. Genet.*, vol. 18, no. 18, pp. 3462–3469, 2009.
- [55] A. Noreau *et al.*, "SYNE1 mutations in autosomal recessive cerebellar ataxia.," *JAMA Neurol.*, vol. 70, no. 10, pp. 1296–31, 2013.
- [56] B. L. Fogel and S. Perlman, "Clinical features and molecular genetics of autosomal recessive cerebellar ataxias," *Lancet Neurology*, vol. 6, no. 3. pp. 245–257, 2007.
- [57] V. Schurig, A. V. Orman, and P. Bowen, "Nonprogressive cerebellar disorder with mental retardation and autosomal recessive inheritance in Hutterites," *Am. J. Med. Genet.*, vol. 9, no. 1, pp. 43–53, 1981.
- [58] M. A. Basson and R. J. Wingate, "Congenital hypoplasia of the cerebellum: developmental causes and behavioral consequences," *Front. Neuroanat.*, vol. 7, 2013.
- [59] U. Tan and M. Tan, "Unertan syndrome: A new variant of unertan syndrome: Running on all fours in two upright-walking children," *Int. J. Neurosci.*, vol. 119, no. 7, pp. 909–918, 2009.
- [60] H. C. Glass *et al.*, "Autosomal recessive cerebellar hypoplasia in the Hutterite population.," *Dev. Med. Child Neurol.*, vol. 47, no. 10, pp. 691–5, 2005.

- [61] U. Tan, “Two families with quadrupedalism, mental retardation, no speech, and infantile hypotonia (Uner Tan Syndrome Type-II); a novel theory for the evolutionary emergence of human bipedalism,” *Front. Neurosci.*, no. 8 APR, 2014.
- [62] K. M. Boycott *et al.*, “Homozygous deletion of the very low density lipoprotein receptor gene causes autosomal recessive cerebellar hypoplasia with cerebral gyral simplification,” *Am. J. Hum. Genet.*, vol. 77, no. 3, p. 477—483, 2005.
- [63] T. J. Dixon-Salazar *et al.*, “Exome Sequencing Can Improve Diagnosis and Alter Patient Management,” *Sci. Transl. Med.*, vol. 4, no. 138, p. 138ra78-138ra78, 2012.
- [64] U. Tan, “Unertan syndrome: review and report of four new cases,” *Int. J. Neurosci.*, vol. 118, no. 2, pp. 211–225, 2008.
- [65] U. Tan, “Uner tan syndrome: history, clinical evaluations, genetics, and the dynamics of human quadrupedalism,” *Open Neurol. J.*, vol. 4, pp. 78–89, 2010.
- [66] R. S. Desikan *et al.*, “An automated labeling system for subdividing the human cerebral cortex on MRI scans into gyral based regions of interest,” *Neuroimage*, vol. 31, no. 3, pp. 968–980, 2006.
- [67] B. Fischl *et al.*, “Whole brain segmentation: Automated labeling of neuroanatomical structures in the human brain,” *Neuron*, vol. 33, no. 3, pp. 341–355, 2002.
- [68] I. Cabrita *et al.*, “Differential effects of anoctamins on intracellular calcium signals,” *FASEB J.*, vol. 31, no. 5, pp. 2123–2134, 2017.

- [69] P. Wanitchakool *et al.*, “Cellular defects by deletion of ANO10 are due to deregulated local calcium signaling,” *Cell. Signal.*, vol. 30, pp. 41–49, 2017.
- [70] “Ensembl Genome Browser: Anoctamin10 [Human], (ENSG00000160746),” 2017. [Online]. Available: [https://www.ensembl.org/Homo\\_sapiens/Gene/Summary?db=core;g=ENSG00000160746;r=3:43354859-43691594](https://www.ensembl.org/Homo_sapiens/Gene/Summary?db=core;g=ENSG00000160746;r=3:43354859-43691594). [Accessed: 04-Nov-2017].
- [71] R. Schreiber and K. Kunzelmann, “Expression of anoctamins in retinal pigment epithelium (RPE),” *Pflugers Arch. Eur. J. Physiol.*, vol. 468, no. 11–12, pp. 1921–1929, 2016.
- [72] A. Kasumu and I. Bezprozvanny, “Deranged calcium signaling in purkinje cells and pathogenesis in spinocerebellar ataxia 2 (SCA2) and other ataxias,” *Cerebellum*, vol. 11, no. 3, pp. 630–639, 2012.
- [73] L. Yin *et al.*, “Glucose stimulates calcium-activated chloride secretion in small intestinal cells,” *AJP Cell Physiol.*, vol. 306, no. 7, pp. C687–C696, 2014.
- [74] M. Strazzabosco, “Transport systems in cholangiocytes: Their role in bile formation and cholestasis,” in *Yale Journal of Biology and Medicine*, 1997, vol. 70, no. 4, pp. 427–434.
- [75] Y. Kim, S. Chattopadhyay, S. Locke, and D. A. Pearce, “Interaction among Btn1p, Btn2p, and Ist2p reveals potential interplay among the vacuole, amino acid levels, and ion homeostasis in the yeast *Saccharomyces cerevisiae*,” *Eukaryot. Cell*, vol. 4, no. 2, pp. 281–288, 2005.
- [76] M. Sala-Rabanal, Z. Yurtsever, K. N. Berry, C. G. Nichols, and X. T. J. Brett, “Modulation of TMEM16A channel activity by the von Willebrand factor type A (VWA) domain of the calcium-activated chloride channel regulator 1

- (CLCA1),” *J. Biol. Chem.*, vol. 292, no. 22, pp. 9164–9174, 2017.
- [77] F. Huang, X. Wong, and L. Y. Jan, “International Union of Basic and Clinical Pharmacology. LXXXV: calcium-activated chloride channels,” *Pharmacol. Rev.*, vol. 64, no. 1, pp. 1–15, 2012.
- [78] A. de Angeli, S. Thomine, J.-M. Frachisse, G. Ephritikhine, F. Gambale, and H. Barbier-Brygoo, “Anion channels and transporters in plant cell membranes,” *FEBS Lett.*, vol. 581, no. 12, pp. 2367–2374, 2007.
- [79] “Chloride channels,” *Br. J. Pharmacol.*, vol. 158, no. Suppl1, pp. 130–134, 2009.
- [80] T. J. Jentsch, “Chloride channels are different,” *Nature*, vol. 415, no. 6869, pp. 276–277, 2002.
- [81] B. D. Safratowich, C. Lor, L. Bianchi, and L. Carvelli, “Amphetamine activates an amine-gated chloride channel to generate behavioral effects in *caenorhabditis elegans*,” *J. Biol. Chem.*, vol. 288, no. 30, pp. 21630–21637, 2013.
- [82] N. Pedemonte and L. J. V. Galiotta, “Structure and Function of TMEM16 Proteins (Anoctamins),” *Physiol. Rev.*, vol. 94, no. 2, pp. 419–459, 2014.
- [83] M. I. Hollenhorst, K. Richter, and M. Fronius, “Ion transport by pulmonary epithelia,” *Journal of Biomedicine and Biotechnology*, vol. 2011, 2011.
- [84] G. M. Solomon, S. Vamsee Raju, M. T. Dransfield, and S. M. Rowe, “Therapeutic Approaches to Acquired Cystic Fibrosis Transmembrane Conductance Regulator Dysfunction in Chronic Bronchitis,” *Ann Am Thorac Soc.*, vol. 13, no. S2, pp. S169–S176, 2016.
- [85] M. Schreiber and L. Salkoff, “A novel calcium-sensing domain in the BK

- channel,” *Biophys. J.*, vol. 73, no. 3, pp. 1355–1363, 1997.
- [86] C. Hartzell, I. Putzier, and J. Arreola, “CALCIUM-ACTIVATED CHLORIDE CHANNELS,” *Annu. Rev. Physiol.*, vol. 67, no. 1, pp. 719–758, Mar. 2005.
- [87] Q. Xiao, K. Yu, P. Perez-Cornejo, Y. Cuia, J. Arreolac, and H. H. Criss, “Voltage- and calcium-dependent gating of TMEM16A/Ano1 chloride channels are physically coupled by the first intracellular loop,” *PNAS*, pp. 8891–8896, 2011.
- [88] V. V. Matchkov *et al.*, “Bestrophin-3 (vitelliform macular dystrophy 2-like 3 protein) is essential for the cGMP-dependent calcium-activated chloride conductance in vascular smooth muscle cells,” *Circ. Res.*, vol. 103, no. 8, pp. 864–872, 2008.
- [89] S. Das *et al.*, “Topology of NGEF, a prostate-specific cell:cell junction protein widely expressed in many cancers of different grade level,” *Cancer Res.*, vol. 68, no. 15, pp. 6306–6312, 2008.
- [90] S. Chattopadhyay, N. E. Muzaffar, F. Sherman, and D. A. Pearce, “The yeast model for batten disease: Mutations in btn1, btn2, and hsp30 alter pH homeostasis,” *J. Bacteriol.*, vol. 182, no. 22, pp. 6418–6423, 2000.
- [91] S. Chattopadhyay and D. A. Pearce, “Interaction with Btn2p is required for localization of Rsg1p: Btn2p-mediated changes in arginine uptake in *Saccharomyces cerevisiae*,” *Eukaryot. Cell*, vol. 1, no. 4, pp. 606–612, 2002.
- [92] “The Human Protein Atlas Database (version 88.38) ANO10 Tissue Atlas,” 2016. [Online]. Available: <https://www.proteinatlas.org/ENSG00000160746-ANO10/tissue>. [Accessed: 05-Nov-2017].

- [93] I. Jun *et al.*, “Cancer, ANO9/TMEM16J promotes tumourigenesis via EGFR and is a novel therapeutic target for pancreatic,” *Br. J. Cancer*, vol. 117, pp. 1798–1809, 2017.
- [94] U. Duvvuri *et al.*, “TMEM16A induces MAPK and contributes directly to tumorigenesis and cancer progression,” *Cancer Res.*, vol. 72, no. 13, pp. 3270–3281, 2012.
- [95] W. Liu, M. Lu, B. Liu, Y. Huang, and K. Wang, “Inhibition of Ca(2+)-activated Cl(-) channel ANO1/TMEM16A expression suppresses tumor growth and invasiveness in human prostate carcinoma,” *Cancer Lett.*, vol. 326, no. 1, pp. 41–51, 2012.
- [96] A. Britschgi *et al.*, “Calcium-activated chloride channel ANO1 promotes breast cancer progression by activating EGFR and CAMK signaling,” *Proc. Natl. Acad. Sci.*, vol. 110, no. 11, pp. E1026–E1034, 2013.
- [97] S. Simon *et al.*, “DOG1 regulates growth and IGFBP5 in gastrointestinal stromal tumors,” *Cancer Res.*, vol. 73, no. 12, pp. 3661–3670, 2013.
- [98] D. R. P. Sauter, I. Novak, S. F. Pedersen, E. H. Larsen, and E. K. Hoffmann, “ANO1 (TMEM16A) in pancreatic ductal adenocarcinoma (PDAC),” *Pflugers Arch. Eur. J. Physiol.*, vol. 467, no. 7, pp. 1495–1508, 2015.
- [99] M. Dutertre *et al.*, “Estrogen regulation and physiopathologic significance of alternative promoters in breast cancer,” *Cancer Res.*, vol. 70, no. 9, pp. 3760–3770, 2010.
- [100] T. K. Bera *et al.*, “NGEP, a gene encoding a membrane protein detected only in prostate cancer and normal prostate,” *Proc. Natl. Acad. Sci. U. S. A.*, vol. 101, no. 9, pp. 3059–3064, 2004.

- [101] M. Katoh and M. Katoh, "Identification and characterization of human TP53I5 and mouse Tp53i5 genes in silico.," *Int. J. Oncol.*, vol. 25, no. 1, pp. 225–230, 2004.
- [102] A. Bill *et al.*, "ANO1 interacts with EGFR and correlates with sensitivity to EGFR-targeting therapy in head and neck cancer," *Oncotarget*, vol. 6, no. 11, pp. 9173–9188, 2015.
- [103] "The Human Protein Atlas Database (version 88.38) ANO10 Pathology Atlas," 2016. [Online]. Available: <https://www.proteinatlas.org/ENSG00000160746-ANO10/pathology>. [Accessed: 05-Nov-2017].
- [104] A. Sailer and H. Houlden, "Recent advances in the genetics of cerebellar ataxias," *Curr. Neurol. Neurosci. Rep.*, vol. 12, no. 3, pp. 227–236, 2012.
- [105] C. Marcel, E. J. Kamsteeg, H. Scheffer, M. Koenig, and C. Tranchant, "A new mutation in anoctamin 10 gene associated with isolated autosomal recessive cerebellar ataxia," *Mov. Disord.*, vol. 27, p. S186, 2012.
- [106] R. Schreiber, D. Faria, B. V. Skryabin, P. Wanitchakool, J. R. Rock, and K. Kunzelmann, "Anoctamins support calcium-dependent chloride secretion by facilitating calcium signaling in adult mouse intestine," *Pflugers Arch. Eur. J. Physiol.*, vol. 467, no. 6, pp. 1203–1213, 2015.
- [107] "Human Protein Atlas (version 88.38) WDR81 Tissue Atlas," 2012. [Online]. Available: <https://www.proteinatlas.org/ENSG00000167716-WDR81/tissue>. [Accessed: 05-Nov-2017].
- [108] "GeneCards: Human Gene Database, WD Repeat Domain 81 (WDR81) Gene (Protein Coding)." [Online]. Available: <http://www.genecards.org/cgi->

- bin/carddisp.pl?gene=WDR81. [Accessed: 05-Nov-2017].
- [109] “Ensemble Human WDR81(ENSG00000167716),” 2017. [Online]. Available: [https://www.ensembl.org/Homo\\_sapiens/Gene/Summary?db=core;g=ENSG00000167716;r=17:1716523-1738599](https://www.ensembl.org/Homo_sapiens/Gene/Summary?db=core;g=ENSG00000167716;r=17:1716523-1738599). [Accessed: 05-Nov-2017].
- [110] R. Rapiteanu, L. J. Davis, J. C. Williamson, R. T. Timms, J. Paul Luzio, and P. J. Lehner, “A Genetic Screen Identifies a Critical Role for the WDR81-WDR91 Complex in the Trafficking and Degradation of Tetherin,” *Traffic*, vol. 17, no. 8, pp. 940–958, 2016.
- [111] X. Liu *et al.*, “The BEACH-containing protein WDR81 coordinates p62 and LC3C to promote aggrephagy,” *J. Cell Biol.*, vol. 216, no. 5, pp. 1301–1320, 2017.
- [112] M. Traka *et al.*, “WDR81 Is Necessary for Purkinje and Photoreceptor Cell Survival,” *J. Neurosci.*, vol. 33, no. 16, pp. 6834–6844, 2013.
- [113] C. Xu and J. Min, “Structure and function of WD40 domain proteins,” *Protein and Cell*, vol. 2, no. 3, pp. 202–214, 2011.
- [114] A. R. Cullinane, A. A. Schäffer, and M. Huizing, “The BEACH Is Hot: A LYST of Emerging Roles for BEACH-Domain Containing Proteins in Human Disease,” *Traffic*, vol. 14, no. 7, pp. 749–766, 2013.
- [115] S. S. Pao, I. T. Paulsen, and M. H. Saier, “Major facilitator superfamily,” *Microbiol. Mol. Biol. Rev.*, vol. 62, no. 1, pp. 1–34, 1998.
- [116] M. H. Saier *et al.*, “The major facilitator superfamily,” *J. Mol. Microbiol. Biotechnol.*, 1999.
- [117] N. Von Muhlinen *et al.*, “An essential role for the ATG8 ortholog LC3C in antibacterial autophagy,” *Autophagy*, vol. 9, no. 5, pp. 784–786, 2013.



- [118] O. Sarac, S. Gulsuner, Y. Yildiz-Tasci, T. Ozcelik, and T. Kansu, “Neuro-ophthalmologic findings in humans with quadrupedal locomotion,” *Ophthalmic Genet.*, vol. 33, no. 4, pp. 249–252, 2012.
- [119] E. Donnard *et al.*, “Mutational analysis of genes coding for cell surface proteins in colorectal cancer cell lines reveal novel altered pathways, druggable mutations and mutated epitopes for targeted therapy.,” *Oncotarget*, vol. 5, no. 19, pp. 9199–213, 2014.
- [120] “Ensemble Human VLDLR (ENSG00000147852),” 2017. [Online]. Available:  
[https://www.ensembl.org/Homo\\_sapiens/Gene/Summary?db=core;g=ENSG00000147852;r=9:2621834-2660053](https://www.ensembl.org/Homo_sapiens/Gene/Summary?db=core;g=ENSG00000147852;r=9:2621834-2660053). [Accessed: 05-Nov-2017].
- [121] “NCBI VLDLR Very Low Density Lipoprotein Receptor [Homo sapiens (Human)], 7436,” 2017. [Online]. Available:  
<https://www.ncbi.nlm.nih.gov/gene/7436>. [Accessed: 05-Nov-2017].
- [122] “GeneCards: Human Gene Database, Vry Low Density Lipoprotein Receptor (VLDLR) Gene (Protein Coding).” .
- [123] J. Doehner and I. Knuesel, “Reelin-mediated Signaling during Normal and Pathological Forms of Aging.,” *Aging Dis.*, vol. 1, no. 1, pp. 12–29, 2010.
- [124] G. D’Arcangelo, G. G. Miao, S.-C. Chen, H. D. Scares, J. I. Morgan, and T. Curran, “A protein related to extracellular matrix proteins deleted in the mouse mutant reeler,” *Nature*, vol. 374, no. 6524, pp. 719–723, 1995.
- [125] G. D’Arcangelo, “Reelin in the Years: Controlling Neuronal Migration and Maturation in the Mammalian Brain,” *Adv. Neurosci.*, vol. 2014, pp. 1–19, 2014.

- [126] T. Miyata, K. Nakajima, K. Mikoshiba, and M. Ogawa, "Regulation of Purkinje cell alignment by reelin as revealed with CR-50 antibody.," *J. Neurosci.*, vol. 17, no. 10, pp. 3599–3609, 1997.
- [127] M. Larouche, U. Beffert, J. Herz, and R. Hawkes, "The reelin receptors Apoer2 and Vldlr coordinate the patterning of purkinje cell topography in the developing mouse cerebellum," *PLoS One*, vol. 3, no. 2, 2008.
- [128] S. Niu, A. Renfro, C. C. Quattrocchi, M. Sheldon, and G. D'Arcangelo, "Reelin Promotes Hippocampal Dendrite Development through the VLDLR/ApoER2-Dab1 Pathway," *Neuron*, vol. 41, no. 1, pp. 71–84, 2004.
- [129] A. M. DiBattista *et al.*, "Very low density lipoprotein receptor regulates dendritic spine formation in a RasGRF1/CaMKII dependent manner.," *Biochim. Biophys. Acta*, vol. 1853, no. 5, pp. 904–17, 2015.
- [130] P. J. Tacke *et al.*, "LDL receptor deficiency unmasks altered VLDL triglyceride metabolism in VLDL receptor transgenic and knockout mice.," *J. Lipid Res.*, vol. 41, no. 12, pp. 2055–62, 2000.
- [131] H. Tao and T. Hajri, "Very low density lipoprotein receptor promotes adipocyte differentiation and mediates the proadipogenic effect of peroxisome proliferator-activated receptor gamma agonists," *Biochem. Pharmacol.*, vol. 82, no. 12, pp. 1950–1962, 2011.
- [132] H. a Mulhaupt *et al.*, "Expression of very low density lipoprotein receptor in the vascular wall. Analysis of human tissues by in situ hybridization and immunohistochemistry.," *Am. J. Pathol.*, vol. 148, no. 6, pp. 1985–1997, 1996.
- [133] "Human Protein Atlas (version 88.38) VLDLR Tissue Atlas," 2009. [Online].

Available: <https://www.proteinatlas.org/ENSG00000147852-VLDLR/tissue>.

[Accessed: 05-Nov-2017].

- [134] L. E. Kolb *et al.*, “Novel VLDLR microdeletion identified in two Turkish siblings with pachygyria and pontocerebellar atrophy,” *Neurogenetics*, vol. 11, no. 3, pp. 319–325, 2010.
- [135] K. Okuizumi *et al.*, “Genetic association of the very low density lipoprotein (VLDL) receptor gene with sporadic Alzheimer’s disease,” *Nat. Genet.*, vol. 11, no. 2, pp. 207–209, 1995.
- [136] A. Sentürk, S. Pfennig, A. Weiss, K. Burk, and A. Acker-Palmer, “Ephrin Bs are essential components of the Reelin pathway to regulate neuronal migration,” *Nature*, vol. 472, no. 7343, pp. 356–360, 2011.
- [137] G. S. Gerhard and K. C. Cheng, “A call to fins! Zebrafish as a gerontological model,” *Aging cell*, vol. 1, no. 2, pp. 104–111, 2002.
- [138] “Why Zebrafish?,” 2017. [Online]. Available: <https://www.fishforpharma.com/why-zebrafish-17>, (Leiden University).  
[Accessed: 05-Nov-2017].
- [139] R. W. Friedrich, G. A. Jacobson, and P. Zhu, “Circuit Neuroscience in Zebrafish,” *Current Biology*, vol. 20, no. 8, 2010.
- [140] K. Dooley and L. I. Zon, “Zebrafish: a model system for the study of human disease,” *Curr. Opin. Genet. Dev.*, vol. 10, no. 3, pp. 252–256, 2000.
- [141] K. Howe *et al.*, “The zebrafish reference genome sequence and its relationship to the human genome,” *Nature*, vol. 496, no. 7446, pp. 498–503, 2013.
- [142] G. J. Lieschke and P. D. Currie, “Animal models of human disease: Zebrafish swim into view,” *Nature Reviews Genetics*, vol. 8, no. 5, pp. 353–367, 2007.

- [143] E. Kabashi, E. Brustein, N. Champagne, and P. Drapeau, “Zebrafish models for the functional genomics of neurogenetic disorders,” *Biochimica et Biophysica Acta - Molecular Basis of Disease*, vol. 1812, no. 3. pp. 335–345, 2011.
- [144] M. F. Wullimann, B. Rupp, and H. Reichert, *Neuroanatomy of the zebrafish brain: A topological atlas*. 1996.
- [145] Y. Liu, D. Li, and Z. Yuan, “Photoacoustic Tomography Imaging of the Adult Zebrafish by Using Unfocused and Focused High-Frequency Ultrasound Transducers,” *Appl. Sci.*, vol. 6, no. 12, p. 392, 2016.
- [146] J. Ganz, J. Kaslin, D. Freudenreich, A. Machate, M. Geffarth, and M. Brand, “Subdivisions of the adult zebrafish subpallium by molecular marker analysis Julia Ganz,” *J. Comp. Neurol.*, vol. 520, no. Sfb 655, pp. 633–655, 2011.
- [147] M. B. Orger, M. C. Smear, S. M. Anstis, and H. Baier, “Perception of Fourier and non-Fourier motion by larval zebrafish,” *Nat. Neurosci.*, vol. 3, no. 11, pp. 1128–1133, 2000.
- [148] G. S. Gerhard *et al.*, “Life spans and senescent phenotypes in two strains of Zebrafish (*Danio rerio*),” *Exp. Gerontol.*, vol. 37, no. 8–9, pp. 1055–1068, 2002.
- [149] H. B. Schonthaler *et al.*, “The zebrafish mutant bumper shows a hyperproliferation of lens epithelial cells and fibre cell degeneration leading to functional blindness,” *Mech. Dev.*, 2010.
- [150] A. Arslan-Ergul and M. M. Adams, “Gene expression changes in aging Zebrafish (*Danio rerio*) brains are sexually dimorphic,” *BMC Neurosci.*, vol. 15, no. 1, p. 29, 2014.

- [151] C. M. Small, G. E. Carney, Q. Mo, M. Vannucci, and A. G. Jones, “A microarray analysis of sex- and gonad-biased gene expression in the zebrafish: Evidence for masculinization of the transcriptome,” *BMC Genomics*, vol. 10, no. 1, p. 579, 2009.
- [152] I. Skromne and V. E. Prince, “Current perspectives in zebrafish reverse genetics: Moving forward,” *Developmental Dynamics*, vol. 237, no. 4. pp. 861–882, 2008.
- [153] “GeneTools, LCC: Morpholino Antisense Oligos-A Brief Introduction to Morpholino Antisense.” [Online]. Available: [http://www.gene-tools.com/morpholino\\_antisense\\_oligos](http://www.gene-tools.com/morpholino_antisense_oligos). [Accessed: 05-Nov-2017].
- [154] B. R. Bill, A. M. Petzold, K. J. Clark, L. A. Schimmenti, and S. C. Ekker, “A Primer for Morpholino Use in Zebrafish,” *Zebrafish*, vol. 6, no. 1, pp. 69–77, 2009.
- [155] J. Summerton, “Morpholino antisense oligomers: The case for an RNase H-independent structural type,” *Biochimica et Biophysica Acta - Gene Structure and Expression*, vol. 1489, no. 1. pp. 141–158, 1999.
- [156] J. S. Eisen and J. C. Smith, “Controlling morpholino experiments: don’t stop making antisense,” *Development*, vol. 135, no. 10, pp. 1735–1743, 2008.
- [157] P. A. Morcos, “Achieving targeted and quantifiable alteration of mRNA splicing with Morpholino oligos,” *Biochem. Biophys. Res. Commun.*, vol. 358, no. 2, pp. 521–527, 2007.
- [158] I. Stancheva, A. L. Collins, I. B. Van den Veyver, H. Zoghbi, and R. R. Meehan, “Erratum: A Mutant Form of MeCP2 Protein Associated with Human Rett Syndrome Cannot Be Displaced from Methylated DNA by Notch

- in *Xenopus* Embryos (Molecular Cell (2003) 12(2) (425–435)(10.1016/S1097-2765(03)00276-4)(S1097276503002764)),” *Molecular Cell*, vol. 63, no. 1. p. 179, 2016.
- [159] “STRING: Protein-Protein Interaction Network,” 2017. [Online]. Available: <http://version10.string-db.org/>. [Accessed: 06-Nov-2017].
- [160] C. von Mering, M. Huynen, D. Jaeggi, S. Schmidt, P. Bork, and B. Snel, “STRING: A database of predicted functional associations between proteins,” *Nucleic Acids Research*, vol. 31, no. 1. pp. 258–261, 2003.
- [161] D. Szklarczyk *et al.*, “The STRING database in 2011: Functional interaction networks of proteins, globally integrated and scored,” *Nucleic Acids Res.*, vol. 39, no. SUPPL. 1, 2011.
- [162] S. Brohée, K. Faust, G. Lima-Mendez, G. Vanderstocken, and J. van Helden, “Network analysis tools: From biological networks to clusters and pathways,” *Nat. Protoc.*, vol. 3, no. 10, pp. 1616–1629, 2008.
- [163] D. Szklarczyk *et al.*, “STRING v10: Protein-protein interaction networks, integrated over the tree of life,” *Nucleic Acids Res.*, vol. 43, no. D1, pp. D447–D452, 2015.
- [164] D. Szklarczyk *et al.*, “The STRING database in 2017: quality-controlled protein-protein association networks, made broadly accessible,” *Nucleic Acids Res.*, vol. 45, no. D1, pp. D362–D368, 2017.
- [165] “MotifScan: Protein Annotation and Domain Identification Database.” [Online]. Available: [http://myhits.isb-sib.ch/cgi-bin/motif\\_scan](http://myhits.isb-sib.ch/cgi-bin/motif_scan). [Accessed: 06-Nov-2017].
- [166] M. Pagni, V. Ioannidis, L. Cerutti, M. Zahn-Zabal, C. V. Jongeneel, and L.

- Falquet, “MyHits: A new interactive resource for protein annotation and domain identification,” *Nucleic Acids Res.*, vol. 32, no. WEB SERVER ISS., 2004.
- [167] M. Pagni *et al.*, “MyHits: Improvements to an interactive resource for analyzing protein sequences,” *Nucleic Acids Res.*, vol. 35, no. SUPPL.2, 2007.
- [168] M. P. Liang, D. L. Brutlag, and R. B. Altman, “Automated construction of structural motifs for predicting functional sites on protein structures,” *Pac. Symp. Biocomput.*, pp. 204–15, 2003.
- [169] “NCBI (National Center for Biotechnology Information) Tool,” 2017.  
[Online]. Available: <https://www.ncbi.nlm.nih.gov>. [Accessed: 06-Nov-2017].
- [170] “Ensembl Genome Browser,” 2017. [Online]. Available:  
<http://www.ensembl.org/index.html>. [Accessed: 06-Nov-2017].
- [171] “UCSC (University of California Santa Cruz) Genome Browser,” 2017.  
[Online]. Available: <http://genome.ucsc.edu>. [Accessed: 06-Nov-2017].
- [172] J. Ostell and J. McEntyre, “The NCBI Handbook,” *NCBI Bookshelf*, pp. 1–8, 2007.
- [173] P. S. Cooper *et al.*, “Education resources of the National Center for Biotechnology Information,” *Brief. Bioinform.*, vol. 11, no. 6, pp. 563–569, 2010.
- [174] E. W. Sayers *et al.*, “Database resources of the National Center for Biotechnology Information,” *Nucleic Acids Res.*, vol. 37, no. SUPPL. 1, 2009.
- [175] T. Hubbard *et al.*, “The Ensembl genome database project,” *Nucleic Acids Res.*, vol. 30, no. 1, pp. 38–41, 2002.
- [176] P. Flicek *et al.*, “Ensembl’s 10th year,” *Nucleic Acids Res.*, vol. 38, no.

SUPPL.1, 2009.

- [177] A. Yates *et al.*, “Ensembl 2016,” *Nucleic Acids Res.*, vol. 44, no. D1, pp. D710–D716, 2016.
- [178] W. J. Kent *et al.*, “The Human Genome Browser at UCSC,” *Genome Res.*, vol. 12, no. 6, pp. 996–1006, 2002.
- [179] P. A. Fujita *et al.*, “The UCSC genome browser database: Update 2011,” *Nucleic Acids Res.*, vol. 39, no. SUPPL. 1, 2011.
- [180] “BLAST: Basic Local Alignment Search Tool.” [Online]. Available: <https://blast.ncbi.nlm.nih.gov/Blast.cgi>. [Accessed: 06-Nov-2017].
- [181] S. F. Altschul, W. Gish, W. Miller, E. W. Myers, and D. J. Lipman, “Basic local alignment search tool,” *J. Mol. Biol.*, vol. 215, no. 3, pp. 403–410, 1990.
- [182] “Primer 3 web (Version 4.1.0): Pick Primers From a DNA sequence.” [Online]. Available: <http://primer3.ut.ee/>.
- [183] “Universal Probe Library: design your array in three easy steps,” 2017. [Online]. Available: [https://lifescience.roche.com/en\\_tr/brands/universal-probe-library.html](https://lifescience.roche.com/en_tr/brands/universal-probe-library.html). [Accessed: 06-Nov-2017].
- [184] T. Madden, “Chapter 16 : The BLAST Sequence Analysis Tool,” *NCBI Handbook[internet]*, pp. 1–15, 2002.
- [185] I. Lobo, “Basic Local Alignment Search Tool (BLAST),” *Nat. Educ.*, vol. 1, no. 1, p. 215, 2008.
- [186] C. Camacho *et al.*, “BLAST plus: architecture and applications,” *BMC Bioinformatics*, vol. 10, no. 421, p. 1, 2009.
- [187] S. Rozen and H. J. Skaletsky, “Primer3,” *Bioinformatics Methods and Protocols Methods in Molecular Biology*, vol. 3. pp. 1–41, 1998.



- [188] A. Untergasser *et al.*, “Primer3-new capabilities and interfaces,” *Nucleic Acids Res.*, vol. 40, no. 15, 2012.
- [189] P. Mouritzen *et al.*, “ProbeLibrary: A new method for faster design and execution of quantitative real-time PCR,” *Nat. Methods*, vol. 2, no. 4, pp. 313–316, 2005.
- [190] “EMBL-EBI: Pairwise Sequence Alignment,” 2017. [Online]. Available: <https://www.ebi.ac.uk/Tools/psa/%0D>. [Accessed: 06-Nov-2017].
- [191] “EMBL-EBI: Cluster Omega,” 2017. [Online]. Available: <https://www.ebi.ac.uk/Tools/msa/clustalo/>. [Accessed: 06-Nov-2017].
- [192] T. Kulikova *et al.*, “EMBL Nucleotide Sequence Database in 2006,” *Nucleic Acids Res.*, vol. 35, no. SUPPL. 1, 2007.
- [193] H. McWilliam *et al.*, “Analysis Tool Web Services from the EMBL-EBI,” *Nucleic Acids Res.*, vol. 41, no. Web Server issue, 2013.
- [194] J. Ye, S. McGinnis, and T. L. Madden, “BLAST: Improvements for better sequence analysis,” *Nucleic Acids Res.*, vol. 34, no. WEB. SERV. ISS., 2006.
- [195] R. C. Edgar and S. Batzoglou, “Multiple sequence alignment,” *Current Opinion in Structural Biology*, vol. 16, no. 3. pp. 368–373, 2006.
- [196] S. McGinnis and T. L. Madden, “BLAST: At the core of a powerful and diverse set of sequence analysis tools,” *Nucleic Acids Res.*, vol. 32, no. WEB SERVER ISS., 2004.
- [197] F. Sievers and D. G. Higgins, “Clustal omega, accurate alignment of very large numbers of sequences,” *Methods Mol. Biol.*, vol. 1079, pp. 105–116, 2014.
- [198] F. Sievers *et al.*, “Fast, scalable generation of high-quality protein multiple

- sequence alignments using Clustal Omega,” *Mol. Syst. Biol.*, vol. 7, 2011.
- [199] J. Daugelaite, A. O’ Driscoll, and R. D. Sleator, “An Overview of Multiple Sequence Alignments and Cloud Computing in Bioinformatics,” *ISRN Biomath.*, vol. 2013, pp. 1–14, 2013.
- [200] “NCBI: Gene,” 2017. [Online]. Available: <https://www.ncbi.nlm.nih.gov/gene/>. [Accessed: 06-Nov-2017].
- [201] B. L. Aken *et al.*, “The Ensembl gene annotation system,” *Database*, vol. 2016, p. baw093, 2016.
- [202] “Expression Atlas (Gene expression across species and biological conditions),” 2017. [Online]. Available: <https://www.ebi.ac.uk/gxa/home>. [Accessed: 06-Nov-2017].
- [203] NCBI Resource Coordinators, “Database Resources of the National Center for Biotechnology Information,” *Nucleic Acids Res.*, vol. 45, no. D1, pp. D12–D17, 2017.
- [204] A. Piovesan, M. Caracausi, F. Antonaros, M. C. Pelleri, and L. Vitale, “GeneBase 1.1: A tool to summarize data from NCBI gene datasets and its application to an update of human gene statistics,” *Database*, vol. 2016, 2016.
- [205] J.-Y. Jung, T. F. DeLuca, T. H. Nelson, and D. P. Wall, “A literature search tool for intelligent extraction of disease-associated genes,” *J. Am. Med. Informatics Assoc.*, vol. 21, no. 3, pp. 399–405, 2014.
- [206] R. Petryszak *et al.*, “Expression Atlas update—an integrated database of gene and protein expression in humans, animals and plants,” *Nucleic Acids Res.*, vol. 44, no. October 2015, p. gkv1045, 2015.
- [207] M. Kapushesky *et al.*, “Gene Expression Atlas update--a value-added database

- of microarray and sequencing-based functional genomics experiments,” *Nucleic Acids Res.*, vol. 40, no. D1, pp. D1077–D1081, 2012.
- [208] R. Petryszak *et al.*, “Expression Atlas update - A database of gene and transcript expression from microarray- and sequencing-based functional genomics experiments,” *Nucleic Acids Res.*, vol. 42, no. D1, 2014.
- [209] M. Schonlau, “The Clustergram : A graph for visualizing hierarchical and non-hierarchical cluster analyses,” *Stata J.*, vol. 3, pp. 316–327, 2002.
- [210] S. Nam *et al.*, “Gene expression profile of the hypothalamus in DNP-KLH immunized mice following electroacupuncture stimulation,” *Evidence-based Complement. Altern. Med.*, vol. 2011, 2011.
- [211] D. K. Agrafiotis *et al.*, “Advanced Biological and Chemical Discovery (ABCD): Centralizing discovery knowledge in an inherently decentralized world,” *J. Chem. Inf. Model.*, vol. 47, no. 6, pp. 1999–2014, 2007.
- [212] D. K. Agrafiotis, D. Bandyopadhyay, and M. Farnum, “Radial clustergrams: Visualizing the aggregate properties of hierarchical clusters,” *J. Chem. Inf. Model.*, vol. 47, no. 1, pp. 69–75, 2007.
- [213] G. Cerruela García, I. Luque Ruiz, and M. Á. Gómez-Nieto, “Analysis and study of molecule data sets using snowflake diagrams of weighted maximum common subgraph trees,” *J. Chem. Inf. Model.*, vol. 51, no. 6, pp. 1216–1232, 2011.
- [214] S. van Dam, U. Vösa, A. van der Graaf, L. Franke, and J. P. de Magalhães, “Gene co-expression analysis for functional classification and gene–disease predictions,” *Brief. Bioinform.*, 2017.
- [215] H. Imai *et al.*, “Dynamic changes in the gene expression of zebrafish Reelin

- receptors during embryogenesis and hatching period,” *Dev. Growth Differ.*, vol. 54, no. 2, pp. 253–263, 2012.
- [216] M. W. Pfaffl, “A new mathematical model for relative quantification in real-time RT-PCR,” *Nucleic Acids Res.*, vol. 29, no. 9, p. 45e–45, 2001.
- [217] “Ensembl Genome Browser (Release 91): Anoctamin 10a [Zebrafish], ENSDART00000126041.1,” 2017. [Online]. Available: [https://www.ensembl.org/Danio\\_rerio/Transcript/Summary?db=core;g=ENSDARG00000057736;r=16:8067642-8125189;t=ENSDART00000126041](https://www.ensembl.org/Danio_rerio/Transcript/Summary?db=core;g=ENSDARG00000057736;r=16:8067642-8125189;t=ENSDART00000126041). [Accessed: 06-Nov-2017].
- [218] “Promega: PGEM-T® Easy Vector Systems (1360),” 2017. [Online]. Available: <https://worldwide.promega.com/products/pcr/pcr-cloning/pgem-t-easy-vector-systems/?catNum=A1360>. [Accessed: 06-Nov-2017].
- [219] D. M. Parichy, “Evolution of danio pigment pattern development,” *Heredity*, vol. 97, no. 3, pp. 200–210, 2006.
- [220] B. S. Carter, J. S. Fletcher, and R. C. Thompson, “Analysis of messenger RNA expression by in situ hybridization using RNA probes synthesized via in vitro transcription,” *Methods*, vol. 52, no. 4, pp. 322–331, 2010.
- [221] P. A. Morcos, “GeneTools, LCC: Morpholino oligos can block translation or nuclear processing of mRNA.” [Online]. Available: [http://www.gene-tools.com/choosing\\_the\\_optimal\\_target](http://www.gene-tools.com/choosing_the_optimal_target). [Accessed: 05-Nov-2017].
- [222] “UniProtKB - P68400 (CSK21\_HUMAN) Casein Kinase II Subunit Alpha.” [Online]. Available: <https://www.uniprot.org/uniprot/P68400>. [Accessed: 01-Jul-2018].
- [223] “UniProtKB - P67870 (CSK2B\_HUMAN) Casein Kinase 2 Subunit Beta.”

- [Online]. Available: <https://www.uniprot.org/uniprot/P67870>. [Accessed: 01-Jul-2018].
- [224] S. Türkmen *et al.*, “CA8 mutations cause a novel syndrome characterized by ataxia and mild mental retardation with predisposition to quadrupedal gait,” *PLoS Genet.*, vol. 5, no. 5, 2009.
- [225] D. W. Litchfield, “Protein kinase CK2: structure, regulation and role in cellular decisions of life and death,” *Biochem. J.*, vol. 369, no. Pt 1, pp. 1–15, 2003.
- [226] N. Mazarakis, A. Edwards, and H. Mehmet, “Apoptosis in neural development and disease,” *Arch. Dis. Child. Fetal Neonatal Ed.*, vol. 77, no. 3, pp. F165–F170, 1997.
- [227] I. Chowers *et al.*, “Gene expression variation in the adult human retina,” *Hum. Mol. Genet.*, vol. 12, no. 22, pp. 2881–2893, 2003.
- [228] T. E. Scheetz *et al.*, “Regulation of gene expression in the mammalian eye and its relevance to eye disease,” *Proc. Natl. Acad. Sci. U. S. A.*, vol. 103, no. 13, pp. 14429–14434, 2006.
- [229] A. Balreira *et al.*, “ANO10 mutations cause ataxia and coenzyme Q10 deficiency,” *J. Neurol.*, vol. 261, no. 11, pp. 2192–2198, 2014.
- [230] M. Caceres *et al.*, “Elevated gene expression levels distinguish human from non-human primate brains,” *Proc. Natl. Acad. Sci.*, vol. 100, no. 22, pp. 13030–13035, 2003.
- [231] O. Y. Naumova, M. Lee, S. Y. Rychkov, N. V. Vlasova, and E. L. Grigorenko, “Gene Expression in the Human Brain: The Current State of the Study of Specificity and Spatiotemporal Dynamics,” *Child Dev.*, vol. 84, no.

- 1, pp. 76–88, 2013.
- [232] A. J. L. Barton, R. C. A. Pearson, A. Najlerahim, and P. J. Harrison, “Pre- and Postmortem Influences on Brain RNA,” *Journal of Neurochemistry*, vol. 61, no. 1, pp. 1–11, 1993.
- [233] H. Zhang *et al.*, “Brain-specific Crmp2 deletion leads to neuronal development deficits and behavioural impairments in mice,” *Nat. Commun.*, vol. 7, 2016.
- [234] D. Randall and C. Daxboeck, *Gills - Anatomy, Gas Transfer, and Acid-Base Regulation*, vol. 10, 1984.
- [235] D. J. Randall, D. Baumgarten, and M. Malyusz, “The relationship between gas and ion transfer across the gills of fishes,” *Comp. Biochem. Physiol. -- Part A Physiol.*, vol. 41, no. 3, pp. 629–637, 1972.
- [236] A. Pyle *et al.*, “Respiratory chain deficiency in nonmitochondrial disease,” *Neurol. Genet.*, vol. 1, no. 1, 2015.
- [237] G. De Michele *et al.*, “Cerebellar ataxia and hypogonadism. A clinicopathological report,” *Clin. Neurol. Neurosurg.*, vol. 92, no. 1, pp. 67–70, 1990.
- [238] M. Cavallin *et al.*, “WDR81 mutations cause extreme microcephaly and impair mitotic progression in human fibroblasts and Drosophila neural stem cells,” *Brain*, vol. 140, no. 10, pp. 2597–2609, 2017.
- [239] M. Anheim *et al.*, “Ataxia with oculomotor apraxia type 2: Clinical, biological and genotype/phenotype correlation study of a cohort of 90 patients,” *Brain*, vol. 132, no. 10, pp. 2688–2698, 2009.
- [240] H. Luksch, “Optic Tectum: Sensorimotor Integration,” in *Encyclopedia of*

*Neuroscience*, 2009, pp. 263–269.

- [241] S. Franklin, “The Peripheral and Central Nervous System,” in *Conn’s Translational Neuroscience*, 2016, pp. 113–129.
- [242] D. Purves *et al.*, “Neuroscience. 2nd edition,” *Sunderland (MA): Sinauer Associates; 2001.*, 2001. .
- [243] G. De Michele and A. Filla, “Other autosomal recessive and childhood ataxias,” *Handb. Clin. Neurol.*, vol. 103, pp. 343–357, 2011.
- [244] Y. Jossin, I. Bar, N. Ignatova, F. Tissir, C. L. De Rouvroit, and A. M. Goffinet, “The Reelin signaling pathway: Some recent developments,” *Cerebral Cortex*, vol. 13, no. 6. pp. 627–633, 2003.
- [245] F. Tissir and A. M. Goffinet, “Reelin and brain development,” *Nat. Rev. Neurosci.*, vol. 4, no. 6, pp. 496–505, 2003.
- [246] S. Streit, C. W. Michalski, M. Erkan, J. Kleeff, and H. Friess, “Northern blot analysis for detection and quantification of RNA in pancreatic cancer cells and tissues,” *Nat. Protoc.*, vol. 4, no. 1, pp. 37–43, 2009.
- [247] F. R. H. JONES, “The Swimbladder and the Vertical Movement of Teleostean Fishes,” *J. Exp. Biol.*, vol. 28, no. 4, p. 553 LP-566, 1951.
- [248] T. Gabaldón and E. V. Koonin, “Functional and evolutionary implications of gene orthology,” *Nature Reviews Genetics*, vol. 14, no. 5. pp. 360–366, 2013.
- [249] F. Yang *et al.*, “Identifying pathogenicity of human variants via paralog-based yeast complementation,” *PLoS Genet.*, vol. 13, no. 5, 2017.
- [250] K. Liu *et al.*, “Negative regulation of phosphatidylinositol 3-phosphate levels in early-to-late endosome conversion,” *J. Cell Biol.*, 2016.
- [251] J. J. Liu *et al.*, “Inactivation of PI3k/Akt signaling pathway and activation of

- caspase-3 are involved in tanshinone I-induced apoptosis in myeloid leukemia cells in vitro,” *Ann. Hematol.*, vol. 89, no. 11, pp. 1089–1097, 2010.
- [252] K. D. Courtney, R. B. Corcoran, and J. A. Engelman, “The PI3K pathway as drug target in human cancer,” *Journal of Clinical Oncology*, vol. 28, no. 6. pp. 1075–1083, 2010.
- [253] B. D. Manning and A. Toker, “AKT/PKB Signaling: Navigating the Network,” *Cell*, vol. 169, no. 3. pp. 381–405, 2017.
- [254] J. P. MacKeigan, D. J. Taxman, D. Hunter, H. S. Earp, L. M. Graves, and J. P.-Y. Ting, “Inactivation of the antiapoptotic phosphatidylinositol 3-kinase-Akt pathway by the combined treatment of taxol and mitogen-activated protein kinase kinase inhibition.,” *Clin. Cancer Res.*, vol. 8, no. 7, pp. 2091–2099, 2002.
- [255] N. Bencsik *et al.*, “Protein kinase D promotes plasticity-induced F-actin stabilization in dendritic spines and regulates memory formation,” *J. Cell Biol.*, vol. 210, no. 5, pp. 771–783, 2015.
- [256] G. H. Lee and G. D’Arcangelo, “New Insights into Reelin-Mediated Signaling Pathways,” *Front. Cell. Neurosci.*, vol. 10, 2016.
- [257] S. C. Goetz, K. F. Liem, and K. V. Anderson, “The spinocerebellar ataxia-associated gene tau tubulin kinase 2 controls the initiation of ciliogenesis,” *Cell*, vol. 151, no. 4, pp. 847–858, 2012.
- [258] N. F. Liachko *et al.*, “The Tau Tubulin Kinases TTBK1/2 Promote Accumulation of Pathological TDP-43,” *PLoS Genet.*, vol. 10, no. 12, 2014.
- [259] C. J. L. M. Smeets and D. S. Verbeek, “Cerebellar ataxia and functional genomics: Identifying the routes to cerebellar neurodegeneration,” *Biochimica*



*et Biophysica Acta - Molecular Basis of Disease*, vol. 1842, no. 10. pp. 2030–2038, 2014.

- [260] H. Houlden *et al.*, “Mutations in TTBK2, encoding a kinase implicated in tau phosphorylation, segregate with spinocerebellar ataxia type 11,” *Nat. Genet.*, vol. 39, no. 12, pp. 1434–1436, 2007.
- [261] K. Araki, H. Meguro, E. Kushiya, C. Takayama, Y. Inoue, and M. Mishina, “Selective expression of the glutamate receptor channel  $\delta 2$  subunit in cerebellar Purkinje cells,” *Biochem. Biophys. Res. Commun.*, vol. 197, no. 3, pp. 1267–1276, 1993.
- [262] C. Takayama, S. Nakagawa, M. Watanabe, M. Mishina, and Y. Inoue, “Light- and electron-microscopic localization of the glutamate receptor channel delta 2 subunit in the mouse Purkinje cell,” *Neurosci Lett*, vol. 188, no. 2, pp. 89–92, 1995.
- [263] L. B. Hills *et al.*, “Deletions in GRID2 lead to a recessive syndrome of cerebellar ataxia and tonic upgaze in humans,” *Neurology*, vol. 81, no. 16, pp. 1378–1386, 2013.
- [264] N. Kashiwabuchi *et al.*, “Impairment of Motor Coordination, Purkinje-Cell Synapse Formation, and Cerebellar Long-Term Depression in Glur-Delta-2 Mutant Mice,” *Cell*, vol. 81, no. 2, pp. 245–252, 1995.
- [265] L. J. Hsu *et al.*, “Transforming growth factor  $\beta 1$  signaling via interaction with cell surface hyal-2 and recruitment of WWOX/WOX1,” *J. Biol. Chem.*, vol. 284, no. 23, pp. 16049–16059, 2009.
- [266] J.-Y. Lo, Y.-T. Chou, F.-J. Lai, and L.-J. Hsu, “Regulation of cell signaling and apoptosis by tumor suppressor WWOX,” *Exp. Biol. Med.*, vol. 240, no. 3,

pp. 383–391, 2015.

- [267] X. Liu *et al.*, “Post-translational modifications as key regulators of TNF-induced necroptosis,” *Cell death & disease*, vol. 7, no. 7. p. e2293, 2016.
- [268] I. Bosanac, T. Michikawa, K. Mikoshiba, and M. Ikura, “Structural insights into the regulatory mechanism of IP 3 receptor,” in *Biochimica et Biophysica Acta - Molecular Cell Research*, 2004.
- [269] J. Ousingsawat *et al.*, “Anoctamin 6 mediates effects essential for innate immunity downstream of P2X7 receptors in macrophages,” *Nat. Commun.*, vol. 6, p. 6245, 2015.
- [270] C. A. Ballinger *et al.*, “Identification of CHIP, a novel tetratricopeptide repeat-containing protein that interacts with heat shock proteins and negatively regulates chaperone functions,” *Mol Cell Biol*, vol. 19, no. 6, pp. 4535–4545, 1999.
- [271] J. Jiang *et al.*, “CHIP is a U-box-dependent E3 ubiquitin ligase: Identification of Hsc70 as a target for ubiquitylation,” *J. Biol. Chem.*, vol. 276, no. 46, pp. 42938–42944, 2001.
- [272] T. Yonezawa *et al.*, “The ubiquitin ligase STUB1 regulates stability and activity of RUNX1 and RUNX1–RUNX1T1,” *J. Biol. Chem.*, vol. 292, no. 30, pp. 12528–12541, 2017.
- [273] S. B. Qian, H. McDonough, F. Boellmann, D. M. Cyr, and C. Patterson, “CHIP-mediated stress recovery by sequential ubiquitination of substrates and Hsp70,” *Nature*, vol. 440, no. 7083, pp. 551–555, 2006.
- [274] M. J. Berridge, “Inositol trisphosphate and calcium signalling mechanisms,” *Biochimica et Biophysica Acta - Molecular Cell Research*, vol. 1793, no. 6.

pp. 933–940, 2009.

- [275] M. J. Berridge, “Inositol trisphosphate and calcium signalling,” *Nature*, vol. 361, no. 6410, pp. 315–325, 1993.
- [276] M. D. Bootman and M. J. Berridge, “The elemental principles of calcium signaling,” *Cell*, vol. 83, no. 5. pp. 675–678, 1995.
- [277] E. Finch, T. Turner, and S. Goldin, “Calcium as a coagonist of inositol 1,4,5-trisphosphate-induced calcium release,” *Science (80-. )*, vol. 252, no. 5004, pp. 443–446, 1991.
- [278] G. A. Mignery and T. C. Südhof, “The ligand binding site and transduction mechanism in the inositol-1,4,5-triphosphate receptor,” *EMBO J.*, vol. 9, no. 12, pp. 3893–8, 1990.
- [279] C. W. Taylor, P. C. A. Da Fonseca, and E. P. Morris, “IP3receptors: The search for structure,” *Trends in Biochemical Sciences*, vol. 29, no. 4. pp. 210–219, 2004.
- [280] J. Burgess and E. Raven, “Calcium in biological systems,” *Advances in Inorganic Chemistry*, vol. 61. pp. 251–366, 2009.
- [281] J. Evenas, A. Malmendal, and S. Forsen, “Calcium,” *Curr. Opin. Chem. Biol.*, vol. 2, pp. 293–302, 1998.
- [282] G. Auburger, N. E. Sen, D. Meierhofer, A. N. Başak, and A. D. Gitler, “Efficient Prevention of Neurodegenerative Diseases by Depletion of Starvation Response Factor Ataxin-2,” *Trends in Neurosciences*, vol. 40, no. 8. pp. 507–516, 2017.
- [283] D. Meierhofer, M. Halbach, N.-E. Sen, S. Gispert, and G. Auburger, “Atxn2-Knock-Out mice show branched chain amino acids and fatty acids pathway

- alterations.,” *Mol. Cell. Proteomics*, 2016.
- [284] I. Lastres-Becker *et al.*, “Mammalian ataxin-2 modulates translation control at the pre-initiation complex via PI3K/mTOR and is induced by starvation,” *Biochim. Biophys. Acta - Mol. Basis Dis.*, vol. 1862, no. 9, pp. 1558–1569, 2016.
- [285] D. Nonis *et al.*, “Ataxin-2 associates with the endocytosis complex and affects EGF receptor trafficking,” *Cell. Signal.*, vol. 20, no. 10, pp. 1725–1739, 2008.
- [286] A. Kang *et al.*, “Ataxin-1 is involved in tumorigenesis of cervical cancer cells via the EGFR–RAS–MAPK signaling pathway,” *Oncotarget*, vol. 8, no. 55, pp. 94606–94618, 2017.
- [287] H. G. Serra, C. E. Byam, J. D. Lande, S. K. Tousey, H. Y. Zoghbi, and H. T. Orr, “Gene profiling links SCA1 pathophysiology to glutamate signaling in Purkinje cells of transgenic mice,” *Hum. Mol. Genet.*, vol. 13, no. 20, pp. 2535–2543, 2004.
- [288] J. Silbereis, E. Cheng, Y. M. Ganat, L. R. Ment, and F. M. Vaccarino, “Precursors with glial fibrillary acidic protein promoter activity transiently generate GABA interneurons in the postnatal cerebellum,” *Stem Cells*, vol. 27, no. 5, pp. 1152–1163, 2009.
- [289] C. R. Edamakanti, J. Do, M. Didonna, Alessandro, Martina, and P. Opal, “Mutant ataxin1 disrupts cerebellar development in spinocerebellar ataxia type 1,” *J. Clin. Invest.*, pp. 1–14, 2018.
- [290] J. C. Darnell and E. Klann, “The translation of translational control by FMRP: Therapeutic targets for FXS,” *Nature Neuroscience*, vol. 16, no. 11, pp. 1530–1536, 2013.

- [291] I. J. Weiler *et al.*, “Fragile X mental retardation protein is necessary for neurotransmitter-activated protein translation at synapses,” *Proc. Natl. Acad. Sci. U. S. A.*, vol. 101, no. 50, pp. 17504–17509, 2004.
- [292] R. L. Strack and S. R. Jaffrey, “Using RNA Mimics of GFP to Image RNA Dynamics in Mammalian Cells,” in *Fluorescence Microscopy: Super-Resolution and other Novel Techniques*, 2014, pp. 83–91.
- [293] F. Tassone and E. Berry-Kravis, *The fragile X-associated tremor ataxia syndrome (FXTAS)*. 2010.
- [294] J. Zhang, L. Hou, E. Klann, and D. L. Nelson, “Altered hippocampal synaptic plasticity in the FMR1 gene family knockout mouse models,” *J. Neurophysiol.*, vol. 101, no. 5, pp. 2572–80, 2009.
- [295] L. Arnaud, B. A. Ballif, and J. A. Cooper, “Regulation of Protein Tyrosine Kinase Signaling by Substrate Degradation during Brain Development,” *Mol. Cell. Biol.*, vol. 23, no. 24, pp. 9293–9302, 2003.
- [296] H. Ishikawa and W. F. Marshall, “Ciliogenesis: Building the cell’s antenna,” *Nature Reviews Molecular Cell Biology*, vol. 12, no. 4. pp. 222–234, 2011.
- [297] E. M. Valente, R. O. Rosti, E. Gibbs, and J. G. Gleeson, “Primary cilia in neurodevelopmental disorders,” *Nature Reviews Neurology*, vol. 10, no. 1. pp. 27–36, 2014.
- [298] Y. Miyoshi *et al.*, “A new mouse allele of glutamate receptor delta 2 with cerebellar atrophy and progressive ataxia,” *PLoS One*, vol. 9, no. 9, 2014.
- [299] B. Osta, G. Benedetti, and P. Miossec, “Classical and paradoxical effects of TNF- $\alpha$  on bone homeostasis,” *Front. Immunol.*, vol. 5, no. 48, pp. 1–9, 2014.
- [300] L. Kubickova, L. Sedlarikova, R. Hajek, and S. Sevcikova, “TGF- $\beta$  – an

- excellent servant but a bad master,” *J. Transl. Med.*, vol. 10, no. 183, pp. 1–24, 2012.
- [301] P. Maroni, E. Matteucci, P. Bendinelli, and M. A. Desiderio, “Functions and Epigenetic Regulation of Wwox in Bone Metastasis from Breast Carcinoma: Comparison with Primary Tumors,” *Int. J. Mol. Sci.*, vol. 18, no. 1, p. 1, 2017.
- [302] S.-W. Park, J. Ludes-Meyers, D. B. Zimonjic, M. E. Durkin, N. C. Popescu, and C. M. Aldaz, “Frequent downregulation and loss of WWOX gene expression in human hepatocellular carcinoma,” *Br. J. Cancer*, vol. 91, no. 4, pp. 753–759, 2004.
- [303] D. M. A. Van den Heuvel, O. Harschnitz, L. H. van den Berg, and R. J. Pasterkamp, “Taking a risk: A therapeutic focus on ataxin-2 in amyotrophic lateral sclerosis?,” *Trends in Molecular Medicine*, vol. 20, no. 1, pp. 25–35, 2014.
- [304] S. Ben-Salem, A. M. Al-Shamsi, A. John, B. R. Ali, and L. Al-Gazali, “A Novel Whole Exon Deletion in WWOX Gene Causes Early Epilepsy, Intellectual Disability and Optic Atrophy,” *J. Mol. Neurosci.*, vol. 56, no. 1, pp. 17–23, May 2015.
- [305] S. M. Pulst, “Degenerative ataxias, from genes to therapies,” *Neurology*, vol. 86, no. 24, pp. 2284–2290, 2016.
- [306] J. R. Brouwer, R. Willemsen, and B. A. Oostra, “The FMR1 Gene and Fragile X-Associated Tremor/Ataxia Syndrome,” *Am. J. Med. Genet. B. Neuropsychiatr. Genet.*, vol. 0, no. 6, pp. 782–798, 2009.
- [307] M. F. Bear, K. M. Huber, and S. T. Warren, “The mGluR theory of fragile X mental retardation,” *Trends in Neurosciences*, vol. 27, no. 7, pp. 370–377,

2004.

- [308] L. Huang *et al.*, “Missense mutations in ITPR1 cause autosomal dominant congenital nonprogressive spinocerebellar ataxia,” *Orphanet J. Rare Dis.*, vol. 7, no. 1, 2012.
- [309] D. A. Fruman, H. Chiu, B. D. Hopkins, S. Bagrodia, L. C. Cantley, and R. T. Abraham, “The PI3K Pathway in Human Disease,” *Cell*, vol. 170, no. 4, pp. 605–635, 2017.
- [310] J. T. Weber, “Altered calcium signaling following traumatic brain injury,” *Front. Pharmacol.*, vol. 3, p. 60, 2012.
- [311] C. G. Lau *et al.*, “Regulation of NMDA receptor Ca<sup>2+</sup> signalling and synaptic plasticity,” *Biochem. Soc. Trans.*, vol. 37, no. Pt 6, pp. 1369–74, 2009.
- [312] M. K. Hsu, C. L. Pan, and F. C. Chen, “Functional divergence and convergence between the transcript network and gene network in lung adenocarcinoma,” *Onco. Targets. Ther.*, vol. 9, pp. 335–347, 2016.
- [313] Y. Wang, P. N. J. Schnegelsberg, J. Dausman, and R. Jaenisch, “Functional redundancy of the muscle-specific transcription factors Myf5 and myogenin,” *Nature*, 1996.
- [314] C. S. Von Koch *et al.*, “Generation of APLP2 KO mice and early postnatal lethality in APLP2/APP double KO mice,” *Neurobiol. Aging*, 1997.
- [315] D. Santamaría *et al.*, “Cdk1 is sufficient to drive the mammalian cell cycle,” *Nature*, 2007.
- [316] K. M. Cadigan, U. Grossniklaus, and W. J. Gehring, “Functional redundancy: the respective roles of the two sloppy paired genes in *Drosophila* segmentation,” *Proc. Natl. Acad. Sci.*, 1994.

- [317] M. Gonzalez-Gaitan, M. Rothe, E. A. Wimmer, H. Taubert, and H. Jackle, "Redundant functions of the genes knirps and knirps-related for the establishment of anterior Drosophila head structures.," *Proc. Natl. Acad. Sci.*, 1994.
- [318] F. M. Hoffmann, "Drosophila abl and genetic redundancy in signal transduction," *Trends in Genetics*. 1991.
- [319] R. Cohen, T. Yokoi, J. P. Holland, a E. Pepper, and M. J. Holland, "Transcription of the constitutively expressed yeast enolase gene ENO1 is mediated by positive and negative cis-acting regulatory sequences.," *Mol. Cell. Biol.*, 1987.
- [320] S. Nedvetzki *et al.*, "RHAMM, a receptor for hyaluronan-mediated motility, compensates for CD44 in inflamed CD44-knockout mice: A different interpretation of redundancy," *Proc. Natl. Acad. Sci.*, 2004.
- [321] J. E. Garcia, A. Puentes, and M. E. Patarroyo, "Developmental biology of sporozoite-host interactions in Plasmodium falciparum malaria: Implications for vaccine design," *Clinical Microbiology Reviews*. 2006.
- [322] M. A. El-Brolosy and D. Y. R. Stainier, "Genetic compensation: A phenomenon in search of mechanisms," *PLoS Genetics*. 2017.
- [323] A.-L. Barabási and Z. N. Oltvai, "Network biology: understanding the cell's functional organization," *Nat. Rev. Genet.*, 2004.
- [324] E. Davidson and M. Levin, "Gene regulatory networks.," *Proc. Natl. Acad. Sci. U. S. A.*, 2005.
- [325] X. Teng *et al.*, "Genome-wide consequences of deleting any single gene," *Mol. Cell*, 2013.



- [326] P. Chen, D. Wang, H. Chen, Z. Zhou, and X. He, “The nonessentiality of essential genes in yeast provides therapeutic insights into a human disease,” *Genome Res.*, 2016.
- [327] H. J. Muller, “Further studies on the nature and causes of gene mutations,” *International Congress of Genetics*. 1932.
- [328] A. S. Mukherjee and W. Beermann, “Synthesis of ribonucleic acid by the x-chromosomes of *Drosophila melanogaster* and the problem of dosage compensation [55],” *Nature*. 1965.
- [329] M. L. Barr and E. G. Bertram, “A morphological distinction between neurones of the male and female, and the behaviour of the nucleolar satellite during accelerated nucleoprotein synthesis [2],” *Nature*. 1949.
- [330] E. Heard and C. M. Disteche, “Dosage compensation in mammals: Fine-tuning the expression of the X chromosome,” *Genes and Development*. 2006.
- [331] M. F. Lyon, “Gene action in the X-chromosome of the mouse (*mus musculus* L.),” *Nature*, 1961.
- [332] W. C. Liew and L. Orban, “Zebrafish sex: A complicated affair,” *Brief. Funct. Genomics*, 2014.
- [333] T. E. Sztal, E. A. McKaige, C. Williams, A. A. Ruparelia, and R. J. Bryson-Richardson, “Genetic compensation triggered by actin mutation prevents the muscle damage caused by loss of actin protein,” *PLoS Genet.*, 2018.
- [334] D. I. Perez, C. Gil, and A. Martinez, “Protein kinases CK1 and CK2 as new targets for neurodegenerative diseases,” *Medicinal Research Reviews*. 2011.
- [335] K. Kawakami, “Transposon tools and methods in zebrafish,” *Developmental Dynamics*, vol. 234, no. 2. pp. 244–254, 2005.

- [336] M. Ferg, O. Armant, L. Yang, T. Dickmeis, S. Rastegar, and U. Strähle, “Gene transcription in the zebrafish embryo: Regulators and networks,” *Brief. Funct. Genomics*, vol. 13, no. 2, pp. 131–143, 2014.
- [337] M. Jinek, K. Chylinski, I. Fonfara, M. Hauer, J. A. Doudna, and E. Charpentier, “A Programmable Dual-RNA-Guided DNA Endonuclease in Adaptive Bacterial Immunity,” *Science (80-. )*, vol. 337, no. 6096, pp. 816–821, 2012.
- [338] A. Kaminski, M. T. Howell, and R. J. Jackson, “Initiation of encephalomyocarditis virus RNA translation: the authentic initiation site is not selected by a scanning mechanism,” *EMBO J.*, vol. 9, no. 11, pp. 3753–9, 1990.
- [339] K. M. Kwan *et al.*, “The Tol2kit: A multisite gateway-based construction Kit for Tol2 transposon transgenesis constructs,” *Dev. Dyn.*, vol. 236, no. 11, pp. 3088–3099, 2007.
- [340] K. Kawakami, “Transgenesis and Gene Trap Methods in Zebrafish by Using the Tol2 Transposable Element,” *Methods Cell Biol.*, vol. 77, pp. 201–222, 2004.
- [341] K. Kawakami and T. Noda, “Transposition of the Tol2 Element, an Ac-Like Element from the Japanese Medaka Fish *Oryzias latipes*, in Mouse Embryonic Stem Cells,” *Genetics*, vol. 166, no. 2, pp. 895–899, 2004.
- [342] K. Kawakami, H. Takeda, N. Kawakami, M. Kobayashi, N. Matsuda, and M. Mishina, “A transposon-mediated gene trap approach identifies developmentally regulated genes in zebrafish,” *Dev. Cell*, vol. 7, no. 1, pp. 133–144, 2004.

- [343] K. Kawakami and A. Shima, "Identification of the Tol2 transposase of the medaka fish *Oryzias latipes* that catalyzes excision of a nonautonomous Tol2 element in zebrafish *Danio rerio*," *Gene*, vol. 240, no. 1, pp. 239–244, 1999.
- [344] K. Kawakami, K. Imanaka, M. Itoh, and M. Taira, "Excision of the Tol2 transposable element of the medaka fish *Oryzias latipes* in *Xenopus laevis* and *Xenopus tropicalis*," *Gene*, vol. 338, no. 1, pp. 93–98, 2004.
- [345] Z. Ivics, P. B. Hackett, R. H. Plasterk, and Z. Izsvák, "Molecular reconstruction of sleeping beauty, a Tc1-like transposon from fish, and its transposition in human cells," *Cell*, 1997.
- [346] P. Blader and U. Strähle, "Zebrafish developmental genetics and central nervous system development.," *Hum. Mol. Genet.*, 2000.
- [347] R. Ward, "Vertebrate Central Nervous System," *Life Sci.*, 2001.
- [348] A. V. Kalueff, A. M. Stewart, and R. Gerlai, "Zebrafish as an emerging model for studying complex brain disorders," *Trends in Pharmacological Sciences*. 2014.
- [349] J. M. Fadool and J. E. Dowling, "Zebrafish: A model system for the study of eye genetics," *Progress in Retinal and Eye Research*. 2008.


# APPENDIX

## PERMISSIONS FROM THE REPRODUCED FIGURES OF PUBLISHED STUDIES

**Figure 1.1. The anatomy of the cerebellum is illustrated. (A) The internal structures of the cerebellum including, cerebellar cortex in grey matter, and fastigial nucleus, globose nucleus, emboliform nucleus in white matter were shown (Reused by courtesy of Professor Heshmat S.W. Haroun) [16].**

Copy right for Cerebellar Nuclei and connections in Man

Inbox x


**Goksemin Fatma SENGUL** <gokseminsengul@gmail.com>  
to heshmatsabet

Jun 5 (6 days ago) ☆

Dear Professor Heshmat Sabet;

I am Goksemin Fatma Sengul from Bilkent University. I want to use one figure from your paper entitled as Cerebellar Nuclei and Connections in Man. Can you prove the copy right permission for this paper to reuse it in my thesis? I could not replace with any other picture from the one in the paper. So, I would be glad if you can help about this issue.


Best

**Heshmat Haroun**  
to me

Jun 5 (6 days ago) ☆

Dear Goksemin Fatma

Thank you for the email. Regarding the use of my paper in your thesis, you can easily do that but with reference to me and the publisher. I didn't understand exactly what do you from the figure mentioned in the paper. Please clarify your request and I shall not hesitate to help.

**Goksemin Fatma SENGUL** <gokseminsengul@gmail.com>  
to Heshmat

Jun 5 (6 days ago) ☆


Dear Professor Heshmat Haroun;

I want to use Figure 1. to describe the morphological and structural aspects of the cerebellum. Let me introduce my thesis a bit. I am working on a movement disorder which is cerebellar ataxia. Therefore, I open a session in my thesis describes cerebellum. My PI suggested me to put pictures with regards to cerebellum since I mentioned about its functional, morphological and structural aspects of it, I want to put your figure to tell the details about functional and structural areas in the cerebellum. Sorry, if I forgot to mention about these details in my first email. Right now, the required thing is that copy right permission to reuse this figure. Since you are the only person has rights of the paper, copy right center ([www.copyright.com](http://www.copyright.com)) also suggested to contact directly with you to reuse your picture in my thesis. I appreciate your helps and understandings about this issue.

Here is the article that I want to use  
Figure 1

Haroun, H. S. W., "Cerebellar nuclei and connections in man.", *Anatomy Physiology Biochem Int J (APBIJ)*, vol. 1, issue 1, pp. ID555552, 2016.

Best


**Heshmat Haroun**  
to me

Jun 5 (6 days ago) ☆

Dear Goksemin Fatma

Thank you for your second mail. I would like to tell you that I have no objection to use any part of my article with my best wishes for you along your thesis.

Best Regards

**Goksemin Fatma SENGUL** <gokseminsengul@gmail.com>  
to Heshmat

Jun 5 (6 days ago) ☆

Dear Professor Heshmat Haroun;

I am glad and thank you so much for approving my reuse your picture in my thesis and also your good luck wishes.

Best

**Figure 1.1. The anatomy of the cerebellum is illustrated.(B)The functional structures of the cerebellum containing cerebrocerebellum, spinocerebellum and vestibulocerebellum were depicted (Reprinted with permission from Sinauer Association) [17].**


no-reply@copyright.com  
Kime: Goksemin Fatma Sengul  
[Copyright.com](https://copyright.com) Order Confirmation

5 Haziran 2018 19:31

N

Do Not Reply Directly to This Email  
To ensure that you continue to receive our emails,  
please add [copyright@marketing.copyright.com](mailto:copyright@marketing.copyright.com) to your [address book](#).

**Thank You for Your Order with  
Copyright Clearance Center**



**Dear Goksemin Sengul,**


Thank you for placing your order with [Copyright Clearance Center](#).

Order Summary:  
Order Date: 06/05/2018  
Confirmation Number: 11722029  
Items in order: 1  
Order Total: \$ 0.00

To view or print your order details or terms and conditions,  
click the following link and log in: [Order link](#)

Need additional permissions? [Go here](#).

How was your experience? [Click here to give us feedback](#).



If you need assistance, please visit our online help ([www.copyright.com/help](http://www.copyright.com/help)).  
Please do not reply to this message. This e-mail address is not monitored for responses.

**Toll Free: +1.855.239.3415**  
**Local: +1.978.646.2600**  
**[info@copyright.com](mailto:info@copyright.com)**  
**[www.copyright.com](http://www.copyright.com)**

Please visit [Copyright Clearance Center](#) for more information.

This email was sent by Copyright Clearance Center  
222 Rosewood Drive, Danvers, MA 01923 USA

To view the privacy policy, please [go here](#).

Figure 1.2. Magnetic resonance imaging of patient with ARCA3 is represented. (A) Sagittal T1=weighted sequence is shown. (B) Transverse T1=weighted sequence is indicated (Reprinted with the permission of JAMA Neurology and by the courtesy of Professor Michel Koenig) [30].

goksemin  
Kime: michel.koenig@inserm.fr  
Copyright permission for paper

8 Haziran 2018 21:25  
Gönderilen - Google



Dear Professor Michel Koenig;

I am Goksemin Fatma Sengul from Bilkent University. I want to use your figure 1 from the article named as **Autosomal recessive cerebellar ataxia type 3 due to ANO10 mutations: delineation and genotype-phenotype correlation study** published in Jama Neurology in 2014. I want to reuse Figure 1 to describe the changes in the brains of patient with ARCA3. Therefore, I want to ask that may I use your Figure 1 to tell my points clearly in my thesis. I appreciate your understandings and helps.

I attached the article.

Best  
Goksemin

Michel Koenig  
Kime: goksemin  
Ynt: Copyright permission for paper

Evvelsi gün 12:29



Dear Dr Goksemin Sengul,

yes please, use figure 1 of the JAMA Neurol 2014 paper for your thesis. Please, do not forget to cite the paper.

Best regards,

Pr Michel Koenig, MD-PhD  
Laboratoire de Génétique Moléculaire  
EA7402 Institut Universitaire de Recherche Clinique  
641 avenue du Doyen Gaston Giraud  
34093 Montpellier Cedex 5, France  
e-mail: [michel.koenig@inserm.fr](mailto:michel.koenig@inserm.fr)  
Tel: 33 (0)4 1175 9879  
Fax: 33 (0)4 1175 9882

goksemin

Kime: Michel Koenig

Ynt: Copyright permission for paper

Evvelsi gün 12:31

Gönderilen - Google

G

Dear Professor Michel Koenig;

I ensure you that I will cite your paper and add reproduced by the courtesy of Professor Michel Koenig and JAMA Neurology. I appreciate your positive return.

Best  
Goksemin

no-reply@copyright.com

Kime: fatma.sengul@bilkent.edu.tr

RESPONSE REQUIRED for your request to American Medical Association

Bugün 18:54

N

# JAMA Neurology

## Accept your approved request

Dear Mrs. Goksemin Sengul,

American Medical Association has approved your recent request described below. Before you can use this content, **you must accept** the license fee and terms set by the publisher.

Use this [link](#) to accept (or decline) the publisher's fee and terms for this order.

### Order Summary

Licensee: Goksemin Sengul  
Order Date: Jun 8, 2018  
Order Number: 501406607  
Publication: JAMA Neurology  
Title: Autosomal Recessive Cerebellar Ataxia Type 3 Due to : Delineation and Genotype-Phenotype Correlation Study  
Type of Use: Dissertation/Thesis

View or print complete [details](#) of your request.

Sincerely,

Copyright Clearance Center

Tel: +1-855-239-3415 / +1-978-646-2777  
[customercare@copyright.com](mailto:customercare@copyright.com)  
<https://myaccount.copyright.com>



RightsLink®

**Figure 1.3. (A) Computerized axial tomography (CAT) scan of CAMRQ1 affected individual with enhanced contrast is shown. (B) The coronal section of the brain is depicted. (C) The sagittal section of brain is illustrated. Reductions in the volumes of the cerebellum and vermis were clearly detected in all images (Reprinted with permission from John Wiley and Sons) [57].**

☆ no-reply@copyright.com

8 Haziran 2018 14:40

Kime: fatma.sengul@bilkent.edu.tr

Thank you for your order with RightsLink / John Wiley and Sons

N



## Thank you for your order!

Dear Mrs. Goksemin Sengul,

Thank you for placing your order through Copyright Clearance Center's RightsLink® service.

### Order Summary

Licensee: Goksemin Sengul  
Order Date: Jun 8, 2018  
Order Number: 4364180408484  
Publication: American Journal of Medical Genetics Part A  
Title: Nonprogressive cerebellar disorder with mental retardation and autosomal recessive inheritance in hutterites  
Type of Use: Dissertation/Thesis  
Order Total: 0.00 USD

View or print complete [details](#) of your order and the publisher's terms and conditions.

Sincerely,

Copyright Clearance Center

Tel: +1-855-239-3415 / +1-978-646-2777  
[customercare@copyright.com](mailto:customercare@copyright.com)  
<https://myaccount.copyright.com>



RightsLink®



Figure 1.4. MRI-based morphological analysis of control and CAMRQ2 affected individuals' brains are shown. (A) The midsagittal MRI images of control and CAMRQ2 affected individuals were illustrated. The highlighted numbers:(1) corpus callosum, (2) third ventricle, (3) fourth ventricle, (4) cerebellum on the right top image indicated brain areas where the volumetric changes became apparent. (B) The lateral and medial schematic representations of cortical regions are depicted. The highlighted numbers, (5) BA45, (6) BA44, (7) BA6, (8) precentral, (9) superior temporal, (10) superior parietal, (11) lateral occipital, (12) fusiform, (13) isthmus cingulated, (14) posterior cingulated, (15) frontal pole, (16) medial orbitofrontal, (17) temporal pole (Reprinted by the courtesy of Professor Tayfun Özçelik) [47].

goksemin

Kime: tozcelik@bilkent.edu.tr

Copyright for the Gulsuner et al 2011

8 Haziran 2018 21:02

Gönderilen - Google

G

Sayın Prof. Dr. Tayfun Hocam;

Ben Michelle Adams'ın MSc öğrencisi Goksemin Fatma Sengul. Tezimde kullanmak için sizin 2011 yılında Genome Research adlı dergide yayınladığınız **Homozygosity mapping and targeted genomic sequencing reveal the gene responsible for cerebellar hypoplasia and quadrupedal locomotion in a consanguineous kindred** isimli yayınınızın brinci figürünü CAMRQ2 hastalarının beyin bölgelerindeki değişimi anlatmak için kullanmak istiyorum. Copyright center sayfasından izin almak istediğimde maalesef onların bana bu hakkı sağlayamayacaklarını öğrendim. Onların tavsiyesi üzerine hem Journal editörüne hem de size kullanım iznini danışmak için mail attım. Eğer izniniz olursa tezimde bahsettiğim makalenin ilk figürünü kullanmak istiyorum. Yardım ve anlayışınız için tesekkürler.

Makaleyi ekte bulabilirsiniz.

İyi çalışmalar  
Saygılarımla  
Göksemin

**Tayfun Ozcelik**

Kime: goksemin

Ynt: Copyright for the Gulsuner et al 2011

8 Haziran 2018 21:42

TO

Sevgili Göksemin,

Tabii, benim açımdan hiçbir sakıncası yok. Memnun olurum.

Tayfun Özçelik

Sayın Prof. Dr. Tayfun Hocam;  
Ben Michelle Adams'ın MSc öğrencisi Goksemin Fatma Sengul. Tezimde  
kullanmak için sizin 2011 yılında Genome Research adlı dergide

Daha Fazlasını Gör

İyi çalışmalar  
Saygılarımla  
Göksemin

--  
Tayfun Ozcelik  
Professor of Human Genetics  
Bilkent University  
Department of Molecular Biology and Genetics  
Bilkent - Ankara 06800  
Turkey  
Tel: +90-312-2902139  
Fax: +90-312-2665097  
e-mail: [tozcelik@bilkent.edu.tr](mailto:tozcelik@bilkent.edu.tr)

**goksemin**

Kime: Tayfun Ozcelik

Ynt: Copyright for the Gulsuner et al 2011

8 Haziran 2018 21:43

All Mail - Google

G

Sayın Prof. Dr. Tayfun Hocam;

İzniniz için çok teşekkürler.

İyi akşamlar  
Göksemin

Figure 1.5. The proposed topology and functional transmembrane domains of Anoctamin family member proteins are depicted (Reprinted with the permission from American Society for Pharmacology and Experimental Therapeutics) [77].



*Council*

**John D. Schuetz**  
President  
St. Jude Children's Research  
Hospital

**Edward T. Morgan**  
President-Elect  
Emory University School of  
Medicine

**David R. Sibley**  
Past President  
Bethesda, Maryland

**John J. Tesmer**  
Secretary/Treasurer  
University of Michigan

**Margaret E. Gnegy**  
Secretary/Treasurer-Elect  
University of Michigan Medical  
School

**Charles P. France**  
Past Secretary/Treasurer  
The University of Texas Health  
Science Center at San Antonio

**Wayne L. Backes**  
Councilor  
Louisiana State University Health  
Sciences Center

**Carol L. Beck**  
Councilor  
Thomas Jefferson University

**Alan V. Smrcka**  
Councilor  
University of Michigan Medical  
School

**Mary E. Vore**  
Chair, Board of Publications  
Trustees  
University of Kentucky

**Brian M. Cox**  
FASEB Board Representative  
Bethesda, MD

**Michael W. Wood**  
Chair, Program Committee  
Neupharm LLC

**Judith A. Siuciak**  
Executive Officer

June 8, 2018

Goksemin Fatma Sengul  
Neuroscience  
Bilkent University  
Universiteler Mahallesi  
Ankara  
Turkey

Email: fatma.sengul@bilkent.edu.tr

Dear Goksemin Fatma Sengul:

This is to grant you permission to reproduce the following figure in your thesis titled "The expression analysis of three movement-disorder related genes following the knockdown of ano10, wdr81 and vldlr in Zebrafish (*Danio rerio*)" for the Bilkent University Interdisciplinary Neuroscience Graduate Program:

Figure 3 from F Huang, X Wong, and LY Jan (2012) International Union of Basic and Clinical Pharmacology. LXXXV: Calcium-Activated Chloride Channels, *Pharmacol Rev*, 64(1): 1-15; DOI: <https://doi.org/10.1124/pr.111.005009>

Permission to reproduce the figure is granted for worldwide use in all languages, translations, and editions, and in any format or medium including print and electronic. The authors and the source of the materials must be cited in full, including the article title, journal title, volume, year, and page numbers.

Sincerely yours,

Richard Dodenhoff  
Journals Director

Transforming Discoveries into Therapies  
ASPET - 9650 Rockville Pike - Bethesda, Maryland 20814 - Office: 301-634-7060 - [aspet.org](http://aspet.org)



**Figure 1.6. The schematic *in silico* representation of functional domains within the transmembrane WDR81 protein is depicted (Reprinted by the courtesy of Professor Michelle Adams and with the permission from Springer Nature BMC Neuroscience) [33].**

**Goksemin Fatma ŞENGÜL**

Kime: Michelle Adams

Permisssion to reproduce figures from Doldur-Ballı et al.

Bugün 00:58

Gönderilen - Google

GF

Dear Professor Michelle Adams;

I would plan to reuse the Figure 4 and Supplementary Figure 1 of Fusun's paper. I went to the copyright and they suggested that all rights of the paper is belong to the author, Doldur-Ballı et al. However, I thought that I need to take the permission from the correspondence author, you to reuse the Figure 4 and Supplementary Figure 1 of paper named as Characterization of a novel zebrafish (*Danio rerio*) gene, *wdr81*, associated with cerebellar ataxia, mental retardation and dysequilibrium syndrome (CAMRQ). Therefore, I would like to ask you that may I use these figure 4 and Supplementary Fig 1 in my thesis if you allow? I will immediately contact with her. I appreciate your helps.

Best  
Goksemin

--

Goksemin Fatma SENGÜL  
MSc. Student, Neuroscience  
Michelle Adams Lab, UNAM 505B  
Bilkent University  
06800 Bilkent, Ankara, Turkey

**Michelle Adams**

Kime: Goksemin Fatma ŞENGÜL

Ynt: Permisssion to reproduce figures from Doldur-Ballı et al.

Bugün 08:46

MA

Dear Goksemin,

You have my permission to reproduce these figures in your thesis.

Michelle Adams

[Goksemin Fatma ŞENGÜL adlı kişiye ait metnin Daha Fazlasını Gör](#)

Michelle Adams, PhD  
Professor of Neuroscience and Psychology  
Neuroscience Graduate Program Director  
Psychology Department  
Bilkent University  
06800 Bilkent  
Ankara - TURKEY  
+90 (312) 290-1090 (Psychology office)  
+90 (312) 290-3093 (Brain Research Center office)  
+90 (312) 290-3415 (Department of Psychology Main office)  
+90 (312) 290-2561 (Fax)

## SPRINGER NATURE

Dear Dr. Sengul,

Thank you for contacting Springer Nature.

Reproduction of figures or tables from any article is permitted free of charge and without formal written permission from the publisher or the copyright holder, provided that the figure/table is original, BioMed Central is duly identified as the original publisher, and that proper attribution of authorship and the correct citation details are given as acknowledgment.

With kind regards,

---

**Joel Lagmay**

Global Open Research Support Executive  
Global Open Research Support

**Springer Nature**

T +44 (0)203 192 2009

[www.springernature.com](http://www.springernature.com)

---

Springer Nature is a leading research, educational and professional publisher, providing quality content to our communities through a range of innovative platforms, products and services. Every day, around the globe, our imprints, books, journals and resources reach millions of people – helping researchers, students, teachers & professionals to discover, learn and achieve.

---

In the US: Springer Customer Service Center LLC, 233 Spring Street, New York, NY 10013

Registered Address: 2711 Centerville Road Wilmington, DE 19808 USA

State of Incorporation: Delaware, Reg. No. 4538065

Rest of World: Springer Customer Service Center GmbH,

Tiergartenstraße 15 – 17, 69121 Heidelberg

Registered Office: Heidelberg | Amtsgericht Mannheim, HRB 336546

Managing Directors: Martin Mos, Dr. Ulrich Vest

-----Your Question/Comment -----

Dear who is my concern:

I am Goksemin Fatma Sengul from Bilkent University. I want to reproduce Figure 4 and Supplementary from the paper entitled as  
Characterization of a novel zebrafish (*Danio rerio*) gene, *wdr81*, associated with cerebellar ataxia, mental retardation and dysequilibrium syndrome (CAMRQ)

Figure 1 in my thesis. I want to reuse these Figures to compare the WMISH results of *wdr81* with my other two targeted genes and as well as to describe the domains in the *wdr81* protein to speculate about its novel or known functions. I contacted with the copyright center and officer suggested me to directly right to the first author or corresponding author. However, the corresponding author suggested me to take the actual permission from you. Therefore, I decide to write to the BMC journal. I want to ask that may I use Figure 4 and Supplementary Fig 1 from the study that was published in BMC in 2015. I appreciate all of your helps and understandings.

Best wishes  
Goksemin

---

**Figure 1.7. A schematic representation of Reelin signaling pathway during early development (Reprinted with the permission from Aging and Disease) [123].**

goksemin

Kime: Editorial Office

Copyright for reprint

Evvelsi gün 00:16

Gönderilen - Google

G

Dear who I concern;

I am Goksemin Fatma Sengul from Bilkent University. I want to reprint Figure 1 from the paper

Reelin-mediated Signaling during Normal and Pathological Forms of Aging published in Aging and Disease in 2010. I cannot find the copyright part in the permission session. I consult with Copyright center and they suggested me to directly right to you for the approval of the putting the Figure my into my thesis to suggest the role of vldlr regulated Reelin signaling pathway in synaptic plasticity and in f-actin stabilization&microtuble stabilization. Therefore, I would like to ask you that may I use this Figure to convey my stamemnts more clearly. I appreciate your understandings.

You can find the article in attachements.



Reelin-mediated

Editorial Office

Kime: goksemin

RE: Copyright for reprint

Evvelsi gün 01:24

E

H, Goksemin

Yes, you can use the figure 1 in your thesis.

Kunlin Jin, M.D., Ph.D.

Editor-in-Chief

Aging and Disease

[www.aginganddisease.org](http://www.aginganddisease.org)

[goksemin](#) adlı kişiye ait metnin **Daha Fazlasını Gör**

**goksemin**

Kime: Editorial Office

Ynt: Copyright for reprint

Evvelsi gün 01:30

Gönderilen - Google

G

Dear Kunlin Jin;

I have additional question. Should I write reprinted with the permission from Aging and Disease or do you suggest something else?

Best

9 Haz 2018 tarihinde 01:24 saatinde, [editorial@aginganddisease.org](mailto:editorial@aginganddisease.org) şunları yazdı:

[editorial@aginganddisease.org](#) adlı kişiye ait metnin **Daha Fazlasını Gör**

**Editorial Office**

Kime: goksemin

Ynt: Copyright for reprint

Evvelsi gün 02:15

EO

My email was permission

Sent from my iPhone

[goksemin](#) adlı kişiye ait metnin **Daha Fazlasını Gör**

**goksemin**

Kime: Editorial Office

Ynt: Copyright for reprint

Evvelsi gün 02:20

Gönderilen - Google

G

Dear Kunlin Jun;

Should I wrote by the courtesy of Kunlin Jun did I understand wrong?

Best

9 Haz 2018 tarihinde 02:15 saatinde, Editorial Office <[editorial@aginganddisease.org](mailto:editorial@aginganddisease.org)> şunları yazdı:

[Editorial Office](#) adlı kişiye ait metnin **Daha Fazlasını Gör**

**Editorial Office**

Kime: goksemin

RE: Copyright for reprint

Bugün 18:31

E

Please feel free to use figure 1. You own the copy right.

Kunlin Jin, M.D., Ph.D.

Editor-in-Chief

Aging and Disease

[www.aginganddisease.org](http://www.aginganddisease.org)

[goksemin](#) adlı kişiye ait metnin **Daha Fazlasını Gör**



**Figure 1.8. The depiction of orthologous genes among zebrafish, human, mouse, and chicken genomes. This image was obtained from orthology relationships through Ensemble Campara 63. If a gene has been duplicated in one lineage, it is accepted as one single shared gene in the overlapping region (Reprinted with the permission from Springer Nature) [141].**

no-reply@copyright.com

Evvelsi gün 00:51

Kime: Goksemin Fatma Sengul

N

Thank you for your order with RightsLink / Springer Nature

**SPRINGER NATURE**

### Thank you for your order!

Dear Mrs. Goksemin Sengul,

Thank you for placing your order through Copyright Clearance Center's RightsLink® service.

#### Order Summary

Licensee: Goksemin Sengul  
Order Date: Jun 8, 2018  
Order Number: 4364420795269  
Publication: Nature  
Title: The zebrafish reference genome sequence and its relationship to the human genome  
Type of Use: Thesis/Dissertation  
Order Total: 0.00 USD

View or print complete [details](#) of your order and the publisher's terms and conditions.

Sincerely,

Copyright Clearance Center

Tel: +1-855-239-3415 / +1-978-646-2777  
[customercare@copyright.com](mailto:customercare@copyright.com)  
<https://myaccount.copyright.com>



RightsLink®

**Figure 1.9. Representation of the zebrafish organs. The upper image depicts a dorsal view of brain and nervous system whereas the picture below indicates internal organs. The abbreviations for the structures of the brain and nervous system; OB: Olfactory bulb, Tel: Telencephalon, Ha: Habenula, Ctec: Commissura tecti, TeO: Optic tectum, CCe: Corpus cerebelli, EG: Eminentia granularis, CC: Crista cerebellaris, LVB: Facial lobe, MO: Medulla oblongatis, MS: Medulla spinalis (Reprinted with the permission from Birkhä user Verlag) [144], (Reprinted with the permission from Special Issue Biomedical Ultrasound) [145].**

no-reply@copyright.com  
Kime: fatma.sengul@bilkent.edu.tr  
[Copyright.com](#) Order Confirmation


Evvelsi gün 01:18

N

Do Not Reply Directly to This Email

To ensure that you continue to receive our emails,  
please add [copyright@marketing.copyright.com](mailto:copyright@marketing.copyright.com) to your [address book](#).

**Thank You for Your Order with  
Copyright Clearance Center**



**Dear Goksemin Sengul,**


Thank you for placing your order with [Copyright Clearance Center](#).

Order Summary:  
Order Date: 06/08/2018  
Confirmation Number: 11722744  
Items in order: 1  
Order Total: \$ 0.00

To view or print your order details or terms and conditions,  
click the following link and log in: [Order link](#)

Need additional permissions? [Go here](#).

How was your experience? [Click here to give us feedback](#).



If you need assistance, please visit our online help ([www.copyright.com/help](http://www.copyright.com/help)).

Please do not reply to this message. This e-mail address is not monitored for responses.

**Toll Free: +1.855.239.3415**  
**Local: +1.978.646.2600**  
[info@copyright.com](mailto:info@copyright.com)  
[www.copyright.com](http://www.copyright.com)

Please visit [Copyright Clearance Center](#) for more information.

This email was sent by Copyright Clearance Center  
222 Rosewood Drive, Danvers, MA 01923 USA

To view the privacy policy, please [go here](#).

**Figure 1. 10. Lateral view of adult female (F) zebrafish is shown in above and male (M) zebrafish is shown in below. Abbreviations; wt: wild type, L: Left side of the bodies (Adapted from Elsevier) [149].**

no-reply@copyright.com

9 Haziran 2018 02:14

N

Kime: Goksemin Fatma Sengul

Thank you for your order with RightsLink / Elsevier



### Thank you for your order!

Dear Mrs. Goksemin Sengul,

Thank you for placing your order through Copyright Clearance Center's RightsLink® service.

#### Order Summary

Licensee: Goksemin Sengul  
Order Date: Jun 8, 2018  
Order Number: 4364451248150  
Publication: Mechanisms of Development  
Title: The zebrafish mutant bumper shows a hyperproliferation of lens epithelial cells and fibre cell degeneration leading to functional blindness  
Type of Use: reuse in a thesis/dissertation  
Order Total: 0.00 USD

View or print complete [details](#) of your order and the publisher's terms and conditions.

Sincerely,

Copyright Clearance Center

Tel: +1-855-239-3415 / +1-978-646-2777  
[customercare@copyright.com](mailto:customercare@copyright.com)  
<https://myaccount.copyright.com>



RightsLink®

**Figure 1.11. An illustration of splice-blocking morpholino (MO) effects. (A) The normal endogenous splicing mechanism is shown. (B) The first possible route of SD MO action is targeting the splice donor site and inhibiting the binding of U1 complex. (C) The second possible route of SA MO action is targeting to the splice acceptor side and inhibiting the binding of U2AF (AF) spliceosomal component thereby following the subsequent recruitment of the U2 complex. In both cases, the lariat formation process does not occur, the splicing event is halted and a new mRNA transcript is not generated. Abbreviations: splice donor site targeting morpholino (SD MO); Splice acceptor site targeting morpholino (SA MO) (Reprinted with the permission from Mary Ann Liebert, Inc) [154].**

no-reply@copyright.com

Kime: fatma.sengul@bilkent.edu.tr

[Copyright.com](http://Copyright.com) Order Confirmation


Evvelsi gün 02:59

N

Do Not Reply Directly to This Email

To ensure that you continue to receive our emails,  
please add [copyright@marketing.copyright.com](mailto:copyright@marketing.copyright.com) to your [address book](#).

**Thank You for Your Order with  
Copyright Clearance Center**



**Dear Goksemin Sengul,**


Thank you for placing your order with [Copyright Clearance Center](#).

Order Summary:  
Order Date: 06/08/2018  
Confirmation Number: 11722753  
Items in order: 1  
Order Total: \$TBD

To view or print your order details or terms and conditions,  
click the following link and log in: [Order link](#)

Need additional permissions? [Go here](#).

How was your experience? [Click here to give us feedback](#).



If you need assistance, please visit our online help ([www.copyright.com/help](http://www.copyright.com/help)).

Please do not reply to this message. This e-mail address is not monitored for responses.

**Toll Free: +1.855.239.3415**  
**Local: +1.978.646.2600**  
[info@copyright.com](mailto:info@copyright.com)  
[www.copyright.com](http://www.copyright.com)

Please visit [Copyright Clearance Center](#) for more information.

This email was sent by Copyright Clearance Center  
222 Rosewood Drive, Danvers, MA 01923 USA

To view the privacy policy, please [go here](#).

**Figure 1.12. The mechanism of action of translation blocking morpholinos. A) The normal endogenous translation mechanism is depicted. B) The translation-inhibiting morpholino targets to the 5'UTR and prevents the scanning of 40S ribosomal subunit, thereby inhibiting the starting and elongation steps of the translation process (Reprinted with the permission from Mary Ann Liebert, Inc) [154].**

no-reply@copyright.com  
Kime: fatma.sengul@bilkent.edu.tr  
[Copyright.com](http://Copyright.com) Order Confirmation


9 Haziran 2018 02:59

N

Do Not Reply Directly to This Email

To ensure that you continue to receive our emails,  
please add [copyright@marketing.copyright.com](mailto:copyright@marketing.copyright.com) to your address book.

**Thank You for Your Order with  
Copyright Clearance Center**



**Dear Goksemin Sengul,**


Thank you for placing your order with [Copyright Clearance Center](http://Copyright Clearance Center).

Order Summary:  
Order Date: 06/08/2018  
Confirmation Number: 11722753  
Items in order: 1  
Order Total: \$TBD

To view or print your order details or terms and conditions,  
click the following link and log in: [Order link](#)

Need additional permissions? [Go here](#).

How was your experience? [Click here to give us feedback](#).



If you need assistance, please visit our online help ([www.copyright.com/help](http://www.copyright.com/help)).

Please do not reply to this message. This e-mail address is not monitored for responses.

**Toll Free: +1.855.239.3415**  
**Local: +1.978.646.2600**  
[info@copyright.com](mailto:info@copyright.com)  
[www.copyright.com](http://www.copyright.com)

Please visit [Copyright Clearance Center](http://Copyright Clearance Center) for more information.

This email was sent by Copyright Clearance Center  
222 Rosewood Drive, Danvers, MA 01923 USA

To view the privacy policy, please [go here](#).

**Figure 3.4. Whole mount *in situ* hybridization (WMISH) was performed with Zebrafish embryos in order to show the localization of *wdr81*, *vldlr*, *ano10A* mRNA transcription certain common nervous system areas. (A) The expression pattern of *wdr81* in early developmental stages of Zebrafish (Doldur-Ballı *et al.*, 2015) (Adapted by the courtesy of Professor Michelle Adams and with the permission from the Springer Nature BMC Neuroscience) [33]. Abbreviations, Ce: cerebellum, Di: diencephalon, FB: forebrain region, HB: hindbrain region, Hy: hypothalamus, MB: midbrain region, MLF: medial longitudinal, OV: Optic vesicle, Le: Lens, hpf: hour post fertilization, dpf: day post fertilization [33].**

Goksemin Fatma ŞENGÜL

Kime: Michelle Adams

Permisssion to reproduce figures from Doldur-Ballı et al.

Bugün 00:58

Gönderilen - Google

GF

Dear Professor Michelle Adams;

I would plan to reuse the Figure 4 and Supplementary Figure 1 of Fusun's paper. I went to the copyright and they suggested that all rights of the paper is belong to the author, Doldur-Ballı et al. However, I thought that I need to take the permission from the correspondence author, you to reuse the Figure 4 and Supplementary Figure 1 of paper named as Characterization of a novel zebrafish (*Danio rerio*) gene, *wdr81*, associated with cerebellar ataxia, mental retardation and dysequilibrium syndrome (CAMRQ). Therefore, I would like to ask you that may I use these figure 4 and Supplementary Fig 1 in my thesis if you allow? I will immediately contact with her. I appreciate your helps.

Best  
Goksemin

Goksemin Fatma SENGÜL  
MSc. Student, Neuroscience  
Michelle Adams Lab, UNAM 505B  
Bilkent University  
06800 Bilkent, Ankara, Turkey

Michelle Adams

Kime: Goksemin Fatma ŞENGÜL

Ynt: Permisssion to reproduce figures from Doldur-Ballı et al.

Bugün 08:46

MA

Dear Goksemin,

You have my permission to reproduce these figures in your thesis.

Michelle Adams

[Goksemin Fatma ŞENGÜL adlı kişiye ait metnin Daha Fazlasını Gör](#)

Michelle Adams, PhD  
Professor of Neuroscience and Psychology  
Neuroscience Graduate Program Director  
Psychology Department  
Bilkent University  
06800 Bilkent  
Ankara - TURKEY  
+90 (312) 290-1090 (Psychology office)  
+90 (312) 290-3093 (Brain Research Center office)  
+90 (312) 290-3415 (Department of Psychology Main office)  
+90 (312) 290-2561 (Fax)

## SPRINGER NATURE

Dear Dr. Sengul,

Thank you for contacting Springer Nature.

Reproduction of figures or tables from any article is permitted free of charge and without formal written permission from the publisher or the copyright holder, provided that the figure/table is original, BioMed Central is duly identified as the original publisher, and that proper attribution of authorship and the correct citation details are given as acknowledgment.

With kind regards,

---

**Joel Lagmay**

Global Open Research Support Executive  
Global Open Research Support

**Springer Nature**

T +44 (0)203 192 2009

[www.springernature.com](http://www.springernature.com)

---

Springer Nature is a leading research, educational and professional publisher, providing quality content to our communities through a range of innovative platforms, products and services. Every day, around the globe, our imprints, books, journals and resources reach millions of people – helping researchers, students, teachers & professionals to discover, learn and achieve.

---

In the US: Springer Customer Service Center LLC, 233 Spring Street, New York, NY 10013

Registered Address: 2711 Centerville Road Wilmington, DE 19808 USA

State of Incorporation: Delaware, Reg. No. 4538065

Rest of World: Springer Customer Service Center GmbH, Tiergartenstraße 15 – 17, 69121 Heidelberg

Registered Office: Heidelberg | Amtsgericht Mannheim, HRB 336546

Managing Directors: Martin Mos, Dr. Ulrich Vest

-----Your Question/Comment -----

Dear who is my concern:

I am Goksemin Fatma Sengul from Bilkent University. I want to reproduce Figure 4 and Supplementary from the paper entitled as

Characterization of a novel zebrafish (*Danio rerio*) gene, *wdr81*, associated with cerebellar ataxia, mental retardation and dysequilibrium syndrome (CAMRQ)

Figure 1 in my thesis. I want to reuse these Figures to compare the WMISH results of *wdr81* with my other two targeted genes and as well as to describe the domains in the *wdr81* protein to speculate about its novel or known functions. I contacted with the copyright center and officer suggested me to directly right to the first author or corresponding author. However, the corresponding author suggested me to take the actual permission from you. Therefore, I decide to write to the BMC journal. I want to ask that may I use Figure 4 and Supplementary Fig 1 from the study that was published in BMC in 2015. I appreciate all of your helps and understandings.

Best wishes  
Goksemin

---



Figure 3.4. Whole mount *in situ* hybridization (WMISH) was performed with Zebrafish embryos in order to show the localization of *wdr81*, *vldlr*, *ano10A* mRNA transcription certain common nervous system areas. (B) The expression pattern of *vldlr* in early developmental stages of Zebrafish (Imai, *et al.*, 2012) (Adapted from the Development, Growth&Differentiation) [215]. Abbreviations, Ce: cerebellum, Di: diencephalon, FB: forebrain region, HB: hindbrain region, Hy: hypothalamus, MB: midbrain region, MLF: medial longitudinal, OV: Optic vesicle, Le: Lens, hpf: hour post fertilization, dpf: day post fertilization [215].

no-reply@copyright.com

8 Haziran 2018 22:22

Kime: fatma.sengul@bilkent.edu.tr

Thank you for your order with RightsLink / John Wiley and Sons

N



## Thank you for your order!

Dear Mrs. Goksemin Sengul,

Thank you for placing your order through Copyright Clearance Center's RightsLink® service.

### Order Summary

Licensee: Goksemin Sengul  
 Order Date: Jun 8, 2018  
 Order Number: 4364360939639  
 Publication: Development, Growth & Differentiation  
 Title: Dynamic changes in the gene expression of zebrafish Reelin receptors during embryogenesis and hatching period  
 Type of Use: Dissertation/Thesis  
 Order Total: 0.00 USD

View or print complete [details](#) of your order and the publisher's terms and conditions.

Sincerely,

Copyright Clearance Center

Tel: +1-855-239-3415 / +1-978-646-2777  
[customercare@copyright.com](mailto:customercare@copyright.com)  
<https://myaccount.copyright.com>



RightsLink®

**Figure 5.1. The illustration of Tol2 transposon system. (A) The suitable recombination sites addition through PCR to the gene of interest vector in order to insert it into the pME is depicted. Although it is not shown in this figure, the inserts of p5E and p3E entry vectors are also exposed to similar restriction sites addition PCR amplification to make them also proper for the insertion into their specific pDONR plasmids by using BP reactions. (B) The schematic drawing of combination of three entry plasmids within the one expression pDest vector using LR reaction. Abbreviations in the figure stands for pDONR: donor plasmid, attB1-4, attP1-4, attL1-4, attR1-4: recombination specific sequences, p5E: 5' elements containing plasmid, pME: middle entry plasmid, p3E: 3' elements containing plasmid, EGFP: enhanced green fluorescent protein sequence (Adapted from John Wiley and Sons) [339].**

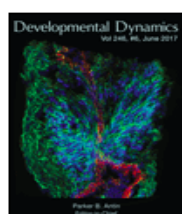
no-reply@copyright.com

Kime: fatma.sengul@bilkent.edu.tr

Thank you for your order with RightsLink / John Wiley and Sons

Evvelsi gün 03:31

N



### Thank you for your order!

Dear Mrs. Goksemin Sengul,

Thank you for placing your order through Copyright Clearance Center's RightsLink® service.

#### Order Summary

Licensee: Goksemin Sengul  
 Order Date: Jun 8, 2018  
 Order Number: 4364481325022  
 Publication: Developmental Dynamics  
 Title: The Tol2kit: A multisite gateway-based construction kit for Tol2 transposon transgenesis constructs  
 Type of Use: Dissertation/Thesis  
 Order Total: 0.00 USD

View or print complete [details](#) of your order and the publisher's terms and conditions.

Sincerely,

Copyright Clearance Center

Tel: +1-855-239-3415 / +1-978-646-2777  
[customercare@copyright.com](mailto:customercare@copyright.com)  
<https://myaccount.copyright.com>



RightsLink®